

**ESKOM**

**NUCLEAR SITES  
SITE SAFETY REPORTS**

**NUMERICAL MODELLING OF  
COASTAL PROCESSES**

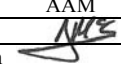
**DUYNEFONTEIN**

**Report No. 1010/4/101**

**SEPTEMBER 2009**



**PRESTEDGE RETIEF DRESNER WIJNBERG (PTY) LTD  
CONSULTING PORT AND COASTAL ENGINEERS**

<b>Numerical Modelling of Coastal Processes - Duynefontein Report 1010/4/101</b>					
<b>Revision</b>	<b>Date</b>	<b>Author</b>	<b>Checked</b>	<b>Status</b>	<b>Approved</b>
00	March 2008	SAL	AAM/GKP	Draft for Comment	AAM
01	March 2008	SAL	AAM/GKP	For Use	AAM
02	March 2008	SAL	AAM/GKP	For Use	AAM
03	September 2009	SAL	AAM/GKP	For Use	AAM 

Keywords: Numerical modelling, waves, water levels, currents, thermal plume, sediment transport, tsunamis, Duynefontein

**ESKOM****NUCLEAR SITES  
SITE SAFETY REPORTS****NUMERICAL MODELLING OF COASTAL PROCESSES  
DUYNEFONTEIN****TABLE OF CONTENTS**

	<b>PAGE NO.</b>
<b>1. INTRODUCTION .....</b>	<b>1</b>
<b>1.1 Background.....</b>	<b>1</b>
<b>1.2 Scope of work.....</b>	<b>1</b>
<b>1.3 Limitations .....</b>	<b>2</b>
<b>1.4 Conventions and terminology.....</b>	<b>2</b>
<b>2. DESCRIPTION OF NUMERICAL MODELS.....</b>	<b>3</b>
<b>2.1 Introduction .....</b>	<b>3</b>
<b>2.2 Wave refraction model.....</b>	<b>3</b>
<b>2.3 Cross-shore hydrodynamic model.....</b>	<b>4</b>
<b>2.4 Two-dimensional hydrodynamic model.....</b>	<b>5</b>
<b>2.5 Three-dimensional hydrodynamic model.....</b>	<b>5</b>
<b>2.6 Two-dimensional sediment transport model.....</b>	<b>6</b>
<b>2.7 Suspended sediment model.....</b>	<b>6</b>
<b>2.8 Extreme value analysis.....</b>	<b>7</b>
<b>2.9 CORMIX near-field dilution model.....</b>	<b>7</b>
<b>3. FIELD MEASUREMENTS.....</b>	<b>8</b>
<b>4. WATER LEVELS .....</b>	<b>10</b>
<b>4.1 Tides.....</b>	<b>10</b>
<b>4.2 Extraction of storm surge .....</b>	<b>10</b>
<b>4.3 Extreme value analysis of storm surge .....</b>	<b>11</b>
<b>5. TSUNAMI FLOODING.....</b>	<b>12</b>
<b>5.1 Background.....</b>	<b>12</b>
<b>5.2 Distant tsunamis .....</b>	<b>12</b>
5.2.1 Sources .....	12
5.2.2 Model setup .....	15
5.2.3 Model calibration.....	15
5.2.4 Results .....	16
<b>5.3 Local tsunamis .....</b>	<b>17</b>
5.3.1 Sources .....	17
5.3.2 Modelling approach.....	18
5.3.3 Model setup .....	18
5.3.4 Slumps modelled .....	19
5.3.5 Results .....	20
5.3.6 Discussion .....	21
<b>5.4 Conclusions .....</b>	<b>21</b>
<b>5.5 Recommendations.....</b>	<b>22</b>
<b>6. WAVES .....</b>	<b>23</b>
<b>6.1 Waves measured at the site.....</b>	<b>23</b>
<b>6.2 Offshore hindcast data .....</b>	<b>23</b>
<b>6.3 Model setup.....</b>	<b>24</b>

<b>6.4</b>	<b>Model calibration.....</b>	<b>24</b>
<b>6.5</b>	<b>Extreme value analysis of wave height .....</b>	<b>25</b>
<b>6.6</b>	<b>Wave transformation across surf-zone.....</b>	<b>26</b>
<b>7.</b>	<b>SEA TEMPERATURE .....</b>	<b>27</b>
<b>7.1</b>	<b>Temperature measured at site.....</b>	<b>27</b>
<b>7.2</b>	<b>Extreme value analysis of temperature .....</b>	<b>28</b>
<b>8.</b>	<b>CURRENTS.....</b>	<b>30</b>
<b>8.1</b>	<b>Background.....</b>	<b>30</b>
<b>8.2</b>	<b>Currents measured at site.....</b>	<b>30</b>
<b>8.3</b>	<b>Hydrodynamic modelling.....</b>	<b>30</b>
8.3.1	Model setup .....	30
8.3.2	Model calibration.....	32
8.3.3	Selection of representative hydrodynamic conditions .....	33
<b>9.</b>	<b>THERMAL PLUME DISPERSION.....</b>	<b>35</b>
<b>9.1</b>	<b>Background.....</b>	<b>35</b>
<b>9.2</b>	<b>Discharge characteristics .....</b>	<b>35</b>
<b>9.3</b>	<b>Intake and outfall layouts tested .....</b>	<b>37</b>
9.3.1	Background .....	37
9.3.2	Layout 0: Existing Koeberg Layout .....	37
9.3.3	Layout 1: Offshore tunnel intake and offshore tunnel outfall.....	38
9.3.4	Layout 2: Basin intake and offshore tunnel outfall.....	38
9.3.5	Layout 3: Offshore tunnel intake and nearshore channel outfall 3 km north.....	39
9.3.6	Layout 4: Offshore tunnel intake and nearshore channel outfall 4.5 km north.....	39
9.3.7	Layout 5: Basin intake and nearshore channel outfall .....	39
<b>9.4</b>	<b>Model setup.....</b>	<b>40</b>
<b>9.5</b>	<b>Results.....</b>	<b>41</b>
9.5.1	Near-field dilution .....	41
9.5.2	Far-field temperature and dilution .....	43
9.5.3	Recirculation.....	43
<b>10.</b>	<b>SEDIMENT TRANSPORT .....</b>	<b>45</b>
<b>10.1</b>	<b>Background.....</b>	<b>45</b>
<b>10.2</b>	<b>Sediment grain size.....</b>	<b>45</b>
<b>10.3</b>	<b>Sediment transport rates.....</b>	<b>47</b>
10.3.1	Model setup .....	47
10.3.2	Schematisation of wave and wind climate.....	47
10.3.3	Model calibration.....	47
10.3.4	Results .....	48
<b>10.4</b>	<b>Suspended sediment concentrations .....</b>	<b>49</b>
10.4.1	Background .....	49
10.4.2	Measured suspended sediment concentrations .....	50
10.4.3	Model setup .....	51
10.4.4	Conditions modelled.....	51
10.4.5	Results .....	51
<b>11.</b>	<b>CONCLUSIONS AND RECOMMENDATIONS.....</b>	<b>53</b>

## REFERENCES

## FIGURES

**APPENDIX A: Reference list of DHI applications of the MIKE model to power plants and marine outfalls**

**APPENDIX B: Report on calibration of wave hindcast data by Fugro Oceanor**

**APPENDIX C: Council for Geoscience Report: A Probabilistic Tsunami Hazard Assessment for Coastal South Africa from Distant Tsunamogenic Areas**

**APPENDIX D: Council for Geoscience Report: Potential Sources of Tsunami Along the South African Coast**

**APPENDIX E: Data Reports on Oceanographic Measurements by Lwandle Technologies**

**LIST OF TABLES**

Table 3.1: Data collection programme .....	8
Table 3.2: Data measurement sites .....	9
Table 4.1: Predicted tidal levels at Cape Town .....	10
Table 4.2: Extreme tidal residuals at Cape Town .....	11
Table 5.1: Distant tsunami sources modelled .....	13
Table 5.2: Fault parameters and vertical seabed displacement .....	14
Table 5.3: Modelled water levels at Duynefontein due to distant tsunamis .....	17
Table 5.4: Slump parameters modelled .....	20
Table 5.5: Modelled water levels at Duynefontein due to a theoretical 80 km <sup>3</sup> slump .....	21
Table 6.1: Extreme wave climate at -30 m CD .....	26
Table 7.1: Summary statistics of seawater temperatures measured at Duynefontein Site .....	28
Table 7.2: Extreme Seawater temperatures at 3 m depth .....	29
Table 8.1: Summary statistics of current speeds measured at the Duynefontein Site .....	30
Table 9.1: Reactor combinations tested in thermal plume model .....	35
Table 9.2: Seawater cooling requirements .....	35
Table 9.3: Near-field dilution model inputs .....	41
Table 9.4: Near-field dilution results for summer .....	42
Table 9.5: Near-field dilution results for winter .....	42
Table 9.6: Thermal Recirculation results .....	44
Table 10.1: Sediment grain size analysis for Duynefontein .....	46
Table 10.2: Measured total suspended solids (TSS) at Duynefontein Site .....	50
Table 10.3: Preliminary estimate of sand volume drawn into cooling water intake in 20 m depth .....	52

## LIST OF FIGURES

- Figure 1.1 : Locality map for Duynefontein site.
- Figure 1.2 : Bathymetry and location of instruments deployed at Duynefontein.
- Figure 4.1 : Analysis of storm surge: Measured tide, predicted tide and residual at Cape Town. Full 40 year dataset.
- Figure 4.2 : Analysis of storm surge: Measured tide, predicted tide and residual at Cape Town. Fourteen days including the May 1984 storm event.
- Figure 4.3 : Extreme value analysis of positive storm surge at Cape Town.
- Figure 4.4 : Extreme value analysis of negative storm surge at Cape Town.
- Figure 5.1 : Model bathymetry used for tsunami modelling of Sumatra and Karachi earthquake events.
- Figure 5.2 : Calibration of tsunami model: Measured and modelled water levels due to the tsunami in the Port of Port Elizabeth for the 26 December 2004 Sumatra event.
- Figure 5.3 : Maximum water levels predicted during tsunami event. Source is Sumatra A: 26 December 2004 earthquake,  $M_w = 9.2$ .
- Figure 5.4 : Minimum water levels predicted during tsunami event. Source is Sumatra A: 26 December 2004 earthquake,  $M_w = 9.2$ .
- Figure 5.5 : Maximum water levels predicted during tsunami event. Source is Sumatra B: maximum credible earthquake determined by the Council for Geoscience,  $M_w = 9.2$ .
- Figure 5.6 : Minimum water levels predicted during tsunami event. Source is Sumatra B: maximum credible earthquake determined by the Council for Geoscience,  $M_w = 9.2$ .
- Figure 5.7 : Maximum water levels predicted during tsunami event. Source is a Sumatra C: maximum plausible event from Borrero et al (2006),  $M_w = 9.3$ .
- Figure 5.8 : Minimum water levels predicted during tsunami event. Source is a Sumatra C: maximum plausible event from Borrero et al (2006),  $M_w = 9.3$ .
- Figure 5.9 : Maximum water levels predicted during tsunami event. Source is Karachi A: maximum credible earthquake determined by the Council for Geoscience,  $M_w = 8.4$ .
- Figure 5.10 : Minimum water levels predicted during tsunami event. Source is Karachi A: maximum credible earthquake determined by the Council for Geoscience,  $M_w = 8.4$ .
- Figure 5.11 : Model bathymetry used for tsunami modelling of the South Sandwich Islands earthquake events.
- Figure 5.12 : Maximum water levels predicted during tsunami event. Source is South Sandwich Islands A: maximum credible earthquake determined by the Council for Geoscience,  $M_w = 7.6$ .
- Figure 5.13 : Minimum water levels predicted during tsunami event. Source is South Sandwich Islands A: maximum credible earthquake determined by the Council for Geoscience,  $M_w = 7.6$ .
- Figure 5.14 : Maximum water levels predicted during tsunami event. Source is South Sandwich Islands B: magnitude increased to  $M_w = 8.0$ .
- Figure 5.15 : Minimum water levels predicted during tsunami event. Source is South Sandwich Islands B: magnitude increased to  $M_w = 8.0$ .
- Figure 5.16 : Top: Main morphological and structural features of submarine slumps (Dingle, 1977). Bottom: Parameters defining slump model (Watts et al, 2003).
- Figure 5.17 : Location of slump zones around Southern Africa shown in pink (Dingle et al, 1987).
- Figure 5.18 : Model bathymetry used for tsunami modelling due to slumps on the South African shelf margin. Locations of the three slumps modelled are indicated.
- Figure 5.19 : Details of the Agulhas Slump (Dingle, 1977).
- Figure 5.20 : Maximum water levels predicted during tsunami event. Source is theoretical Agulhas Slump with volume of slumped sediment =  $80 \text{ km}^3$ .
- Figure 5.21 : Minimum water levels predicted during tsunami event. Source is theoretical Agulhas Slump with volume of slumped sediment =  $80 \text{ km}^3$ .
- Figure 5.22 : Maximum water levels predicted during tsunami event. Source is theoretical Cape Town Slump (South) with volume of slumped sediment =  $80 \text{ km}^3$ .

- Figure 5.23 : Minimum water levels predicted during tsunami event. Source is theoretical Cape Town Slump (South) with volume of slumped sediment = 80 km<sup>3</sup>.
- Figure 5.24 : Maximum water levels predicted during tsunami event. Source is theoretical Cape Town Slump (North) with volume of slumped sediment = 80 km<sup>3</sup>.
- Figure 5.25 : Minimum water levels predicted during tsunami event. Source is theoretical Cape Town Slump (North) with volume of slumped sediment = 80 km<sup>3</sup>.
- Figure 6.1 : Wave measurements at Duynefontein Sites A and B. Time-series of wave parameters (refer to Figure 1.2 for instrument positions).
- Figure 6.2 : Wave measurements at Duynefontein Site A. Wave rose and histogram of wave heights.
- Figure 6.3 : Wave measurements at Duynefontein Site B. Wave rose and histogram of wave heights.
- Figure 6.4 : Time-series of offshore wave hindcast parameters. Position is 40 km south-west of Cape Town in 200 m depth at position E 18.0°, S 34.0°.
- Figure 6.5 : Rose and histogram of offshore wave hindcast data. Position is 40 km south-west of Cape Town in 200 m depth at position E 18.0°, S 34.0°.
- Figure 6.6 : Numerical mesh used for wave refraction modelling.
- Figure 6.7 : Calibration of wave model. Measured and modelled time-series of wave parameters at Site A.
- Figure 6.8 : Calibration of wave model. Measured and modelled time-series of wave parameters at Site B.
- Figure 6.9 : Example of wave refraction from offshore to Duynefontein site. Deepwater wave condition:  $H_{m0} = 9.5$  m,  $T_p = 16.5$  s, Mean direction = 224°.
- Figure 6.10 : Example of wave refraction from offshore to Duynefontein site. Deepwater wave condition:  $H_{m0} = 9.5$  m,  $T_p = 16.5$  s, Mean Dir = 224°.
- Figure 6.11 : Characterisation of storm waves refracted to -30 m CD depth contour at Duynefontein site. Point 1. Includes only storms where the offshore  $H_{m0} > 4.0$  m.
- Figure 6.12 : Extreme value analysis of waves at -30 m CD depth at Duynefontein (Point 1).
- Figure 6.13 : Example of cross-shore wave transformation modelling from -30 m CD depth to shoreline.
- Figure 7.1 : Seawater temperatures measured at Duynefontein for SSR.
- Figure 7.2 : Seawater temperatures measured at Duynefontein showing decrease in temperature with depth.
- Figure 7.3 : Seawater temperatures measured at 08:00 inside cooling water intake basin at Koeberg. Site C, Water depth = 3 m, Instrument depth = 3 m.
- Figure 7.4 : Histograms of measured seawater temperatures in the cooling water intake basin at Koeberg. Left: Temperature measured at 08:00. Right: Difference between the maximum daily temperature and the temperature at 08:00.
- Figure 7.5 : Extreme Value Analysis of measured seawater temperatures at 08:00 in the cooling water intake basin at Koeberg.
- Figure 8.1 : Current measurements at Site A, water depth = 10 m (refer to Figure 1.2 for position). Time-series of surface and bottom currents.
- Figure 8.2 : Current measurements at Site B, water depth = 30 m (refer to Figure 1.2 for position). Time-series of surface and bottom currents.
- Figure 8.3 : Current measurements at Sites A and B. Surface and seabed current rose plots.
- Figure 8.4 : Numerical mesh and bathymetry used for hydrodynamic modelling.
- Figure 8.5 : Calibration of hydrodynamic model: current speed and direction. Measured and modelled time-series of currents at Site A for period February to March 2008.
- Figure 8.6 : Calibration of hydrodynamic model: current speed and direction. Measured and modelled time-series of currents at Site A for period July 2008.
- Figure 8.7 : Calibration of hydrodynamic model: current speed and direction. Measured and modelled time-series of currents at Site B for period July 2008.
- Figure 8.8 : Calibration of hydrodynamic model: thermal plume dispersion. Modelled surface temperatures at 11:00 and measured surface temperatures between 11:20 and 11:50 on 14 October 1985.
- Figure 8.9 : Calibration of hydrodynamic model: thermal plume dispersion. Modelled surface temperatures at 12:00 and measured surface temperatures between 11:30 and 12:15 on 16 October 1985.
- Figure 8.10 : Calibration of hydrodynamic model: thermal plume dispersion. Modelled surface temperatures at 12:00 and measured surface temperatures between 11:18 and 12:10 on 18 October 1985.

- Figure 8.11 : Wave and wind time-series used in hydrodynamic and plume modelling. 14 day summer simulation period.
- Figure 8.12 : Wave and wind time-series used in hydrodynamic and plume modelling. 14 day winter simulation period.
- Figure 8.13 : Wave and wind time-series used in hydrodynamic and plume modelling. 14 day calm simulation period.
- Figure 9.1 : Layout 1: Offshore tunnel intake and offshore tunnel outfall.
- Figure 9.2 : Layout 2: Basin intake and offshore tunnel outfall.
- Figure 9.3 : Layout 3: Offshore tunnel intake and nearshore channel outfall 3 km north.
- Figure 9.4 : Layout 4: Offshore tunnel intake and nearshore channel outfall 4.5 km north.
- Figure 9.5 : Layout 5: Basin intake and nearshore channel outfall.
- Figure 9.6 : Near-field dilution modelling results (summer).
- Figure 9.7 : Example of modelled currents and thermal plume near water surface at a time when the currents are northward.
- Figure 9.8 : Example of modelled currents and thermal plume near water surface at a time when the currents are southward.
- Figure 9.9 : Thermal plume modelling: Mean increase in temperature due to power station. Layout 0: Existing Koeberg Layout. Power output: Koeberg = 1800 MWe.
- Figure 9.10 : Thermal plume modelling: Maximum increase in temperature due to power station. Layout 0: Existing Koeberg Layout. Power output: Koeberg = 1800 MWe.
- Figure 9.11 : Thermal plume modelling: Mean increase in temperature due to power station. Layout 0: Existing Koeberg Layout plus PBMR. Power output: Koeberg = 1800 MWe, PBMR = 165 MWe.
- Figure 9.12 : Thermal plume modelling: Maximum increase in temperature due to power station. Layout 0: Existing Koeberg Layout plus PBMR. Power output: Koeberg = 1800 MWe, PBMR = 165 MWe.
- Figure 9.13 : Thermal plume modelling: Mean increase in temperature due to power station. Layout 1: Offshore tunnel intake and offshore tunnel outfall. Power output: Koeberg = 1800 MWe, PBMR = 165 MWe, Nuclear-1 = 4000 MWe.
- Figure 9.14 : Thermal plume modelling: Maximum increase in temperature due to power station. Layout 1: Offshore tunnel intake and offshore tunnel outfall. Power output: Koeberg = 1800 MWe, PBMR = 165 MWe, Nuclear-1 = 4000 MWe.
- Figure 9.15 : Thermal plume modelling: Mean increase in temperature due to power station. Layout 1: Offshore tunnel intake and offshore tunnel outfall. Power output: Koeberg = 1800 MWe, PBMR = 165 MWe, Nuclear-1 + expansion = 8250 MWe.
- Figure 9.16 : Thermal plume modelling: Maximum increase in temperature due to power station. Layout 1: Offshore tunnel intake and offshore tunnel outfall. Power output: Koeberg = 1800 MWe, PBMR = 165 MWe, Nuclear-1 + expansion = 8250 MWe.
- Figure 9.17 : Thermal plume modelling: Mean increase in temperature due to power station. Layout 2: Basin intake and offshore tunnel outfall. Power output: Koeberg = 1800 MWe, PBMR = 165 MWe, Nuclear-1 + expansion = 8250 MWe.
- Figure 9.18 : Thermal plume modelling: Maximum increase in temperature due to power station. Layout 2: Basin intake and offshore tunnel outfall. Power output: Koeberg = 1800 MWe, PBMR = 165 MWe, Nuclear-1 + expansion = 8250 MWe.
- Figure 9.19 : Thermal plume modelling: Mean increase in temperature due to power station. Layout 3: Offshore tunnel intake and nearshore channel outfall 3 km north. Power output: Koeberg = 1800 MWe, PBMR = 165 MWe, Nuclear-1 + expansion = 8250 MWe.
- Figure 9.20 : Thermal plume modelling: Maximum increase in temperature due to power station. Layout 3: Offshore tunnel intake and nearshore channel outfall 3 km north. Power output: Koeberg = 1800 MWe, PBMR = 165 MWe, Nuclear-1 + expansion = 8250 MWe.
- Figure 9.21 : Thermal plume modelling: Mean increase in temperature due to power station. Layout 4: Offshore tunnel intake and nearshore channel outfall 4.5 km north. Power output: Koeberg = 1800 MWe, PBMR = 165 MWe, Nuclear-1 + expansion = 8250 MWe.

- Figure 9.22 : Thermal plume modelling: Maximum increase in temperature due to power station. Layout 4: Offshore tunnel intake and nearshore channel outfall 4.5 km north. Power output: Koeberg = 1800 MWe, PBMR = 165 MWe, Nuclear-1 + expansion = 8250 MWe.
- Figure 9.23 : Thermal plume modelling: Mean increase in temperature due to power station. Layout 5: Basin intake and nearshore channel outfall. Power output: Koeberg = 1800 MWe, PBMR = 165 MWe, Nuclear-1 + expansion = 8250 MWe.
- Figure 9.24 : Thermal plume modelling: Maximum increase in temperature due to power station. Layout 5: Basin intake and nearshore channel outfall. Power output: Koeberg = 1800 MWe, PBMR = 165 MWe, Nuclear-1 + expansion = 8250 MWe.
- Figure 9.25 : Thermal plume modelling: time-series of recirculation results showing the increase in temperature at the intakes for the various layouts and power outputs modelled.
- Figure 10.1 : Sediment transport modelling. Measured  $D_{50}$  grain size.
- Figure 10.2 : Sediment transport modelling. Testing of wave and current modules in a simplified model comprising a uniform 1:67 beach slope with a wave approaching  $30^\circ$  from normal.
- Figure 10.3 : Sediment transport modelling. Testing of the coupled wave, current and sediment transport model for a simplified case with a uniform 1:67 beach slope and a wave approaching  $30^\circ$  from normal.
- Figure 10.4 : Sediment transport modelling: Potential net sediment transport for  $D_{50} = 0.2$  mm. Layout 0: Existing Koeberg Layout. Overview plot.
- Figure 10.5 : Sediment transport modelling: Potential net sediment transport for  $D_{50} = 0.2$  mm. Layout 0: Existing Koeberg Layout. Detailed view.
- Figure 10.6 : Sediment transport modelling: Potential net sediment transport for  $D_{50} = 0.2$  mm. Layout 2: Basin intake and offshore tunnel outfall. Overview plot.
- Figure 10.7 : Sediment transport modelling: Potential net sediment transport for  $D_{50} = 0.2$  mm. Layout 2: Basin intake and offshore tunnel outfall. Detailed view.
- Figure 10.8 : Sediment transport modelling: Potential net sediment transport for  $D_{50} = 0.2$  mm. Layout 3: Offshore tunnel intake and nearshore channel outfall. Overview plot.
- Figure 10.9 : Sediment transport modelling: Potential net sediment transport for  $D_{50} = 0.2$  mm. Layout 3: Offshore tunnel intake and nearshore channel outfall. Detailed view.
- Figure 10.10 : Sediment transport modelling: Potential net sediment transport for  $D_{50} = 0.2$  mm. Layout 5: Basin intake and nearshore channel outfall. Overview plot.
- Figure 10.11 : Sediment transport modelling: Potential net sediment transport for  $D_{50} = 0.2$  mm. Layout 5: Basin intake and nearshore channel outfall. Detailed view.
- Figure 10.12 : Sediment transport modelling. Alongshore transport rates. Layout 0.  $D_{50} = 0.2$  mm.
- Figure 10.13 : Sediment transport modelling. Influence of season on net alongshore transport rates. Layout 0.  $D_{50} = 0.2$  mm.
- Figure 10.14 : Sediment transport modelling. Influence of grain size on net alongshore transport rates. Layout 0.  $D_{50} = 0.2$  mm.
- Figure 10.15 : Sediment transport modelling. Influence of layout on net alongshore transport rates.  $D_{50} = 0.2$  mm.
- Figure 10.16 : Measured total suspended solids and sampling positions.
- Figure 10.17 : Example of modelled vertical profile of suspended sand concentration.

## **1. INTRODUCTION**

### **1.1 Background**

Eskom have embarked on a Nuclear Sites Programme as part of their overall Nuclear Programme. The purpose of the programme is to identify the most suitable nuclear sites to meet the requirements of sufficiency for a “Strategic reserve of banked potential sites” through a Nuclear Siting Investigation Programme implemented to internationally accepted standards, according to best practice and in line with authority requirements (e.g. the National Nuclear Regulator) as appropriate.

To this end, Eskom have embarked on a programme to prepare licenceable Site Safety Reports (SSR’s) for three sites, namely Duynefontein, Bantamsklip and Thyspunt. SSR’s are licensing documents that are submitted to the national nuclear regulatory authority in support of obtaining a site licence. The data incorporated into the SSR’s contain site-related information spanning the site life-cycle phases from Nuclear Siting Investigations through construction, commissioning, operation, decommissioning, to site reuse and thereafter.

Prestedge Retief Dresner Wijnberg (Pty) Ltd (PRDW), as part of a multi-disciplinary team preparing the SSR’s, are responsible for the Oceanography and Coastal Engineering Chapters of the Site Safety Report, which are required to be prepared in accordance with Eskom’s Technical Specification for this work. This report on the Numerical Modelling of Coastal Processes, along with the Coastal Engineering Investigations Report (PRDW, 2009), detail the studies undertaken in support of the SSR Chapter on Oceanography and Coastal Engineering. Due to space constraints the SSR contains a summary of the methodology and results, whilst these two supporting reports provide additional details on the studies undertaken. This report describes the Duynefontein site (see Figures 1.1 and 1.2 for location), whilst similar reports have been prepared for the Bantamsklip and Thyspunt sites.

### **1.2 Scope of work**

The scope of work is to characterise the following parameters at the Duynefontein site:

- Water levels
- Tsunami flooding
- Wave height, period and direction
- Seawater temperatures
- Currents
- Thermal plume dispersion and recirculation for typical intake and outfall configurations
- Sediment transport
- Suspended sediment concentrations.

### 1.3 Limitations

As required by Eskom's Technical Specification for this work, this study analyses return periods up to  $1:10^6$  years for water levels, waves and sea temperatures. Since these predictions are based on the available measured or hindcast datasets covering only the last 13 to 30 years, the predictions for return periods longer than 50 to 100 years need to be interpreted with caution.

### 1.4 Conventions and terminology

The following conventions and terminology are used in this report:

- Wave direction is the direction from which the wave is coming, measured clockwise from true north.
- Wind direction is the direction from which the wind is coming, measured clockwise from true north.
- Current direction is the direction towards which the current is flowing, measured clockwise from true north.
- $H_{m0}$  is the significant wave height, determined from the zeroth moment of the wave energy spectrum. It is approximately equal to the average of the highest one-third of the waves in a given sea state.
- $T_p$  is the peak wave period, defined as the wave period with maximum wave energy density in the wave energy spectrum.
- Mean wave direction is defined as the mean direction calculated from the full two-dimensional wave spectrum by weighting the energy at each frequency.
- $D_N$  is the diameter for which N% of the sediment, by mass, has a smaller diameter, e.g.  $D_{50}$  is the median grain diameter.
- Time is South African Standard Time (Time Zone -2).
- Seabed and water levels are measured relative to Chart Datum, which corresponds to Lowest Astronomical Tide (LAT) for Cape Town. Chart Datum is 0.825 m below Mean Sea Level or Land Levelling Datum (South African Tide Tables, 2008).
- The map projection system is as follows:
 

Map projection:	Gauss Conformal
Datum:	Hartebeesthoek 94
Spheroid:	WGS84
Scale factor:	1
Central meridian:	19°E
Reference system:	WG19
Co-ordinates:	Eastings (X, increasing eastwards) Northings (Y, increasing northwards)
Distance units:	International metre

## **2. DESCRIPTION OF NUMERICAL MODELS**

### **2.1 Introduction**

The numerical modelling has been undertaken using the MIKE suite of models developed by Danish Hydraulics Institute (DHI). The MIKE suite of models is the most comprehensive professional coastal engineering software suite currently available. This means that all the modelling for this project is being conducted using the same suite of integrated models, thus employing the same pre- and post-processing tools, numerical grids, data structures, and allowing direct coupling of the output of one model with the input to the next model. This increases the reliability of the results by minimising any errors associated with interfacing models and data structures from different sources.

The software is under continual development, testing and application by Danish Hydraulic Institute's more than 750 employees based in more than 25 countries worldwide. Major software updates occur annually and minor updates occur quarterly on average. The latest version is Release 2008 Service Pack 3, which is being used for the modelling described below. The software has been employed by DHI alone on more than 80 power, desalination and industrial plants worldwide.

A reference list of DHI applications of the MIKE model to power plants and marine outfalls is included in Appendix A. Validation documents, user manuals and scientific documentation for each model is available on request.

### **2.2 Wave refraction model**

The MIKE 21 Spectral Waves Flexible Mesh model (DHI, 2008a) is used for wave refraction modelling. The model simulates the growth, decay and transformation of wind-generated waves and swell in offshore and coastal areas using unstructured meshes.

MIKE 21 SW includes two different formulations:

- Directional decoupled parametric formulation
- Fully spectral formulation.

The directional decoupled parametric formulation is based on a parameterization of the wave action conservation equation. The parameterization is made in the frequency domain by introducing the zeroth and first moment of the wave action spectrum as dependent variables.

The fully spectral formulation is based on the wave action conservation equation, where the directional-frequency wave action spectrum is the dependent variable.

MIKE 21 SW includes the following physical phenomena:

- Wave growth by action of wind
- Non-linear wave-wave interaction
- Dissipation due to white-capping
- Dissipation due to bottom friction
- Dissipation due to depth-induced wave breaking
- Refraction and shoaling due to depth variations
- Wave-current interaction
- Effect of time-varying water depth and flooding and drying.

The discretization of the governing equation in geographical and spectral space is performed using cell-centred finite volume method. In the geographical domain, an unstructured mesh technique is used. The time integration is performed using a fractional step approach where a multi-sequence explicit method is applied for the propagation of wave action.

MIKE 21 SW is also used in connection with the calculation of the sediment transport, which for a large part is determined by wave conditions and associated wave-induced currents. The wave-induced current is generated by the gradients in radiation stresses that occur in the surf zone. MIKE 21 SW can be used to calculate the wave conditions and associated radiation stresses. Subsequently the wave-induced flow is calculated using the MIKE 21 Flow Model FM.

### **2.3 Cross-shore hydrodynamic model**

The cross-shore hydrodynamic engine of the LITPACK model (DHI, 2008b) has been applied to model wave set-up and the transformation of wave heights across the surf-zone.

The hydrodynamic model includes a description of propagation, shoaling and breaking of waves, calculation of the driving forces due to radiation stress gradients, momentum balance for the cross-shore and longshore direction giving the wave set-up and the longshore current velocities. The model can be applied on complex coastal profiles with longshore bars. In the case of a longshore bar the broken waves can reform in the trough onshore of the bar. The waves can be treated as regular or irregular, and the effect of directional spreading can be included in the description.

For irregular waves, the Battjes and Janssen approach is applied in this study. The statistical description of the wave heights is a truncated Rayleigh distribution where the upper bound is the local maximum wave height. The mean wave energy balance equation is applied to calculate the RMS-value of the wave heights across the coastal/beach profile. The wave period is fixed.

## 2.4 Two-dimensional hydrodynamic model

The two-dimensional hydrodynamic model used is the MIKE 21 Flow Model (DHI, 2008c). The model is used to simulate tsunami propagation and transformation. MIKE 21 is a general purpose numerical modelling system for the simulation of water levels and flows in estuaries, bays and coastal areas. The model solves the two-dimensional shallow water equations (conservation of mass and vertically-integrated momentum) on a series of dynamically-nested rectangular grids using the Alternating Direction Implicit (ADI) technique. The solver is second to third-order accurate in the convective momentum terms.

MIKE 21 Flow includes the following physical phenomena relevant to tsunami simulations:

- Bottom friction
- Flooding and drying, i.e. tsunami run-up on a beach
- Coriolis forcing.

## 2.5 Three-dimensional hydrodynamic model

The three-dimensional hydrodynamic model used is the MIKE 3 Flow Flexible Mesh Model (DHI, 2008d). The model is used to simulate the three-dimensional tidal, wind and wave-driven currents and the thermal plume dispersion. The model is based on the numerical solution of the three-dimensional incompressible Reynolds averaged Navier-Stokes equations invoking the assumptions of Boussinesq and of hydrostatic pressure. The model consists of the continuity, momentum, temperature, salinity and density equations and is closed by a  $k$ - $\epsilon$  vertical turbulence closure scheme. Horizontal eddy viscosity is modelled with the Smagorinsky formulation.

The time integration of the shallow water equations and the transport equations is performed using a semi-implicit scheme, where the horizontal terms are treated explicitly and the vertical terms are treated implicitly. In the vertical direction a structured mesh, based on a sigma-coordinate transformation is used, while the geometrical flexibility of the unstructured flexible mesh comprising triangles or rectangles is utilised in the horizontal plane.

MIKE 3 Flow Model includes the following physical phenomena:

- Currents due to tides
- Currents due to wind stress on the water surface
- Currents due to waves: the second order stresses due to breaking of short period waves can be included using the radiation stresses computed in the MIKE 21 SW model
- Coriolis forcing
- Bottom friction
- Flooding and drying

- Advection and dispersion of heat, salt and other constituents
- Effect of water temperature and salinity on density and turbulence (baroclinic mode)
- Heat exchange with the atmosphere: the exchange is calculated for the processes of long wave radiation, sensible heat flux (convection), short wave radiation and latent heat flux (evaporation).

## 2.6 Two-dimensional sediment transport model

The sediment transport model used is the MIKE 21 Flow Model FM, Sand Transport Model (DHI, 2008e). The model comprises a dynamic coupling between the following modules:

- Spectral wave module
- Hydrodynamic module
- Sand transport module.

The spectral wave module is MIKE 21 SW as described in Section 2.2. The hydrodynamic module is the MIKE 21 Flow Flexible Mesh Model, which is the two-dimensional version of the model described in Section 2.5.

The Sand Transport Module calculates the transport of non-cohesive sediment based on the combination of flow conditions from the hydrodynamic module and wave conditions from the wave module. For the case of combined wave and currents, sediment transport rates are derived by linear interpolation in a sediment transport lookup table. The values in the table are calculated by the quasi three-dimensional sediment transport model (STPQ3D). STPQ3D calculates instantaneous and time-averaged hydrodynamics and sediment transport in two horizontal directions. As the model calculates the bed load and the suspended load separately, the values in the sediment transport table are the total load.

The temporal and vertical variations of shear stress, turbulence, flow velocity and sediment concentrations are resolved. The time evolution of the boundary layer due to combined wave/current motion is solved by means of an integrated momentum approach. The force balance includes contributions from the near bed wave orbital motion, forces associated with wave breaking (gradients of radiation stresses) and the sloping water surface. Note that equilibrium sediment transport conditions are assumed, i.e. the sediment transport reacts instantaneously to the wave and current conditions.

## 2.7 Suspended sediment model

The LITSTP engine of the LITPACK model (DHI, 2008b) has been applied to model the suspended sediment concentration profiles for estimating the volume of sediment drawn into the cooling water intake. The model solves the vertical diffusion equation on an intrawave period grid to provide a detailed description of the suspended sediment concentration both vertically and over the wave period.

The model accounts for waves and currents at arbitrary angles, breaking/non-breaking waves, plane/ripple-covered bed, uniform/graded bed material, effect of bed slope and the effect of streaming. The sediment is divided into 30 size fractions based on a log-normal grading curve characterized by the median grain diameter  $D_{50}$  and the sediment grading defined by  $(D_{84}/D_{16})^{0.5}$ . The model output is the time-averaged vertical profile of suspended sediment concentration. The model only simulates non-cohesive sediments with grain sizes greater than 0.063 mm, i.e. sand particles.

## 2.8 Extreme value analysis

The EVA toolbox (DHI, 2008f) comprises a comprehensive suite of routines for performing extreme value analysis. These include:

- A pre-processing facility for extraction of the extreme value series from the record of observations.
- Support of two different extreme value models, the annual maximum series model and the partial duration series model.
- Support of a large number of probability distributions, including exponential, generalised Pareto, Gumbel, generalised extreme value, Weibull, Frechét, gamma, Pearson Type 3, Log-Pearson Type 3, log-normal, and square-root exponential distributions.
- Three different estimation methods: method of moments, maximum likelihood method, and method of L-moments.
- Three validation tests for independence and homogeneity of the extreme value series.
- Calculation of five different goodness-of-fit statistics.
- Support of two different methods for uncertainty analysis, Monte Carlo simulation and Jackknife resampling.
- Comprehensive graphical tools, including histogram and probability plots.

## 2.9 CORMIX near-field dilution model

The CORMIX Ver 5.0 GTS model (Doneker *et al*, 2007) has been used to simulate the near-field dilution of the thermal plume, i.e. the dilution that occurs as the plume rises from the diffuser ports towards the water surface. CORMIX employs an expert system approach based on flow classification using length scales to determine the discharge/environment interaction and the flow processes that control initial near-field mixing and the transition to far-field plume behaviour. Note that CORMIX is not part of the MIKE suite of models from DHI.

### 3. FIELD MEASUREMENTS

A comprehensive data collection programme has been developed and implemented at the Duynefontein site. The objective of this programme is to provide baseline data for:

- Evaluation of the site and Nuclear Power Plant (NPP) safety
- Design of coastal structures at the site
- Calibrating the numerical models to confirm the accuracy of the numerical models used for estimation of both frequent and rare events.

The data collection programme is summarised in Table 3.1. The programme commenced in January 2008 and is scheduled to be completed in August 2010, resulting in 32 months of data. The data measured until February 2009 is presented in this report, under the relevant report section as indicated in Table 3.1. Technical details of the instrumentation employed and additional results are provided in Appendix E.

**TABLE 3.1: DATA COLLECTION PROGRAMME**

<b>Parameter</b>	<b>Description</b>	<b>Results (in this report unless indicated)</b>
Bathymetry	Multi-beam bathymetric survey	Section 6.3
Beach Profiles	Measured quarterly since April 2008	Coastal Engineering Report (PRDW, 2009)
Sediment Grain Sizes	Beach and nearshore samples in March 2008	Section 10.2
Wave Data	Measured at the site since January 2008. Also 15 years of offshore hindcast data.	Section 6.1
Water Levels	28.9 years of tidal data from Cape Town	Section 4.2
Currents	Measured at the site since January 2008.	Section 8.2
Seawater Temperature	Measured at the site since 1987	Section 7.1
Salinity	Measured at the site since January 2008	Section 7.1
Turbidity	Measured at the site since January 2008	Section 10.4.2
Biofouling	Measured at the site since January 2008	Coastal Engineering Report (PRDW, 2009)

The sites at which data has been measured are plotted in Figure 1.2 and tabulated in Table 3.2. Sites A and B have been established specifically for this SSR and the measurements are being conducted by Lwandle Technologies (Pty) Ltd under sub-contract to PRDW. Site C is inside the existing Koeberg intake basin and seawater temperature data has been measured there since 1987 by C Maxwell on behalf of Eskom. Sites D and E were used for seawater temperature measurements in 2008 by Bayworld on behalf of Eskom (Bayworld, 2008 and 2009).

**TABLE 3.2: DATA MEASUREMENT SITES**

<b>Site name</b>	<b>Oceanographic parameters measured</b>	<b>Measurement agency</b>	<b>Water depth [m]</b>	<b>Position in degrees WGS84 [longitude, latitude]</b>	<b>Position in meters WG19 [X, Y]</b>
Site A	Waves, currents, seawater temperature, salinity	Lwandle Technologies	10	18.4150, -33.6701	-54253, -3727222
Site B	Waves, currents, seawater temperature, salinity	Lwandle Technologies	30	18.3898, -33.6757	-56587 -3727857
Site C	Seawater temperature	C Maxwell	3	18.4227, -33.6774	-53538, -3728028
Site D	Seawater temperature	Bayworld	27	18.3924, -33.6865	-56339, -3729050
Site E	Seawater temperature	Bayworld	50	18.3509, -33.7025	-60177, -3730848

## 4. WATER LEVELS

### 4.1 Tides

The closest port to the Duynefontein site for which long-term tidal data is available is Cape Town (specifically Granger Bay – see Figure 1.1). The predicted tidal levels at Cape Town are as follows (South African Tide Tables, 2008):

**TABLE 4.1: PREDICTED TIDAL LEVELS AT CAPE TOWN**

Parameter	Level [m CD]
Highest Astronomical Tide (HAT)	2.02
Mean High Water Springs (MHWS)	1.74
Mean High Water Neaps (MHWN)	1.26
Mean Level (ML)	0.98
Mean Low Water Neaps (MLWN)	0.70
Mean Low Water Springs (MLWS)	0.25
Lowest Astronomical Tide (LAT)	0.00

These levels are relative to Chart Datum, which is 0.825 m below Mean Sea Level or Land Levelling Datum (South African Tide Tables, 2008).

### 4.2 Extraction of storm surge

The actual water level at a coastal site will differ from the predicted tidal level due to changes in atmospheric pressure and wind effects (collectively referred to as storm surge), as well as other factors including shelf waves, edge waves, wave set-up, wave run-up, seiche and tsunami. In this section only the storm surge component of the water level is estimated based on long-term hourly water level measurements. Tsunamis are considered in Section 5, while shelf waves, edge waves, wave set-up and wave run-up are considered in the Coastal Engineering Investigations Report (PRDW, 2009), along with the combination of all the relevant components to obtain the extreme water levels.

The procedure described below is used to analyse the storm surge. The hourly measured tide for Cape Town for the period 1967 to 2007 was kindly provided by the Hydrographer of the South African Navy (who is not responsible for any transcription errors or errors due to calculations using the data). The data has been corrected to the present Chart Datum (0.825 m below Mean Sea Level) taking into account the changes in Chart Datum level in use between 1978 and 2003 (South African Tide Tables, 2008). The data has then been ‘cleaned’ by removing obviously incorrect spikes and other errors. The MIKE tidal analysis toolkit (DHI, 2008g) is then used to perform a tidal analysis on the data to obtain the tidal constituents and to subsequently perform a tidal prediction for the full period.

The measured tide is then subtracted from predicted tide to obtain the tidal residuals. These residuals are again ‘cleaned’ to remove additional spikes and other errors in the data. Attention is paid to removing as far as possible errors caused by timing errors in the measurements, since these can

significantly corrupt the residual signal. The resulting dataset comprises 28.9 years of residual data. The measured tide, predicted tide and residuals are plotted in Figure 4.1 (the full time-series) and Figure 4.2 (fourteen days including the May 1984 storm when one of the largest residuals was recorded).

### 4.3 Extreme value analysis of storm surge

The residuals are analysed to estimate the positive storm surge (actual water level higher than predicted tide) and negative storm surge (actual water level higher lower than predicted tide) with return periods of 1:1, 1:10, 1:100 and 1:10<sup>6</sup> years. As discussed in Section 1.3, the results for the 1:10<sup>6</sup> year return period need to be interpreted with caution due to the available data comprising only 28.9 years.

The analysis is performed using the EVA (Extreme Value Analysis) toolbox (as described in Section 2.8). The analysis comprises fitting a three parameter Weibull distribution using the Method of Moments to an extreme value series extracted from the input time-series. The extreme value series is selected using the 'peaks over threshold' or 'partial duration series' method, with the threshold defined as the value that is exceeded 8 times per year on average. To ensure independence, two successive events are extracted only if the time between the events exceeds 24 hours. The 95% confidence level to the best estimate is calculated using the Monte Carlo method. The results of the extreme value analysis are presented in Figures 4.3 and 4.4, and Table 4.2.

**TABLE 4.2: EXTREME TIDAL RESIDUALS AT CAPE TOWN**

<b>Return Period</b> [years]	<b>Best estimate</b> <b>positive residual</b> [m]	<b>Upper 95%</b> <b>confidence positive</b> <b>residual</b> [m]	<b>Best estimate</b> <b>negative residual</b> [m]	<b>Upper 95%</b> <b>confidence</b> <b>negative residual</b> [m]
1	0.44	0.46	-0.42	-0.44
10	0.59	0.64	-0.59	-0.65
100	0.74	0.84	-0.76	-0.87
10 <sup>6</sup>	1.31	1.67	-1.46	-1.89

## **5. TSUNAMI FLOODING**

### **5.1 Background**

A tsunami is a train of water waves generated by impulsive disturbances of the water surface due to non-meteorological but geophysical phenomena such as submarine earthquakes, volcanic eruptions, submarine slumps and landslides or ice falls into a body of water. A conservative analysis of the potential effects produced by tsunamis should be performed and the nuclear installation should be designed for a design basis flood with a probable maximum tsunami taken into consideration (IAEA, 2003).

The approach adopted in this study is for the Council for Geoscience to define the distant and local tsunamigenic sources and for PRDW to then model the propagation of the tsunami from the source to the nuclear installation site.

### **5.2 Distant tsunamis**

#### **5.2.1 Sources**

The Council for Geoscience compiled a report (CGS, 2008a) titled 'A Probabilistic Tsunami Hazard Assessment for Coastal South Africa from Distant Tsunamogenic Areas', which is included as Appendix C of this report. The report identifies Sumatra, Karachi and the South Sandwich Islands as tsunamigenic regions which can affect the coastal areas of South Africa. For each region the report provides the maximum credible earthquake magnitude and the corresponding fault parameters.

Given the fault parameters (origin, strike, length, width, dislocation, depth and dip), the vertical displacement of the seabed caused by the earthquake is estimated using the method of Okada (1985). This method assumes that the displacement of the seabed is a result of the fault movement in a semi-infinite elastic homogeneous body. The vertical displacement of the seabed induces a corresponding displacement of the water surface, which is applied as the initial condition for the hydrodynamic model.

For each source region, a number of tests were performed using the hydrodynamic model to investigate which combination of fault parameters resulted in the worst tsunami reaching the nuclear site. Based on these tests, the six tsunami events described in Table 5.1 are presented in this report. The fault parameters and the resulting maximum vertical seabed displacements for each tsunami event are provided in Table 5.2.

**TABLE 5.1: DISTANT TSUNAMI SOURCES MODELLED**

<b>Earthquake event</b>	<b>Description</b>
Sumatra A	This is the actual tsunami event of 26 December 2004. It is used to calibrate the numerical model. The fault parameters applied are those from Grilli <i>et al</i> (2007).
Sumatra B	This is the maximum credible Sumatra earthquake as determined by CGS (2008a). The fault dip is set to the maximum value and the fault depth to the minimum value recommended in CGS (2008a), since model tests indicated that these values resulted in the largest tsunami. As recommended by CGS (2008a), the fault position and strike were selected to result in the highest tsunami reaching South Africa, as determined from model sensitivity tests. This results in the position being moved south of the 26 December 2004 event to near the Mentawai Islands.
Sumatra C	This is a maximum plausible future rupture of the Mentawai section of the Sunda megathrust, as described by Borrero <i>et al</i> (2006).
Karachi A	This is the maximum credible Karachi earthquake as determined by CGS (2008a). The fault dip is set to the maximum value and the fault depth to the minimum value recommended by CGS (2008a), since model tests indicated that these values resulted in the largest tsunami. As recommended by CGS (2008a), the fault position and strike were selected to result in the highest tsunami reaching South Africa, as determined from model sensitivity tests.
South Sandwich Islands A	This is the maximum credible South Sandwich Islands earthquake determined by CGS (2008a). The fault dip is set to 70° and the fault depth to 1 km, since model sensitivity tests indicated that these values resulted in the largest tsunami. As recommended by CGS (2008a), the fault position and strike were selected to result in the highest tsunami reaching South Africa, as determined from model sensitivity tests.
South Sandwich Islands B	This has the same location as South Sandwich Islands A, but the moment magnitude is increased from 7.6 to 8.0 as a sensitivity test.

**TABLE 5.2: FAULT PARAMETERS AND VERTICAL SEABED DISPLACEMENT**

Fault parameter	Segment number <sup>(1)</sup>	Sumatra A	Sumatra B	Sumatra C	Karachi A	South Sandwich A	South Sandwich B
		(26 Dec 2004 event)	(max credible CGS)	(max plausible Borrero )	(max credible CGS)	(max credible CGS)	(M <sub>w</sub> = 8.0)
Origin longitude <sup>(2)</sup> [degrees, +ve East, -ve West]	1	94.10	98.55	98.30	63.00	-26.00	-26.00
	2	93.33	-	100.00	-	-	-
	3	92.71	-	101.40	-	-	-
	4	92.17	-	-	-	-	-
	5	92.44	-	-	-	-	-
Origin latitude <sup>(2)</sup> [degrees, +ve North, -ve South]	1	3.48	-2.08	-2.00	24.5	-56.00	-56.00
	2	5.10	-	-4.20	-	-	-
	3	7.21	-	-6.00	-	-	-
	4	9.68	-	-	-	-	-
	5	11.78	-	-	-	-	-
Strike [degrees] <sup>(3)</sup>	1	323	321	321	270	160	160
	2	348	-	321	-	-	-
	3	338	-	321	-	-	-
	4	356	-	-	-	-	-
	5	10	-	-	-	-	-
Length [km]	1	220	741.3	260	283.1	102.8	162
	2	150	-	360	-	-	-
	3	390	-	140	-	-	-
	4	150	-	-	-	-	-
	5	350	-	-	-	-	-
Width [km]	1	130	166.72	130	96.92	54.75	71
	2	130	-	180	-	-	-
	3	120	-	70	-	-	-
	4	95	-	-	-	-	-
	5	95	-	-	-	-	-
Mean dislocation [m]	1	18	12.82	20	4.18	1.29	2.2
	2	23	-	20	-	-	-
	3	12	-	20	-	-	-
	4	12	-	-	-	-	-
	5	12	-	-	-	-	-
Depth [km] <sup>(4)</sup>		25	25	15	25	1	1
Dip [degrees]		12	15	15	27	70	70
Seismic moment M <sub>0</sub> [N/m] <sup>(5)</sup>		8.3 x 10 <sup>22</sup>	6.4 x 10 <sup>22</sup>	8.7 x 10 <sup>22</sup>	4.6 x 10 <sup>21</sup>	2.9 x 10 <sup>20</sup>	1.0 x 10 <sup>21</sup>
Moment magnitude M <sub>w</sub> [-] <sup>(6)</sup>		9.2	9.2	9.3	8.4	7.6	8.0
Max displacement up [m] <sup>(7)</sup>		9.6	5.4	9.0	1.8	0.8	1.3
Max displacement down [m]		-5.7	-2.3	-3.6	-0.4	-0.4	-0.7

- Notes: (1) The fault may comprise between 1 and 5 fault segments  
(2) The origin is defined as the mid-point of the upper border of the fault  
(3) An observer facing along strike should see the fault dip to the right (degrees clockwise from north)  
(4) Depth is defined as depth from the seabed to the upper border of the fault  
(5)  $M_0 = \mu LWD$ , with  $\mu$  = shear modulus  $\approx 4 \times 10^{10}$  Pa, L = Fault Length, W = Width, D = Dislocation  
(6)  $M_w = (\log_{10} M_0 - 9) / \log_{10} 32$   
(7) The seabed displacement modelled has a complex three-dimensional shape - only the maximum upward and downward displacements are given here.

### 5.2.2 Model setup

The MIKE 21 HD hydrodynamic model (as described in Section 2.4) is used to simulate the propagation of the tsunami wave from the source to the nuclear site. The model solves the two-dimensional shallow water equations (conservation of mass and vertically-integrated momentum) on a series of dynamically-nested rectangular grids using an implicit time scheme. Processes simulated include Coriolis force, bottom shear stress, flooding and drying. The waves are assumed to be non-breaking and the loss of energy and momentum by wave breaking is not simulated.

Nine nested grids were used, with the grid spacing varying from 120 m near the nuclear site to 9720 m at the model boundaries. The model bathymetry is obtained from the following sources:

- ETOPO 2 minute global bathymetry dataset for depths greater than approximately 200 m.
- MIKE C-MAP electronic hydrographic charts (DHI, 2008h) for depths from 200 m to 100 m.
- Multi-beam bathymetric surveys by the Council for GeoScience for depths from 100 m to 30 m.
- Multi-beam bathymetric survey of the inshore zone by Tritan Survey cc for depths from 30 m to 5 m.
- Beach profiles by Tritan Survey cc
- Lidar survey by Southern Mapping Company for land.

The model domain and bathymetry used to simulate tsunamis from the Sumatra and Karachi regions is shown in Figure 5.1, while the bathymetry for the South Sandwich Islands tsunamis is shown in Figure 5.11.

The model time step is 6 s, which ensures a Courant Number of less than 1.0 (although a Courant number up to 20 may be acceptable for stability of the implicit solver, in this case a value of 1 is required for model accuracy). The grid spacings are selected to ensure at least 20 to 30 grid points per tsunami wavelength. The drying depth is set at 0.2 m and the flooding depth is 0.3 m. Bed resistance is specified by a Manning number of 32 m<sup>1/3</sup>/s. Eddy viscosity is found to have an insignificant influence on these simulations and is set to zero. The still water level modelled is Mean Sea Level.

The fault parameters (Table 5.2) are used to calculate the vertical displacement of the seabed caused by the earthquake, which induces a corresponding displacement of the water surface and is applied as the initial condition for the hydrodynamic model.

### 5.2.3 Model calibration

The model is calibrated by simulating the Sumatra tsunami of 26 December 2004. The fault parameters and associated maximum vertical seabed displacement are shown in Table 5.2.

The 26 December 2004 event was measured at a number of tidal stations along the South African coastline, with the largest water level variation measured in the Port of Port Elizabeth (Rabinovich and Thomson, 2007). The measured tidal data for Port Elizabeth was kindly provided by the Hydrographer of the South African Navy. The measured tide is subtracted from predicted tide and then adjusted for the average storm surge of 0.18 m measured during the tsunami. The resulting tsunami signal is shown in Figure 5.2. It should be noted that the maximum crest of the tsunami was not recorded due to an instrument problem. Hartnady and Okal (2007) estimate the maximum crest level to have been approximately 2.11 m above the predicted tidal level. If the 0.18 m average storm surge is taken into account the maximum crest level reduces to 1.93 m.

The modelled tsunami levels inside the Port of Port Elizabeth compare well to the measurements (Figure 5.2). In this case the model slightly under-predicts the maximum water level (model: 1.7 m, measured: approximately 1.9 m) while over-predicting the minimum water level (model: -2.0 m, measured: -1.5 m). The tsunami has a period of between 30 and 40 minutes. These results provide confidence that the model is capable of simulating the tsunami propagation and transformation processes from distant sources.

#### 5.2.4 Results

Results are presented for each of the six tsunami events described in Table 5.1 and Table 5.2. Each simulation continues for approximately 24 hours after the tsunami wave reaches the site, to ensure that the maximum and minimum water levels are simulated. For each tsunami, the results are presented as two figures showing the maximum and minimum water levels relative to Still Water Level at any time during the simulation. Each figure includes a plot of the larger model domain as well as a zoomed-in view near each of the three proposed nuclear sites (Thyspunt, Bantamsklip and Duynefontein). For reference purposes, Port Elizabeth is also shown. The maximum and minimum water levels in the larger model domain are calculated from model output intervals of 10 minutes, which allows the tsunami wave crests to be visualised in the plots. The maximum and minimum water levels in the zoomed-in views are calculated from model output intervals of 1 minute, which ensures that the maximum levels are accurately detected.

The contour plots are presented in Figures 5.3 to 5.15. It can be seen that for tsunamis in the Indian Ocean, the Duynefontein site is relatively sheltered compared to Thyspunt and Port Elizabeth. The Mentawai Islands earthquakes (Sumatra B and C) are seen to direct the tsunami south-westwards towards South Africa, compared to the 26 December 2004 event, which directed more energy westwards towards Sri Lanka.

The maximum and minimum water levels at any position within a 3 km radius of the Duynefontein site have been extracted from the results and are presented below. The 3 km radius accounts for uncertainty regarding the exact location of the nuclear installation, as well as the possibility of flooding from a

flank rather than frontally. The maximum and minimum levels generally occur along the shoreline rather than offshore, due to shoaling and run-up/run-down effects.

**TABLE 5.3: MODELLED WATER LEVELS AT DUYNEFONTEIN DUE TO DISTANT TSUNAMIS**

<b>Earthquake event</b>	<b>Maximum water level [m above SWL]</b>	<b>Minimum water level [m below SWL]</b>
Sumatra A	0.7	-0.7
Sumatra B	0.7	-0.7
Sumatra C	1.0	-1.0
Karachi A	0.1	-0.1
South Sandwich Islands A	0.5	-0.5
South Sandwich Islands B	1.0	-0.8

The Sumatra C and South Sandwich Islands B tsunamis are seen to result in the most extreme water levels. To account for uncertainties in the source parameters as well as in the modelled tsunami propagation and transformation (see the model calibration in Section 5.2.3), it is recommended to increase the modelled results by 0.5 m. This results in a recommended maximum level of 1.5 m and a minimum level of -1.5 m. These are the maximum tsunami-induced water levels relative to Still Water Level. The total water level will additionally include the effect of tide, wave run-up, wave set-up and storm surge, as described in PRDW (2009).

### 5.3 Local tsunamis

#### 5.3.1 Sources

The Council for Geoscience compiled a report (CGS, 2008b) titled ‘Potential Sources of Tsunami Along the South African Coast’, which is included as Appendix D of this report. The possible tsunamigenic sources identified include: cosmic impact, remote submarine seismicity, submarine slides and slumps, meteotsunami, volcanic activity, terrestrial landslides and rockfalls. The summary and recommendations section of the report (CGS, 2008b) is reproduced below:

- The report provides a qualitative account of possible tsunamigenic sources that could threaten the South African coastline. To adequately assess the risk, a quantitative assessment of each source category is required.
- Offshore slump generated tsunami are considered the largest unknown risk factor. Holocene and recent historical records provide graphic evidence of their destructive capability on regional scales. Further research including all available stratigraphic/sedimentological/geomorphological data should be undertaken to better define the risk.
- Meteotsunami (edge waves) may well have been responsible for the 1969 and 2008 tsunami events along the southern African west coast. In depth research into the global frequency, locality and magnitude of meteotsunami should be undertaken to further quantify the risk. In particular, the atmospheric conditions along the west coast prior to the 1969 event should be compared with those of its 2008 counterpart.

- Worst case scenarios need to be defined. For instance, the potential impacts of the coincidence of maximum storm waves, storm surge, astronomical tides and meteotsunami should be modelled.
- Because of the relatively short history of tsunami records along the South African coast, the database should be extended by conducting an investigation of palaeotsunami in the stratigraphic record. No systematic work has yet been conducted along this coast. Areas of focus should be in the vicinity of planned nuclear installations.

### 5.3.2 Modelling approach

The Council for Geoscience report (CGS, 2008b) considers offshore slump generated tsunamis as the largest unknown risk factor for the South African coast. A number of slump regions have been documented where historical slumping has occurred on massive scales in various phases including late Mesozoic (148 million years ago to 65 million years ago), early to late Tertiary (65 Ma to 1.8 Ma) and possibly Quaternary (1.8 Ma to present). However, a quantitative assessment of the risk of occurrence and geometry of future slump events along the South African shelf margin is not available at present. This is in contrast to the distant tsunamigenic sources which are comparatively well defined (Section 5.2).

After discussion with the external reviewer for this study (Prof. C A Fleming), the modelling approach adopted in this study is to simulate the tsunamis generated by a number of theoretical offshore slumps in order to estimate the slump volume required to generate a tsunami at the nuclear installation sites of comparable size to that from the maximum credible distant earthquake described in Section 5.2.

### 5.3.3 Model setup

The MIKE 21 HD hydrodynamic model (as described in Section 2.4) is used to simulate the propagation of the tsunami wave from the source to the nuclear site. The model grid and parameters are the same as used for the distant earthquake sources (Section 5.2.2), except that the time-step is reduced from 6 to 3 s, and for numerical stability the eddy viscosity is increased from 0 to 20 m<sup>2</sup>/s.

Submarine mass failures can be categorised as either slip events, which are typically large translations in landslide masses, or rotational failure leading to a slump event. Since most of the South African events are categorised as slumps (CGS, 2008b), only slumps will be considered in this study. Unlike tsunami generation by earthquakes, which can be accurately modelled using the instantaneous coseismic displacement of the water surface as an initial condition, submarine slumps or slides typically take place over an extended period of time. To simulate slumps or slides the MIKE 21 HD hydrodynamic model has the facility to dynamically change the seabed level as a function of time.

A numerical routine has been developed to define the dynamic changes in seabed level arising from a slump. The submarine slump is simulated as a rigid body moving down a slope (Figure 5.16). The body has a Gaussian shape as specified in Grilli and Watts (2005). The equation describing the slump

motion follows Watts *et al* (2003), where the slump motion is modelled as a rigid body undergoing a rotation around a point described as the centre of rotation of a circle prescribed by the arc of the circular failure plane. The rigid body is subject to external moments due to gravity, added mass and shear stress summed over the failure plane. The slump motion is described with a cosine function and as such experiences an initial angular acceleration, relatively constant maximum angular velocity and a subsequent deceleration before coming to rest in a position such that the centre of mass of the slump is vertically under the axis of rotation. The input parameters required for the slump model are described in the following section.

#### 5.3.4 Slumps modelled

CGS (2008b) describes two historical slump regions relevant to the proposed nuclear sites: the Cape Town and Agulhas Slumps, shown in Figure 5.17. Three theoretical slumps have been modelled, with each slump located within one of the historical slumping regions and directly opposite one of the three proposed nuclear sites, as shown in Figure 5.18.

The magnitude of tsunami generated by a slump depends on a number of parameters, including slump volume, water depth, slump thickness, initial acceleration and maximum velocity of the slump. The geometry of the slumps which have been modelled is based on the measured geometry of the upper or proximal part of the Agulhas Slump, as indicated in Figure 5.19. Setting the slump width equal to the slump length gives a slump volume of 80 km<sup>3</sup>. The slump parameters modelled are given in Table 5.4.

**TABLE 5.4: SLUMP PARAMETERS MODELLED**

Parameter	Agulhas Slump	Cape Town Slump (South)	Cape Town Slump (North)
Volume [km <sup>3</sup> ] <sup>(1)</sup>	80	80	80
Length [km] <sup>(2)</sup>	18	18	18
Width [km] <sup>(3)</sup>	18	18	18
Thickness [km] <sup>(4)</sup>	0.3	0.3	0.3
Rotation [deg] <sup>(5)</sup>	0.4	0.4	0.4
Radius [km] <sup>(6)</sup>	135	135	135
Displacement [km] <sup>(7)</sup>	1.0	1.0	1.0
Centroid longitude [deg]	24.89	18.38	17.18
Centroid latitude [deg]	-35.22	-35.44	-34.37
Strike [deg] <sup>(8)</sup>	75	140	160
Water depth [m]	2000	2000	2000
Initial acceleration [m/s <sup>2</sup> ]	0.011	0.011	0.011
Maximum velocity [m/s]	2.3	2.3	2.3
Duration [minutes] <sup>(9)</sup>	11.3	11.3	11.3

- Notes: (1) Since the slump is elliptic, the volume =  $\pi/4$  x length x width x thickness  
(2) Length of the slump is measured down the slope, see 'b' in Figure 5.16  
(3) Width of the slump is measured across the slope.  
(4) See 'T' in Figure 5.16  
(5) See ' $\phi$ ' in Figure 5.16  
(6) See 'R' in Figure 5.16  
(7) See 'S' in Figure 5.16  
(8) An observer facing along the strike will see the slump moving down to the right (degrees clockwise from north)  
(9) This is the total duration of the slump movement

### 5.3.5 Results

Results are presented for each of the three slump-generated tsunamis described in Table 5.4. Each simulation continues for approximately 10 hours after the tsunami wave reaches the site, to ensure that the maximum and minimum water levels are simulated. For each tsunami, the results are presented as two figures showing the maximum and minimum water levels relative to Still Water Level at any time during the simulation. Each figure includes a plot of the larger model domain as well as a zoomed-in view near each of the three proposed nuclear sites (Thyspunt, Bantamsklip and Duynefontein). The maximum and minimum water levels in the larger model domain are calculated from model output intervals of 10 minutes, which allows the tsunami wave crests to be visualised in the plots. The maximum and minimum water levels in the zoomed-in views are calculated from model output intervals of 1 minute, which ensures that the maximum levels are accurately detected. The contour plots are presented in Figures 5.20 to 5.25.

The maximum and minimum water levels at any position within a 3 km radius of the Duynefontein site have been extracted from the results and are presented below. The 3 km radius accounts for uncertainty regarding the exact location of the nuclear installation, as well as the possibility of flooding from a flank rather than frontally. The maximum and minimum levels generally occur at the shoreline due to shoaling and run-up/run-down effects.

**TABLE 5.5: MODELLED WATER LEVELS AT DUYNEFONTEIN DUE TO A THEORETICAL 80 KM<sup>3</sup> SLUMP**

<b>Slump event</b>	<b>Maximum water level [m above SWL]</b>	<b>Minimum water level [m below SWL]</b>
Agulhas Slump	0.5	-0.5
Cape Town Slump (South)	0.5	-0.5
Cape Town Slump (North)	2.0	-2.0

### 5.3.6 Discussion

The hydrodynamic modelling indicates that a theoretical 80 km<sup>3</sup> slump in the historical Cape Town Slump region is likely to result in a tsunami amplitude of up to 2.0 m at the Duynefontein site, while the same sized slump in the historic Agulhas Slump region results in a 0.5 m amplitude tsunami at Duynefontein.

Compared to the theoretical 80 km<sup>3</sup> slump that has been modelled, the historical Agulhas Slump is one of the largest identified world-wide with an estimated length of 750 km, width of 106 km and volume of 20 000 km<sup>3</sup> (Dingle, 1977). According to Dingle (1977), the slump involved Pliocene sediments and may therefore be Quaternary (1.8 million years to present) in age. The volume of this slump is 250 times larger than the slump that has been modelled, implying a devastating tsunami for which evidence should presumably be contained in the stratigraphic record.

An important factor, however, is whether the slump occurred as a single unit or as a number of smaller events over time. Preliminary numerical modelling indicates that for the Agulhas and Cape Town slump regions, the duration of the tsunami-induced water level disturbance at the shore is 1 to 2 hours, implying that individual slumps separated by longer than this time are effectively separate smaller events rather than one large event.

## 5.4 Conclusions

The maximum tsunami risk from distant earthquake sources is found to be from the Sumatra region, which results in a maximum tsunami level of 1.5 m and a minimum level of -1.5 m (including a 0.5 m safety factor) at the Duynefontein site.

The maximum risk to the Duynefontein site from local sources is likely to be a submarine slump in the historical Cape Town Slump region. The hydrodynamic modelling indicates that a slump volume of less than 80 km<sup>3</sup> is required to generate a tsunami at the Duynefontein site that exceeds the tsunami from the distant Sumatra earthquake. However, a quantitative assessment of the risk of occurrence and geometry of future slump events along the South African shelf margin is not available at present.

Until further geological research is undertaken, it is proposed to base the tsunami risk on the relatively well defined distant earthquake sources. This results in a recommended maximum level of 1.5 m and a

minimum level of -1.5 m. These are the maximum tsunami-induced water levels relative to Still Water Level. The total water level will additionally include the effect of tide, wave run-up, wave set-up and storm surge, as described in PRDW (2009).

## 5.5 Recommendations

Additional research is required to better define the risk from local tsunamigenic sources. The CGS (2008b) report recommends the following approach:

- Further research including all available stratigraphic/sedimentological/geomorphological data should be undertaken to better define the risk from offshore slump generated tsunami.
- In depth research into the global frequency, locality and magnitude of meteotsunami should be undertaken to further quantify the risk. In particular, the atmospheric conditions along the west coast prior to the 1969 event should be compared with those of its 2008 counterpart.
- Because of the relatively short history of tsunami records along the South African coast, the database should be extended by conducting an investigation of palaeotsunami in the stratigraphic record. No systematic work has yet been conducted along this coast. Areas of focus should be in the vicinity of planned nuclear facilities.

## 6. WAVES

### 6.1 Waves measured at the site

Waves have been measured at the Duynefontein site at Site A (water depth of 10 m) starting in January 2008 and at Site B (water depth of 30 m) starting in July 2008. The locations of the two sites are shown in Figure 1.2 and the coordinates are given in Table 3.2. A number of problems including instrument firmware issues have reduced the data return to date. These issues have now been addressed by the instrument manufacturer. Full details of the measurements are given in Appendix E.

The measured wave time-series are plotted in Figure 6.1. The reason for the change in wave directions during the October 2008 and January 2009 deployments is likely to be instrument-related as these changes are not supported by physical wave refraction processes. Wave roses (excluding the data from October 2008 and January 2009) and wave height histograms are shown in Figures 6.2 and 6.3. The largest storm recorded to date occurred on 9 August 2008 during which the significant wave height ( $H_{m0}$ ) reached 6.7 m at Site B and 5.0 m at Site A (Figure 6.1). The dominant wave direction is  $240^\circ$  at both Sites A and B (Figures 6.2 and 6.3).

These data have been used to calibrate the wave models, as described in Section 6.4. Since the currently available datasets (up to February 2009) at Sites A and B have durations of only 8 and 5 months respectively, a 15 year wave hindcast dataset has been refracted inshore and then used for the extreme value analysis of wave height. The wave measurements are ongoing until August 2010 and will continue to provide valuable design data.

### 6.2 Offshore hindcast data

Fifteen years of offshore wave hindcast data was purchased from Fugro Oceanor in Norway. The data covers the period from November 1990 to October 2007, but excluding the period June 1991 to May 1993 (during which the data quality is lower). The data position is approximately 40 km west of Cape Town in 200 m water depth at coordinates E  $18.0^\circ$ , S  $34.0^\circ$  (Figure 6.6). The data comprises two-dimensional wave spectra and wave parameters ( $H_{m0}$ ,  $T_p$ , mean direction) at 6 hourly intervals.

The source of the data are directional wave spectra from the WAM (WAVE Model) numerical model run at the European Centre for Medium Range Weather Forecasting (ECMWF). The model data has been calibrated by Fugro Oceanor against available satellite altimeter data. A full description of the data sources and the calibration and verification procedure is provided in Appendix B.

The full dataset is plotted in the form of a time-series (Figure 6.4), wave rose and wave height histogram (Figures 6.5). The dominant wave direction is  $230^\circ$ , the median  $H_{m0}$  is 2.4 m and the maximum  $H_{m0}$  is 9.7 m.

### 6.3 Model setup

The wave modelling has been conducted using the MIKE Spectral Waves model (as described in Section 2.2). The objective is to transform the hindcast data from offshore to nearshore where it will be used for a number of applications including wave heights for design of coastal structures, wave run-up, wave-driven currents for plume dispersion and sediment transport.

The model mesh extends from the offshore wave hindcast position in 200 m depth to the shoreline. The mesh size varies from 50 m in the area of interest to 2000 m at the offshore boundary (Figure 6.6).

The model bathymetry is obtained from the following sources:

- MIKE C-MAP electronic hydrographic charts (DHI, 2008h) for depths from 200 m to 75 m.
- Multi-beam bathymetric surveys by the Council for GeoScience for depths from 75 m to 20 m.
- Single-beam bathymetric surveys of the Koeberg intake basin and adjacent seabed by Tritan Survey cc
- Beach profiles by Tritan Survey cc
- Lidar survey by Southern Mapping Company for land.

### 6.4 Model calibration

The model is calibrated by refracting the offshore hindcast data to the inshore measurement positions (Sites A and B, see Figure 1.2) for the period February to July 2008. The model parameter settings based on this calibration are described below.

The directionally decoupled parametric formulation is found to give comparable results to the fully spectral formulation and is adopted due to its lower computational cost. For the directional spreading a  $\cos^n(\theta-\theta_m)$  distribution is used, where  $n$  is the directional spreading index and  $\theta_m$  is the mean wave direction. A constant spreading index of  $n = 2.5$  (directional standard deviation =  $30^\circ$ ) gave superior results to more complex formulations where the spreading is made a function of wave period or direction. The directional discretization in the model is  $10^\circ$ . The wave breaking index is 0.8. Bottom friction is modelled with a constant friction factor  $f_w$  equal to 0.015, which is slightly lower than the default value of 0.02.

The resulting model calibration is considered to be good (Figures 6.7 and 6.8). The discrepancy in the wave directions at Site B is considered to be instrument-related, as described in Section 6.1. Since the boundary condition used for the calibration is the offshore wave hindcast data and not measured data, the calibration also confirms the accuracy of these hindcast data.

Figure 6.9 shows an example of the wave refraction from offshore towards the site, while Figure 6.10 shows a more detailed view near the Duynefontein site.

## 6.5 Extreme value analysis of wave height

The calibrated wave model has been used to transform the offshore hindcast data inshore to three positions along the -30 m CD depth contour. Since the objective is to determine the extreme inshore wave climate, the refraction has been performed only at the times in the 15 year record when the offshore  $H_{m0}$  exceeded 4.0 m.

Results are extracted at the three points along the -30 m CD depth contour shown in Figure 6.10. The wave rose for the storm waves refracted to Point 1 is shown in Figure 6.11, as well as the  $H_{m0}$ - $T_p$  relationship.

The wave data refracted to the -30 m CD positions have been analysed to estimate the  $H_{m0}$  with return periods of 1:1, 1:10, 1:100 and 1:10<sup>6</sup> years. As discussed in Section 1.3, the results for the 1:10<sup>6</sup> year return period need to be interpreted with extreme caution, since it is based on only 15 years of data.

The analysis is performed using the EVA (Extreme Value Analysis) toolbox (as described in Section 2.8). The analysis comprises fitting a three parameter Weibull distribution using the Method of Moments to an extreme value series extracted from the input time-series. The extreme value series is selected using the 'peaks over threshold' or 'partial duration series' method, with the threshold defined as the value that is exceeded 8 times per year on average. To ensure independence, two successive events are extracted only if the time between the events exceeds 48 hours. The 95% confidence level to the best estimate is calculated using the Monte Carlo method. The results of the extreme value analysis are presented in Figure 6.12 and Table 6.1.

Included in Table 6.1 are the increased wave heights taking climate change into account, which is assumed to increase the heights by 17% - refer to PRDW (2009) for details on climate change. Also included in Table 6.1 is the estimated  $T_p$  for each wave height, based on the relationship between  $T_p$  and  $H_{m0}$  at -30 m CD (refer to Figure 6.11).

**TABLE 6.1: EXTREME WAVE CLIMATE AT -30 M CD**

	Return Period [years]	No climate change				Climate change (17% increase in $H_{m0}$ )			
		$H_{m0}$ best estimate [m]	$T_p$ [s]	$H_{m0}$ upper 95% confidence [m]	$T_p$ [s]	$H_{m0}$ best estimate [m]	$T_p$ [s]	$H_{m0}$ upper 95% confidence [m]	$T_p$ [s]
Point 1	1	5.7	15.6	5.9	15.9	6.7	16.8	7.0	17.1
	10	7.0	17.1	7.5	17.7	8.2	18.4	8.8	19.0
	100	8.2	18.4	9.0	19.2	9.6	19.7	10.5	20.6
	$10^6$	12.1	22.0	14.6	24.1	14.2	23.7	17.1	25.9
Point 2	1	5.7	15.6	5.9	15.9	6.6	16.7	6.9	17.0
	10	7.0	17.1	7.4	17.6	8.1	18.3	8.7	18.9
	100	8.1	18.3	8.9	19.1	9.5	19.6	10.4	20.5
	$10^6$	12.0	21.9	14.4	23.9	14.0	23.6	16.8	25.8
Point 3	1	5.7	15.6	5.9	15.9	6.6	16.7	6.9	17.0
	10	7.0	17.1	7.5	17.6	8.2	18.4	8.7	18.9
	100	8.1	18.3	9.0	19.2	9.5	19.7	10.5	20.6
	$10^6$	12.1	22.0	14.5	24.0	14.1	23.7	17.0	25.9

## 6.6 Wave transformation across surf-zone

The cross-shore hydrodynamic engine of the LITPACK model (as described in Section 2.3) is used to transfer each of the extreme wave conditions at the -30 m CD position (Table 6.1) inshore to the -5 m CD position, where the resulting wave conditions are required as input to the wave set-up and run-up computations as described in the Coastal Engineering Investigations Report (PRDW, 2009). An example of the model output is shown in Figure 6.13.

## 7. SEA TEMPERATURE

### 7.1 Temperature measured at site

As part of this SSR, seawater temperature has been measured at the Duynefontein site at Site A (water depth of 10 m) starting in January 2008 and at Site B (water depth of 30 m) starting in July 2008. The locations of the two sites are shown in Figure 1.2 and the coordinates are given in Table 3.2. Full details of the measurements are given in Appendix E. The data measured to date is plotted in Figure 7.1. These measurements are ongoing until August 2010 and will continue to provide valuable design data.

Seawater temperature data at Duynefontein for 2008 was also obtained from Eskom/Bayworld (Bayworld, 2008 and 2009) at Site D in 27 m depth and Site E in 50 m depth. The location of these sites is shown in Figure 1.2 and the coordinates are given in Table 3.2. The data is plotted in Figure 7.2.

Long-term temperature data is also available at Koeberg and these data were obtained from Eskom/Charles Maxwell (pers. comm.). For this study the temperatures measured just inside the Koeberg cooling water intake basin has been utilised. The location of these sites is shown in Figure 1.2 and the coordinates are given in Table 3.2. A 5.0 year long dataset was available with hourly data, while a 13.2 year long dataset was available with daily data at 08:00. The daily data is plotted in Figures 7.3 and 7.4. The maximum temperatures are seen to occur during summer.

Summary statistics of the available seawater temperature datasets are provided in Table 7.1 (listed in order of increasing instrument depth). In some cases more than one instrument was deployed at one site, e.g. an ADCP with an onboard temperature sensor was deployed at the seabed along with a mooring with temperature loggers near the seabed and also higher up in the water column. The location of these sites is shown in Figure 1.2 and the coordinates are given in Table 3.2.

**TABLE 7.1: SUMMARY STATISTICS OF SEAWATER TEMPERATURES MEASURED AT DUYNEFONTEIN SITE**

Site	Total water depth [m]	Instrument depth [m]	Sampling interval [hours or minutes]	Length of dataset [months or years]	Minimum temperature [°C]	Mean temperature [°C]	Maximum temperature [°C]
C	3	3	1 hr	5.0 yrs	8.7	13.3	20.1
C	3	3	24 hr	13.2 yrs	9.2	13.1	20.8
A	10	4	10 min	3.5 mths	9.7	13.0	17.4
B	30	9	10 min	1.0 mths	13.3	14.1	15.9
A	10	10	10 min	7.8 mths	9.4	12.4	18.9
A	10	10	10 min	8.2 mths	9.3	12.1	18.8
B	30	19	10 min	1.0 mths	13.3	13.8	15.4
D	27	27	1 hr	10.8 mths	9.1	11.9	17.9
B	30	28	10 min	4.0 mths	9.2	11.2	14.8
B	30	28	10 min	3.3 mths	9.2	10.3	17.9
B	30	29	10 min	1.0 mths	12.8	13.7	14.2
B	30	30	10 min	1.0 mths	12.6	13.7	14.2
E	50	50	1 hr	6.7 mths	9.0	11.4	15.1

The data shows that the water column tends to be mixed in winter, while in summer the water temperature at 3 m depth may be up to 10°C warmer than at 50 m depth. The average water temperatures at depths of 3 m, 10 m, 27 m and 50 m are approximately 13.3°C, 12.3°C, 11.9°C and 11.4°C respectively.

## 7.2 Extreme value analysis of temperature

The temperatures measured just inside the Koeberg cooling water intake basin in a depth of 3 m (Site C) have been used to estimate the extreme seawater temperatures. The data has been analysed to estimate the temperatures with return periods of 1:1, 1:10, 1:100 and 1: 10<sup>6</sup> years. As discussed in Section 1.3, the results for the 1: 10<sup>6</sup> year return period need to be interpreted with caution due to the limited length of the dataset.

The analysis is performed using the EVA (Extreme Value Analysis) toolbox (as described in Section 2.8). The analysis comprises fitting a three parameter Weibull distribution using the Method of Moments to an extreme value series extracted from the input time-series. The extreme value series is selected using the ‘peaks over threshold’ or ‘partial duration series’ method, with the threshold defined as the value that is exceeded 8 times per year on average. To ensure independence, two successive events are extracted only if the time between the events exceeds 48 hours. The 95% confidence level to the best estimate is calculated using the Monte Carlo method. The results of the extreme value analysis are presented in Figure 7.5 and Table 7.2.

For this analysis the longer 13.2 year duration dataset measured daily at 08:00 is used rather the shorter 5.0 year dataset of hourly data. Due to solar heating, the maximum temperature during the day is likely to exceed the temperature at 08:00. An analysis using the 5.0 year dataset of hourly data shows that the maximum daily temperature exceeds the temperature at 08:00 as follows: median = 0.8°C, 95<sup>th</sup>

percentile = 2.5°C and maximum = 4.8°C (see Figure 7.4). Adding the 95<sup>th</sup> percentile value of 2.5°C to the temperature value at 08:00 is considered to be a sufficiently conservative approach to estimate the maximum daily temperature. The resulting maximum temperatures are given in Table 7.2

**TABLE 7.2: EXTREME SEAWATER TEMPERATURES AT 3 M DEPTH**

Return period [years]	Temperature at 08:00		Maximum temperature at any time of day	
	Best estimate [°C]	Upper 95% confidence [°C]	Best estimate [°C]	Upper 95% confidence [°C]
1	17.2	17.6	19.7	20.1
10	19.3	20.3	21.8	22.8
100	21.7	23.4	24.2	25.9
10 <sup>6</sup>	32.5	39.2	35.0	41.7

For the existing Koeberg units, a shut-down of the reactor will be necessary if the intake temperature exceeds 23°C (Eskom, 2006), which according to Table 7.2 has a return period of approximately 30 years (based on the best estimate of maximum temperature at any time of day). It is expected that the cooling water system for future nuclear installations at the site will be designed to allow higher intake temperatures, e.g. one type of Pressurised Water Reactor (PWR) allows a maximum cooling water temperature of 30°C, as well as an extreme temperature of 34.5°C for the safety assessment (Eskom, 2007).

One option for the cooling water intake is a tunnel intake at 20 m depth. The available data indicates that during high temperature events such as the event from 7 to 11 January 2009 (see Figure 7.2), the temperature at a depth of 10 m was approximately 1°C less than at 3 m depth, while the maximum temperature at a depth of 27 m was approximately 2°C less than the maximum temperature at 3 m depth. The ongoing measurements will provide a longer dataset to establish the decrease in extreme temperature with depth. In the interim, it will be conservative to assume that the extreme temperatures at 20 m depth are 1°C less than at 3 m depth.

## 8. CURRENTS

### 8.1 Background

Currents are important for thermal plume dispersion (Section 9) and sediment transport (Section 10) and also for the design of coastal structures such as intakes and outfalls. Currents have thus been measured at the site and a hydrodynamic model has been set up and calibrated to simulate the currents at the site for various environmental forcings and intake/outfall layouts.

### 8.2 Currents measured at site

Currents have been measured at the Duynefontein site at Site A (water depth of 10 m) starting in January 2008 and at Site B (water depth of 30 m) starting in July 2008. The locations of the two sites are shown in Figure 1.2 and the coordinates are given in Table 3.2. The instruments are Acoustic Doppler Current Profilers (ADCPs) which measure the current speed and direction in 0.5 m intervals from the surface to the seabed. A number of problems including instrument firmware issues have reduced the data return to date. These issues have now been addressed by the instrument manufacturer. Full details of the measurements are given in Appendix E.

The data measured to date is plotted in Figures 8.1 to 8.3. The currents at Sites A and B are predominantly wind-driven. The currents near the surface reach 1 m/s and have a dominant direction of 340°, in response to the dominant south-easterly winds. The currents near the seabed are weaker and the directions are more evenly distributed between northward and southward. Summary statistics are presented in Table 8.1.

**TABLE 8.1: SUMMARY STATISTICS OF CURRENT SPEEDS MEASURED AT THE DUYNEFONTEIN SITE**

	Site A (water depth 10 m)		Site B (water depth 30 m)	
	Near surface (-1.8 m)	Near seabed (-7.8 m)	Near surface (-2.0 m)	Near seabed (-25.5 m)
Mean current speed [m/s]	0.17	0.11	0.19	0.07
Maximum current speed [m/s]	0.97	0.87	0.88	0.43

These data have been used to calibrate the hydrodynamic model, as described in Section 8.3.2. The current measurements are ongoing and will provide valuable design data in the future.

### 8.3 Hydrodynamic modelling

#### 8.3.1 Model setup

The MIKE 3 Flow Flexible Mesh three-dimensional hydrodynamic model (as described in Section 2.5) has been set up to simulate the currents and the dispersion of the thermal plume due to winds, waves, tides and buoyancy effects.

The model bathymetry is obtained from the following sources:

- MIKE C-MAP electronic hydrographic charts (DHI, 2008h) for depths from 200 m to 75 m.
- Multi-beam bathymetric surveys by the Council for GeoScience for depths from 75 m to 20 m.
- Single-beam bathymetric surveys of the Koeberg intake basin and adjacent seabed by Tritan Survey cc
- Beach profiles by Tritan Survey cc
- Lidar survey by Southern Mapping Company for land.

The horizontal model grid comprises both triangular and quadrilateral elements with sizes ranging from 50 m in the surf-zone to 1000 m at the offshore boundaries (see Figure 8.4). The vertical grid has five layers having thicknesses from seabed to surface of 20%, 30%, 20%, 20% and 10% of the local water depth.

The predicted tide is applied along the three open boundaries of the model. Since a weak tidal signal is evident in the measured currents, the tidal levels applied in the model are varied along the boundaries. The tidal levels are obtained from a global tide model including the major diurnal ( $K_1$ ,  $O_1$ ,  $P_1$  and  $Q_1$ ) and semidiurnal tidal constituents ( $M_2$ ,  $S_2$ ,  $N_2$  and  $K_2$ ) with a spatial resolution of  $0.25^\circ \times 0.25^\circ$  based on TOPEX/POSEIDON altimetry data (DHI, 2008c).

A wind that varies in time but is constant over the model domain is applied. The wind data used is based on the data measured at a height of 10 m at Koeberg by Eskom, but the wind speed is increased by a factor 1.65 to account for the increase in wind speed offshore. This factor is calculated by comparing the average wind speed measured at Koeberg to the average wind speed at the offshore wave hindcast position (refer to Section 6.2). The default wind drag coefficient  $C_d$  is used, which is a linear variation from 0.001255 at 7 m/s to 0.002425 at 25 m/s.

Wave-driven currents are included by first running the calibrated MIKE Spectral Waves model (refer to Section 6.4) and saving the radiation stresses at three hour intervals. The numerical grid for the wave refraction model corresponds to the hydrodynamic grid in the hydrodynamic domain, but extends further offshore to the 200 m contour (Figure 6.6).

For bed resistance the default roughness height of 0.05 m is applied. Horizontal eddy viscosity and dispersion are computed using the Smagorinsky formulation with a default constant of 0.28. Vertical eddy viscosity is computed using the k- $\epsilon$  vertical turbulence closure scheme, while the vertical eddy dispersion is set to 0.1 times the vertical eddy viscosity. This scaling factor is applied to compensate for additional vertical mixing caused by the use of only 5 vertical layers and the potential smoothing of the vertical density gradient between the buoyant thermal plume and the ambient water. Model sensitivity tests confirm that using a scaling factor of 0.1 results in a measureable decrease in the vertical mixing compared to the default factor of 1.0.

Model sensitivity tests were performed in which ambient thermal stratification as well as heat exchange between the atmosphere and the sea surface were included in the simulation. These two processes were found to have only a small influence on the modelled currents and the temperature increase due to the plume above the background temperature. The simulations have thus been performed using a constant background temperature. It should be borne in mind that the background sea temperature varies on a seasonal, synoptic and diurnal time-scale (refer to Figures 7.1 to 7.3) and the temperature increase due to the thermal plume will be superimposed on this background variability. A constant salinity of 35.0 psu is specified.

### 8.3.2 Model calibration

The hydrodynamic model is first calibrated against measured currents and then against measured thermal plume temperatures.

The model is first calibrated by comparing the modelled current speed and direction to those measured over a three month period at Sites A and B (see Figure 1.2 for the instrument locations). The calibration results are shown in Figures 8.5 to 8.7. The model is seen to accurately reproduce the measured currents, including the vertical shear in current speed and direction through the water column. These results indicate that the key hydrodynamic forcing mechanisms, i.e. wind, wave and tides, are realistically simulated by the model and provide confidence in the predictive capability of the model.

The model is then calibrated by comparing the thermal plume predicted by the model to historical measurements of the plume from the existing Koeberg Nuclear Power Station. The historical measurements were conducted using a skiboat and a helicopter (Rathey and Potgieter, 1987). The skiboat was equipped with a temperature probe mounted 30 cm below the water surface and traversed the study area on a grid pattern in order to measure the ambient water temperature and define the surface extent of the thermal plume. A helicopter equipped with an infrared sea surface temperature recorder was also used and took measurements on a grid pattern from a height of 100 m above the sea surface. Both sets of measurements were then combined to obtain an average picture of the thermal plume over the survey period of approximately 1 hour.

The surveys conducted on 14, 16 and 18 October 1985 were selected for model calibration. During all these surveys both reactors were operational and the discharge rate was  $80 \text{ m}^3/\text{s}$ , the intake temperature was approximately  $13^\circ\text{C}$  and the outfall temperature was approximately  $23^\circ\text{C}$ , i.e. a  $\Delta T$  of  $10^\circ\text{C}$ . To allow a “spin-up” period, the model was run from 10 October to 19 October 1985, with an initial background temperature of  $13^\circ\text{C}$ . The wind applied in the model was the hourly data measured at 10 m height at Koeberg (Eskom, 1985), with the wind speed increased by a factor 1.65 to account for the increase in wind speed offshore (see Section 8.3.1). The wave height and period applied on the offshore boundary of the model were the 6 hourly values measured by a Waverider buoy in 170 m

water depth approximately 15 km west of Slangkop (see Figure 6.6). Since the wave direction was not measured, a constant direction of 230° was assumed, corresponding to the average wave direction obtained from wave hindcast data in this area (see Figure 6.5).

The plume calibration results are plotted in Figures 8.8 to 8.10. Considering the uncertainties in the measurements (e.g. due to the averaging of the plume over the hour long survey period) and the uncertainties in the model inputs (e.g. the assumed wave direction and the constant background temperature field), the model results correspond well to the measurements and thus provide confidence in the predictive capability of the model.

### 8.3.3 Selection of representative hydrodynamic conditions

The Oceanor hindcast dataset (Section 6.2) includes 10 years of simultaneous wave and wind data which are required as input forcing to the hydrodynamic model, along with tidal forcing. However, the computer run-times for the three-dimensional hydrodynamic model limit the period that can be simulated to a number of months. A rigorous procedure was thus developed to select the following periods from the 10 year dataset:

- A 14 day period with typical summer conditions
- A 14 day period with typical winter conditions
- A 14 day period with calm conditions (low waves and wind).

The procedure first calculates the following parameters for each consecutive 14 day period in the 10 year dataset (values in brackets are the weighting factor applied in the cost function):

- The mean wave height (1.0)
- The standard deviation of the wave height (0.2)
- The mean wave direction, weighted by the wave height (1.0)
- The mean peak period (0.4)
- The mean wind speed (1.0)
- The standard deviation of the wind speed (0.2)
- The mean wind direction, weighted by the wind speed (1.0).

The procedure then uses a cost function (i.e. a function that minimises the difference between two values) to locate the 14 day period having parameters closest to the average conditions for each season. The calmest 14 day period was located using a weighting factor of 2.0 for mean wave height and 1.0 for mean wind speed, with all other weights set to zero. The periods located by this process are given below, and the wind and wave conditions for each period are plotted in Figures 8.11 to 8.13.

- 14 day summer period: 2006-01-05 to 2006-01-19
- 14 day winter period: 2001-06-21 to 2001-07-05

- 14 day calm period: 1997-04-08 to 1997-04-22

For the plume dispersion modelling, these three periods have been run sequentially giving a total simulation time of 42 days.

## 9. THERMAL PLUME DISPERSION

### 9.1 Background

The advantage of locating the power station at the coast is that it allows a once-through seawater cooling system to be used. However, the intake and outfall structures need to be designed to minimize recirculation between the outfall and the intake, and to ensure that the potential ecological impacts due to the discharge of heated water and other co-discharges such as chlorine and nuclides are acceptable.

### 9.2 Discharge characteristics

The Site Safety Report is based on a Plant Parameter Envelope (PPE) of 10 000 MWe. The 10 000 MWe for Duynefontein includes the existing Koeberg Nuclear Power Station plus various combinations of PBMR (Pebble Bed Modular Reactor) and conventional nuclear reactors (Nuclear-1 and expansions), as described in Eskom (2008a). Since the plume modelling results will also be used for the Nuclear-1 EIA, the plume due to Nuclear-1 (maximum output of 4000 MWe) has also been modelled. A PBMR with an output of 165 MWe is included. The following four reactor combinations have been tested in the thermal plume dispersion model.

**TABLE 9.1: REACTOR COMBINATIONS TESTED IN THERMAL PLUME MODEL**

Reactor type and power output	Total site output [MWe]	Comment
Koeberg (1800 MWe)	1 800	Existing baseline
Koeberg (1800 MWe) + PBMR (165 MWe)	1 965	PBMR added
Koeberg (1800 MWe) + PBMR (165 MWe) + Nuclear-1 (4000 MWe)	5 965	EIA Report
Koeberg (1800 MWe) + PBMR (165 MWe) + Nuclear-1 + Expansion (8250 MWe)	10 215	Site Safety Report

The cooling water requirements are characterised by the seawater flow rate and the temperature increase between the intake and the outfall ( $\Delta T$ ). The seawater cooling requirements for the various reactors and power outputs modelled in this study are tabulated below and discussed in more detail below the table.

**TABLE 9.2: SEAWATER COOLING REQUIREMENTS**

Reactor type	Power output [MWe]	Seawater flow rate [m <sup>3</sup> /s]	$\Delta T$ [°C]
Koeberg	1 800	86	10
PBMR	165	4	25
Koeberg + PBMR	1 965	90	10.67
Nuclear-1	4 000	184	12
Nuclear-1 + expansion	8 250	380	12

The cooling water requirements for the existing Koeberg Nuclear Power Station are obtained from PRDW (2005).

The cooling water requirements for the conventional nuclear reactors (Nuclear-1 and expansion) are based on data provided by Eskom (2008b), which indicates that a Pressurised Water Reactor (PWR) with a power of 1 650 MWe requires 76 m<sup>3</sup>/s of cooling water and increases the water temperature by 12°C. It is assumed that for other power outputs the flow rate can be scaled linearly in proportion to the power while the temperature increase remains constant.

The following cooling water requirements for the PBMR were extracted from the PBMR EIA report (Eskom, 2008d) and from information provided to PRDW during the PBMR EIA study (PBMR, 2007):

- Power: 400 MWt delivering 165 MWe PBMR
- Seawater flow rate: 4 000 kg/s = approximately 4 m<sup>3</sup>/s
- ΔT: 25°C.

The above values have been used in the thermal plume modelling described in this report. After completion of the thermal plume modelling the following revised cooling water requirements were received (PBMR, 2009):

- Power: 400 MWt delivering 160 MWe PBMR
- Seawater flow rate: 6 000 kg/s = approximately 6 m<sup>3</sup>/s
- ΔT: 12°C.

The most important parameter for the thermal plume dispersion modelling is the total heat flux = flow rate x ΔT. The original PBMR cooling water data as used in the thermal plume modelling has a heat flux that is 39% higher than the revised data, i.e. the model results will be conservative. Eskom have agreed that the thermal plume modelling should not be updated with the revised data until the PBMR design has been finalised (Eskom, 2009).

In addition to the increased temperature, the cooling water discharge may also contain co-discharges such as chlorine, nuclides, etc. Since these co-discharges have not yet been quantified, for this modelling study these are treated as conservative tracers, i.e. they undergo dilution by physical mixing only and any additional biochemical or physical processes are not modelled. The model results provide the achievable dilutions for any discharged constituent. Once the concentration of these constituents has been quantified, the potential impact of these constituents can be assessed by comparing the achievable dilutions from the model results to the dilution required to reduce the concentration at discharge to a level at which no impacts occur.

Reverse Osmosis desalination is being considered to provide fresh water during the earthworks, construction and operation stages of the power station (Eskom, 2008b). During operation of the power installation, the brine discharge from the desalination plant will be mixed with the once-through

cooling water discharge from the power station and discharged at the cooling water outfall. The operational stage desalination plant fresh water output is 4000 m<sup>3</sup>/day (Eskom, 2008b). The brine output flow associated with this is 6000 m<sup>3</sup>/day (or 0.069 m<sup>3</sup>/s), while the cooling water discharge rate for Nuclear-1 with an expected power output of 3300 MWe will be approximately 152 m<sup>3</sup>/s (Eskom 2008b). This means that the brine will be diluted 2 200 times in the pipe prior to discharge into the sea, making the brine effectively undetectable.

During the earthworks and construction stages, however, the cooling water outfall structure will not be completed and the brine will have to be discharged independently of the cooling water. The dilution of the construction stage brine has been modelled in PRDW (2008). Since the brine is not considered to be a site safety issue, it is not considered further in this report.

### **9.3 Intake and outfall layouts tested**

#### **9.3.1 Background**

Since no engineering feasibility studies on the intake and outfall structures have been completed, five conceptual layouts were developed which serve to illustrate the thermal plumes and recirculation that can be anticipated for typical combinations of intake and outfall types. General design considerations for the intake and outfall are discussed in PRDW (2009). The intakes considered are basins and offshore tunnels, while the outfalls considered are nearshore channels and offshore tunnels.

The layouts that were modelled are described below. Note that these conceptual layouts will need to be refined based on geotechnical and engineering considerations. All the new layouts include the existing Koeberg layout. Eskom have indicated that the existing Koeberg Power Station will continue operating during and after construction of the new power station and that this will preclude modifications/extensions to the existing basin structure, i.e. the new intake and outfall structures should be separate from the existing ones.

#### **9.3.2 Layout 0: Existing Koeberg Layout**

This comprises the existing Koeberg basin intake and a nearshore channel outfall. This layout is tested as a baseline case. The intakes openings are located between levels of -1.5 and -6.0 m MSL. The seawater cooling requirements are given in Table 9.2.

Since the PBMR is planned to share the existing Koeberg intake and outfall (Eskom, 2008d), this layout is also used for the “Koeberg + PBMR” combination. In this case the seawater cooling requirements are the sum of the individual Koeberg and PBMR requirements, as given in Table 9.2.

### 9.3.3 Layout 1: Offshore tunnel intake and offshore tunnel outfall

The intakes comprise submarine tunnels extending to a depth of approximately 20 m approximately 2.2 km offshore (see Figure 9.1). Intake structures will be positioned at the end of each intake tunnel with the intake openings positioned 3 to 5 m above the sea bed to prevent the drawing in of large quantities of sediment. To reduce fish entrainment the intake openings should be designed to draw in water horizontally with a velocity of less than 0.3 m/s.

For the purposes of these tests, it is assumed that the reactor units have a power output of 1 650 MWe and that there is one intake tunnel per reactor unit. This requires 5 tunnels for a power output of 8 250 MWe (refer to Table 9.2: “Nuclear-1 + expansion” combination as tested for the Site Safety Report). Each tunnel has a flow of 76 m<sup>3</sup>/s. The diameter of the tunnels is designed to avoid the risk of sediments settling in the tunnel (minimum velocity of 2.5 m/s). On the other hand, the velocity in the tunnels needs to be limited in order to reduce head losses in the tunnel. On this basis a tunnel diameter of 6.5 m is selected. Other configurations (reactor units with a different power outputs or a different number of tunnels) are possible, but the resulting thermal plumes are expected to be similar, provided the total power output remains at 8 250 MWe.

The outfalls comprise submarine tunnels extending to a depth of approximately 30 m approximately 3.5 km offshore. The length of the outfall was chosen to minimise recirculation back to the existing Koeberg intake. Following the same reasoning as the intake tunnels, there are 5 outfall tunnels each with a diameter of 6.5 m. Each outfall ends in a 200 m long diffuser with 5 ports at 50 m spacing. The ports have a diameter of 2 m and discharge vertically upwards from a height of 2 m above the seabed. The diffuser layout was selected to achieve an initial dilution of at least 10 and to ensure that the plume surfaces under all current and ambient stratification conditions. It is preferable that the plume is not trapped near the seabed as there is then an increased risk of ecological impacts at the seabed and also of recirculation back to the intakes, which in this case are located near the seabed in a depth of 20 m. Further details of the diffuser and the near-field modelling is provided in Section 9.5.1. The lengths of the outfall tunnels are staggered to reduce interaction between thermal plumes from adjacent tunnels (see Figure 9.1).

In addition to the 8 250 MWe power output (Nuclear-1 + expansion) tested for the Site Safety Report, this layout is also tested with a 4 000 MWe output (Nuclear-1) as required for the EIA Report (refer to Table 9.2 for the cooling water requirements). In this case only the 2 southerly intake tunnels and the 2 southerly outfall tunnels were installed instead of 5 intakes and 5 outfalls.

### 9.3.4 Layout 2: Basin intake and offshore tunnel outfall

The intake is a basin which is conceptually modelled as an upscaled version of the existing Koeberg basin and is located 2 km north of the existing basin (see Figure 9.2). The basin has the following dimensions (refer to PRDW (2009) for the design criteria used to derive these dimensions):

- Entrance width (measured to centre-line of breakwater): 145 m
- Entrance depth: -12 m CD
- Settling basin width: 530 m
- Settling basin length: 750 m
- Settling basin depth: -7.5 m
- Intake depth: -5 m CD.

The outfalls are the same as for Layout 1, i.e. 5 tunnels extending to a depth of approximately 30 m approximately 3.5 km offshore, with a 200 m long diffuser.

This layout is tested for the 8 250 MWe power output (Nuclear-1 + expansion) and the cooling water requirements are given in Table 9.2.

#### 9.3.5 Layout 3: Offshore tunnel intake and nearshore channel outfall 3 km north

The intakes are the same as Layout 1, i.e. 5 tunnels extending to a depth of approximately 20 m approximately 2.2 km offshore with intake openings positioned 3 to 5 m above the seabed (see Figure 9.3).

The outfall is a nearshore channel located 3 km north of the Koeberg basin which is conceptually modelled as an upscaled version of the existing Koeberg outfall channel. The channel is 100 m wide and is divided into 5 separate channels each 20 m wide (one per reactor unit). The offshore end of the channel is positioned at the 0 m CD beach contour (i.e. the extreme low water mark). The invert level at the offshore end of the channel is -1 m CD, i.e. 1 m below the original beach level.

This layout is tested for the 8 250 MWe power output (Nuclear-1 + expansion) and the cooling water requirements are given in Table 9.2.

#### 9.3.6 Layout 4: Offshore tunnel intake and nearshore channel outfall 4.5 km north

This is the same as Layout 3, except that the nearshore channel outfall has been moved 1.5 km northwards to increase the distance from the existing Koeberg basin to 4.5 km.

This layout is tested for the 8 250 MWe power output (Nuclear-1 + expansion) and the cooling water requirements are given in Table 9.2.

#### 9.3.7 Layout 5: Basin intake and nearshore channel outfall

The intake is a basin which is conceptually modelled as an upscaled and mirror-imaged version of the existing Koeberg basin and is located 2 km north of the existing basin (see Figure 9.5). The design considerations for this layout include:

- It is not possible to place the new outfall south of the new basin, as this will result in severe recirculation from the new outfall to the Koeberg intake.
- Thus the new outfall is north of the new basin and the basin is mirror-imaged so that the main breakwater reduces recirculation from the new outfall to the new intake.

The basin has the following dimensions (refer to PRDW (2009) for the design criteria used to derive these dimensions):

- Entrance width 145 m
- Entrance depth -12 m CD
- Settling basin width 530 m
- Settling basin length 750 m
- Settling basin depth -7.5 m
- Intake depth -4.5 m CD.

The outfall is a nearshore channel located 300 m north of the new basin which is conceptually modelled as an upscaled version of the existing Koeberg outfall channel. The channel is 100 m wide and is divided into 5 separate channels each 20 m wide (one per reactor unit). The offshore end of the channel is positioned at the 0 m CD beach contour (i.e. the extreme low water mark). The invert level at the offshore end of the channel is -1 m CD, i.e. 1 m below the original beach level.

This layout is tested for the 8 250 MWe power output (Nuclear-1 + expansion) and the cooling water requirements are given in Table 9.2.

#### 9.4 Model setup

The MIKE 3 Flow Flexible Mesh three-dimensional hydrodynamic model (as described in Section 2.5) has been set up to simulate the currents and the far-field dispersion of the thermal plume due to winds, waves, tides and buoyancy effects. The setup and calibration of the model is described in Sections 8.3.1 and 8.3.2, respectively. The selection of a 42 day simulation period comprising typical summer conditions, typical winter conditions and extreme calm conditions (low waves and wind) is described in Section 8.3.3.

As discussed in Section 8.3.1, the simulations have been performed using a constant background temperature of 14°C. At the intake point water is withdrawn from the model at the appropriate flow rate (refer to the cooling water requirements in Table 9.2) and then discharged at the outfall point at a temperature  $\Delta T$  higher than the intake temperature. This means that temperature build-up due to recirculation is simulated explicitly.

Layouts 1, 3 and 4 have the intake openings located at a depth of approximately 20 m. The available measurements (Section 7.1) indicate that the temperature at this depth is on average 1 to 2°C colder

than near the surface. This difference has not been included in the modelling which makes the model results conservative.

## 9.5 Results

### 9.5.1 Near-field dilution

Layouts 2 and 3 include an offshore tunnel outfall with a diffuser. In these cases the near-field dilutions (i.e. the dilution that occurs as the plume rises from the diffuser ports toward the water surface) and plume geometry has been modelled using the CORMIX model (see Section 2.9).

In this case it is preferable to design the diffuser to ensure that the plume rises to the surface instead of being trapped near the seabed, since there is then an increased risk of ecological impacts at the seabed and also since the tunnel intakes are located near the seabed and there would then be an increased risk of recirculation.

The CORMIX model inputs are the diffuser characteristics, the discharge characteristics and the ambient currents and stratification. The stratification cases modelled are a well-mixed winter case and strongly stratified summer case with a 6°C increase in temperature from bottom to surface (see Figure 7.2).

**TABLE 9.3: NEAR-FIELD DILUTION MODEL INPUTS**

Parameter	Value
Water depth	30 m
Diffuser length	200 m
Number of ports	5
Port height above seabed	2 m
Port diameter	2 m
Port orientation	Vertical
Discharge flow rate (total for all 5 ports)	76 m <sup>3</sup> /s
Salinity	35 psu
Discharge temperature (winter)	26°C
Discharge temperature (summer)	22°C
Ambient temperature surface (winter)	14°C
Ambient temperature bottom (winter)	14°C
Ambient temperature surface (summer)	16°C
Ambient temperature bottom (summer)	10°C
Ambient current speeds	0.05, 0.1, 0.2, 0.4, 0.8 m/s

The near-field model results include the initial dilutions, the horizontal plume width (reported here as the full width and not the half-width as given in the model output files), and the upper and lower plume boundary (measured upwards from the seabed). The results are extracted at the end of the near-field (i.e. once the vertical rise phase is complete) as well as at fixed distances of 500 m and 1000 m down current of the discharge point. These results are presented below and are plotted in Figure 9.6.

**TABLE 9.4: NEAR-FIELD DILUTION RESULTS FOR SUMMER**

Parameter	Current speed [m/s]				
	0.05	0.1	0.2	0.4	0.8
<b>End of near-field</b>					
Dilution [-]	15.6	14.0	18.2	32.5	63.6
Horizontal plume width [m]	4512	724	258	204	200
Upper plume boundary [m]	30.0	30.0	30.0	30.0	30.0
Lower plume boundary [m]	24.7	15.4	3.3	0.0	0.0
<b>After 500 m</b>					
Dilution [-]	10.0	15.0	21.5	37.5	70.4
Horizontal plume width [m]	4200	960	494	354	260
Upper plume boundary [m]	30.0	30.0	30.0	30.0	30.0
Lower plume boundary [m]	25.7	18.2	13.5	9.9	4.2
<b>After 1000 m</b>					
Dilution [-]	15.1	17.3	24.9	41.8	80.0
Horizontal plume width [m]	4444	1662	868	508	326
Upper plume boundary [m]	30.0	30.0	30.0	30.0	30.0
Lower plume boundary [m]	24.8	22.1	19.1	14.4	6.7

**TABLE 9.5: NEAR-FIELD DILUTION RESULTS FOR WINTER**

Parameter	Current speed [m/s]				
	0.05	0.1	0.2	0.4	0.8
<b>End of near-field</b>					
Dilution [-]	18.0	15.6	19.0	33.4	63.8
Horizontal plume width [m]	5676	932	280	224	202
Upper plume boundary [m]	30.0	30.0	30.0	30.0	30.0
Lower plume boundary [m]	25.2	17.2	4.3	1.7	0.0
<b>After 500 m</b>					
Dilution [-]	11.5	16.4	22.9	37.7	70.6
Horizontal plume width [m]	5284	1124	590	358	272
Upper plume boundary [m]	30.0	30.0	30.0	30.0	30.0
Lower plume boundary [m]	26.7	18.9	15.3	10.0	5.3
<b>After 1000 m</b>					
Dilution [-]	16.3	18.9	26.2	42.6	79.5
Horizontal plume width [m]	5492	1948	990	548	348
Upper plume boundary [m]	30.0	30.0	30.0	30.0	30.0
Lower plume boundary [m]	25.5	22.5	20.0	15.2	8.4

These results show that for all conditions tested the initial dilution exceeds 10 and the plume reaches the water surface. There is little difference between the summer and winter cases, which indicates that for this diffuser configuration the buoyancy and momentum fluxes of the discharge dominate the ambient stratification.

The results show that a realistic coupling between the near- and far-field models can be achieved if the discharge is released into the far-field model over a horizontal width of 400 m (directly above the 200 m long diffuser) and into the upper half of the water column (upper plume boundary 30 m and lower plume boundary 15 m). The resulting far-field approximation of the near-field dilution is shown in Figure 9.6.

### 9.5.2 Far-field temperature and dilution

The thermal plume from the outfall is advected and dispersed by the ambient currents. The currents are seen to be predominantly wave-driven in the surf-zone and wind- and tidally-driven beyond the surf-zone. Figure 9.7 illustrates an example of a wind-driven current generated by a south-easterly wind. Figure 9.8 shows an example of a current generated by obliquely-breaking westerly waves. Since these currents are continually changing as the wave, wind and tidal conditions change, the plume behaviour is dynamic, as illustrated in Figures 9.7 and 9.8 which show the thermal plume at two moments in time.

The model results for each layout have been post-processed to determine the maximum and mean (i.e. time-averaged) increase in temperature above background over the full 42 day simulation period. This has been done for both the surface and seabed layers of the model. The results are presented in Figures 9.9 to 9.24.

Since the background sea temperature varies on a seasonal, synoptic and diurnal time-scale (refer to Figures 7.2 and 7.3), the temperature increase due to the thermal plume will be superimposed on this background variability.

These results can also be interpreted as dilution factors for any co-discharges such as chlorine, nuclides, etc. as follows: divide 12 (the initial temperature increase) by the temperature increase shown in the plots, e.g. the 2°C contour in the plots represents a dilution factor of  $12/2 = 6$ . If the co-discharge is mixed with the cooling water prior to discharge into the sea, the co-discharge will undergo a pre-dilution in the pipe in addition to the subsequent dilution in the sea.

These results show that the maximum increase in temperature is significantly higher and more extensive than the mean increase in temperature. This is due to the dynamic plume behaviour which results in the plume remaining at one position for short periods of time only. The results also illustrate the effect of the buoyancy of the plume due to the increased temperature, which tends to keep the plume near the water surface rather than the seabed, particularly as the plume is advected into deeper water. In the shallow water (less than 5 m) the plume tends to be mixed throughout the water column.

These model results can be used to assess the potential ecological impacts due to the discharge of heated water and other co-discharges such as chlorine and nuclides.

### 9.5.3 Recirculation

The model results have been analysed to determine the recirculation of the thermal plume from the outfalls back to the intakes (both the new intake and the existing Koeberg intake). Note that the hydrodynamic model automatically accounts for recirculation by constantly adjusting the outfall

temperature to be 12°C above the intake temperature at each time-step. The results are plotted in Figure 9.25 and tabulated below.

**TABLE 9.6: THERMAL RECIRCULATION RESULTS**

Layout and reactors	Temperature increase at existing Koeberg intake		Temperature increase at new intake	
	Mean [°C]	Max [°C]	Mean [°C]	Max [°C]
Layout 0: Koeberg (1800 MWe)	0.7	2.8	-	-
Layout 0: Koeberg (1800 MWe) + PBMR (165 MWe)	0.7	3.0	-	-
Layout 1: Koeberg (1800 MWe) + PBMR (165 MWe) + Nuclear-1 (4000 MWe)	0.9	3.0	0.2	1.2
Layout 1: Koeberg (1800 MWe) + PBMR (165 MWe) + Nuclear-1 + expansion (8250 MWe)	1.1	3.2	0.3	1.2
Layout 2: Koeberg (1800 MWe) + PBMR (165 MWe) + Nuclear-1 + expansion (8250 MWe)	1.3	3.1	0.4	1.5
Layout 3: Koeberg (1800 MWe) + PBMR (165 MWe) + Nuclear-1 + expansion (8250 MWe)	3.1	7.9	0.2	1.5
Layout 4: Koeberg (1800 MWe) + PBMR (165 MWe) + Nuclear-1 + expansion (8250 MWe)	2.2	5.7	0.2	1.0
Layout 5: Koeberg (1800 MWe) + PBMR (165 MWe) + Nuclear-1 + expansion (8250 MWe)	2.1	5.8	0.9	3.2

Although recirculation is generally undesirable as it may decrease the efficiency of the cooling system, the allowable recirculation depends on the ambient temperatures (see Section 7.2) as well as the maximum allowable intake temperatures. For the existing Koeberg units, a shut-down of the reactor will be necessary if the intake temperature exceeds 23°C (Eskom, 2006), which is estimated to have a return period of approximately 30 years (see Section 7.2). Any increase in intake temperatures at Koeberg due to the new power station will reduce this return period. It is expected that the cooling water system for future nuclear installations at the site will be designed to allow higher intake temperatures, e.g. one type of Pressurised Water Reactor (PWR) allows a maximum cooling water temperature of 30°C, as well as an extreme temperature of 34.5°C for the safety assessment (Eskom, 2007).

The recirculation results show that the PBMR does not have a significant effect on the intake temperatures at Koeberg.

Layouts 1 to 4 result in acceptable recirculation (maximum increase < 1.5°C) at the new intake, while Layout 5 is marginal (maximum increase 3.2°C at the new intake). However, Layouts 3, 4 and 5 (which all have nearshore channel outfalls) all result in unacceptable increases at the existing Koeberg intake (maximum increase > 5.7°C). It is concluded that for a future power output of 8 250 MWe, only Layout 1 (offshore tunnel intake and offshore tunnel outfall) or Layout 2 (basin intake and offshore tunnel outfall) are feasible at this site due to the risk of recirculation back to the existing Koeberg intake.

## **10. SEDIMENT TRANSPORT**

### **10.1 Background**

The aim of this section is to estimate the net and gross sediment transport rates in the vicinity of the Duynefontein site. In addition, the concentration of suspended sediment in the water column is modelled for various intake depths and wave conditions.

Additional sediment related studies are described in the Coastal Engineering Report (PRDW, 2009). These include the analysis of historical beach plan shapes, beach erosion by storms, set-back due to sea level rise and sediment movement by tsunamis.

### **10.2 Sediment grain size**

Sediment samples were taken from the nearshore (using a Van Veen grab) and from the beach (near the high and low water marks) on 13 March 2008. The grain size analysis is given in Table 10.1 and the spatial variation of the  $D_{50}$  grain size is plotted in Figure 10.1.  $D_N$  is the diameter for which N% of the sediment, by weight, has a smaller diameter. The sediment grading is defined as  $(D_{84}/D_{16})^{0.5}$ . The sand on the beach south of Koeberg has a  $D_{50}$  of approximately 0.2 mm and a grading of approximately 1.2. The sand on the beach north of Koeberg has a  $D_{50}$  of approximately 0.4 mm and a grading of approximately 1.4, reflecting the steeper beach slope and larger waves north of Koeberg. The sand offshore has a  $D_{50}$  of approximately 0.15 mm and a grading of approximately 1.2, reflecting the deposition of finer sediments in deeper water.

**TABLE 10.1: SEDIMENT GRAIN SIZE ANALYSIS FOR DUYNEFONTEIN**

Longitude [deg]	Latitude [deg]	D <sub>95</sub> [mm]	D <sub>90</sub> [mm]	D <sub>84</sub> [mm]	D <sub>75</sub> [mm]	D <sub>50</sub> [mm]	D <sub>25</sub> [mm]	D <sub>16</sub> [mm]	D <sub>10</sub> [mm]	D <sub>5</sub> [mm]	Grading [-]
18.428217	-33.687317	0.24	0.20	0.19	0.17	0.15	0.14	0.13	0.13	0.12	1.2
18.423267	-33.688667	0.20	0.18	0.17	0.16	0.14	0.13	0.13	0.12	0.11	1.2
18.416417	-33.690617	0.24	0.20	0.18	0.17	0.15	0.13	0.13	0.12	0.11	1.2
18.423317	-33.679333	0.23	0.19	0.18	0.16	0.15	0.13	0.13	0.12	0.11	1.2
18.421283	-33.681350	0.20	0.18	0.17	0.16	0.14	0.13	0.13	0.12	0.11	1.2
18.413333	-33.683167	0.20	0.17	0.16	0.15	0.14	0.13	0.12	0.11	0.10	1.2
18.423383	-33.672667	0.91	0.66	0.47	0.33	0.22	0.17	0.16	0.15	0.14	1.7
18.416433	-33.674317	0.18	0.16	0.15	0.14	0.13	0.12	0.11	0.11	0.10	1.1
18.410133	-33.676700	0.21	0.17	0.16	0.15	0.13	0.12	0.11	0.11	0.10	1.2
18.421683	-33.668617	0.49	0.32	0.27	0.22	0.18	0.15	0.14	0.13	0.12	1.4
18.414933	-33.670433	0.20	0.17	0.15	0.15	0.13	0.12	0.11	0.11	0.10	1.2
18.407417	-33.672667	0.19	0.17	0.16	0.15	0.14	0.13	0.12	0.11	0.10	1.2
18.417617	-33.665183	0.25	0.21	0.19	0.18	0.16	0.14	0.13	0.12	0.11	1.2
18.413083	-33.667367	0.20	0.17	0.16	0.15	0.14	0.13	0.12	0.11	0.10	1.2
18.406067	-33.669617	0.20	0.17	0.16	0.15	0.14	0.12	0.12	0.11	0.10	1.2
18.416100	-33.663483	0.26	0.21	0.19	0.17	0.15	0.13	0.12	0.11	0.10	1.3
18.411233	-33.663917	0.24	0.20	0.18	0.16	0.14	0.12	0.12	0.11	0.10	1.2
18.404267	-33.666117	0.22	0.19	0.17	0.16	0.14	0.12	0.12	0.11	0.10	1.2
18.413483	-33.658100	0.31	0.26	0.23	0.20	0.17	0.15	0.14	0.13	0.12	1.3
18.408800	-33.658750	0.22	0.19	0.18	0.16	0.14	0.12	0.10	0.00	0.00	1.4
18.396417	-33.625083	0.96	0.87	0.79	0.72	0.57	0.45	0.41	0.37	0.33	1.4
18.400117	-33.630767	0.95	0.85	0.77	0.69	0.54	0.43	0.39	0.36	0.31	1.4
18.405417	-33.636917	0.88	0.77	0.69	0.61	0.48	0.38	0.34	0.31	0.28	1.4
18.408767	-33.643233	0.82	0.65	0.52	0.43	0.31	0.23	0.21	0.19	0.18	1.6
18.414033	-33.648783	0.78	0.63	0.53	0.45	0.33	0.25	0.22	0.20	0.18	1.5
18.418033	-33.654917	0.81	0.65	0.51	0.44	0.32	0.24	0.21	0.19	0.17	1.6
18.419967	-33.657917	0.77	0.50	0.40	0.34	0.26	0.21	0.19	0.18	0.16	1.4
18.421933	-33.661217	0.00	1.60	1.19	0.86	0.36	0.26	0.23	0.21	0.18	2.3
18.423367	-33.664467	1.37	1.19	1.06	0.93	0.71	0.51	0.43	0.37	0.31	1.6
18.424967	-33.667733	1.43	1.18	1.00	0.87	0.63	0.43	0.36	0.31	0.26	1.7
18.426517	-33.671033	0.69	0.55	0.47	0.40	0.29	0.22	0.19	0.18	0.16	1.5
18.427500	-33.674250	0.76	0.60	0.49	0.40	0.27	0.20	0.18	0.17	0.16	1.6
18.431817	-33.681033	0.60	0.52	0.43	0.34	0.24	0.19	0.18	0.16	0.15	1.6
18.432333	-33.682183	0.41	0.35	0.31	0.27	0.21	0.18	0.16	0.15	0.14	1.4
18.433867	-33.685633	0.26	0.24	0.22	0.20	0.18	0.16	0.15	0.14	0.13	1.2
18.435217	-33.688933	0.26	0.24	0.22	0.20	0.18	0.16	0.15	0.14	0.13	1.2
18.438567	-33.696000	0.24	0.22	0.21	0.19	0.17	0.16	0.15	0.14	0.13	1.2
18.441083	-33.702967	0.23	0.21	0.19	0.18	0.16	0.15	0.14	0.13	0.13	1.2
18.442967	-33.710317	0.21	0.19	0.19	0.18	0.16	0.15	0.14	0.14	0.13	1.1
18.443667	-33.717317	0.23	0.21	0.20	0.19	0.17	0.15	0.15	0.14	0.13	1.2
18.396133	-33.625267	0.10	0.87	0.77	0.68	0.51	0.42	0.38	0.35	0.31	1.4
18.400100	-33.630900	0.97	0.86	0.77	0.68	0.54	0.43	0.39	0.36	0.31	1.4
18.405417	-33.636983	0.66	0.58	0.52	0.47	0.39	0.31	0.28	0.26	0.22	1.4
18.408633	-33.643350	0.55	0.48	0.44	0.39	0.32	0.27	0.24	0.22	0.20	1.3
18.413750	-33.648933	0.56	0.49	0.45	0.40	0.32	0.26	0.24	0.22	0.19	1.4
18.417833	-33.655067	1.04	0.88	0.78	0.66	0.45	0.32	0.29	0.26	0.23	1.6
18.419717	-33.658050	1.01	0.88	0.80	0.70	0.48	0.34	0.30	0.26	0.23	1.6
18.421717	-33.661317	1.32	1.16	1.04	0.92	0.71	0.47	0.40	0.34	0.29	1.6
18.423067	-33.664483	1.05	0.94	0.87	0.79	0.61	0.44	0.38	0.33	0.28	1.5
18.424667	-33.667833	1.27	1.03	0.90	0.77	0.49	0.33	0.29	0.26	0.22	1.8
18.424667	-33.667833	0.96	0.82	0.72	0.61	0.43	0.32	0.29	0.26	0.22	1.6
18.426233	-33.671117	0.55	0.48	0.44	0.40	0.33	0.27	0.25	0.23	0.21	1.3
18.426967	-33.674167	0.62	0.50	0.44	0.38	0.28	0.21	0.19	0.18	0.16	1.5
18.431617	-33.681117	0.50	0.38	0.32	0.27	0.20	0.17	0.16	0.15	0.14	1.4
18.431883	-33.682283	0.34	0.29	0.25	0.23	0.19	0.17	0.16	0.15	0.14	1.3
18.433317	-33.685867	0.33	0.30	0.27	0.24	0.20	0.17	0.16	0.15	0.14	1.3
18.434783	-33.689367	0.28	0.24	0.22	0.20	0.18	0.16	0.16	0.15	0.14	1.2
18.437867	-33.696250	0.33	0.29	0.26	0.24	0.20	0.17	0.16	0.15	0.14	1.3
18.440067	-33.703183	0.31	0.26	0.24	0.22	0.19	0.17	0.16	0.15	0.14	1.2
18.441833	-33.710633	0.32	0.25	0.23	0.21	0.18	0.16	0.15	0.15	0.14	1.2
18.443083	-33.717567	0.26	0.23	0.21	0.20	0.18	0.16	0.15	0.15	0.14	1.2

### 10.3 Sediment transport rates

#### 10.3.1 Model setup

The MIKE 21 Coupled Flexible Mesh model (as described in Section 2.6) is used. The model simulates wave refraction, wave-driven currents, wind-driven currents and non-cohesive sediment transport over a two-dimensional domain. A simpler approach would be to use a one-dimensional model such as LITPACK (DHI, 2008b) to estimate the sediment transport at specific profile positions. However, the complex transport fields around the basin structures and the headlands at Melkbos and Bokpunt dictates a two-dimensional modelling approach.

The model grid and bathymetry are similar to that used in the wave modelling (Figure 6.6) and the plume dispersion modelling (Figure 8.4). The grid is refined to less than 50 m in the nearshore areas.

#### 10.3.2 Schematisation of wave and wind climate

The deepwater wave and wind hindcast data described in Section 6.2 is used to drive the model. The dataset used is the 10 year period from 1997 to 2006 at 6 hourly intervals. These data are binned into 131 conditions which are then simulated in the model.

The bin sizes used for the deepwater wave conditions are as follows: 2 m bins for  $H_{m0}$ , 20° bins for wave direction and 4 s bins for  $T_p$ . Only the longshore component of the wind is considered, since this component drives the longshore currents. The bin size for the longshore wind speed is 10 m/s.

To obtain one representative condition to model from all the conditions falling into one particular bin,  $H_{m0}$  and the wave direction are weighted by the wave energy flux  $H_{m0}^2 T_p$  and the wind speed is weighted by the wind speed squared.

Each of the 131 conditions is modelled for 12 hours to achieve steady state current speeds under the imposed wave and wind forcing. The sediment transport rate and the rate of bed level change at the end of each 12 hour simulation are saved. The sediment transport rates are then weighted by the occurrence of each condition to obtain the annual sediment transport rates. Note that a fixed bed level is applied, i.e. no morphodynamic updating.

#### 10.3.3 Model calibration

The model parameters used in the wave refraction model follow from the model calibration described in Section 6.4. The model parameters used in the hydrodynamic model follow from the model calibration described in Section 8.3.2.

The inputs to the sediment transport model include the grain size. Since this varies over the domain (Figure 10.1), separate simulations are performed using  $D_{50}$  grain sizes of 0.15, 0.2 and 0.3 mm. Based

on a number of preliminary tests the additional parameter settings for the sediment transport model are selected as follows: critical Shields parameter = 0.05, ripples are included, bed slope effects are excluded, the deterministic formulation is used for the bed concentration, streaming is excluded, density currents are excluded, helical flow is excluded, undertow is excluded, the wave theory is Stokes 1<sup>st</sup> order and the wave breaker index = 0.8.

The coupled wave, current and sediment transport model was first tested for a simplified case with a uniform 1:67 beach slope and a wave approaching 30° from normal. The results are seen to be qualitatively correct (Figures 10.2 and 10.3).

The model calibration was to set up the model for the existing Koeberg layout and to compare the modelled net sediment transport entering the intake basin to the measured maintenance dredging volumes. The model includes the Koeberg cooling water intake pumps with an average flow rate of 86 m<sup>3</sup>/s. The grain size is set to  $D_{50} = 0.2$  mm, which is the typical grain size measured inside the basin (PRDW, 2002). The model gives a net sediment transport into the basin of 146 000 m<sup>3</sup>/year (see Figure 10.5, Profile 24), which compares well to the average maintenance dredging volume of approximately 132 000 m<sup>3</sup>/year (PRDW, 2002).

#### 10.3.4 Results

The following layouts have been modelled (refer to Sections 9.2 and 9.3 for details of the layouts and the associated cooling water intake and outfall flow rates):

- Layout 0: Existing Koeberg
- Layout 2: Basin intake and offshore tunnel outfall
- Layout 3: Offshore tunnel intake and nearshore channel outfall
- Layout 5: Basin intake and nearshore channel outfall

The modelled net sediment transports for these layouts are shown in Figures 10.4 to 10.11. It is important to note that these are the potential sediment transport rates, assuming that the seabed is covered with sand. In rocky areas such as Melkbospunt and Bokpunt (see Figure 1.1) the actual sediment transport rates will be lower and will be limited by sediment availability.

The sediment transports have been integrated across the 23 beach profiles indicated in Figures 10.4 to 10.11. For each profile, the accumulated northward transport, the accumulated southward transport, the net transport and the gross transport have been calculated and are presented in Figure 10.12.

These model results show the following:

- Although the sediment transport varies along the beach due to the presence of rip cells, the net transport along the beach is low, i.e. taking the average of the net transport for Sections 4 to 19 gives less than 10 000 m<sup>3</sup>/year, which is within the model accuracy (see Figure 10.12).
- There is little transport out of the cell, i.e. the southward transport at the southern headland (Profile 3) is close to zero, and likewise the northward transport at the northern headland (Profile 21) – see Figures 10.4 and 10.12.
- There is a clear seasonal trend mainly due to changes in wave direction, with a net northward transport in summer which is balanced by a net southward transport in winter (see Figure 10.13).
- The model results indicate that a grain size of  $D_{50} = 0.15$  mm is unstable on the beach as it results in extremely large transport rates (see Figure 10.14).
- Layout 2 changes the transport only locally around the basin (see Figures 10.7 and 10.15).
- Layout 3 has only very localised effects directly in front of the channel outfall (see Figures 10.9 and 10.15).
- Layout 5 has some localised effects around the basin (see Figures 10.11 and 10.15).
- The new layouts do not change the volume of sand drawn into the existing Koeberg basin, predicted to be 146 000 m<sup>3</sup>/year (see Profile 24 in Figures 10.7, 10.9 and 10.11).
- Due to the new basins having entrances in deeper water (12 m) compared to the existing Koeberg basin (5 m) the predicted volume of sand drawn into the basins are only 22 000 m<sup>3</sup>/year for Layout 2 (see Profile 25 in Figure 10.7) and 11 000 m<sup>3</sup>/year for Layout 5 (see Profile 26 in Figure 10.11). These results assume that the entrance depth is maintained at 12 m.

These model results suggest that wave-driven sediment transport will not create significant safety-related problems for the proposed new layouts. Further more detailed morphodynamic modelling will however need to be undertaken as part of the detailed design phase. An assessment of the coastline stability based on aerial photographs, beach profile measurements and cross-shore sediment transport modelling is presented in PRDW (2009).

## 10.4 Suspended sediment concentrations

### 10.4.1 Background

For Layouts 1, 3 and 4 the proposed seawater intake is a tunnel extending to approximately 20 m water depth with the intake opening positioned 3 to 5 m above the seabed. One of the design parameters will be the volume of sand drawn into the intake which will have to be removed from the proposed settling basin located on land in front of the cooling water pump house (Eskom, 2008c). Preliminary modelling is performed to estimate the volume of sand drawn into the intakes.

## 10.4.2 Measured suspended sediment concentrations

To date 44 water samples have been collected and analysed for Total Suspended Solids (TSS), which comprise both organic (e.g. algae) and inorganic (e.g. silt) particles suspended in the water column. The results are tabulated below and plotted in Figure 10.16.

**TABLE 10.2: MEASURED TOTAL SUSPENDED SOLIDS (TSS) AT DUYNEFONTEIN SITE**

Date	Longitude [deg]	Latitude [deg]	Total water depth [m CD]	Measurement depth above seabed [m]	TSS [mg/L]
2008-06-29	18.4150	-33.6701	10	8	<5
	18.4150	-33.6701	10	6	<5
	18.4150	-33.6701	10	4	<5
	18.4150	-33.6701	10	2	<5
	18.4242	-33.6751	3	1	7
	18.4228	-33.6722	4	0	6
	18.4208	-33.6704	5	1	<5
	18.4193	-33.6679	5	1	<5
	18.4173	-33.6651	7	3	<5
	18.4141	-33.6608	7	3	6
2008-07-11	18.4119	-33.6563	6	2	<5
	18.3898	-33.6757	29	25	2
	18.3898	-33.6757	29	17	3
	18.3898	-33.6757	29	9	2
	18.3898	-33.6757	29	1	3
	18.4150	-33.6701	10	6	<2
	18.4150	-33.6701	10	2	<2
	18.4242	-33.6751	3	1	4
	18.4228	-33.6722	4	0	<2
	18.4208	-33.6704	5	1	2
2008-10-18	18.4193	-33.6679	5	1	2
	18.4173	-33.6651	7	3	16
	18.3890	-33.6757	29	25	5
	18.3890	-33.6757	29	17	6
	18.3890	-33.6757	29	9	10
	18.3890	-33.6757	29	1	10
	18.4150	-33.6701	10	6	2
	18.4150	-33.6701	10	2	3
	18.4153	-33.6688	9	5	3
	18.4159	-33.6691	9	5	3
2008-12-06	18.4161	-33.6693	9	5	4
	18.4164	-33.6695	9	5	9
	18.4167	-33.6697	9	5	10
	18.3898	-33.6757	29	25	4
	18.3898	-33.6757	29	17	<2
	18.3898	-33.6757	29	9	4
	18.3898	-33.6757	29	1	5
	18.4150	-33.6701	10	6	7
	18.4150	-33.6701	10	2	4
	18.4150	-33.6688	10	6	4
	18.4152	-33.6685	9	5	5
	18.4152	-33.6683	9	5	4
	18.4152	-33.6681	9	5	10
	18.4153	-33.6678	9	5	14

The average TSS measured is 4 mg/L and the maximum 16 mg/L. There is a trend for the TSS concentration to decrease as the water depth increases (see Figure 10.16). The TSS concentration is

relatively uniform over the water column, implying that these are smaller cohesive sediment particles ( $D_{50} < 0.063$  mm) rather than larger sand particles (which would show a significantly higher concentration near the seabed, see Figure 10.17).

#### 10.4.3 Model setup

The modelling is performed using the LITPACK model, as described in Section 2.7. The model inputs are the water depth,  $D_{50}$  grain size, the sediment grading defined by  $(D_{84}/D_{16})^{0.5}$ , the root-mean-square wave height  $H_{rms} \approx H_{m0}/1.41$ , the zero-crossing wave period  $T_z \approx T_p/1.3$ , wave direction, current speed, current direction and water temperature. The model output is the vertical profile of suspended sand concentration. The model only simulates non-cohesive sediments with grain sizes greater than 0.063 mm, i.e. sand particles.

Based on the settings established in the two-dimensional sediment transport modelling (Section 10.3.3) the parameter settings for the model are selected as follows: critical Shields parameter = 0.05, wave breaking dissipation factor beta = 0.15, ripples are included, bed slope effects are excluded, the deterministic formulation is used for the bed concentration, convective terms are included, density currents are excluded, the wave theory is Stokes 5<sup>th</sup> order and the wave breaker index = 0.8. A graded sand with 30 size fractions is modelled.

#### 10.4.4 Conditions modelled

The conditions modelled are the same 131 binned wave/wind conditions used for the two-dimensional sediment transport simulations (Section 10.3.2). For each condition the two-dimensional model provides the waves and currents throughout the model domain. The wave and current parameters for each condition are extracted at the proposed intake position in 20 m water depth (as shown in Figures 9.1, 9.3 and 9.4) for use in the suspended sediment model. The water temperature (which influences the particle settling velocity) is set to a conservatively high value of 16°C (see Figure 7.2).

The measured sediment grain sizes are presented in Table 10.1 and Figure 10.1. The three sampling positions closest to the proposed intake have a  $D_{50}$  of 0.14 mm. A more conservative  $D_{50}$  of 0.12 mm was also modelled. A conservatively high sediment grading of 1.5 was assumed.

#### 10.4.5 Results

An example of the vertical profile of suspended sand concentration modelled for one input wave/current condition is shown in Figure 10.17. It is seen that the sand concentration decreases logarithmically with increasing distance from the seabed.

The proposed intake opening is positioned 3 to 5 m above the seabed (Eskom, 2008c), while the intake flow rate for a power output of 8 250 MWe is 380 m<sup>3</sup>/s (see Table 9.2). For a particular wave/current condition, a preliminary estimate of the volume of sand drawn into the intake can be calculated as the

suspended sand concentration at the vertical position of the intake opening multiplied by the intake flow rate. It is assumed that the intake structure itself does not influence the suspended sand profile and that the seabed is covered in sand, i.e. no rocks. The extent to which this assumption is true will depend on the detailed design of the intake structure: the intake geometry, the number of intake openings, the intake velocities, the extent of scour protection around the structure, etc. Since these details are not yet available, the results below should be viewed as preliminary.

The sand volume drawn into the intake is calculated for each of the 131 wave/current conditions. The annual sand volume is then calculated by adding the volumes for each condition, taking into account the percentage occurrence of each condition. The final volume is then adjusted from solid volume to bulk volume assuming a sediment porosity of 0.4. In addition to the annual average sand volume, the maximum sand concentration and the maximum short-term sand volume are obtained from the 131 conditions. Results are presented for the proposed intake levels of 3 and 5 m above the seabed, as well as 1 m above seabed to account for the drawing in of sand from below the level of the intake, or for sand build-up around the intake.

**TABLE 10.3: PRELIMINARY ESTIMATE OF SAND VOLUME DRAWN INTO COOLING WATER INTAKE IN 20 M DEPTH**

	Annual sand volume [m <sup>3</sup> /year]	Short-term maximum sand volume [m <sup>3</sup> /day]	Maximum sand concentration [mg/L = ppm by mass]
$D_{50} = 0.14$ mm			
Intake 1 m above seabed	11 000	900	45
Intake 3 m above seabed	5 000	400	20
Intake 5 m above seabed	3 000	300	15
$D_{50} = 0.12$ mm			
Intake 1 m above seabed	20 000	1 800	90
Intake 3 m above seabed	11 000	900	50
Intake 5 m above seabed	7 000	600	30

Note that the model only simulates non-cohesive sediments with grain sizes greater than 0.063 mm, i.e. sand particles. Finer mud and clay particles that may be present in the water column as a background concentration are not modelled. Assuming an average background concentration of 4 mg/L (Section 10.4.2) and a porosity of 0.4, the annual cohesive sediment volume drawn into the cooling water intake would be 30 000 m<sup>3</sup>/year, which is higher than the sand volumes given in Table 10.3. Whether these cohesive particles will have time to settle in the settling basin, or pass through the heat exchangers and be discharged back to sea, will depend on the design and geometry of the settling basin.

The volumes predicted above are significantly lower than the average maintenance dredging at the present Koeberg intake basin of approximately 132 000 m<sup>3</sup>/year (PRDW, 2002).

## 11. CONCLUSIONS AND RECOMMENDATIONS

Numerical models and data analysis frameworks have been set up to characterise the following parameters at the Duynefontein site:

- Water levels
- Tsunami flooding
- Wave height, period and direction
- Seawater temperatures
- Currents
- Thermal plume dispersion and recirculation for typical intake and outfall configurations
- Sediment transport
- Suspended sediment concentrations.

The numerical models have been calibrated using measurements undertaken at the site as part of the ongoing measurement programme.

The results will be used in the Coastal Engineering Investigations Report (PRDW, 2009), the SSR Chapter on Oceanography and Coastal Engineering, as well as other chapters in the SSR dealing with marine ecology and risk assessment. The results will also be used for the EIA study being conducted for Nuclear-1.

The oceanographic measurement programme is scheduled to run until August 2010 and it is strongly recommended that the programme continue as scheduled.

The thermal plume modelling indicates that nearshore channel outfalls will result in unacceptable temperature increases at the existing Koeberg intake and that an offshore tunnel outfall will thus be required. It is recommended that engineering feasibility studies be undertaken to identify the optimum intake and outfall structures.

Additional research is required to better define the risk from local tsunamigenic sources. The Council for Geoscience report (CGS, 2008b) recommends the following approach:

- Further research including all available stratigraphic/sedimentological/geomorphological data should be undertaken to better define the risk from offshore slump generated tsunami.
- In depth research into the global frequency, locality and magnitude of meteotsunami should be undertaken to further quantify the risk. In particular, the atmospheric conditions along the west coast prior to the 1969 event should be compared with those of its 2008 counterpart
- Because of the relatively short history of tsunami records along the South African coast, the database should be extended by conducting an investigation of palaeotsunami in the stratigraphic

record. No systematic work has yet been conducted along this coast. Areas of focus should be in the vicinity of planned nuclear facilities.

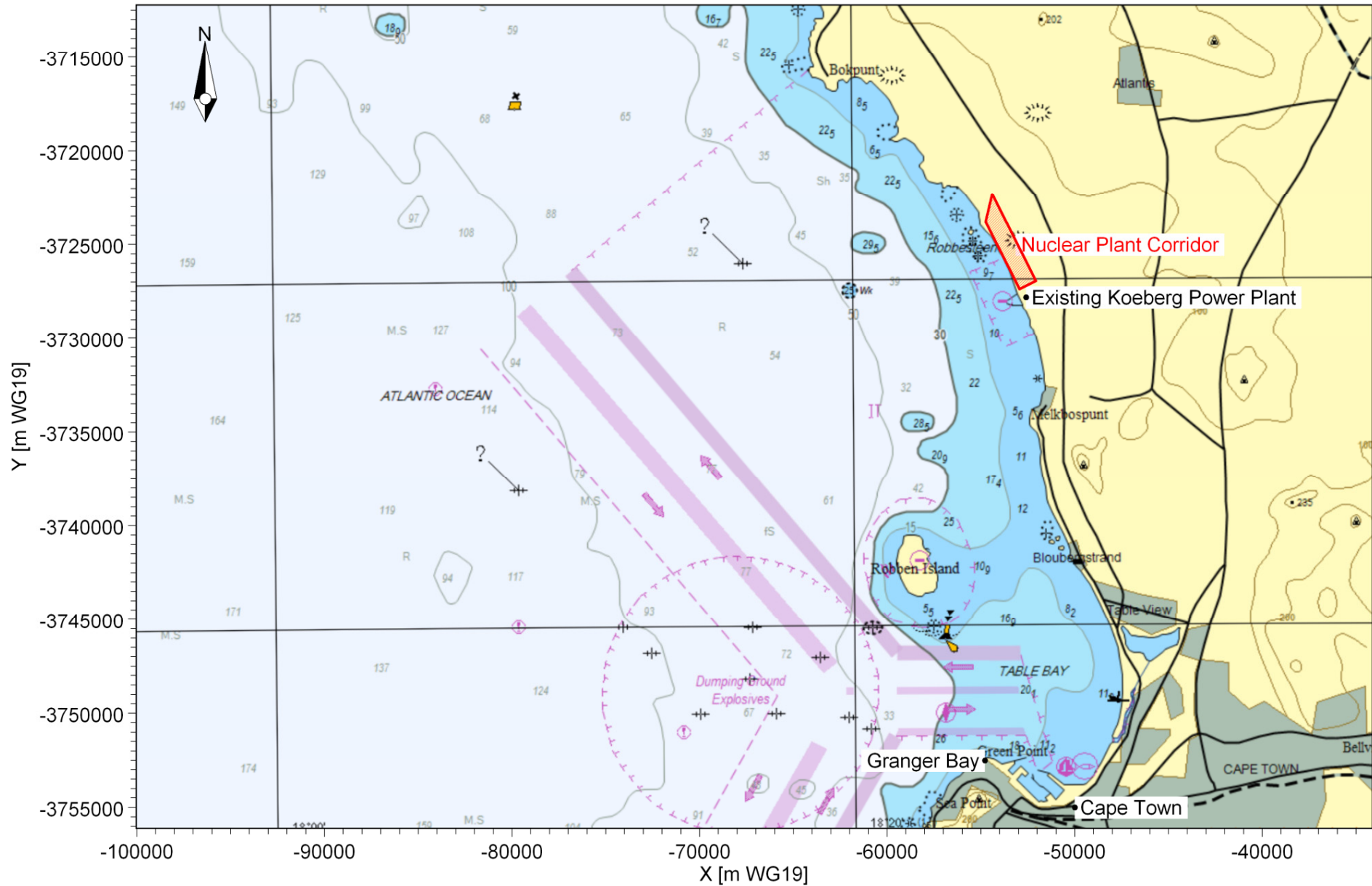
**REFERENCES**

1. Bayworld (2008) Bottom Temperature Studies along the South African Coast. A Bottom Temperature Project to Determine Temperature Ranges Needed for Nuclear Power Station Cooling Systems for ESKOM. Bayworld Centre for Research and Education, Progress Report #1, August 2008.
2. Bayworld (2009) Bottom Temperature Studies along the South African Coast. A Bottom Temperature Project to Determine Temperature Ranges Needed for Nuclear Power Station Cooling Systems for ESKOM. Bayworld Centre for Research and Education, Progress Report #2, February 2009.
3. Borrero J, Sieh K, Chlieh M and Synolakis C (2006). Tsunami Inundation Modeling for Western Sumatra. PNAS, 26 December 2006, vol. 103, no. 52.
4. CGS (2008a) A Probabilistic Tsunami Hazard Assessment for Coastal South Africa from Distant Tsunamogenic areas. By A. Kijko, V. Midzi, J. Ramperthap and M. Singh. Council for Geoscience Report No. 2008 - 0156, Revision 2.
5. CGS (2008b) Potential Sources of Tsunami Along the South African Coast. By D.L. Roberts. Council for Geoscience Report Number: 2008 - 0220
6. DHI (2008a) MIKE 21 SW, Spectral Waves FM Module, User Guide. Danish Hydraulics Software.
7. DHI (2008b) LITPACK, An Integrated Modelling System for Littoral Processes and Coastline Kinetics. User Guide, Danish Hydraulics Software.
8. DHI (2008c) MIKE 21 Flow Model, User Guide. Danish Hydraulics Software
9. DHI (2008d) MIKE 21/3 Coupled Model FM, User Guide. Danish Hydraulics Software.
10. DHI (2008e) MIKE 21 Flow Model FM, Sand Transport Model, User Guide. Danish Hydraulics Software.
11. DHI (2008f) EVA, Extreme Value Analysis, User Guide. Danish Hydraulics Software.
12. DHI (2008g) MIKE 21 Tidal Analysis and Prediction Module, Scientific Documentation. Danish Hydraulics Software.
13. DHI (2008h) MIKE C-MAP, Extraction of World Wide Bathymetry Data and Tidal Information, User Guide. Danish Hydraulics Software.
14. Dingle R (1977) The anatomy of a large submarine slump on a sheared continental margin (SE Africa). Journal of the Geological Society of London 134; 293-310.
15. Dingle R, Birch G, Bremner J, de Decker R, du Plessis A, Engelbrecht J, Fincham M, Fitton T, Flemming B, Gentle R, Goodlad S, Martin A, Mills E, Moir G, Parker R, Robson S, Rogers J, Salmon D, Siesser W, Simpson E, Summerhayes C, Westall C and Winter A (1987). Deep-sea sedimentary environments around southern Africa, South-East Atlantic and South-West Indian Oceans. Annals of the South African Museum 98, 1–27.
16. Doneker, RL, Jirka, GH and Hinton, SW (2007). CORMIX User Manual: A Hydrodynamic Mixing Zone Model and Decision Support System for Pollutant Discharges into Surface

- Waters. Office of Science and Technology, U.S. Environmental Protection Agency, Washington, DC.
17. Eskom (1985) Koeberg meteorological data report, Spring 1985, Koeberg Weather Station.
  18. Eskom (2006) Koeberg Site Safety Report, Chapter 8, Oceanography and Cooling Supply, Rev 3.
  19. Eskom (2007) Areva, EPR Technical Description, Rev A. Received from Eskom, August 2007.
  20. Eskom (2008a) Plant Parameter Envelope for 10 000 MWe for NSIP Site Safety Reports, Document provided by Israel Sekoko, Eskom, on 1 September 2008.
  21. Eskom (2008b) Nuclear-1 consistent EIA data set (Rev. 2). Document (Excel spreadsheet) provided by Andre Nel, Eskom, on 2 October 2008.
  22. Eskom (2008c) Cooling Water Intake and Outfall Works for the Eskom Nuclear-1 Sites, Conceptual Arrangements. Nuclear Programmes Department Nuclear-1, Document No. 300-9, September 2008.
  23. Eskom (2008d) Draft Environmental Impact Assessment Report, Environmental Impact Assessment for a 400 MW(t) Pebble Bed Modular Reactor Demonstration Power Plant. DEAT Reference No: 12/12/20/745, Arcus Gibb, September 2008.
  24. Eskom (2009) 1010 Nuclear Sites - Re: Draft\_P-3257-P.pdf, Email from I Saayman, Eskom, dated 13 August 2009.
  25. Grilli S and Watts P (2005) Tsunami Generation by Submarine Mass Failure, 1: Modelling, Experimental Validation and Sensitivity Analysis. *Journal of Waterway, Port, Coastal and Ocean Engineering*, November/December 2005.
  26. Grilli S, Ioualalen M, Asavanant J, Shi F, Kirby J and Watts P (2007). Source Constraints and Model Simulation of the December 26, 2005, Indian Ocean Tsunami. *Journal of Waterway, Port, Coastal, and Ocean Engineering*, Vol. 133, No. 6, November, 2007.
  27. Hartnady C and Okal E (2007). Mentawai tsunami effect at Port Elizabeth, South Africa on 12-14 September 2007, *South Afr. J. Sci.*, submitted, 2007.
  28. IAEA (2003) Flood Hazard for Nuclear Power Plants on Coastal and River Sites, Safety Guide No. NS-G-3.5. International Atomic Energy Agency.
  29. Okada Y (1985) Surface Deformation to Shear and Tensile Faults in a Half-Space. *Bull. Seism. Soc. Am.*, 75, [4], 1135-1154.
  30. PBMR (2007) Document "Oceanography Info Request 12.11.2007.doc" compiled by PBMR and emailed to PRDW by Paul Furniss, Arcus Gibb, on 26 November 2007.
  31. PBMR (2009) Transmittal of PBMR Information on Thermal Output and Cooling Water Requirements, Letter from PBMR Client Office dated 2009-07-31 with reference P-3257-P (NRR).

32. PRDW (2002) Eskom, Koeberg Nuclear Power Station, Cooling Water Intake Basin, Dredging Strategy, Updated Strategy – May 2002. PRDW Report 201/2/01, May 2002.
33. PRDW (2005) Eskom, Koeberg Nuclear Power Station, Cooling Water Intake Basin and Outfall Structure, Design Base Document. PRDW Report 201/96/7 Rev 02, November 2005.
34. PRDW (2008) Eskom, Nuclear1 EIA: Modelling of Construction Stage Brine Discharge. Report No. 1010/5/001, October 2008.
35. PRDW (2009) Eskom Site Safety Reports, Coastal Engineering Investigations Report, Duynefontein. Prestedge Retief Dresner Wijnberg (Pty) Ltd, Report 1010/2/102 Rev 03, September 2009.
36. Rabinovich A and Thomson R (2007). The 26 December 2004 Sumatra Tsunami: Analysis of Tide Gauge Data from the World Ocean Part 1. Indian Ocean and South Africa. *Pure and Applied Geophysics*, 164 (2007), 261–308.
37. Rattey, D and Potgieter J (1987). Koeberg Nuclear Power Station, Warm Water Plume Report, August 1987.
38. South African Tide Tables (2008) SAN HO-2. Published by the Hydrographer, South African Navy, ISBN 0-9584817-3-3.
39. Watts P, Grilli S, Kirby J, Fryer G and Tappin D (2003). Landslide Tsunami Case Studies Using a Boussinesq Model and a Fully Nonlinear Tsunami Generation Model. *Natural Hazards and Earth System Sciences*, Vol. 3, 2003, pp. 391-402.

## **FIGURES**

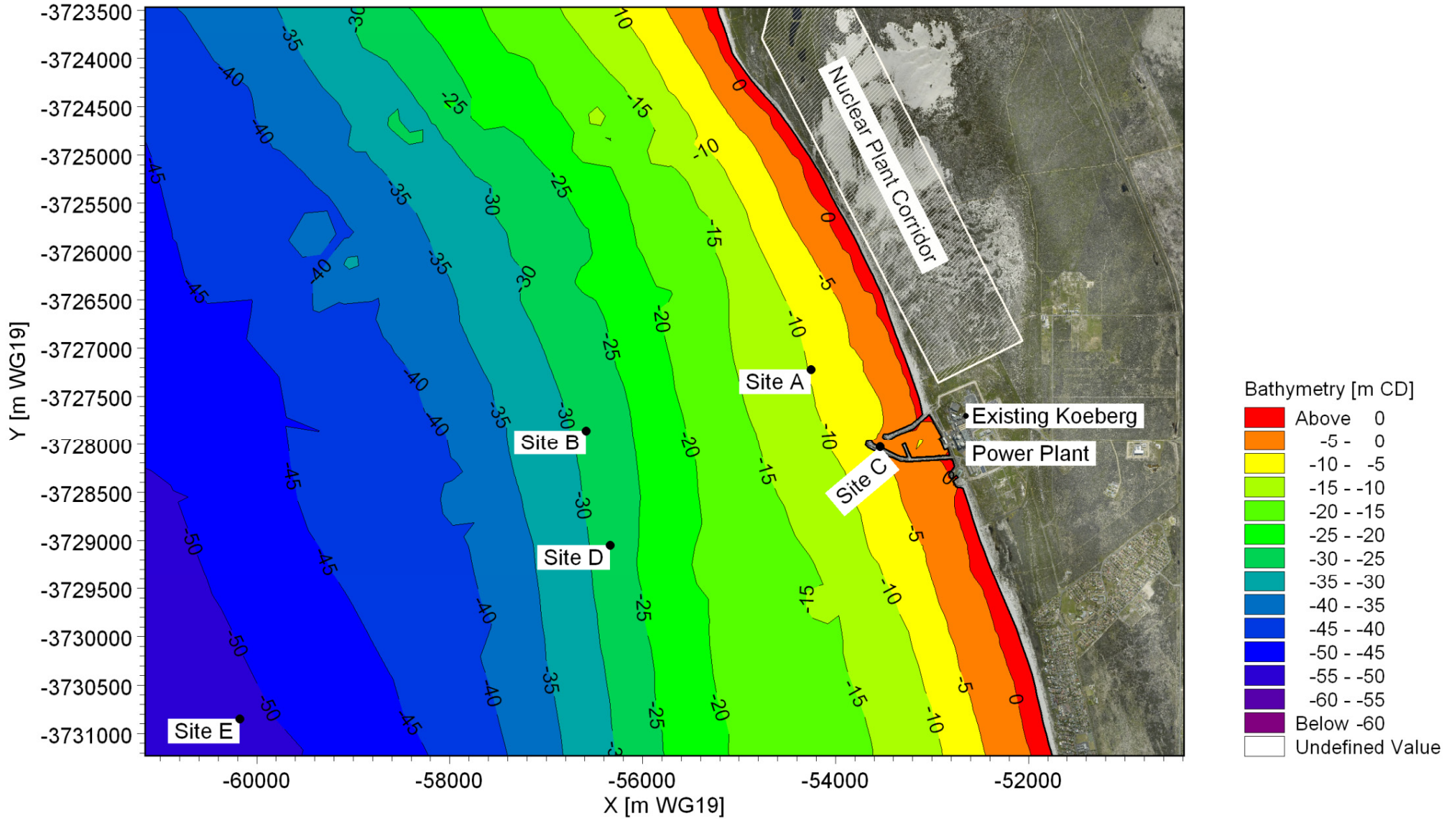


Title:

Locality map for Duynefontein site.

Figure No.

1.1

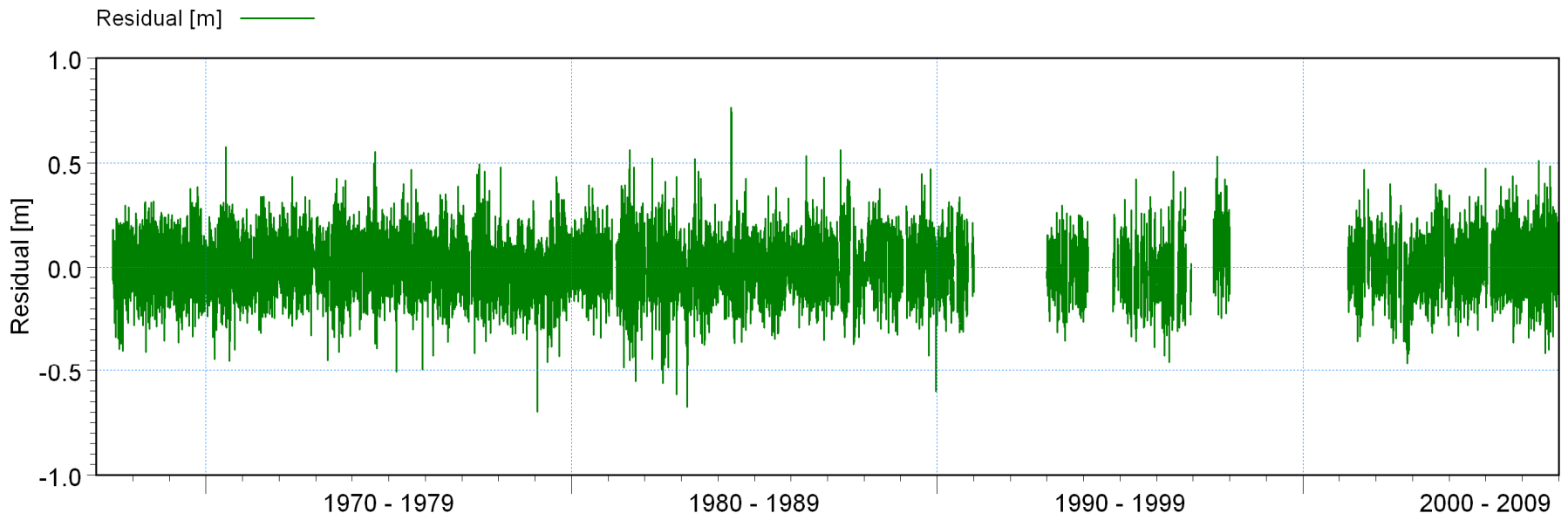
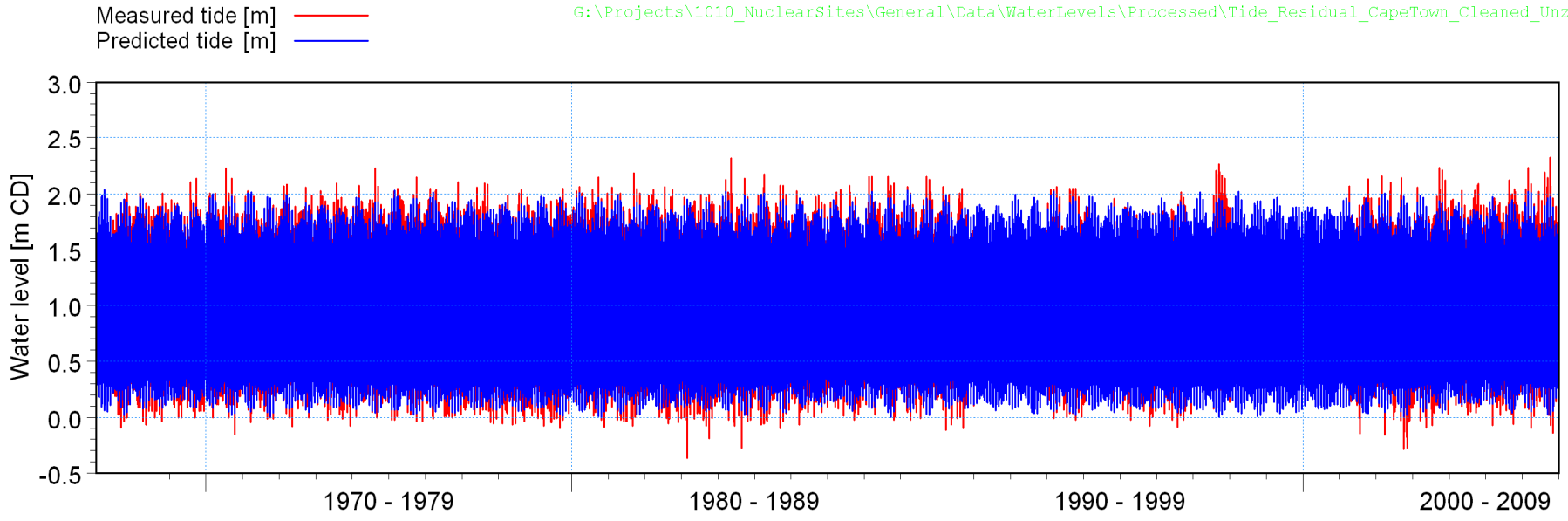


Title:

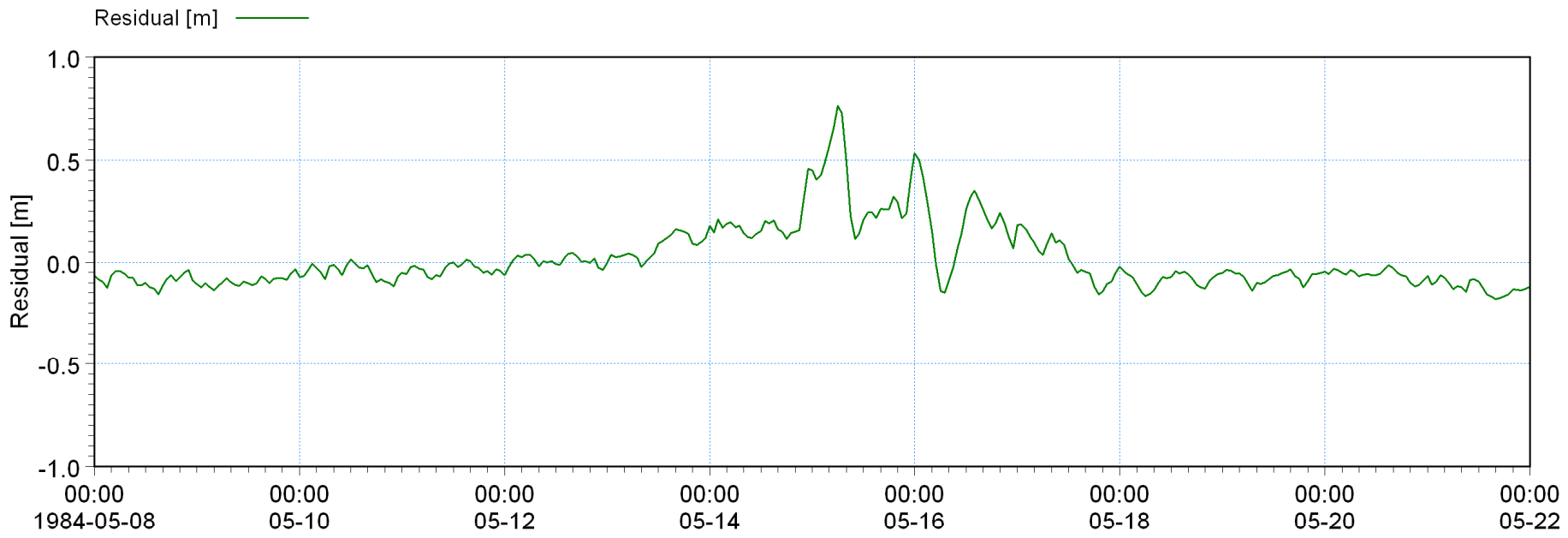
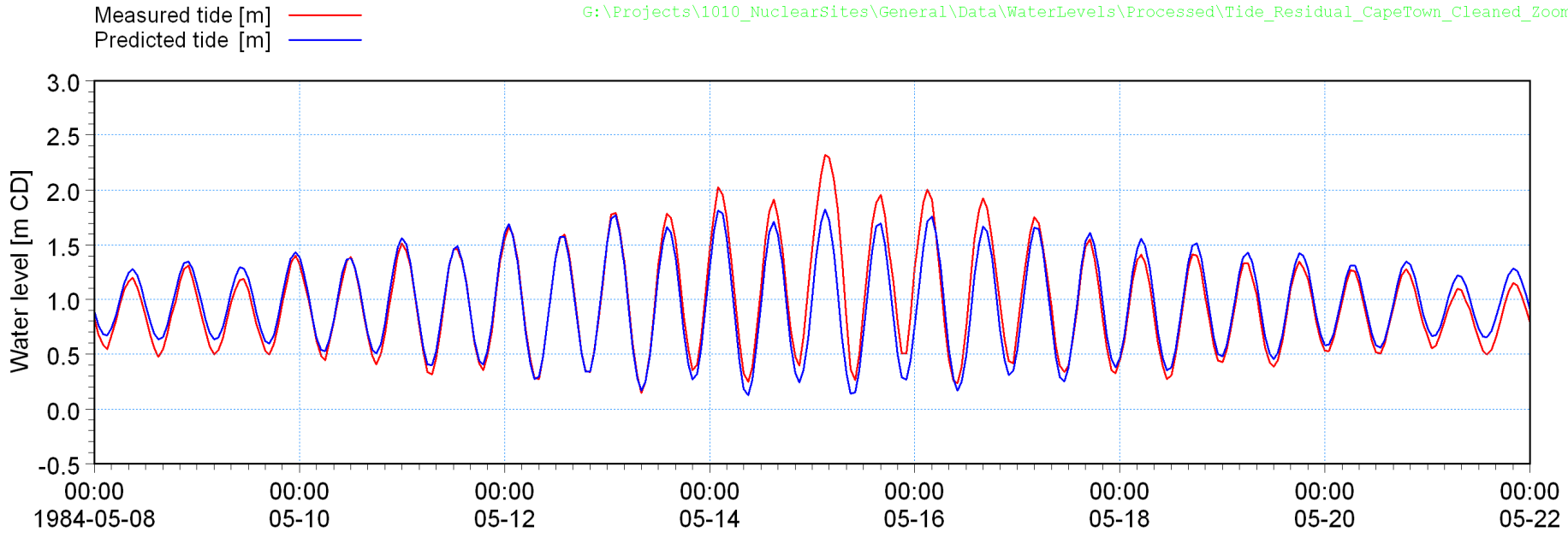
Bathymetry and location of instruments deployed at Duynefontein.

Figure No.

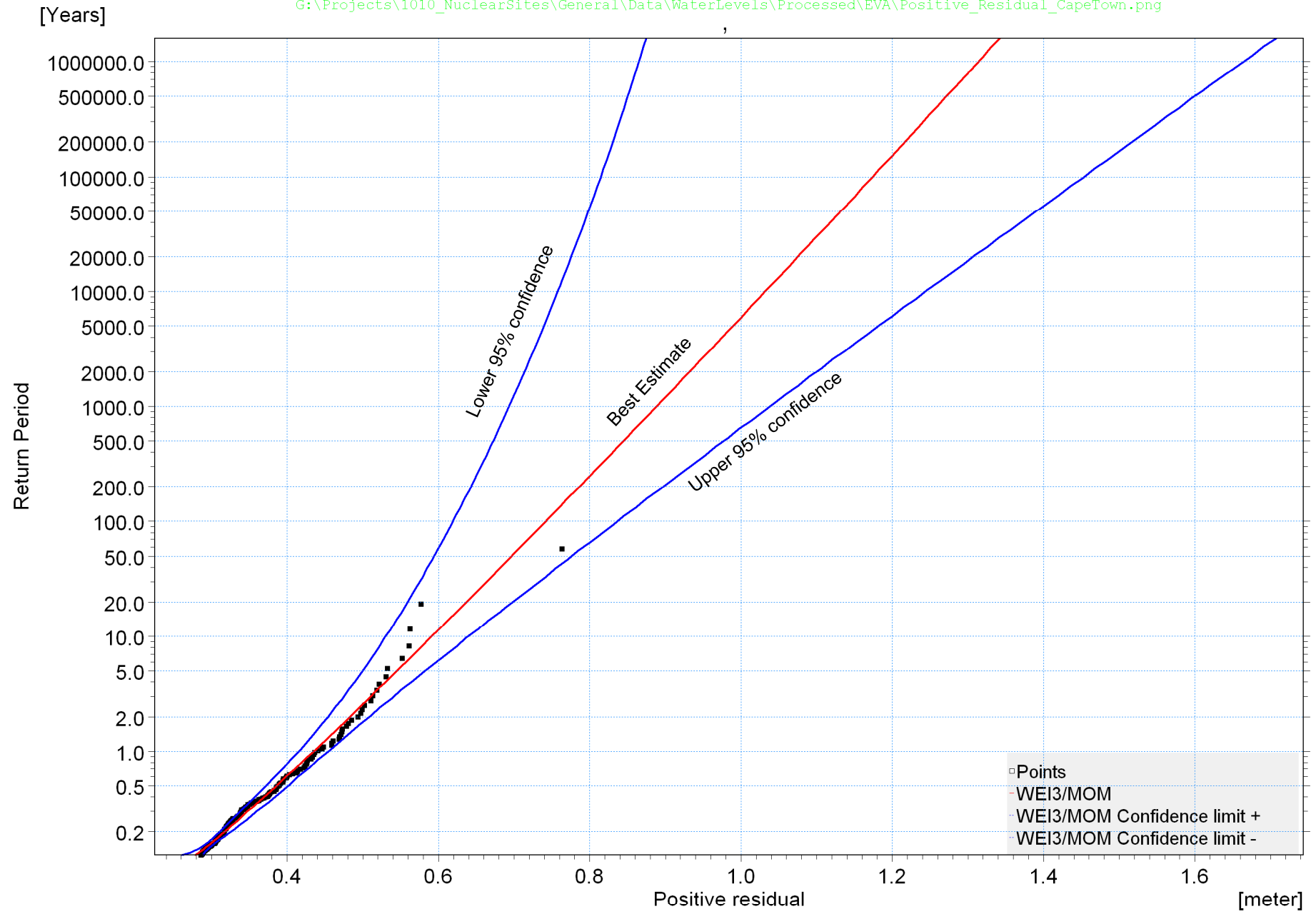
1.2



**Title:**      **Analysis of storm surge: Measured tide, predicted tide and residual at Cape Town. Full 40 year dataset.**



**Title:** Analysis of storm surge: Measured tide, predicted tide and residual at Cape Town. Fourteen days including the May 1984 storm event.

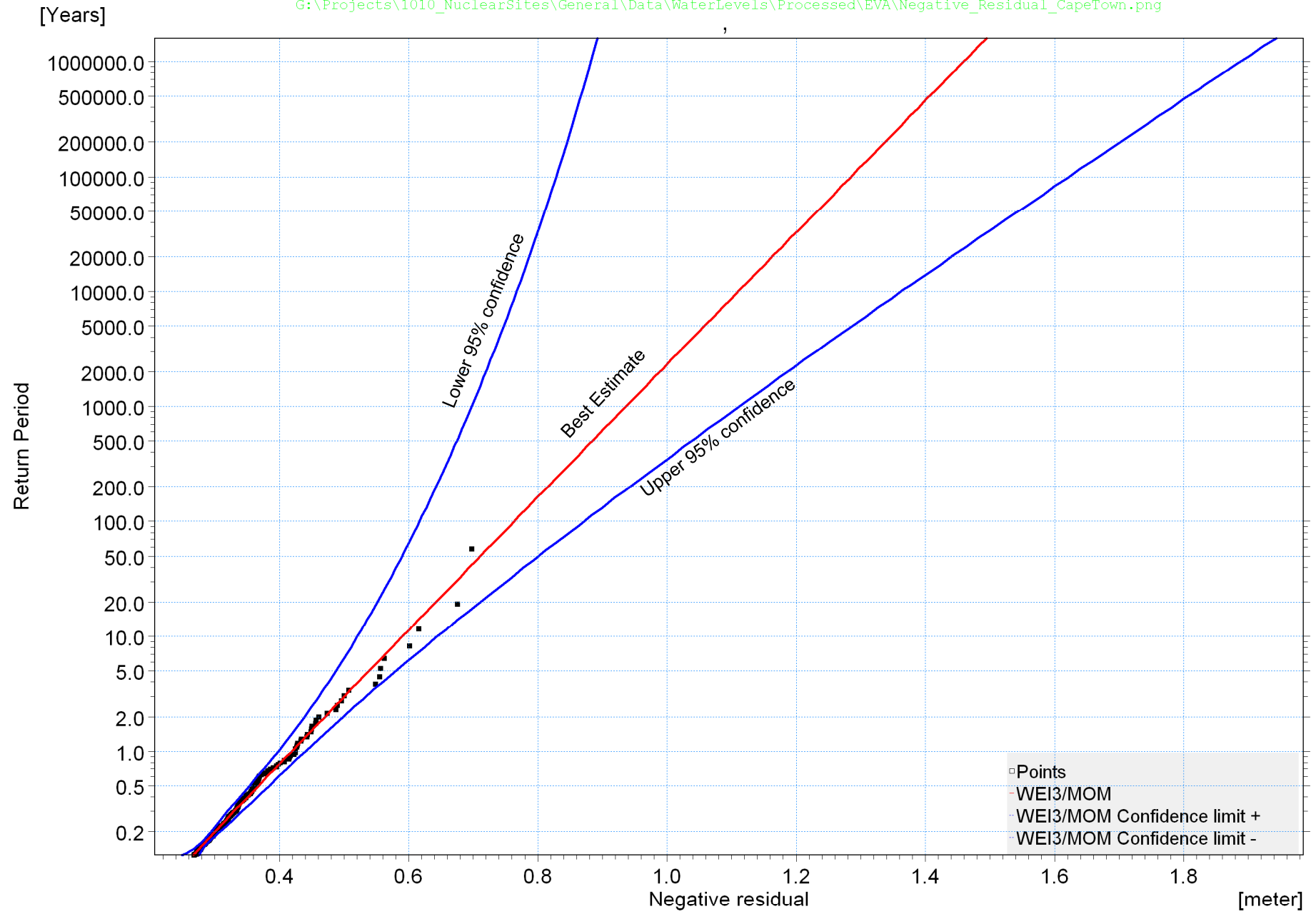


Title:

Extreme value analysis of positive storm surge at Cape Town.

Figure No.

4.3

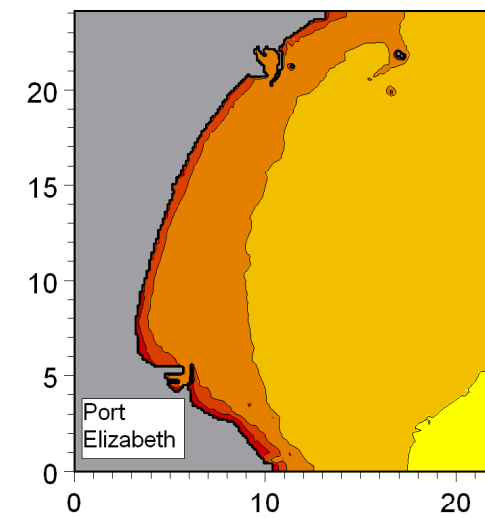
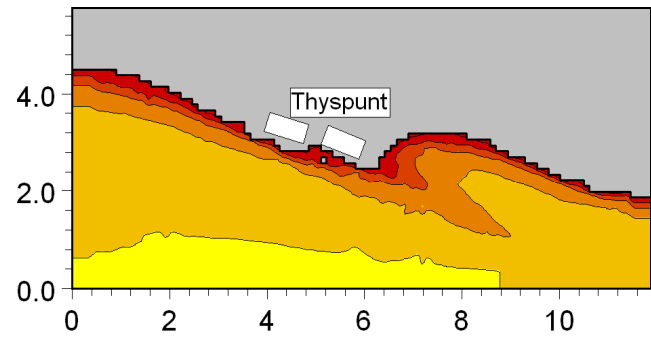
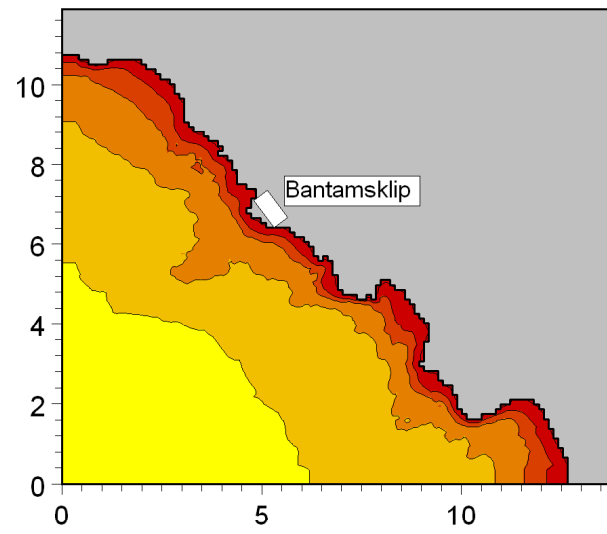
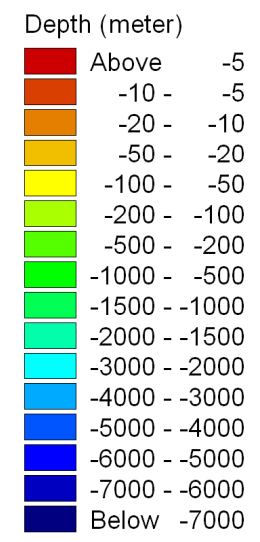
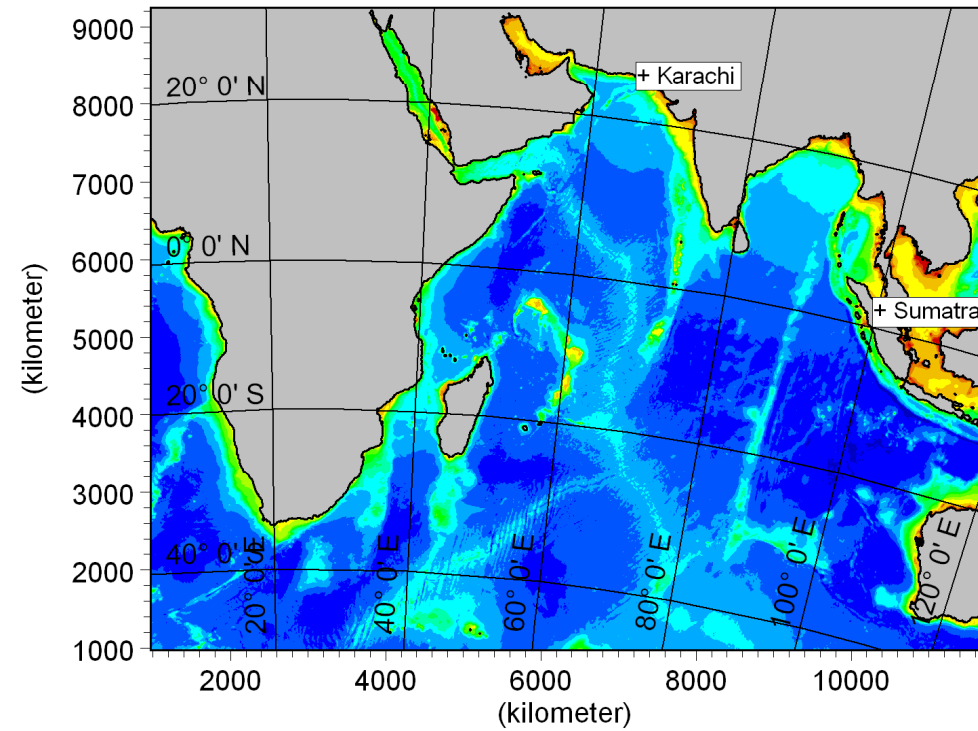
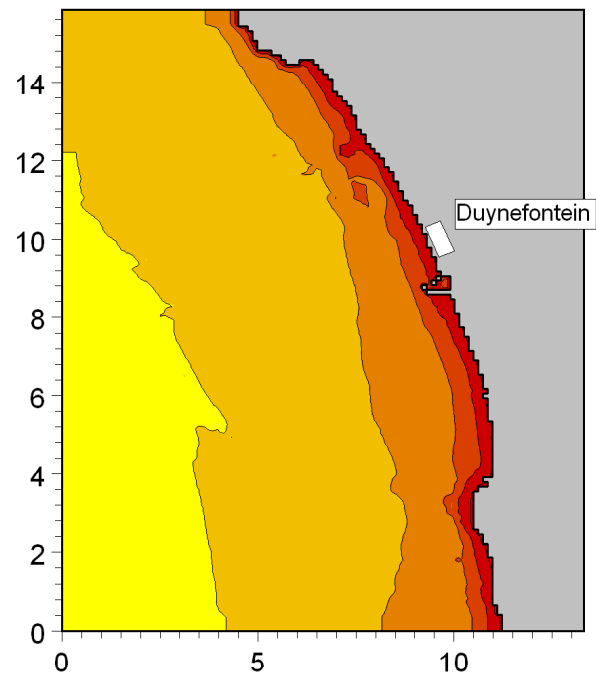


Title:

Extreme value analysis of negative storm surge at Cape Town.

Figure No.

4.4

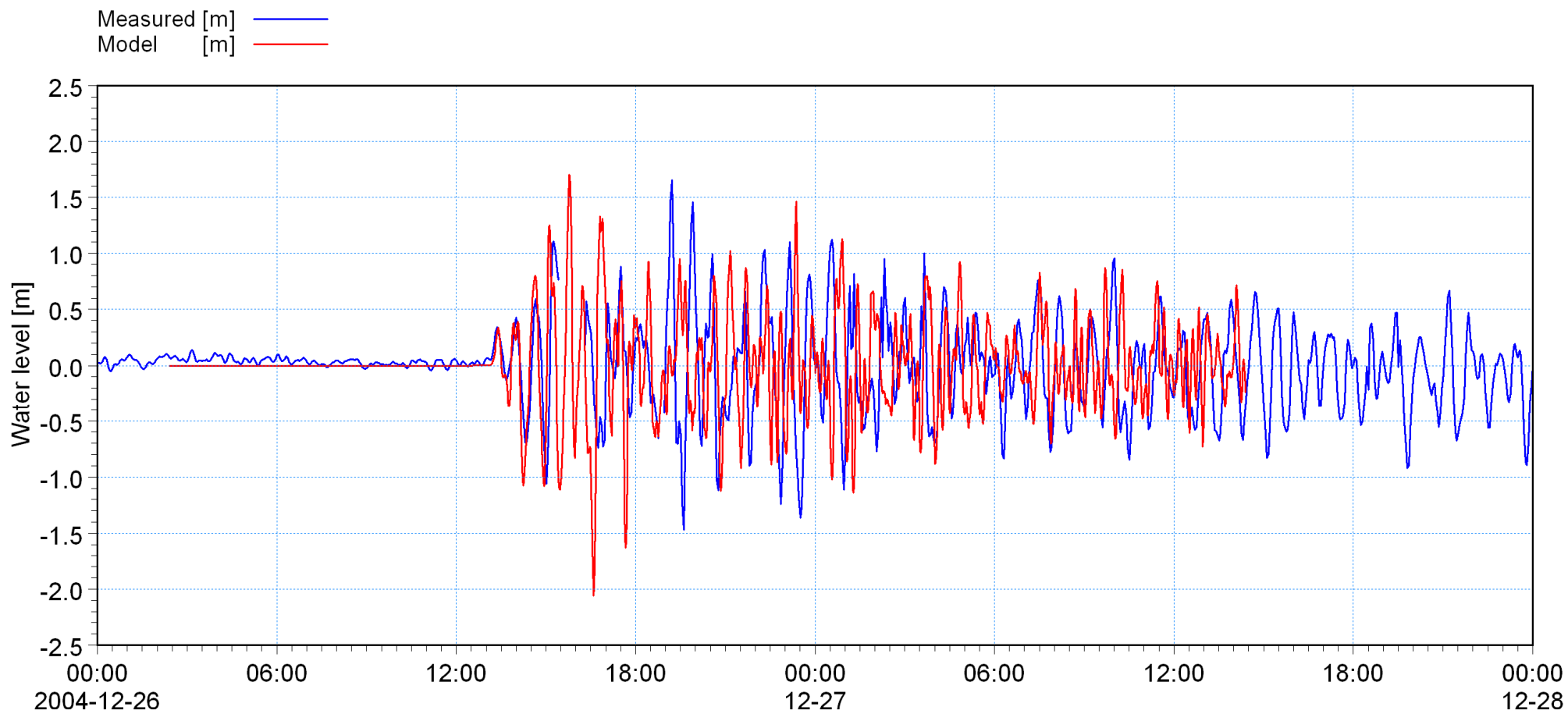


Title:

Model bathymetry used for tsunami modelling of Sumatra and Karachi earthquake events.

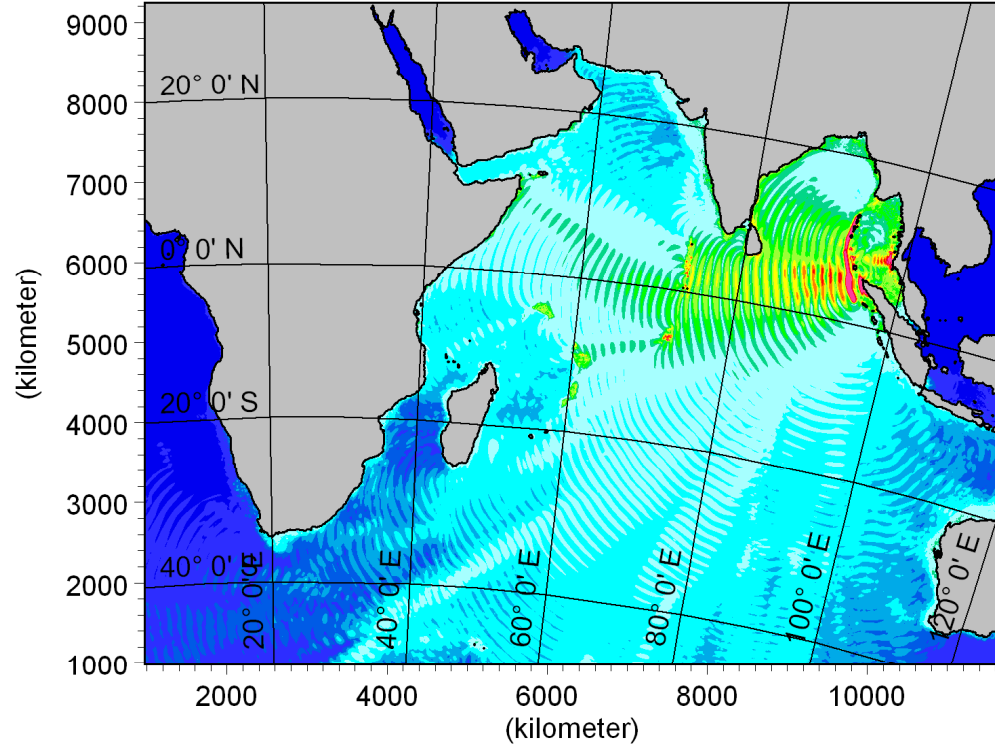
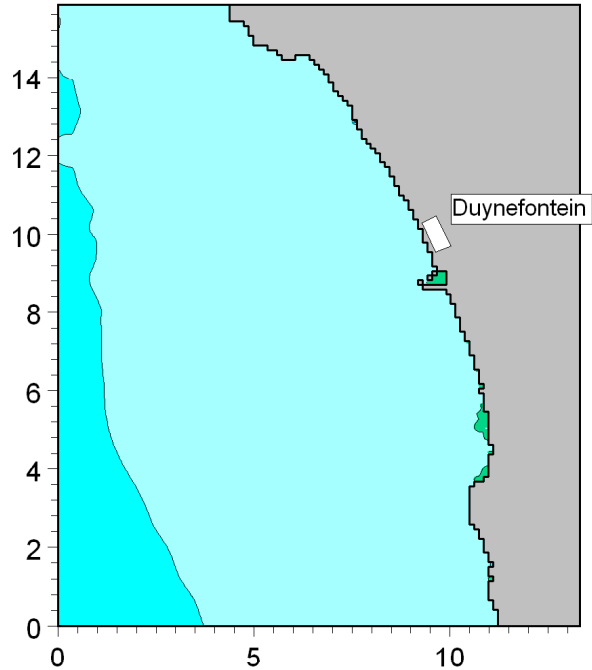
Figure No.

5.1

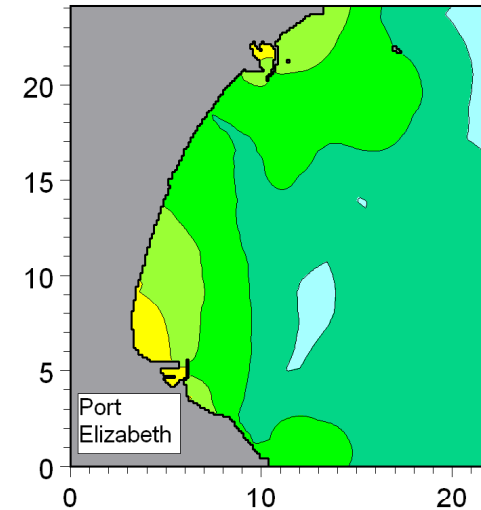
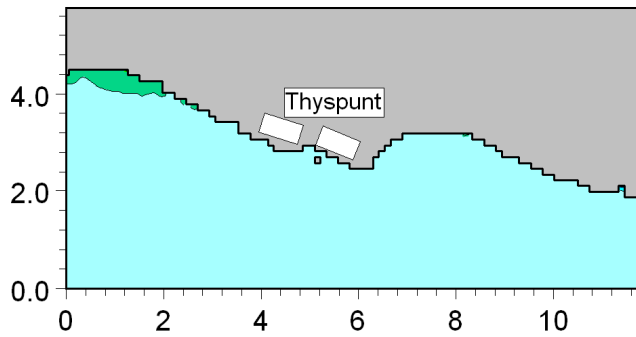
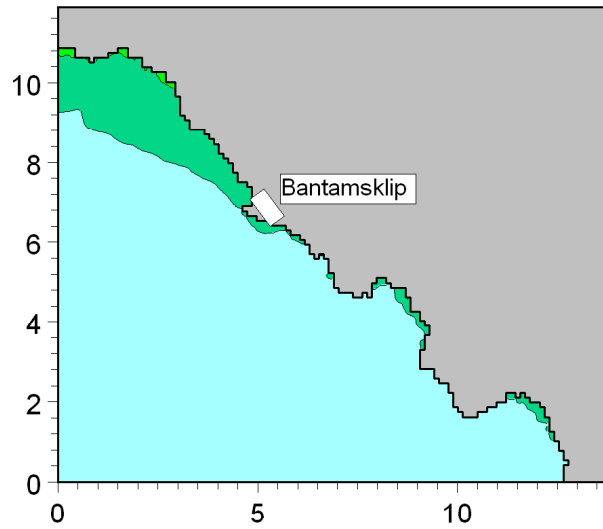
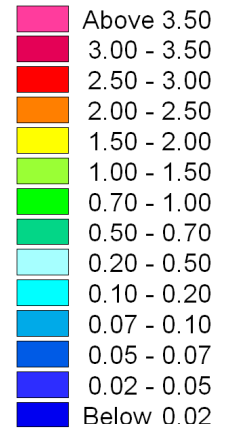


**Title:** Calibration of tsunami model: Measured and modelled water levels due to the tsunami in the Port of Port Elizabeth for the 26 December 2004 Sumatra event.

**Figure No.**  
5.2



Maximum surface elevation (meter)



These are the maximum tsunami-induced water levels above Still Water Level. The total water level will additionally include the effect of tide, wave run-up, wave set-up and storm surge.

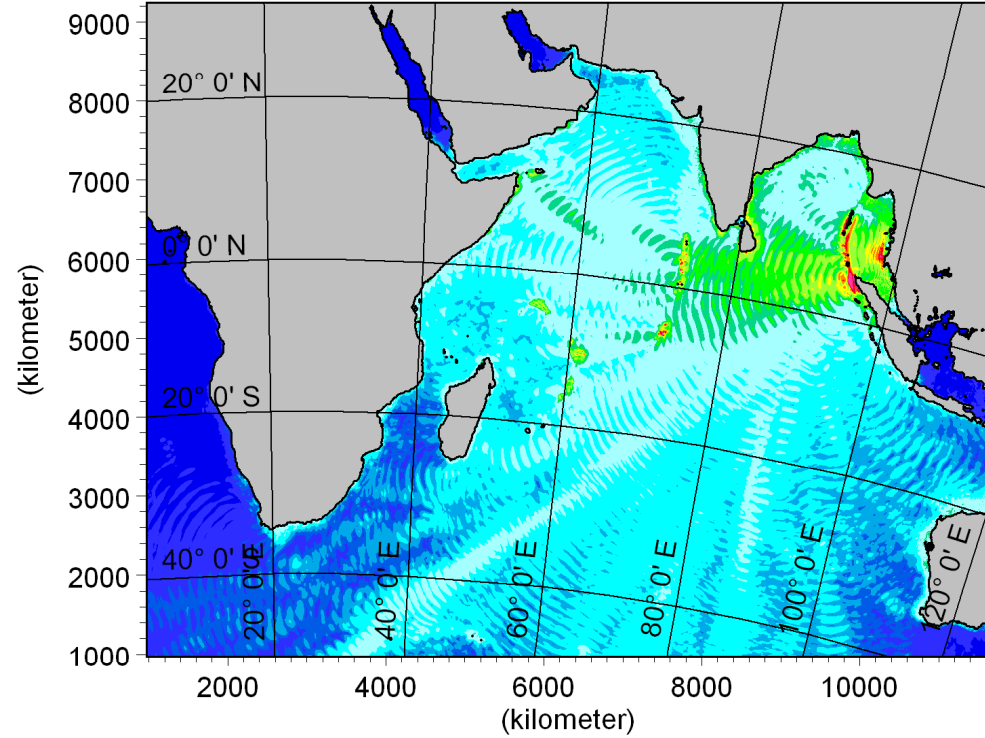
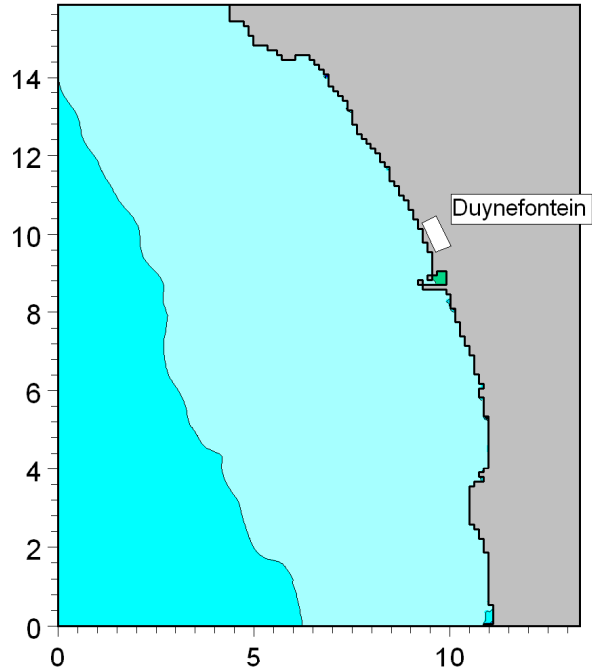


Title:

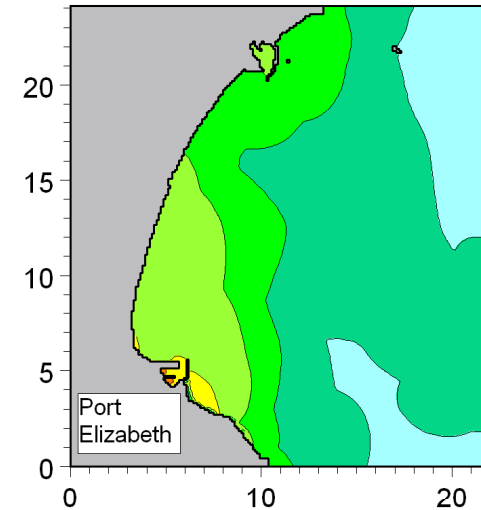
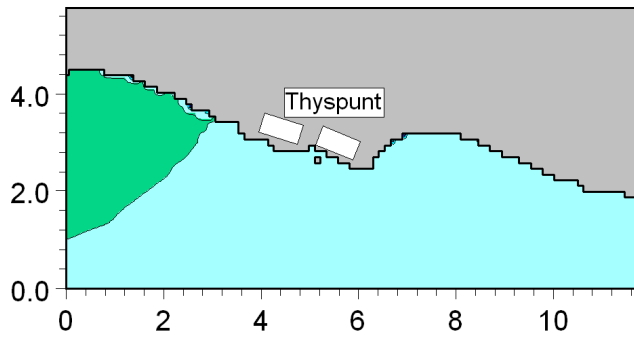
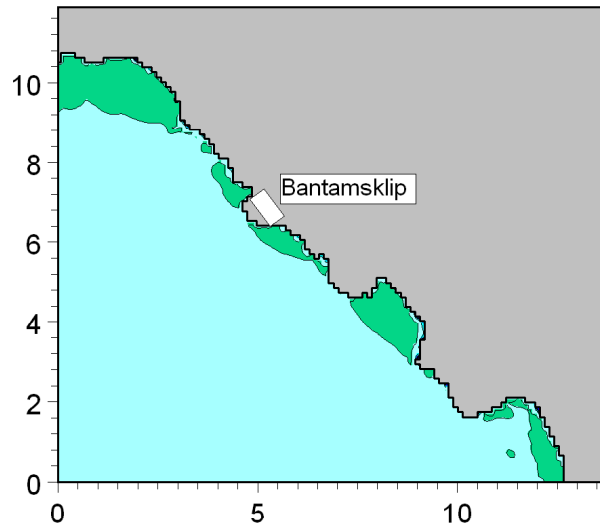
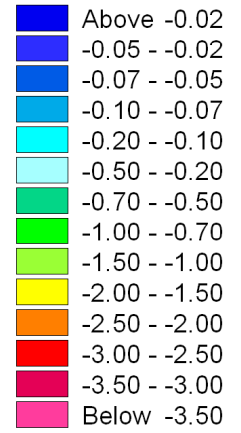
Maximum water levels predicted during tsunami event.  
Source is Sumatra A: 26 December 2004 earthquake, Mw = 9.2.

Figure No.

5.3



Minimum surface elevation (meter)



These are the minimum tsunami-induced water levels below Still Water Level. The total water level will additionally include the effect of tide and storm surge.

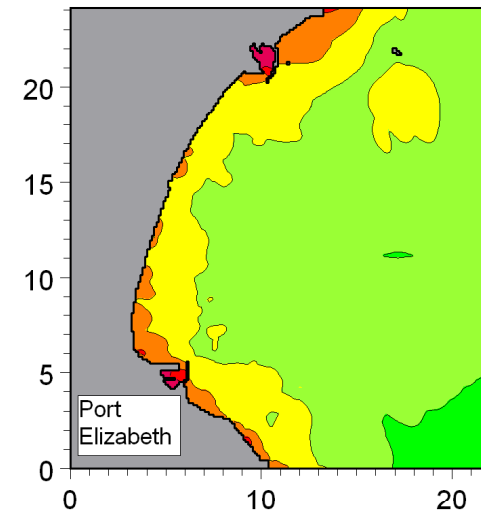
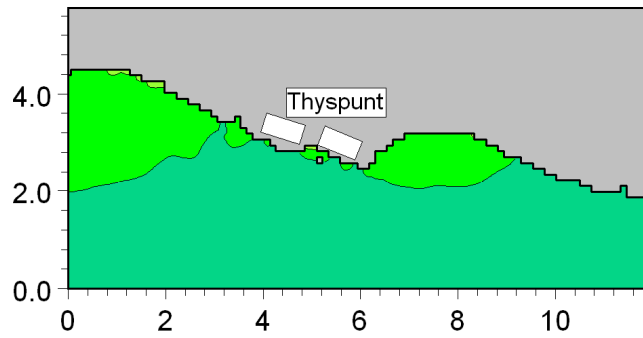
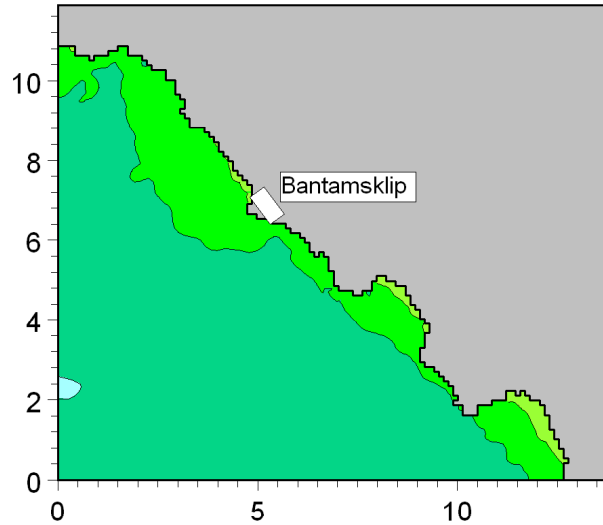
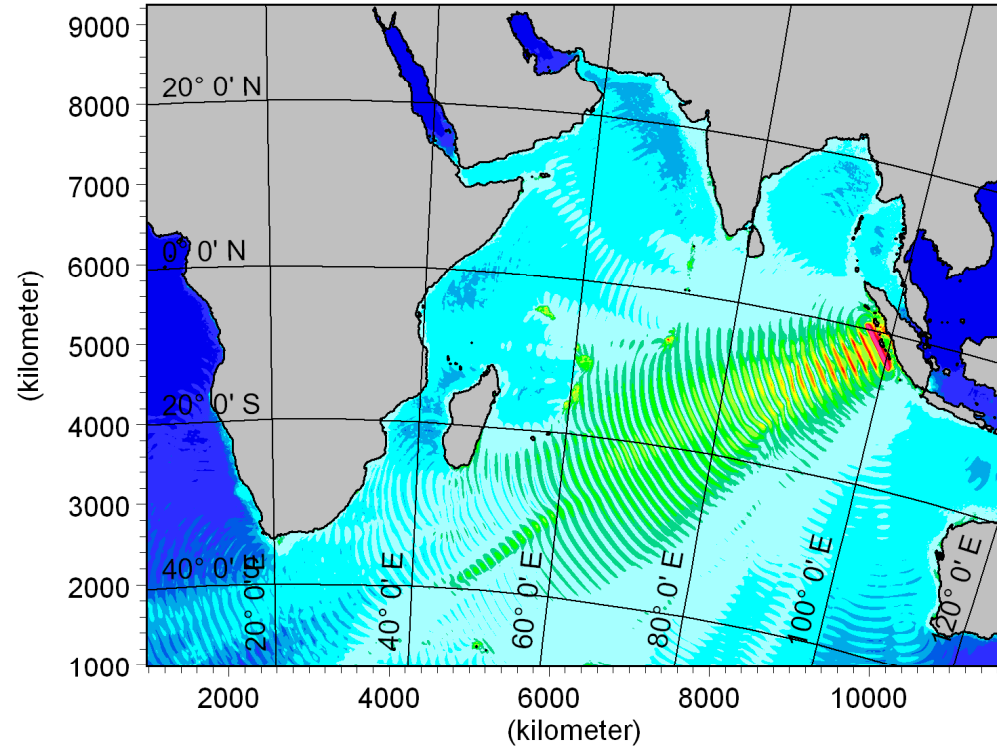
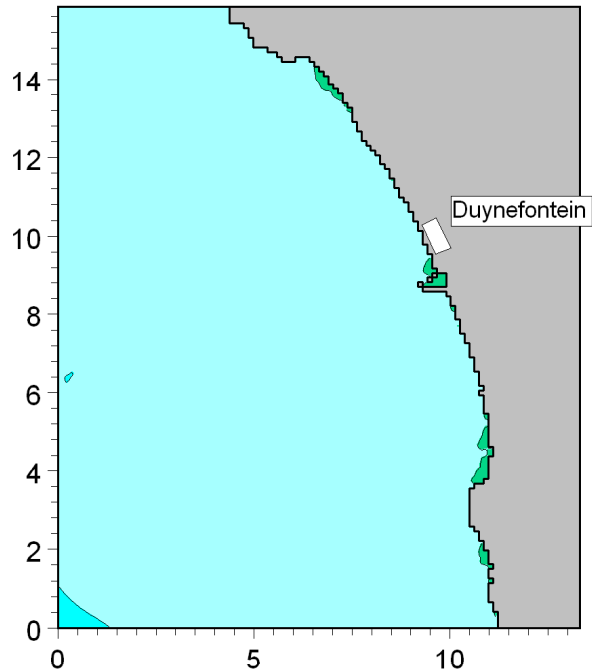


Title:

Minimum water levels predicted during tsunami event.  
Source is Sumatra A: 26 December 2004 earthquake, Mw = 9.2.

Figure No.

5.4

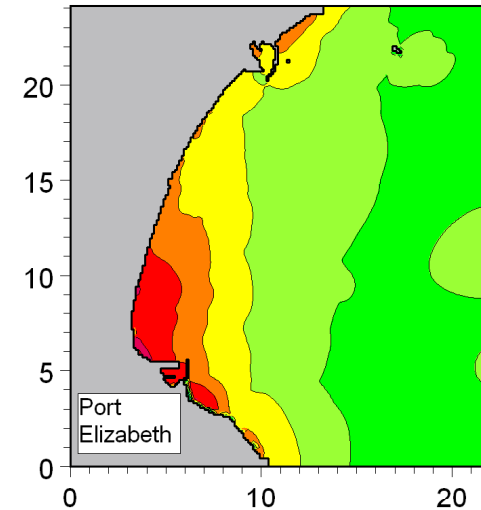
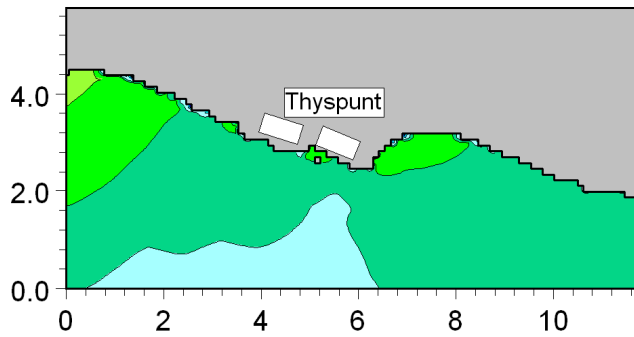
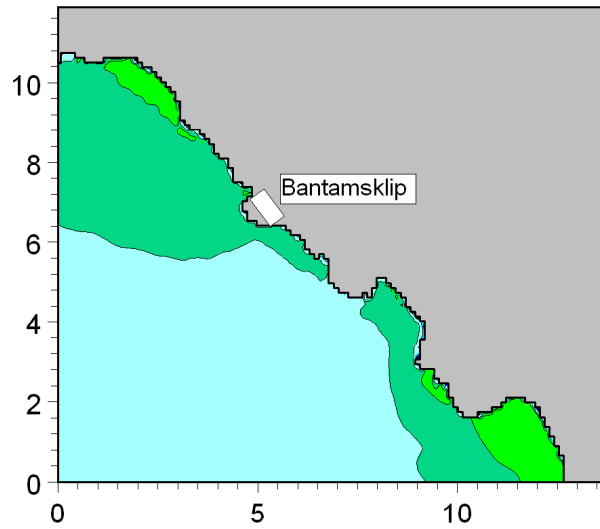
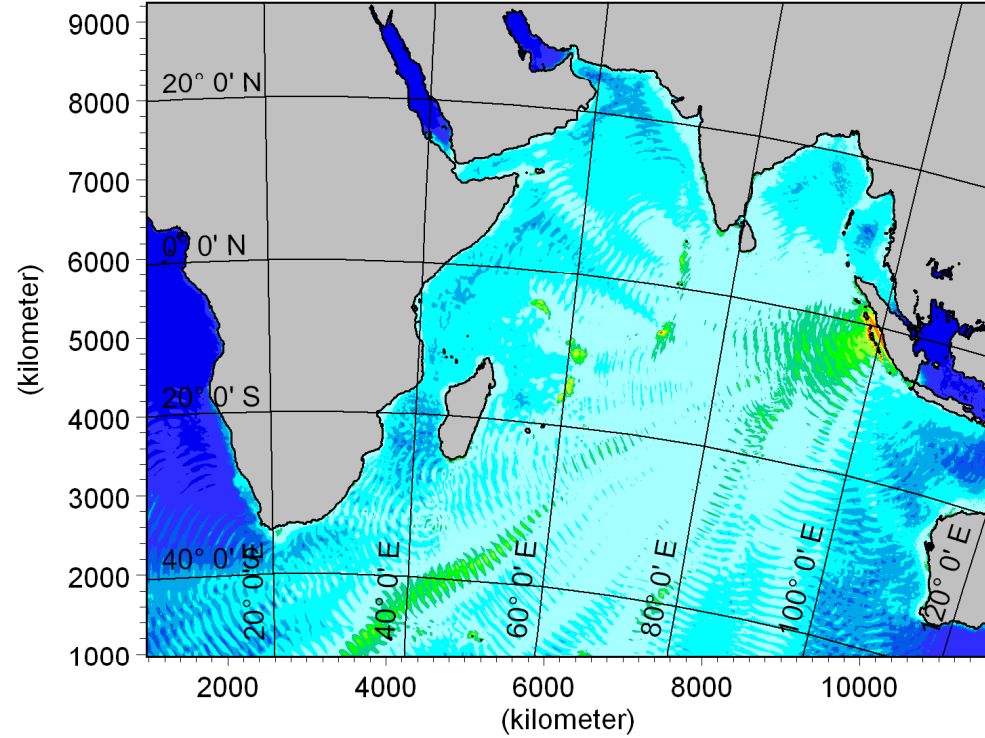
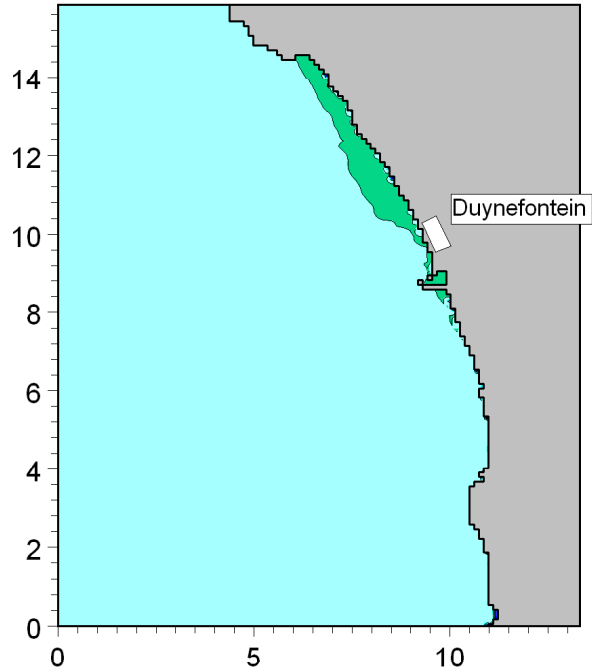


These are the maximum tsunami-induced water levels above Still Water Level. The total water level will additionally include the effect of tide, wave run-up, wave set-up and storm surge.



**Title: Maximum water levels predicted during tsunami event.**  
**Source is Sumatra B: maximum credible earthquake determined by the Council for Geoscience, Mw = 9.2.**

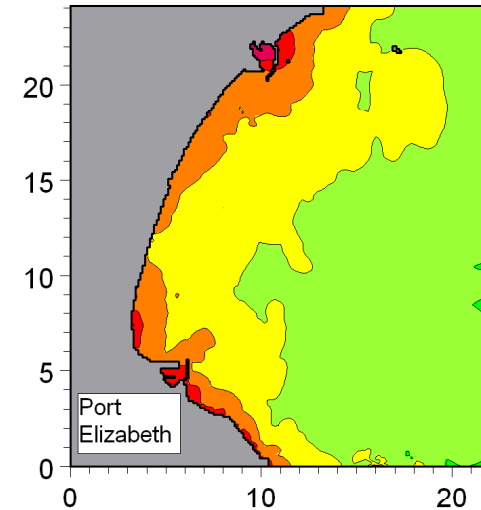
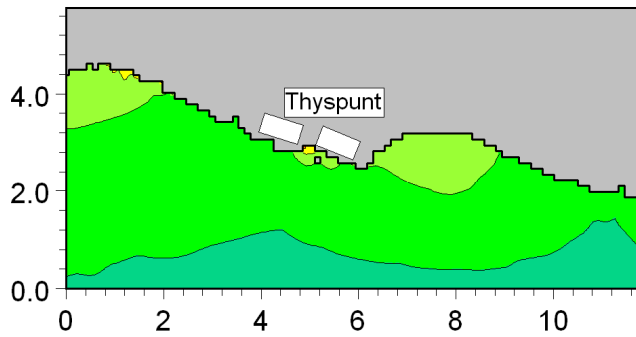
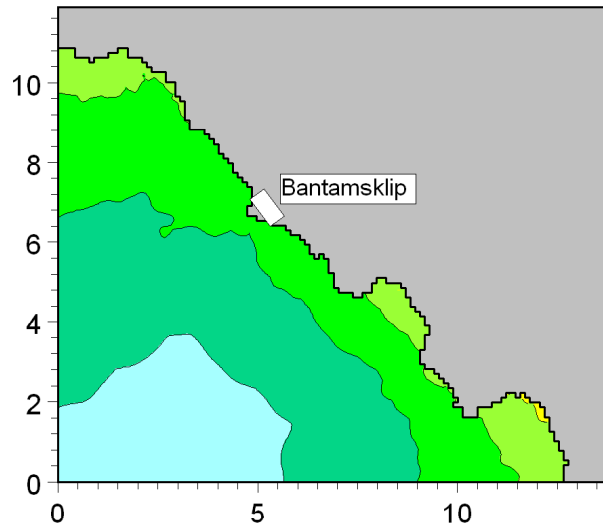
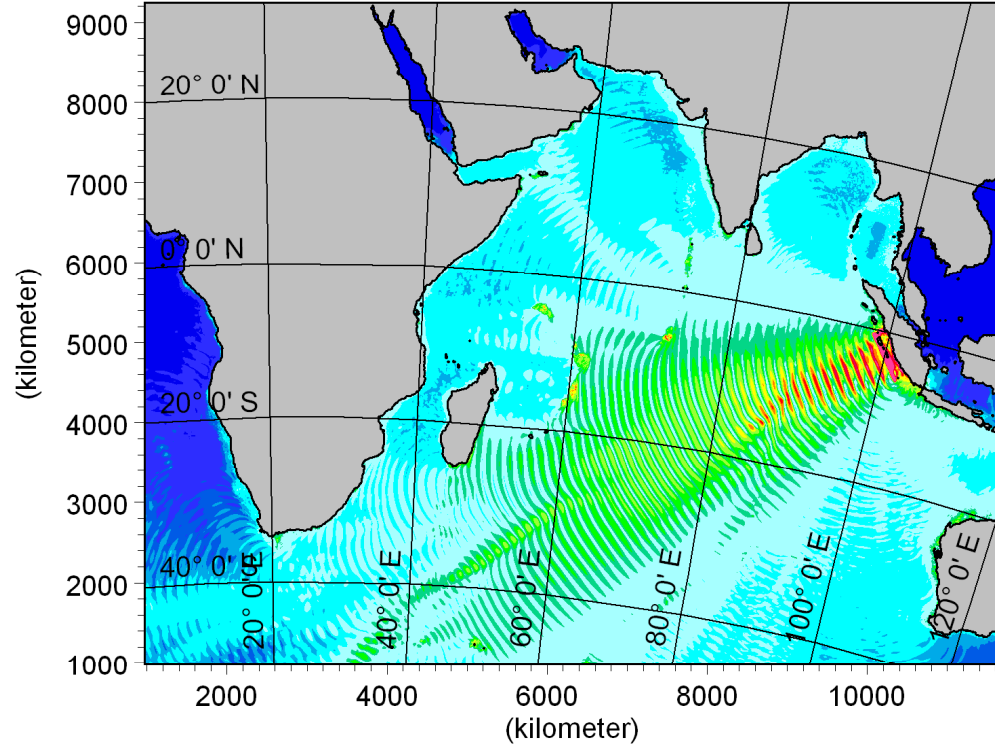
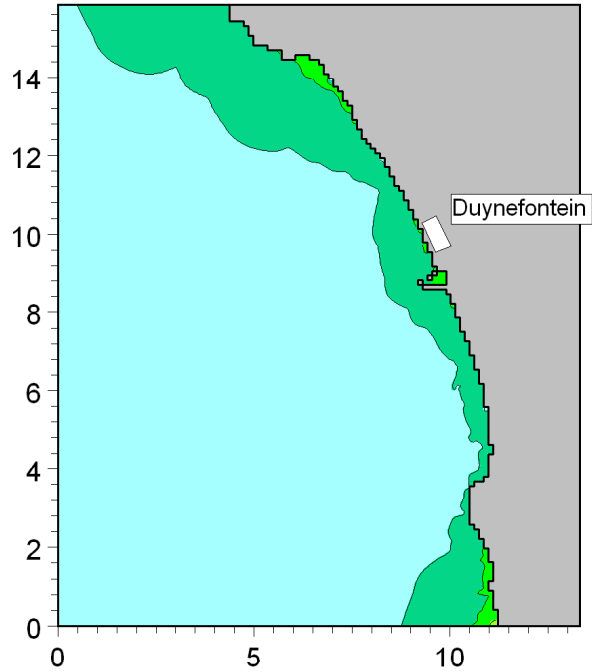
**Figure No. 5.5**



These are the minimum tsunami-induced water levels below Still Water Level. The total water level will additionally include the effect of tide and storm surge.



**Title: Minimum water levels predicted during tsunami event.**  
**Source is Sumatra B: maximum credible earthquake determined by the Council for Geoscience, Mw = 9.2.**



These are the maximum tsunami-induced water levels above Still Water Level. The total water level will additionally include the effect of tide, wave run-up, wave set-up and storm surge.

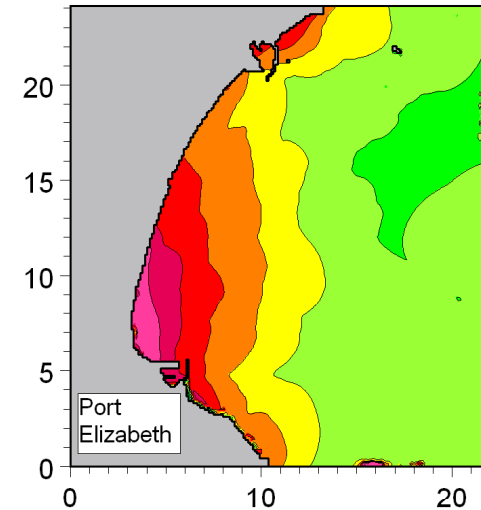
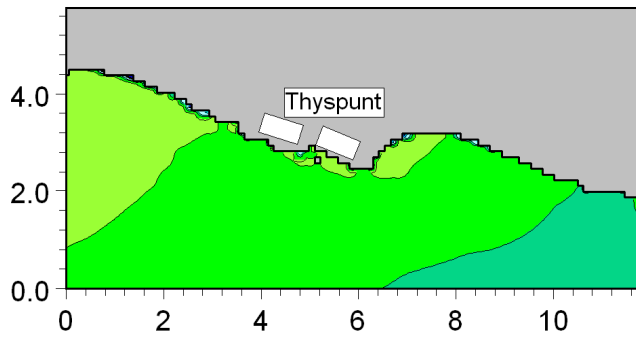
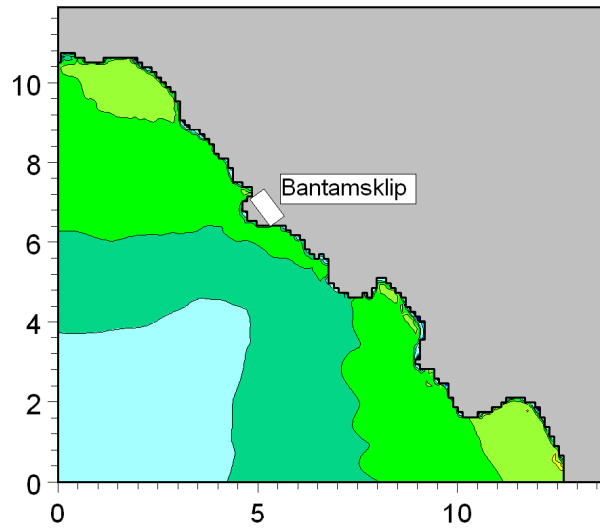
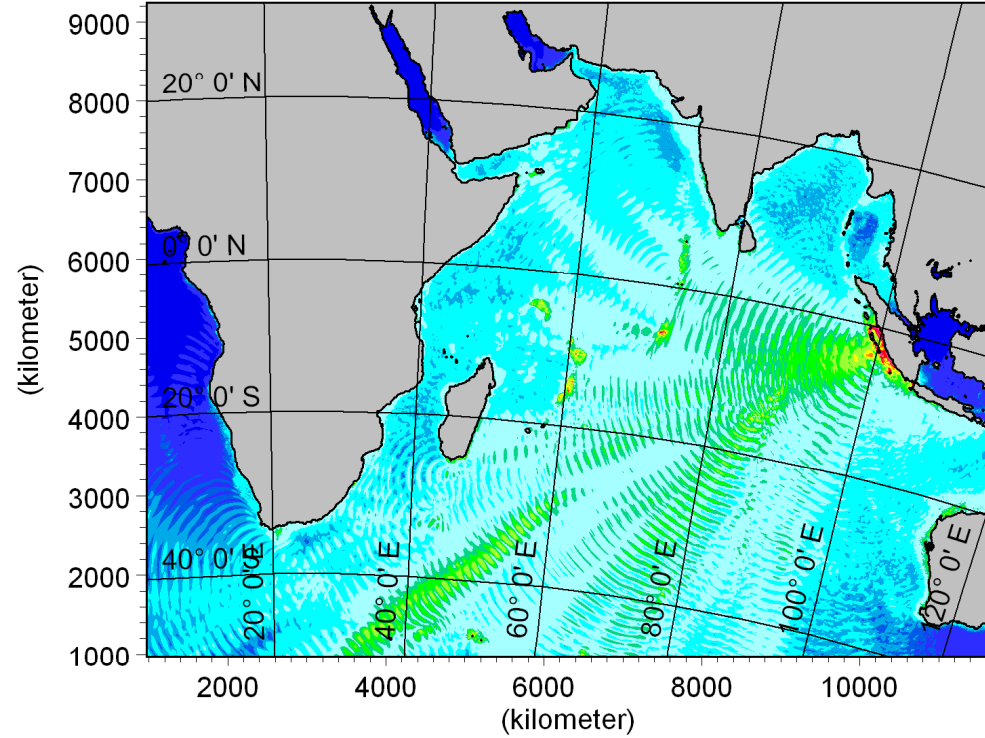
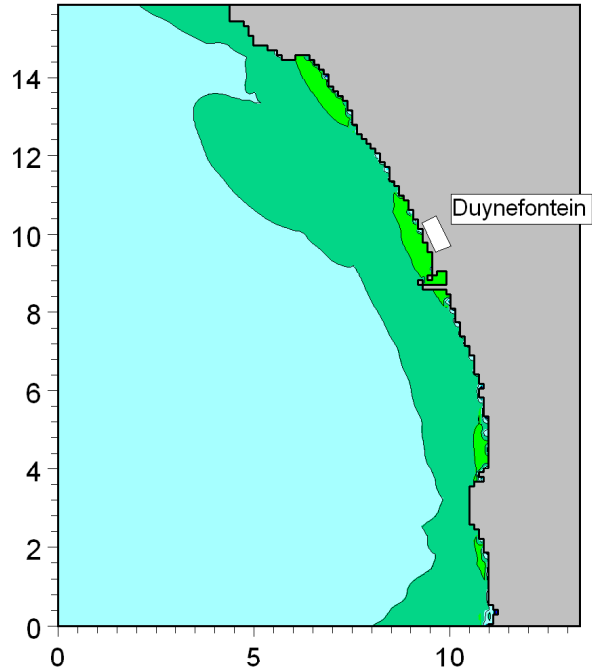


Title:

**Maximum water levels predicted during tsunami event.  
Source is a Sumatra C: maximum plausible event from Borrero *et al* (2006), Mw = 9.3.**

Figure No.

**5.7**



These are the minimum tsunami-induced water levels below Still Water Level. The total water level will additionally include the effect of tide and storm surge.

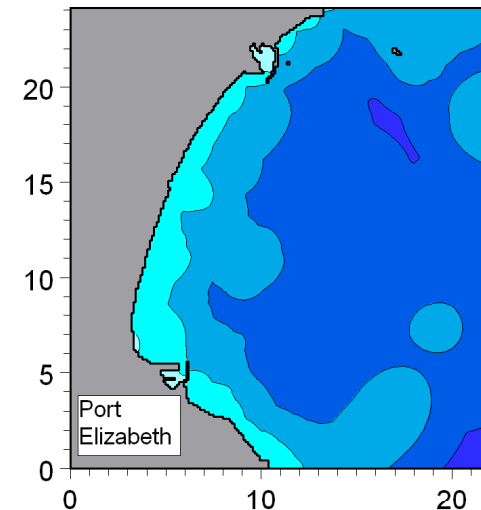
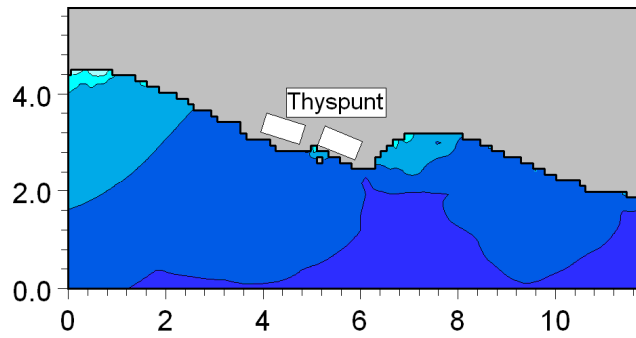
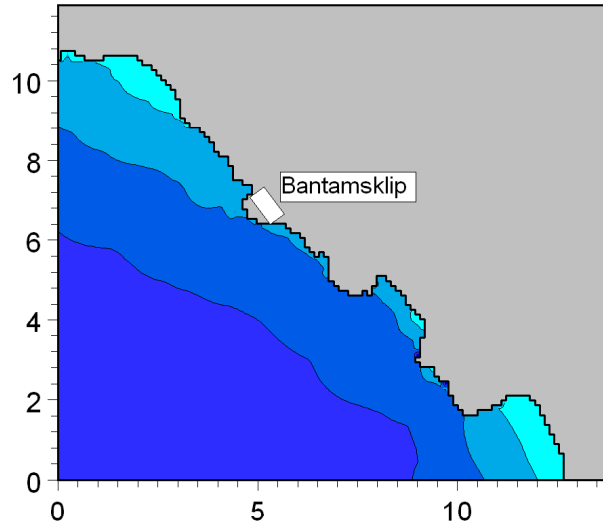
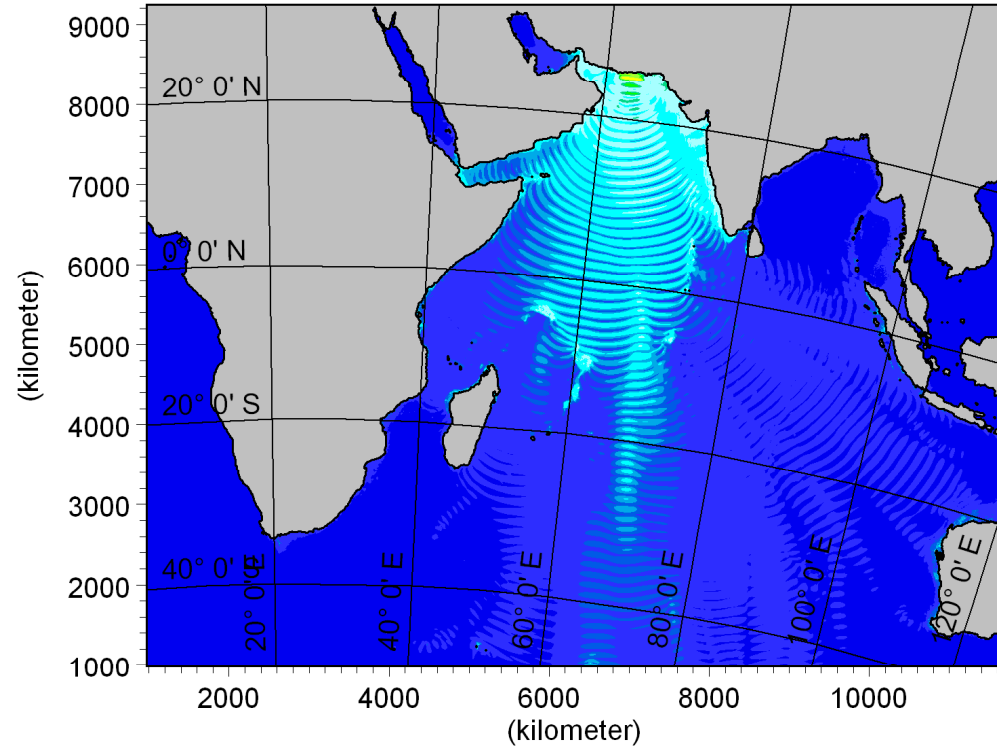
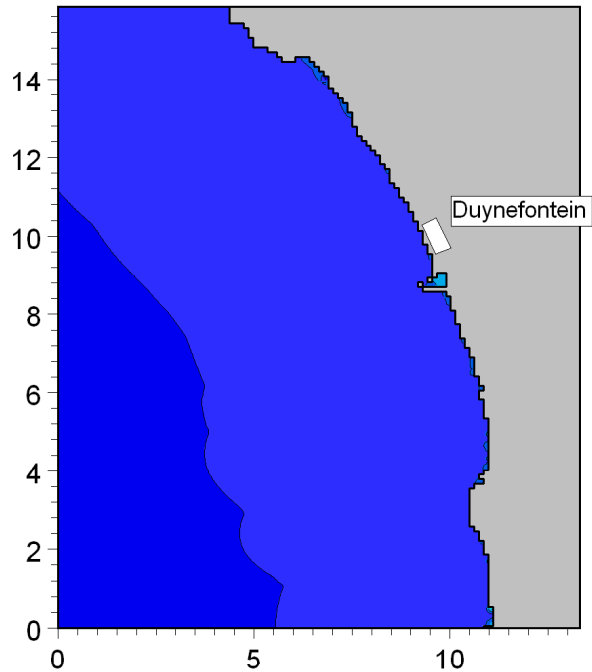


Title:

**Minimum water levels predicted during tsunami event.**  
**Source is a Sumatra C: maximum plausible event from Borrero *et al* (2006), Mw = 9.3.**

Figure No.

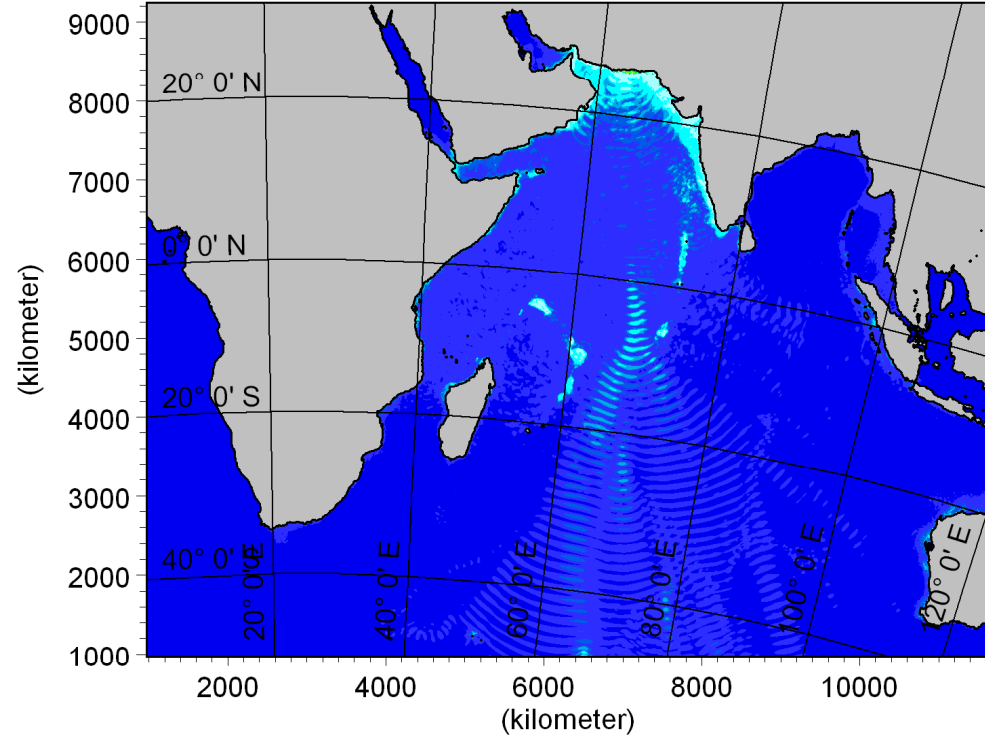
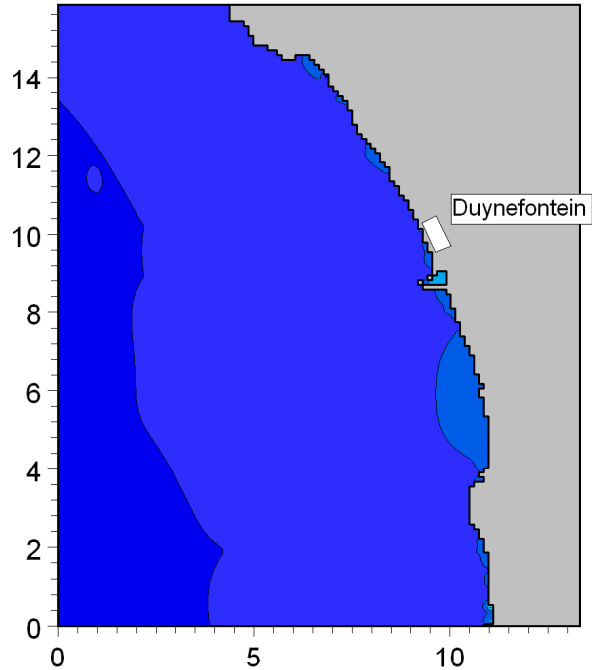
5.8



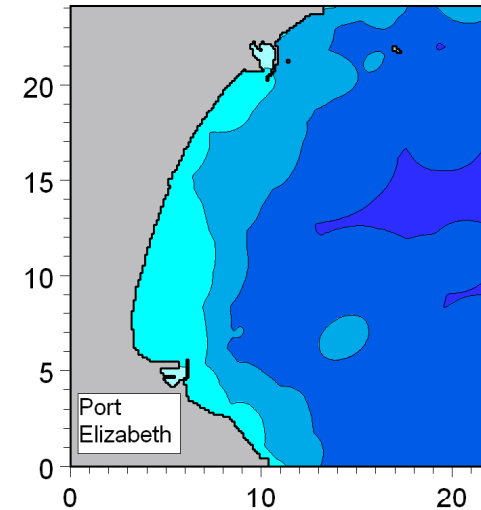
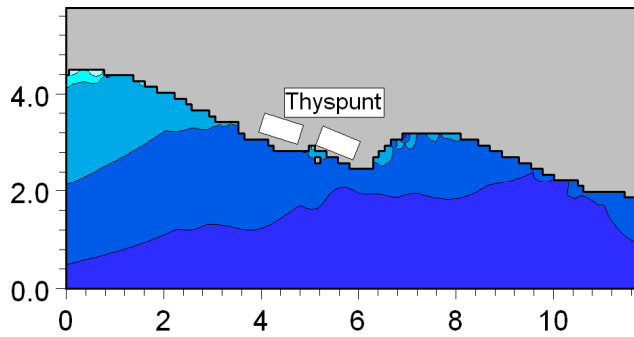
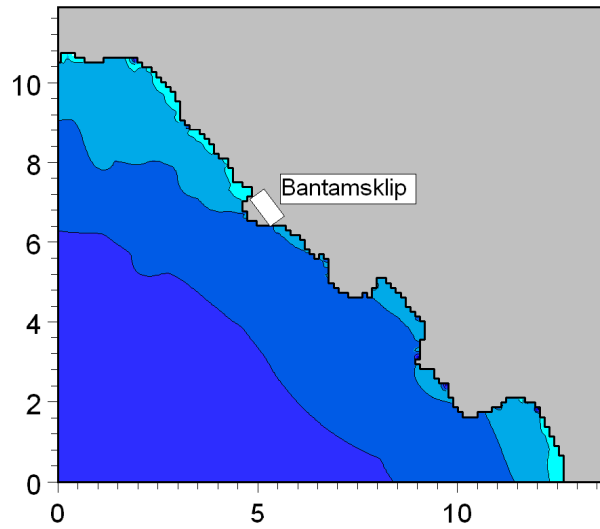
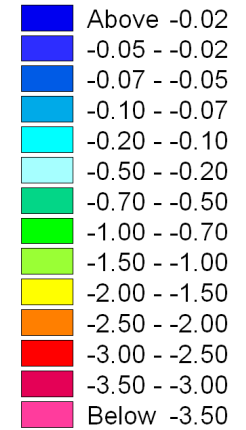
These are the maximum tsunami-induced water levels above Still Water Level. The total water level will additionally include the effect of tide, wave run-up, wave set-up and storm surge.



**Title: Maximum water levels predicted during tsunami event.**  
**Source is Karachi A: maximum credible earthquake determined by the Council for Geoscience, Mw =8.4.**



Minimum surface elevation (meter)

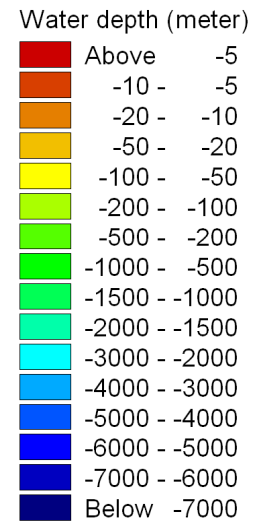
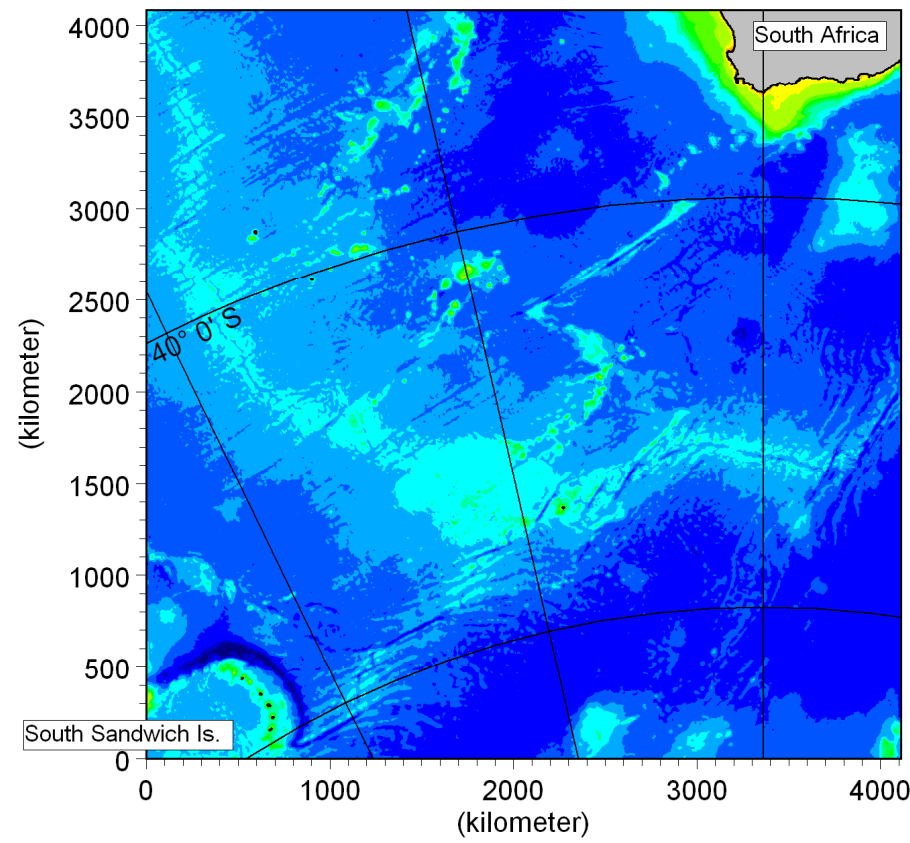
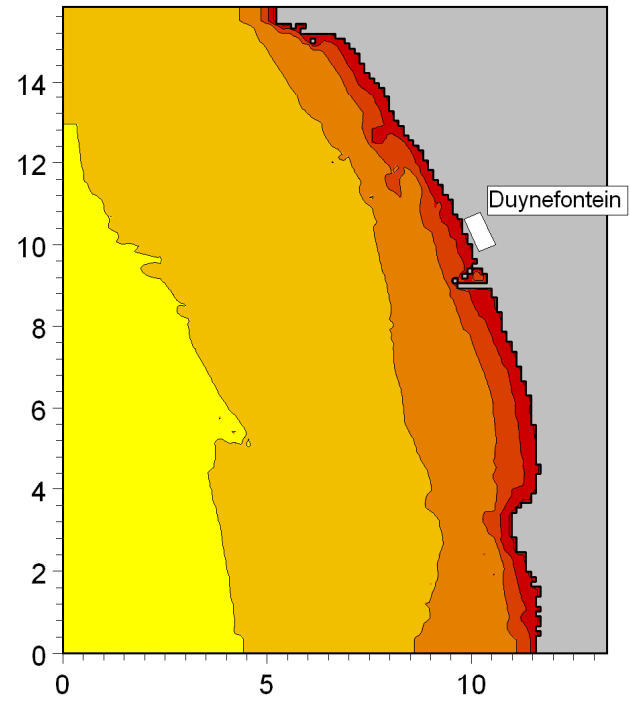
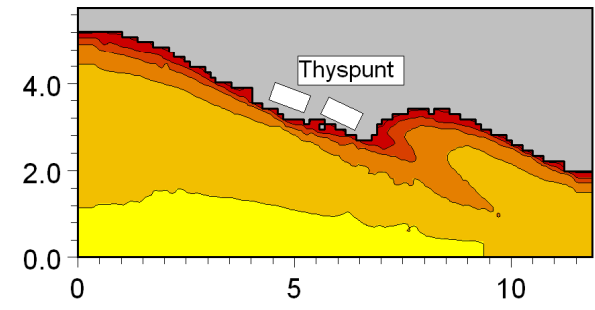
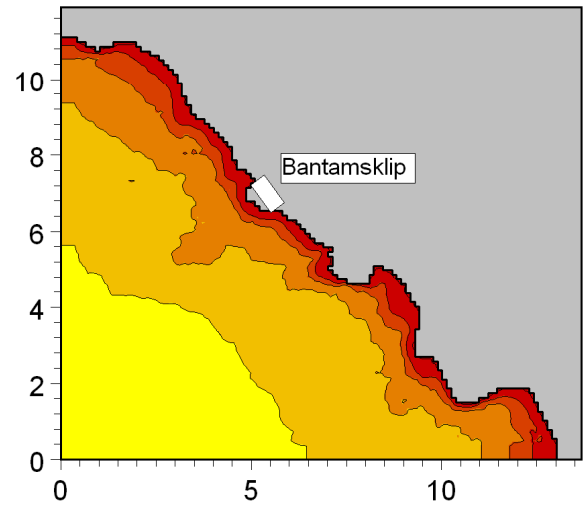


These are the minimum tsunami-induced water levels below Still Water Level. The total water level will additionally include the effect of tide and storm surge.



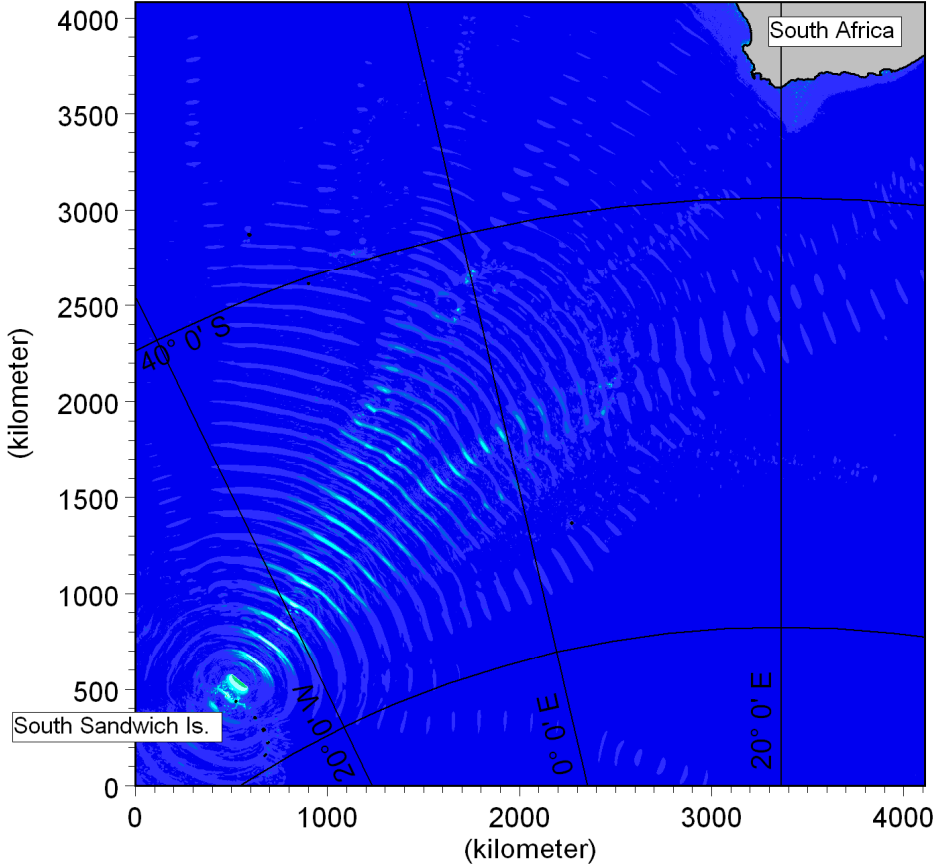
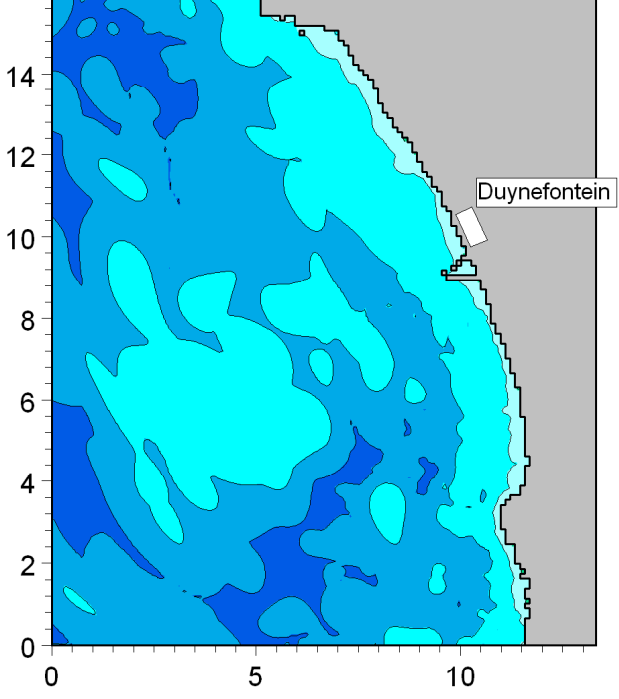
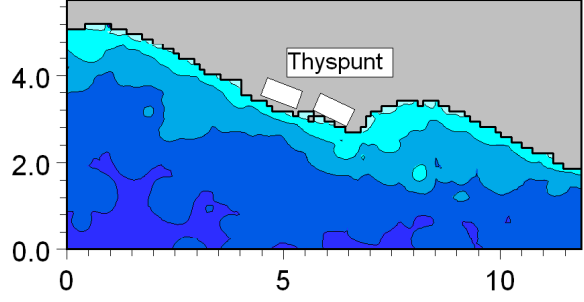
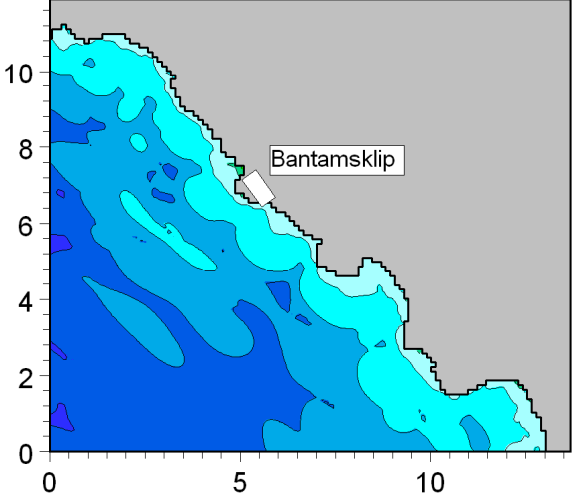
**Title:** Minimum water levels predicted during tsunami event.  
Source is Karachi A: maximum credible earthquake determined by the Council for Geoscience, Mw =8.4.

Run: SouthSandwich01\_MSL\_a



Title: **Model bathymetry used for tsunami modelling of the South Sandwich Islands earthquake events.**

Figure No. **5.11**

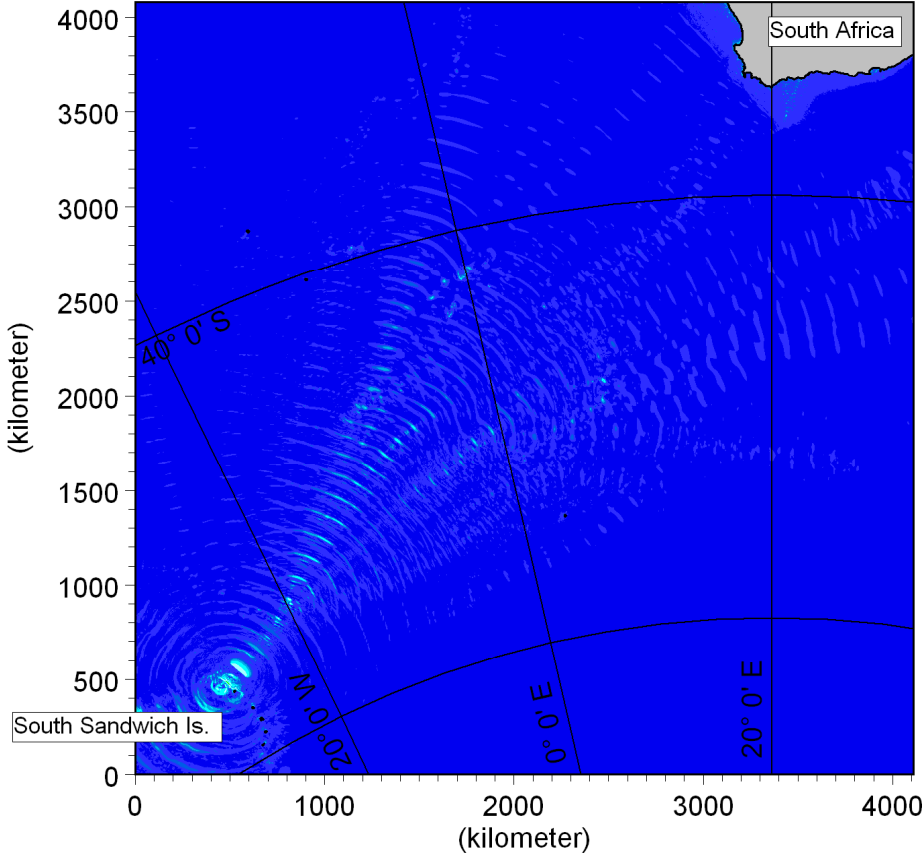
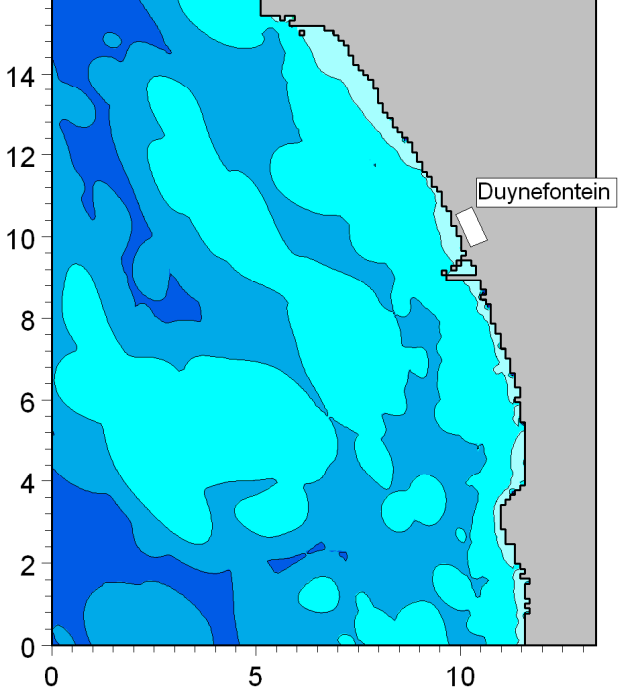
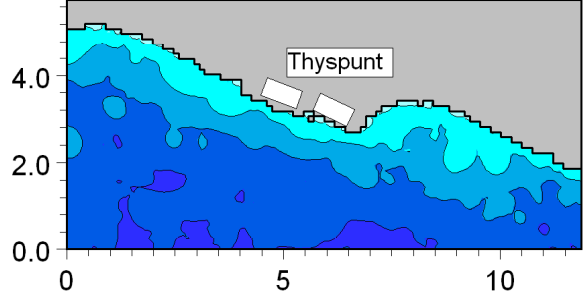
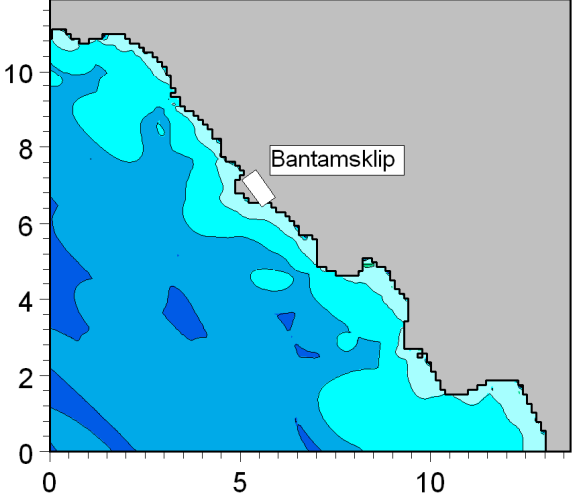


These are the maximum tsunami-induced water levels above Still Water Level. The total water level will additionally include the effect of tide, wave run-up, wave set-up and storm surge.

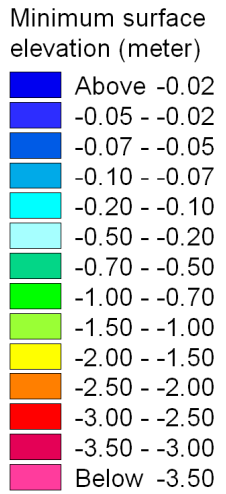
- Maximum surface elevation (meter)
- █ Above 3.50
  - █ 3.00 - 3.50
  - █ 2.50 - 3.00
  - █ 2.00 - 2.50
  - █ 1.50 - 2.00
  - █ 1.00 - 1.50
  - █ 0.70 - 1.00
  - █ 0.50 - 0.70
  - █ 0.20 - 0.50
  - █ 0.10 - 0.20
  - █ 0.07 - 0.10
  - █ 0.05 - 0.07
  - █ 0.02 - 0.05
  - █ Below 0.02



**Title: Maximum water levels predicted during tsunami event. Source is South Sandwich Islands A: maximum credible earthquake determined by the Council for Geoscience, Mw = 7.6.**

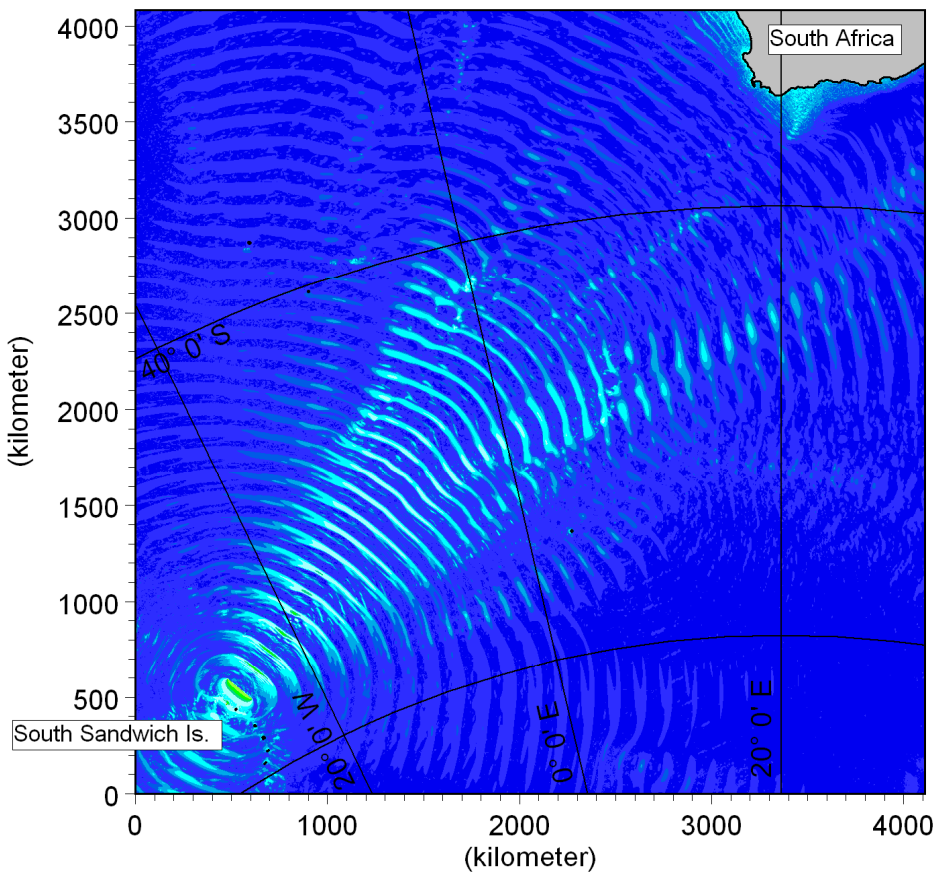
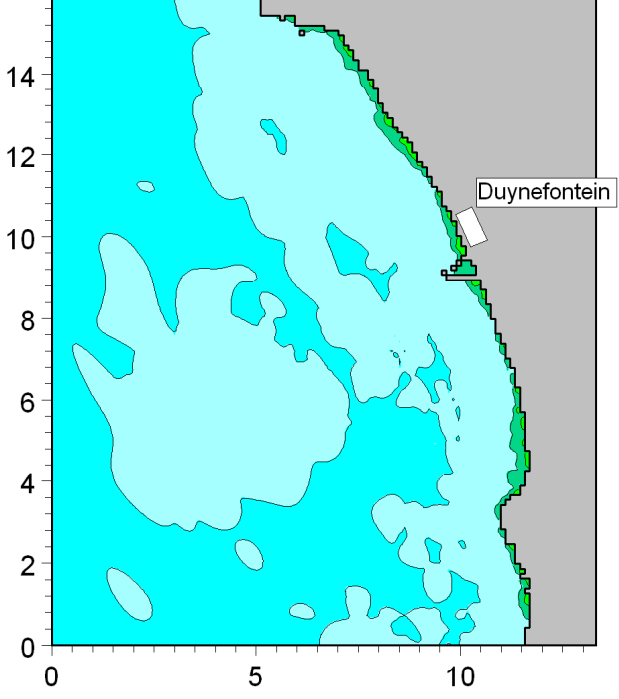
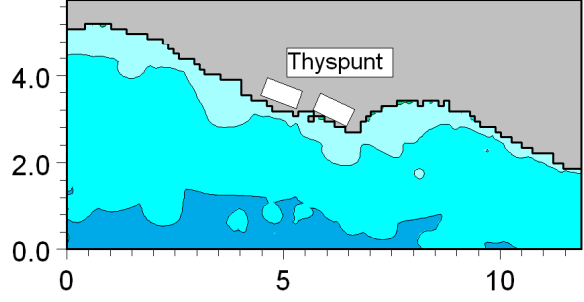
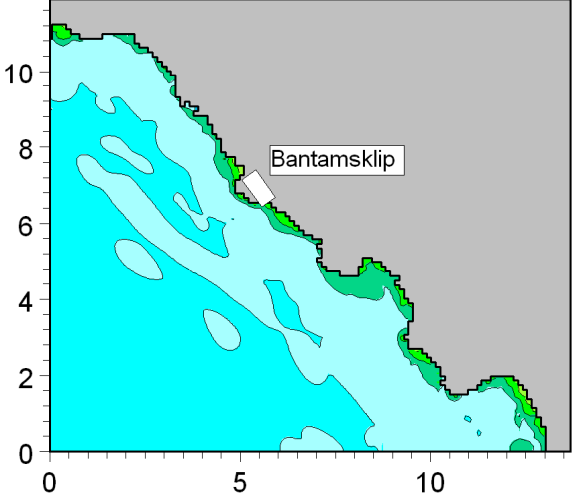


These are the minimum tsunami-induced water levels below Still Water Level. The total water level will additionally include the effect of tide and storm surge.

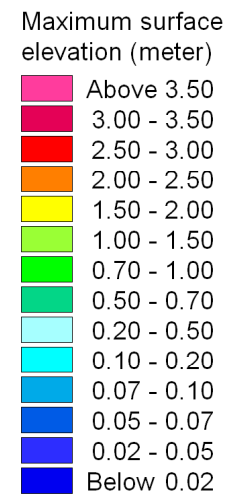


**Title: Minimum water levels predicted during tsunami event. Source is South Sandwich Islands A: maximum credible earthquake determined by the Council for Geoscience, Mw = 7.6.**

Run: SouthSandwich04\_MSL\_a



These are the maximum tsunami-induced water levels above Still Water Level. The total water level will additionally include the effect of tide, wave run-up, wave set-up and storm surge.



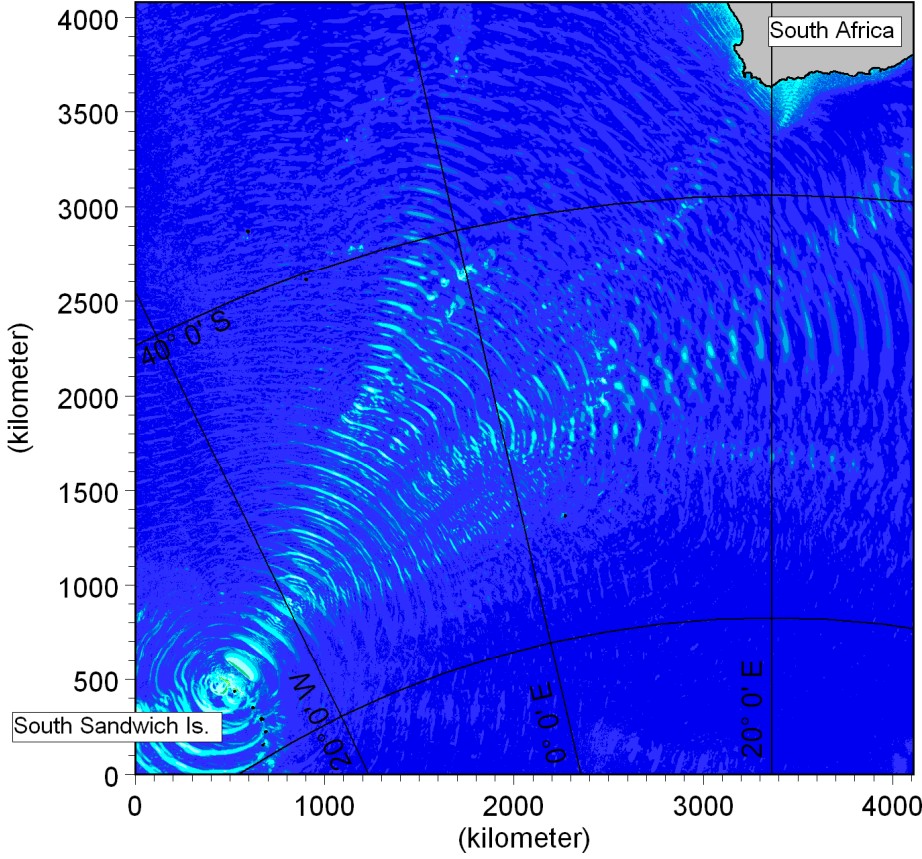
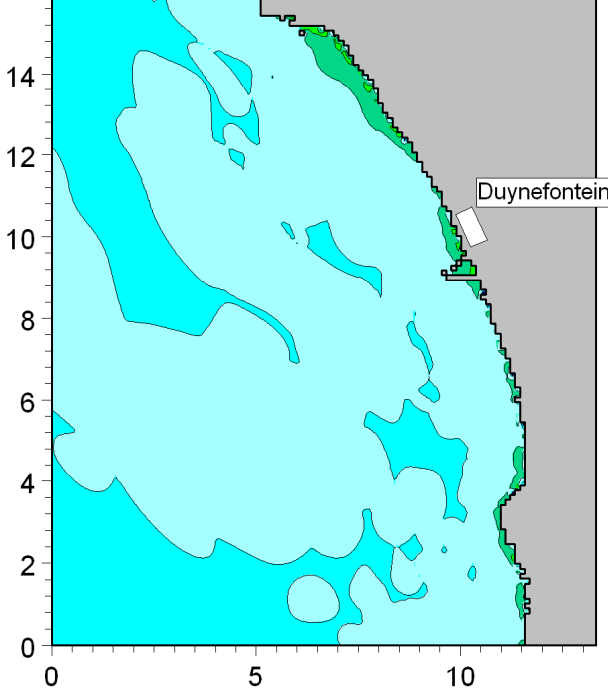
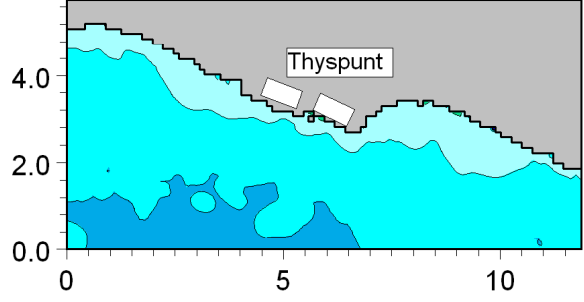
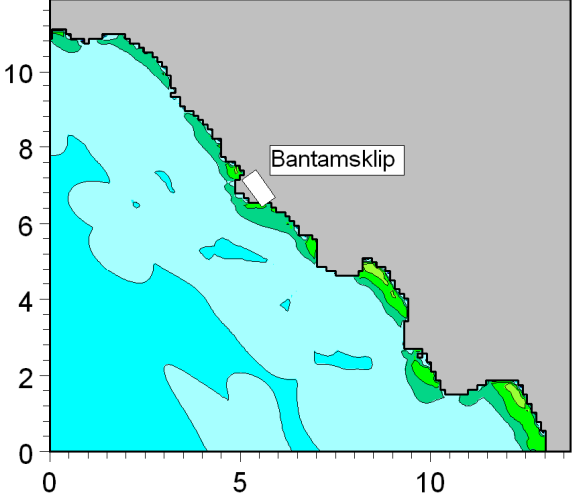
Title:

**Maximum water levels predicted during tsunami event.  
Source is South Sandwich Islands B: magnitude increased to Mw = 8.0.**

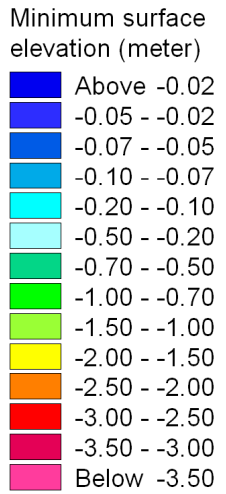
Figure No.

**5.14**

Run: SouthSandwich04\_MSL\_a



These are the minimum tsunami-induced water levels below Still Water Level. The total water level will additionally include the effect of tide and storm surge.

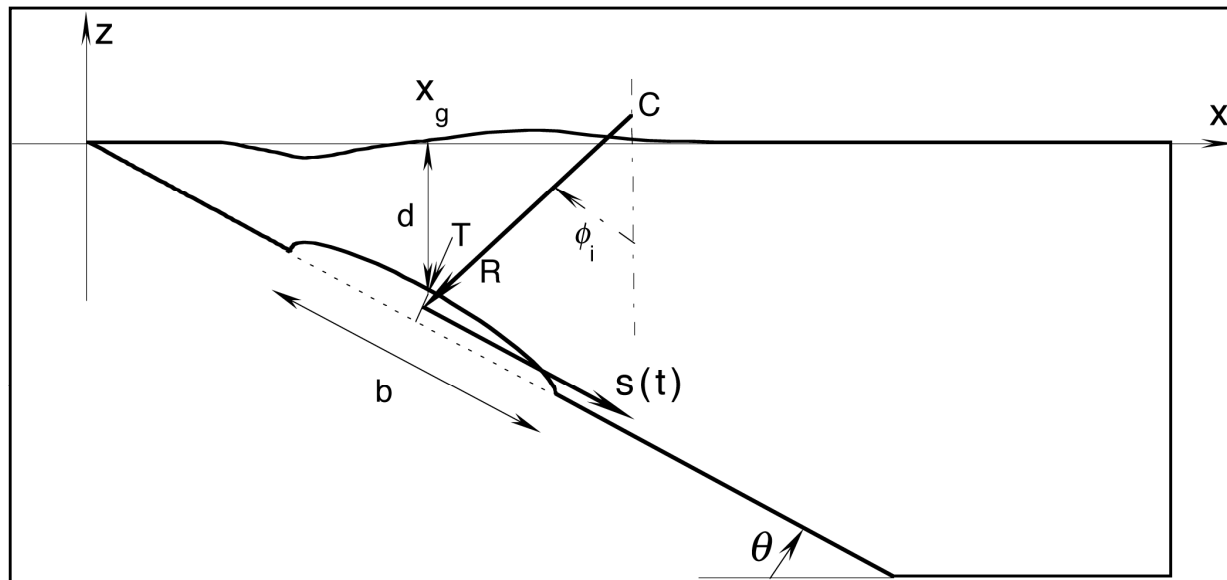
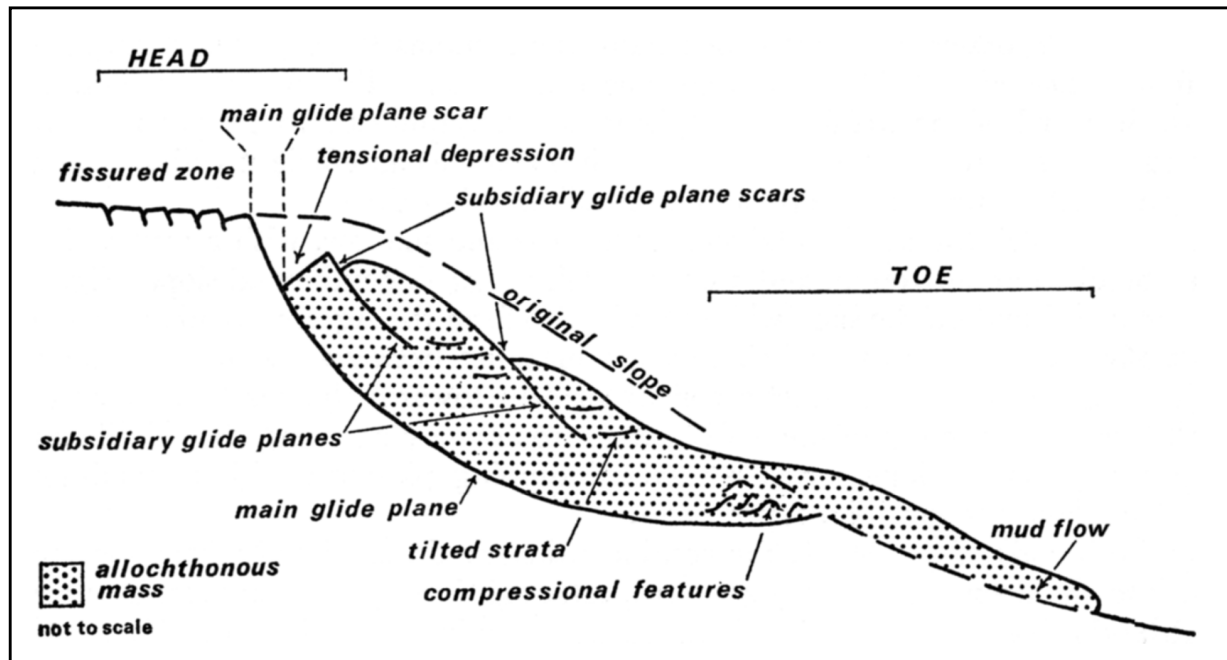


Title:

**Minimum water levels predicted during tsunami event.  
Source is South Sandwich Islands B: magnitude increased to Mw = 8.0.**

Figure No.

**5.15**



Title:

Top: Main morphological and structural features of submarine slumps (Dingle, 1977).  
 Bottom: Parameters defining slump model (Watts et al, 2003).

Figure No.

5.16

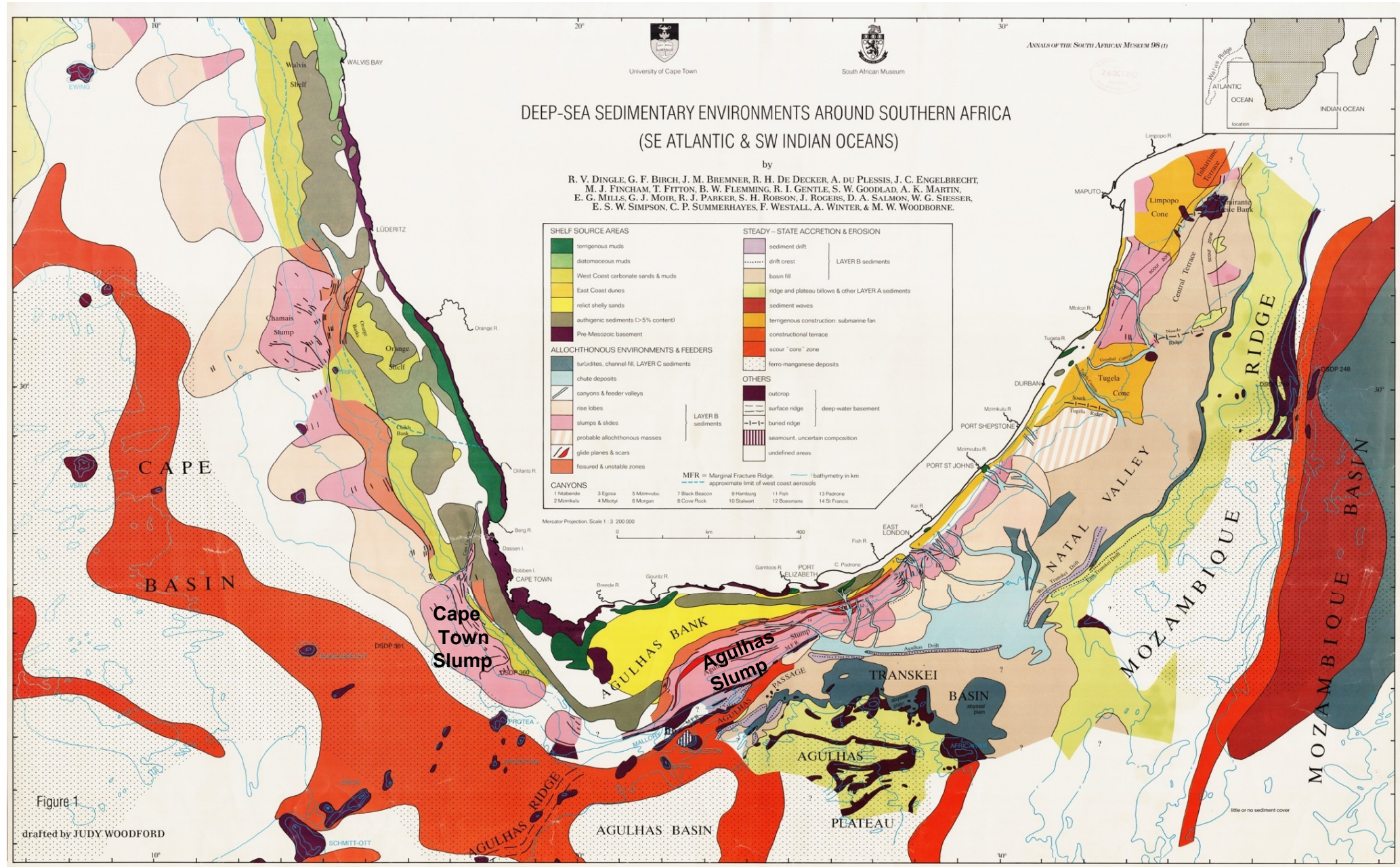


Figure 1  
 drafted by JUDY WOODFORD

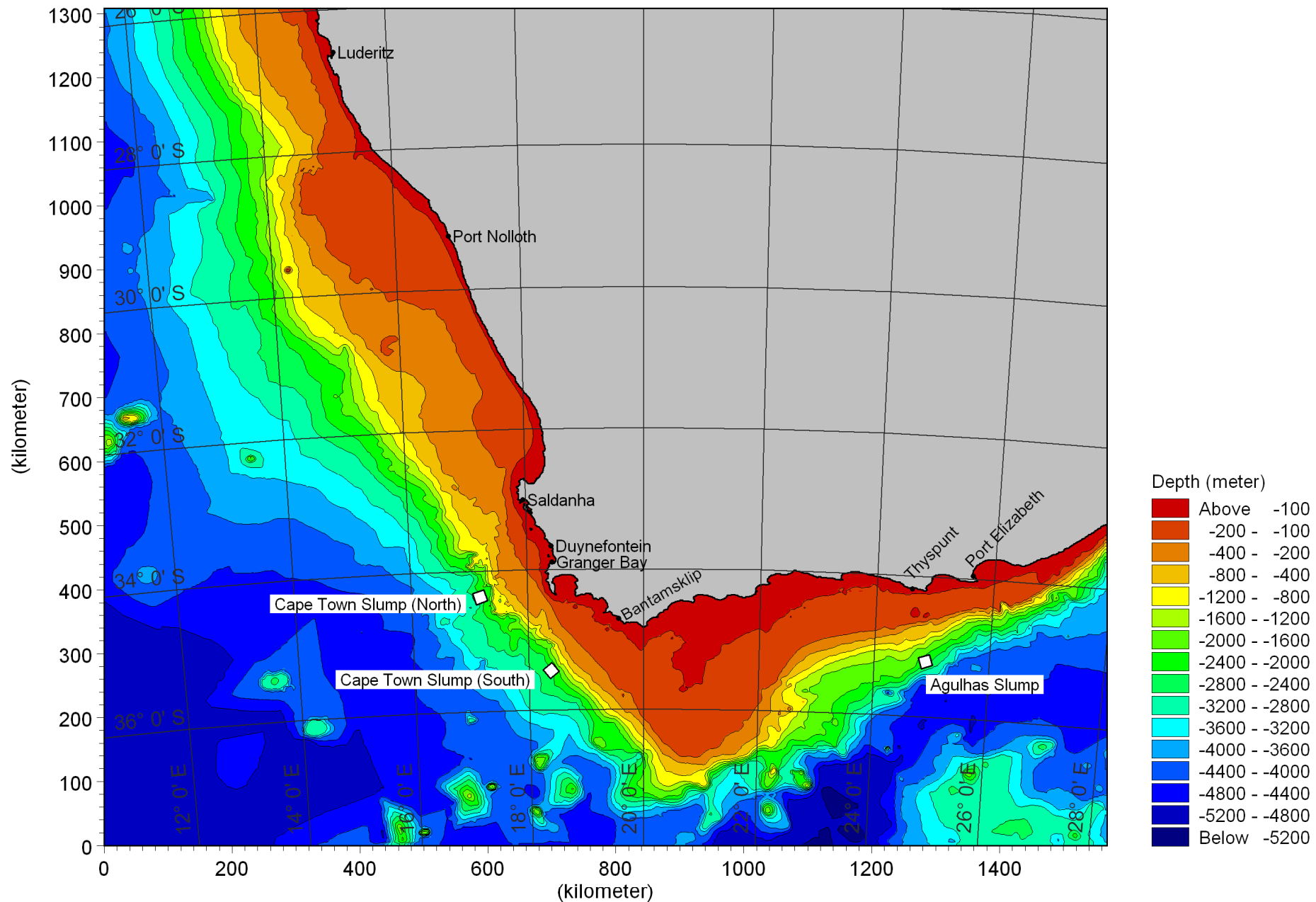


Title:

Location of slump zones around Southern Africa shown in pink (Dingle et al, 1987).

Figure No.

5.17



**Title:** Model bathymetry used for tsunami modelling due to slumps on the South African shelf margin. Locations of the three slumps modelled are indicated.

**Figure No.**  
5.18

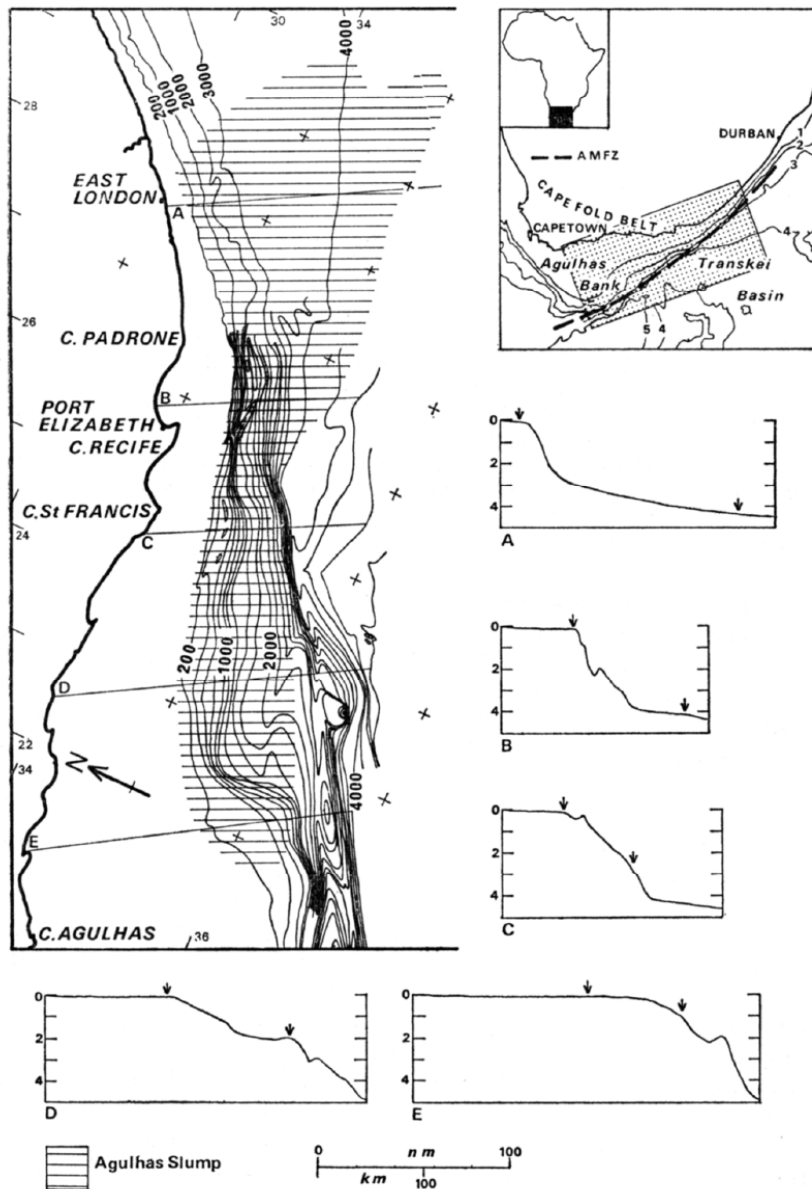


FIG. 1. Bathymetry (in metres) and bathymetric profiles (in kilometres) on the SE Agulhas Bank. Insert shows location of area; AMFZ, Agulhas marginal fracture zone. Arrows on profiles show limits of slump.

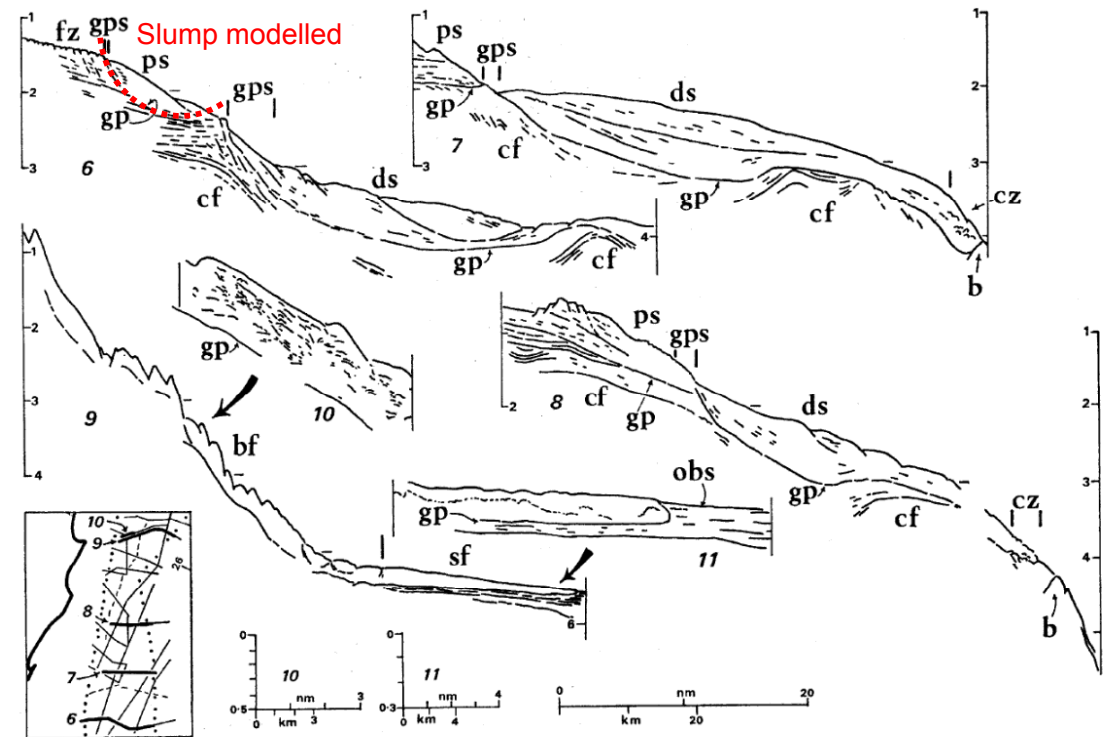


FIG. 6. Replotted (6-9) and traced (10 & 11) seismic profiles across the distal part of the Agulhas Slump. Vertical scales in seconds DT. For abbreviations see explanation to Fig. 4. For location of profile 11 see Fig. 3.

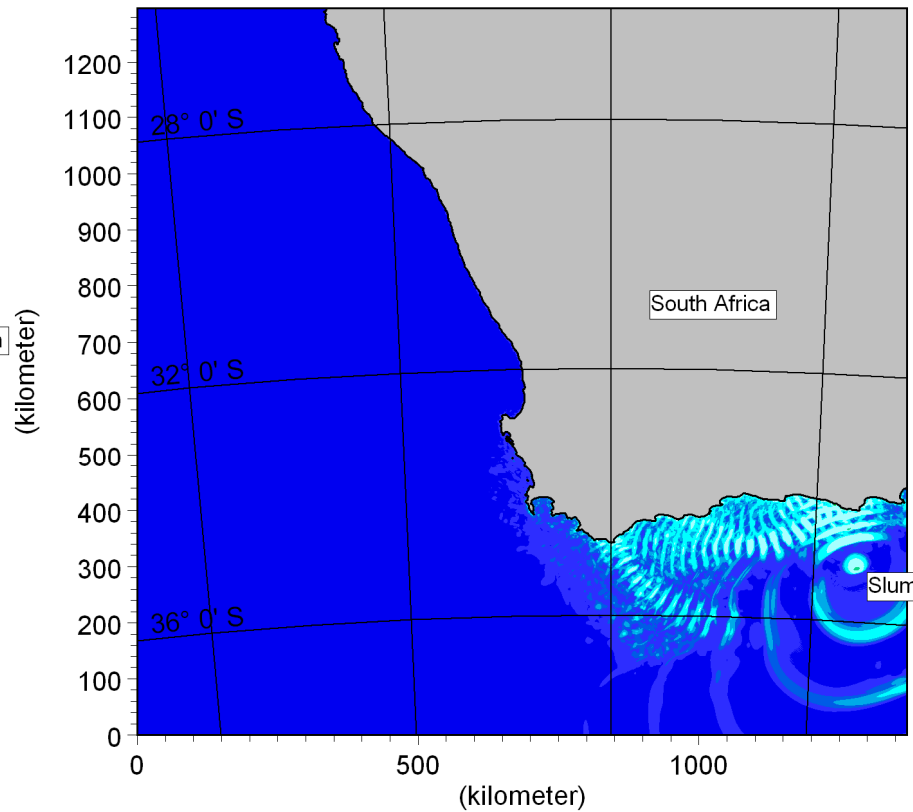
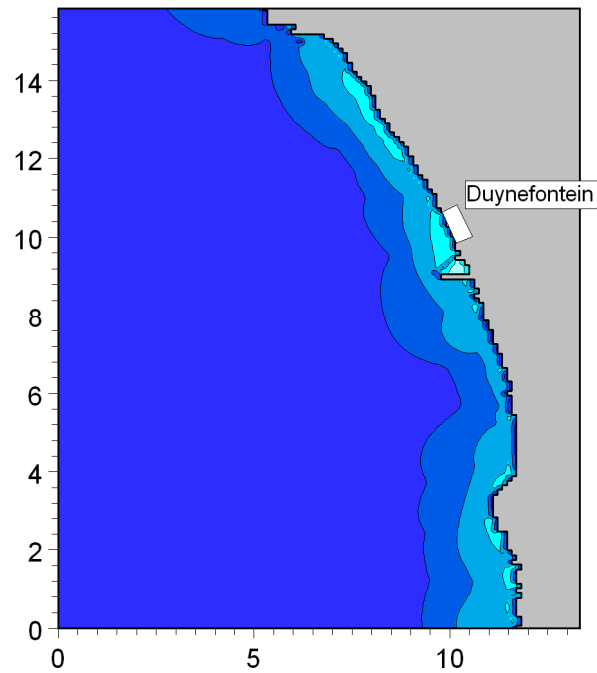
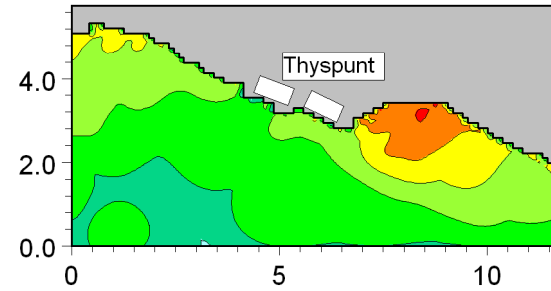
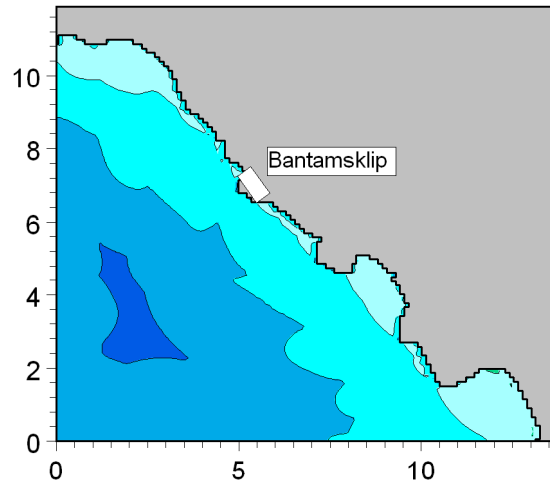


Title:

Details of the Agulhas Slump (Dingle, 1977).

Figure No.

5.19



Maximum surface elevation (meter)

- Above 3.50
- 3.00 - 3.50
- 2.50 - 3.00
- 2.00 - 2.50
- 1.50 - 2.00
- 1.00 - 1.50
- 0.70 - 1.00
- 0.50 - 0.70
- 0.20 - 0.50
- 0.10 - 0.20
- 0.07 - 0.10
- 0.05 - 0.07
- 0.02 - 0.05
- Below 0.02

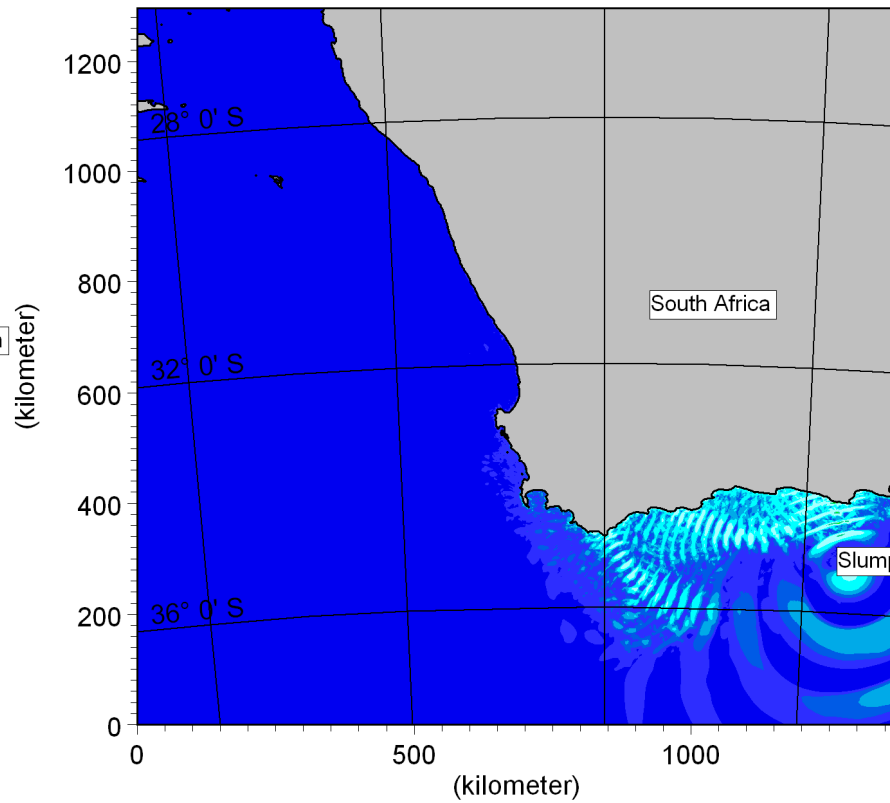
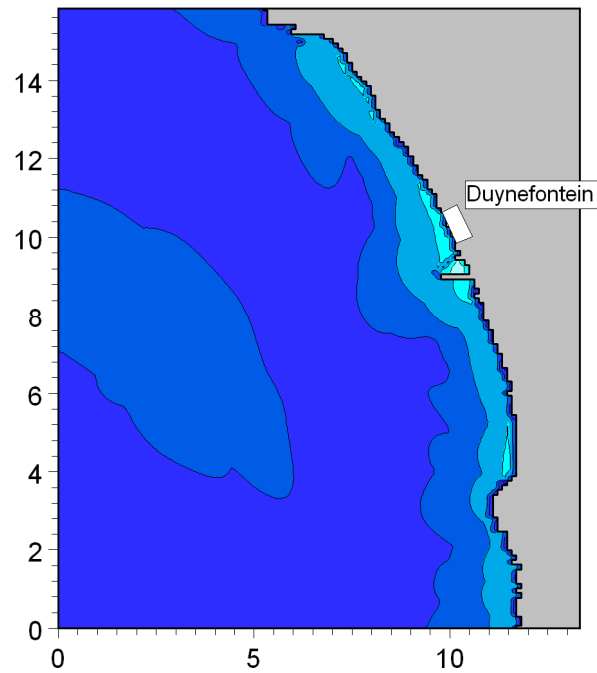
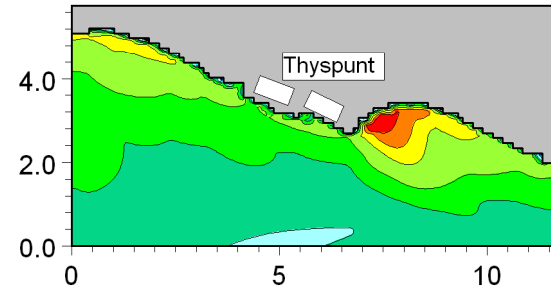
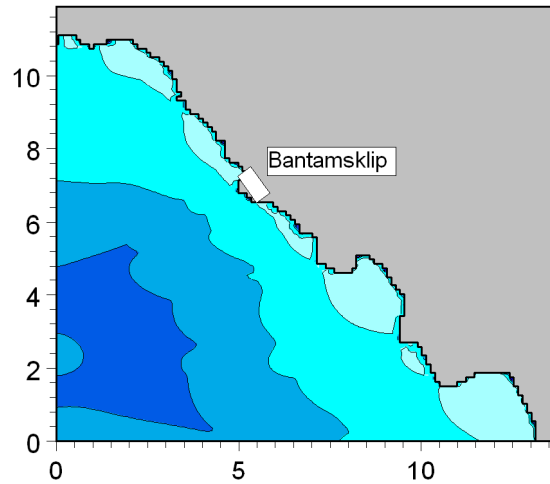


Title:

**Maximum water levels predicted during tsunami event.  
Source is theoretical Agulhas Slump with volume of slumped sediment = 80 km<sup>3</sup>.**

Figure No.

**5.20**



Minimum surface elevation (meter)

- Above -0.02
- 0.05 - -0.02
- 0.07 - -0.05
- 0.10 - -0.07
- 0.20 - -0.10
- 0.50 - -0.20
- 0.70 - -0.50
- 1.00 - -0.70
- 1.50 - -1.00
- 2.00 - -1.50
- 2.50 - -2.00
- 3.00 - -2.50
- 3.50 - -3.00
- Below -3.50



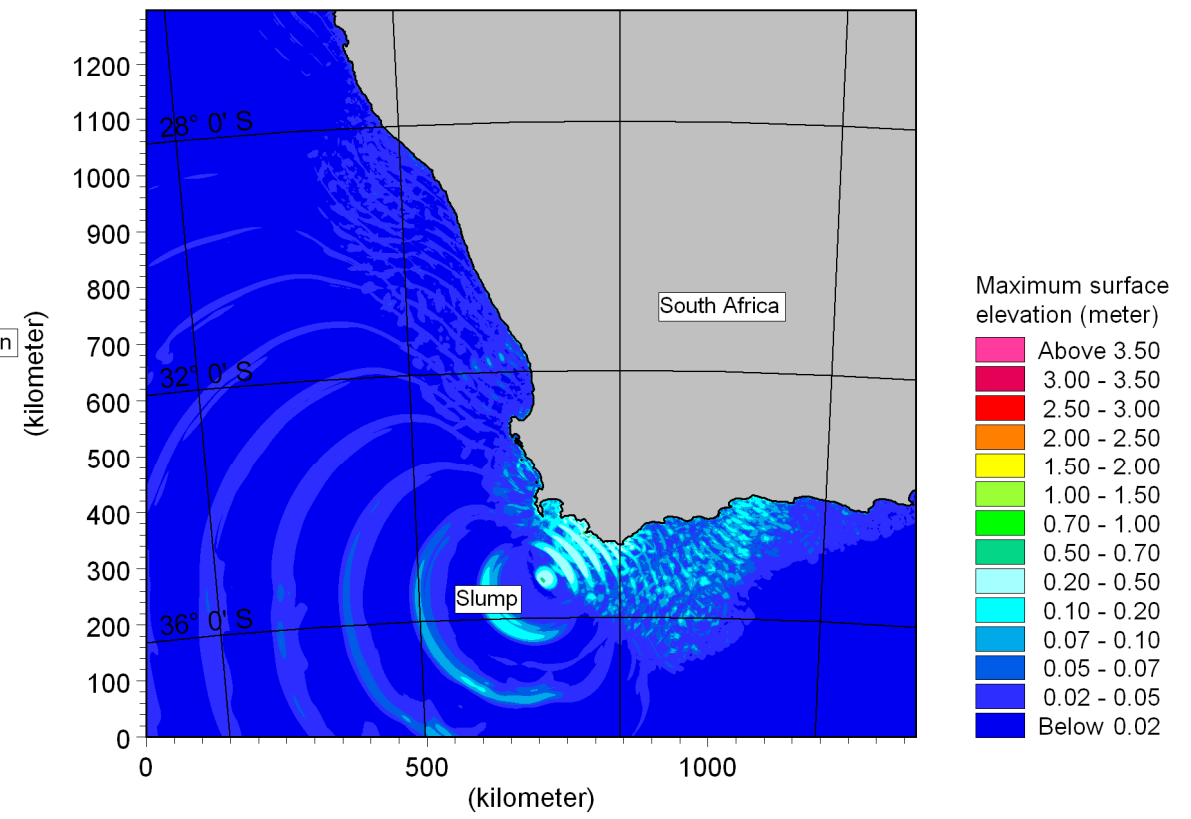
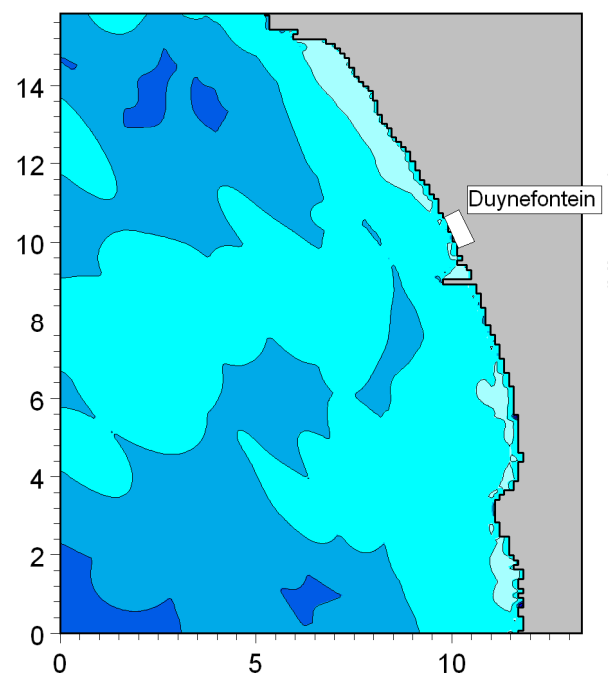
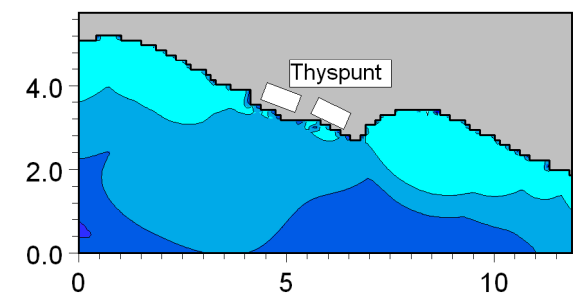
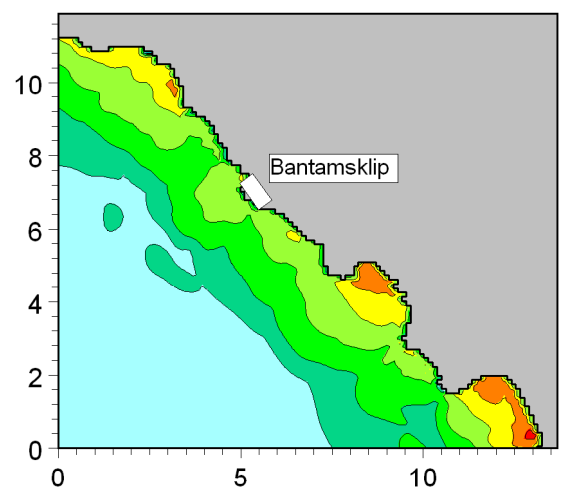
Title:

**Minimum water levels predicted during tsunami event.  
Source is theoretical Agulhas Slump with volume of slumped sediment = 80 km<sup>3</sup>.**

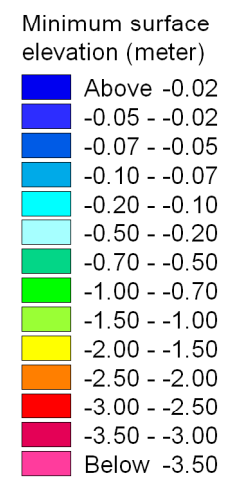
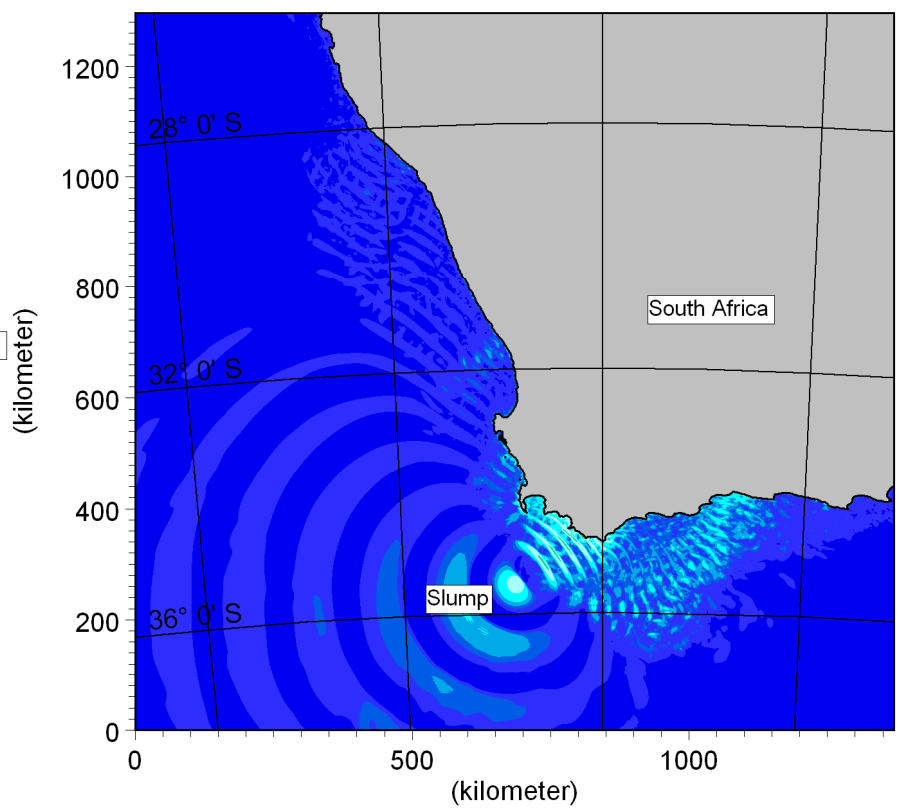
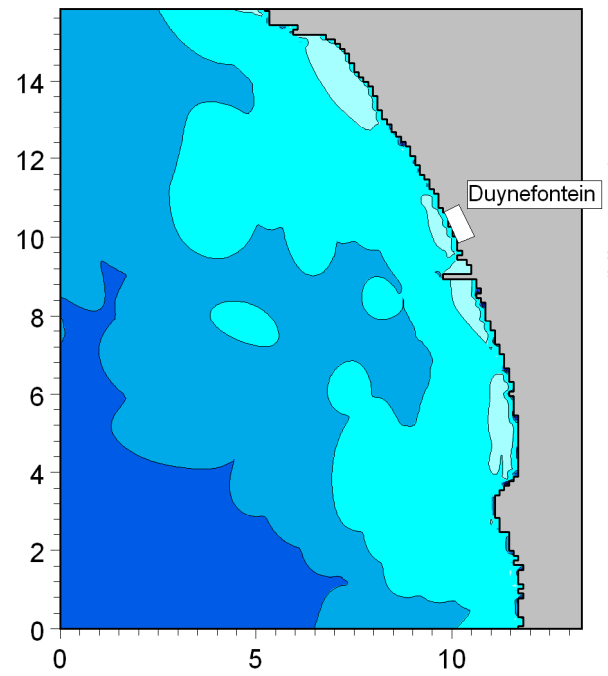
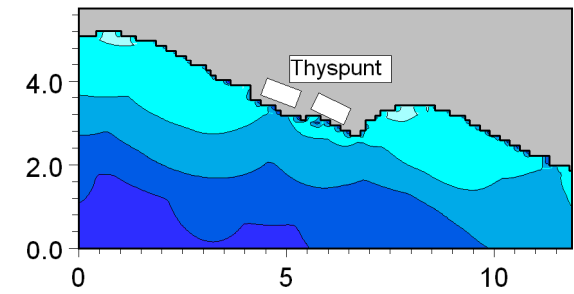
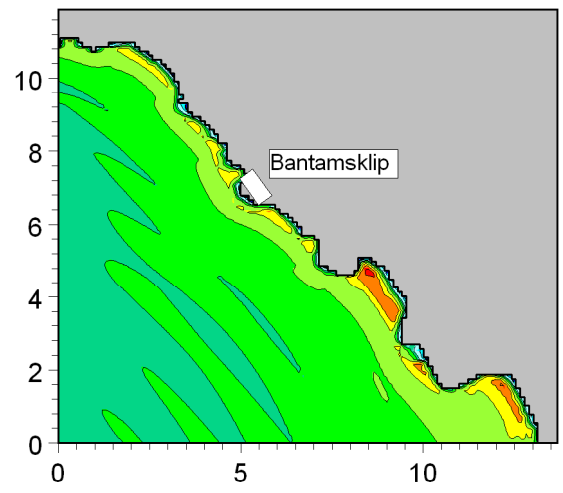
Figure No.

**5.21**

Run: CapeTownSouth01b

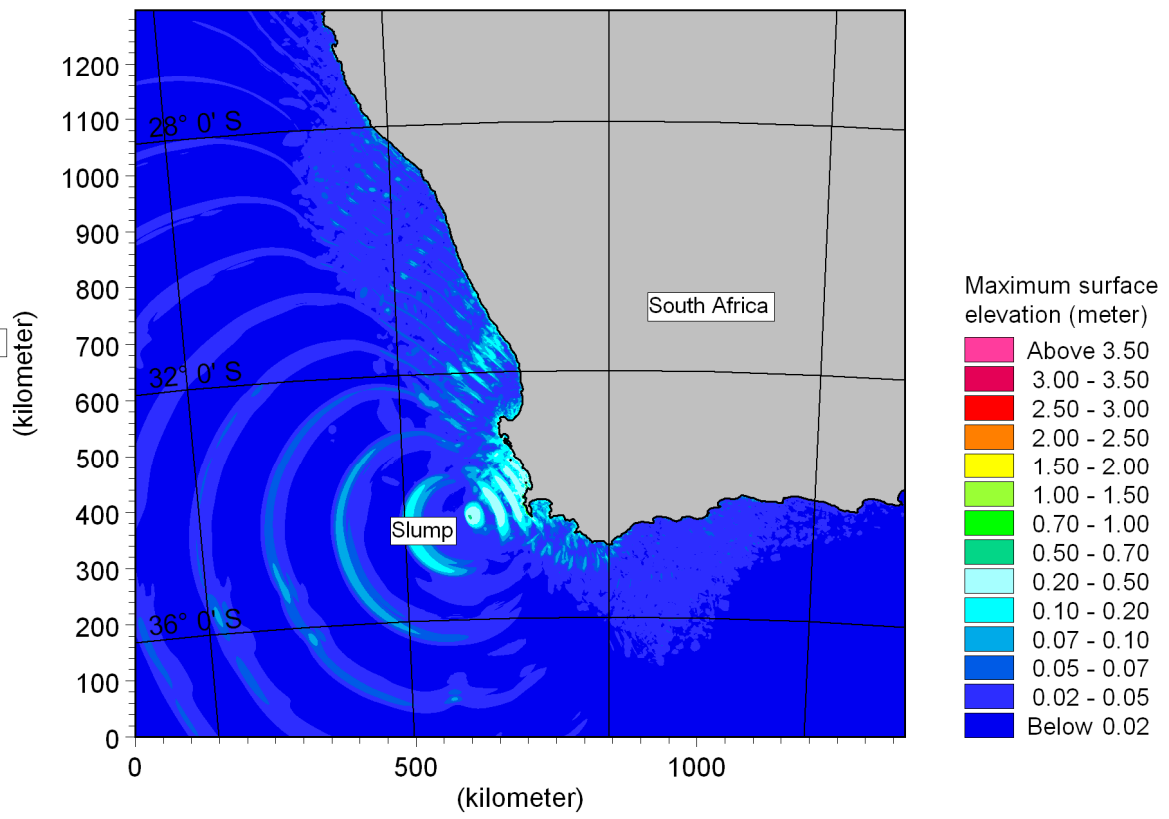
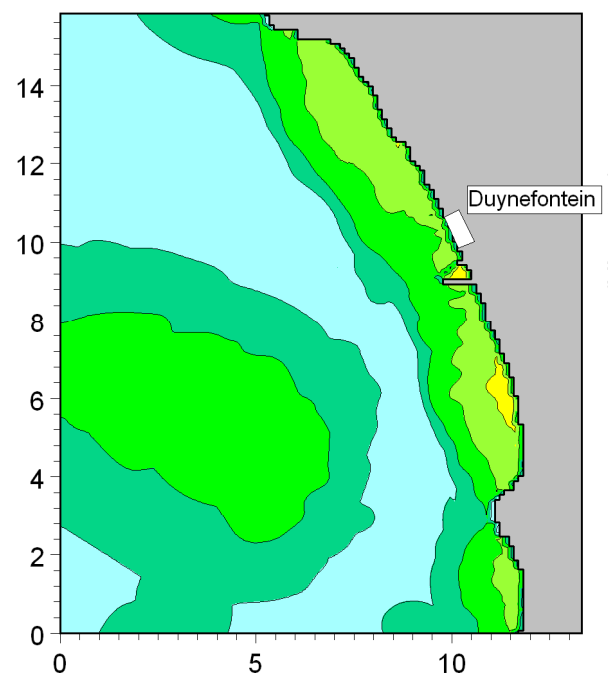
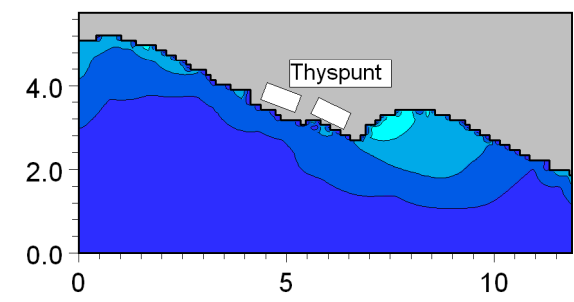
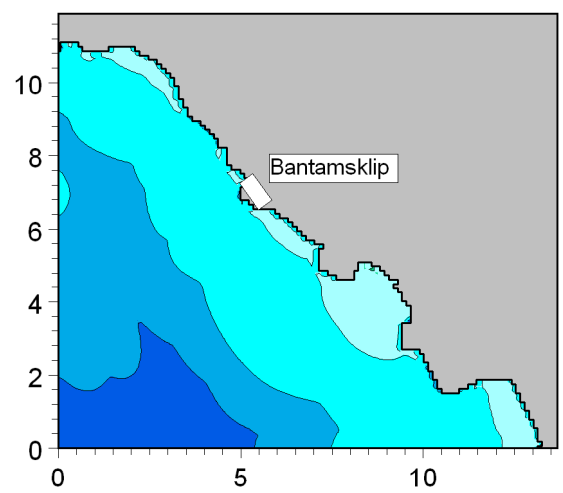


**Title:** Maximum water levels predicted during tsunami event.  
Source is theoretical Cape Town Slump (South) with volume of slumped sediment = 80 km<sup>3</sup>.



**Title:** Minimum water levels predicted during tsunami event.  
Source is theoretical Cape Town Slump (South) with volume of slumped sediment = 80 km<sup>3</sup>.

Run: CapeTownNorth01b



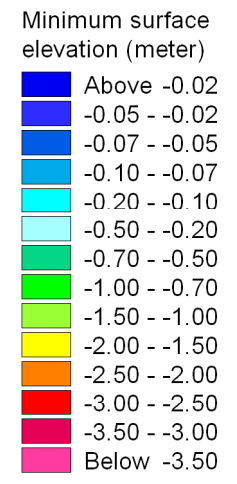
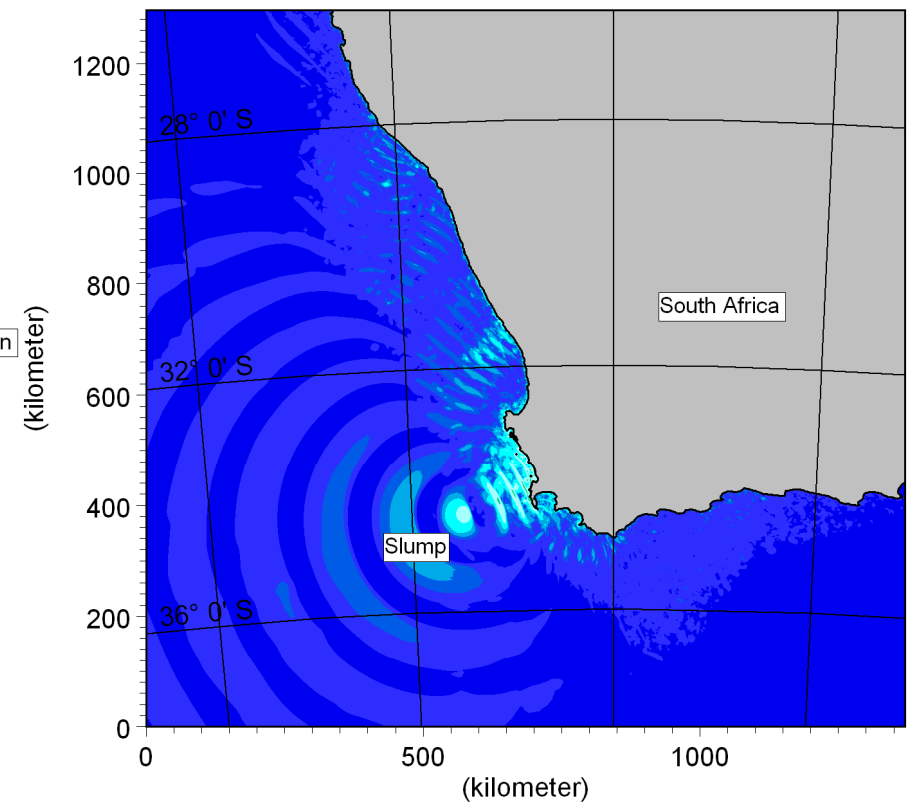
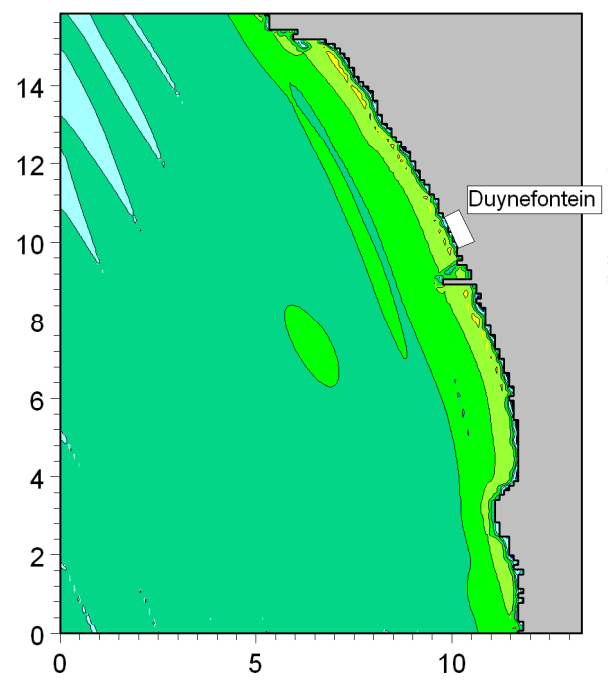
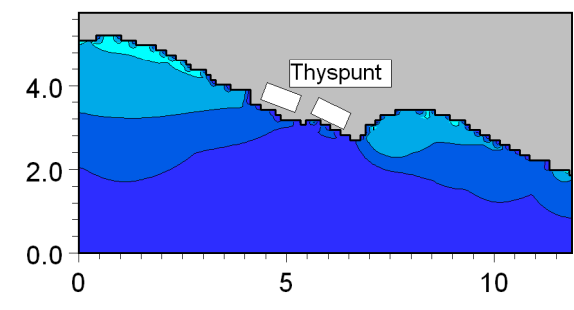
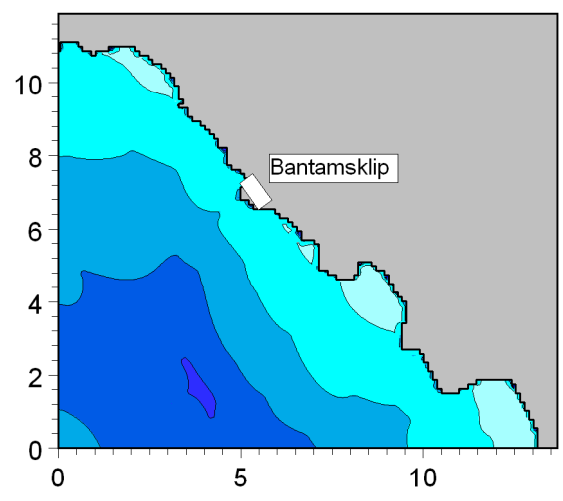
Title:

**Maximum water levels predicted during tsunami event.  
Source is theoretical Cape Town Slump (North) with volume of slumped sediment = 80 km<sup>3</sup>.**

Figure No.

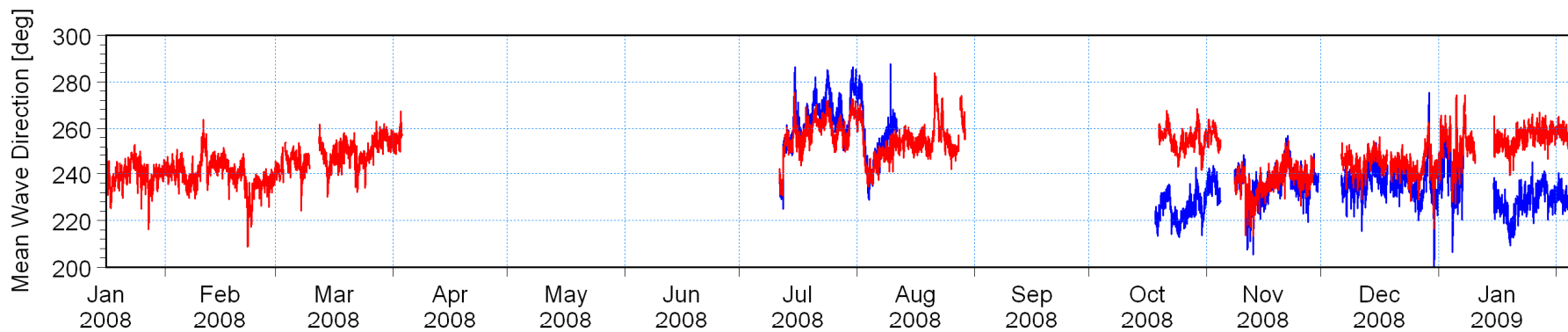
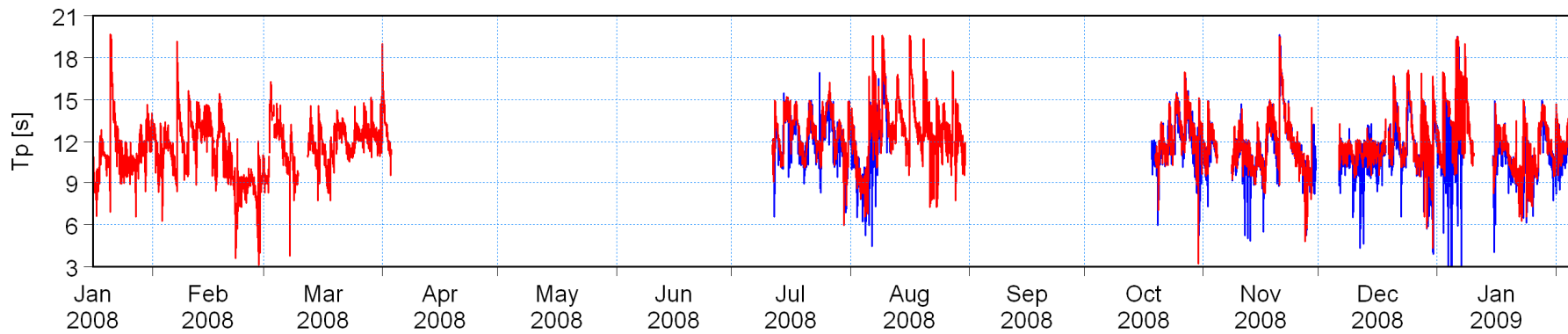
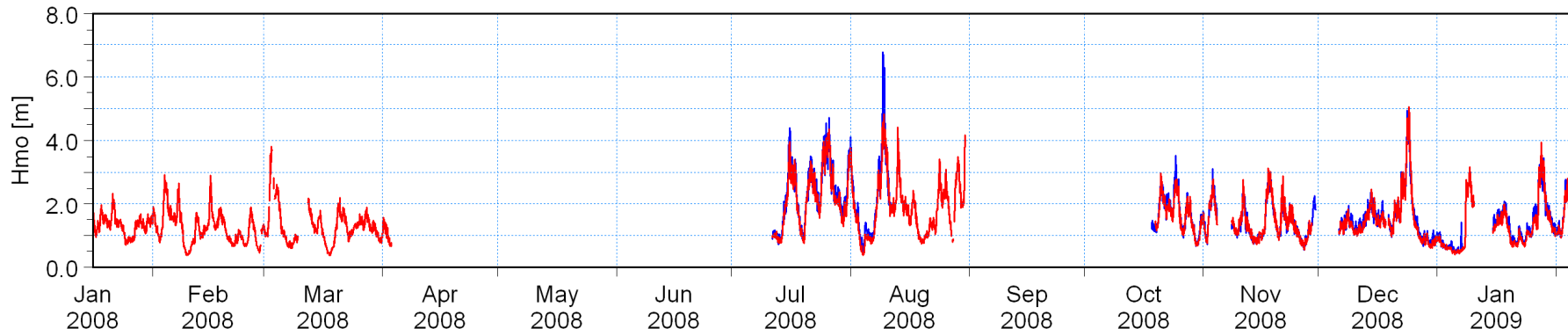
**5.24**

Run: CapeTownNorth01b



**Title:** Minimum water levels predicted during tsunami event.  
Source is theoretical Cape Town Slump (North) with volume of slumped sediment = 80 km<sup>3</sup>.

Site B (Water depth = 30 m) [m] — blue line  
Site A (Water depth = 10 m) [m] — red line



Title:

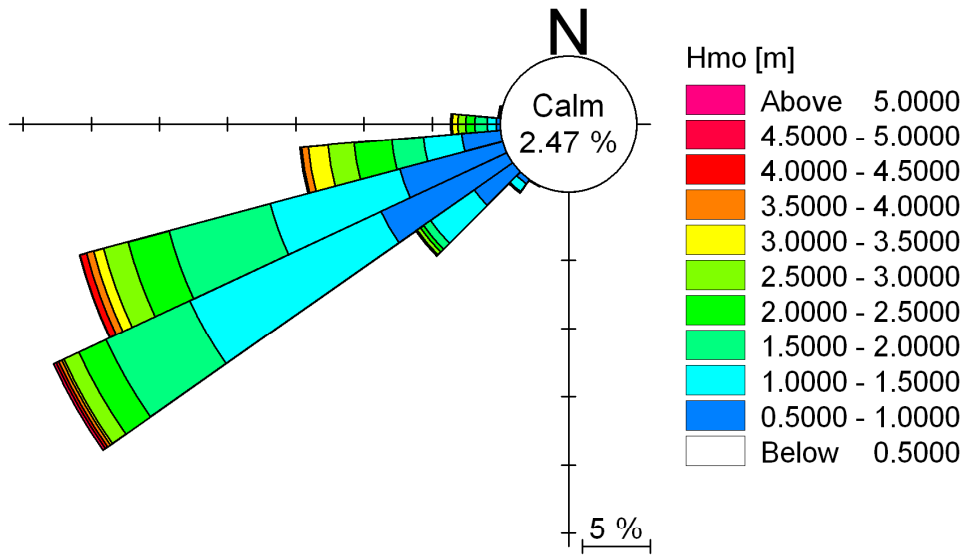
**Wave measurements at Duynefontein Sites A and B.  
Time-series of wave parameters (refer to Figure 1.2 for instrument positions).**

Figure No.

6.1

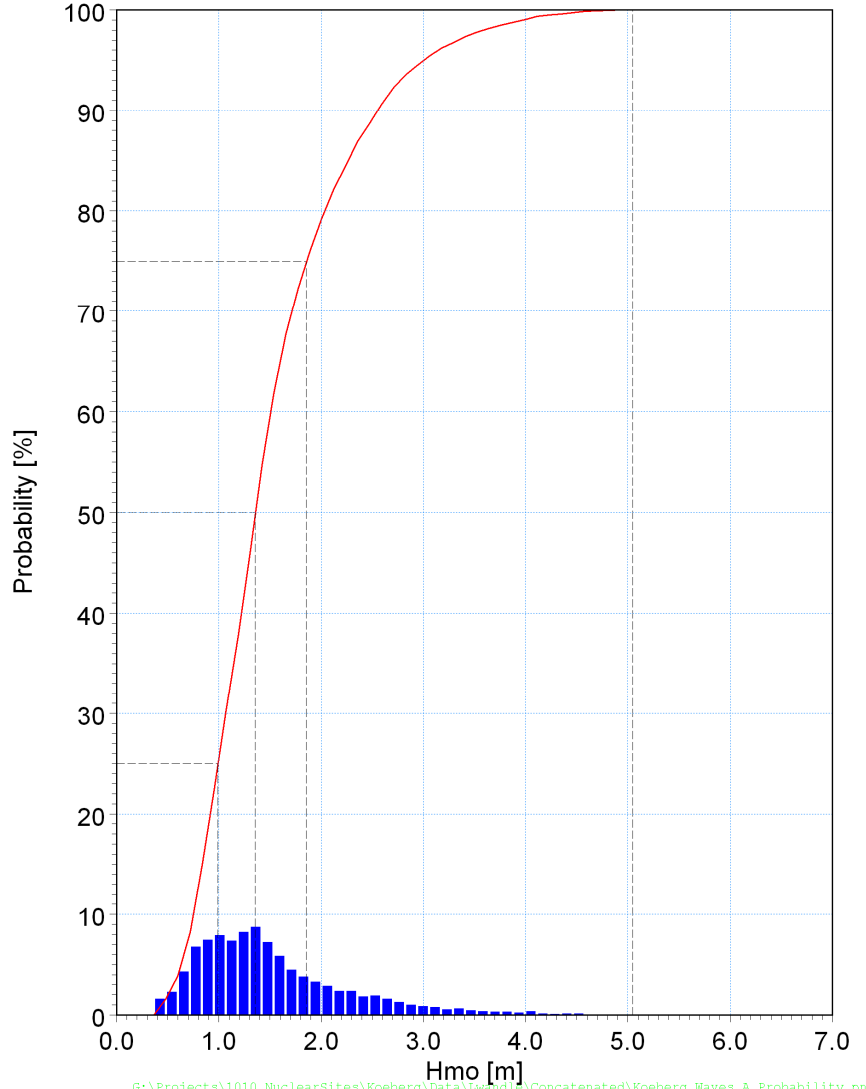
Wave Rose

G:\Projects\1010\_NuclearSites\Koeberg\Data\Lwandle\Concatenated\Koeberg\_Waves\_A\_Rose.png



Wave Height Histogram

000.0%: 0.37078  
 025.0%: 0.98876  
 050.0%: 1.35320  
 075.0%: 1.85392  
 100.0%: 5.04805



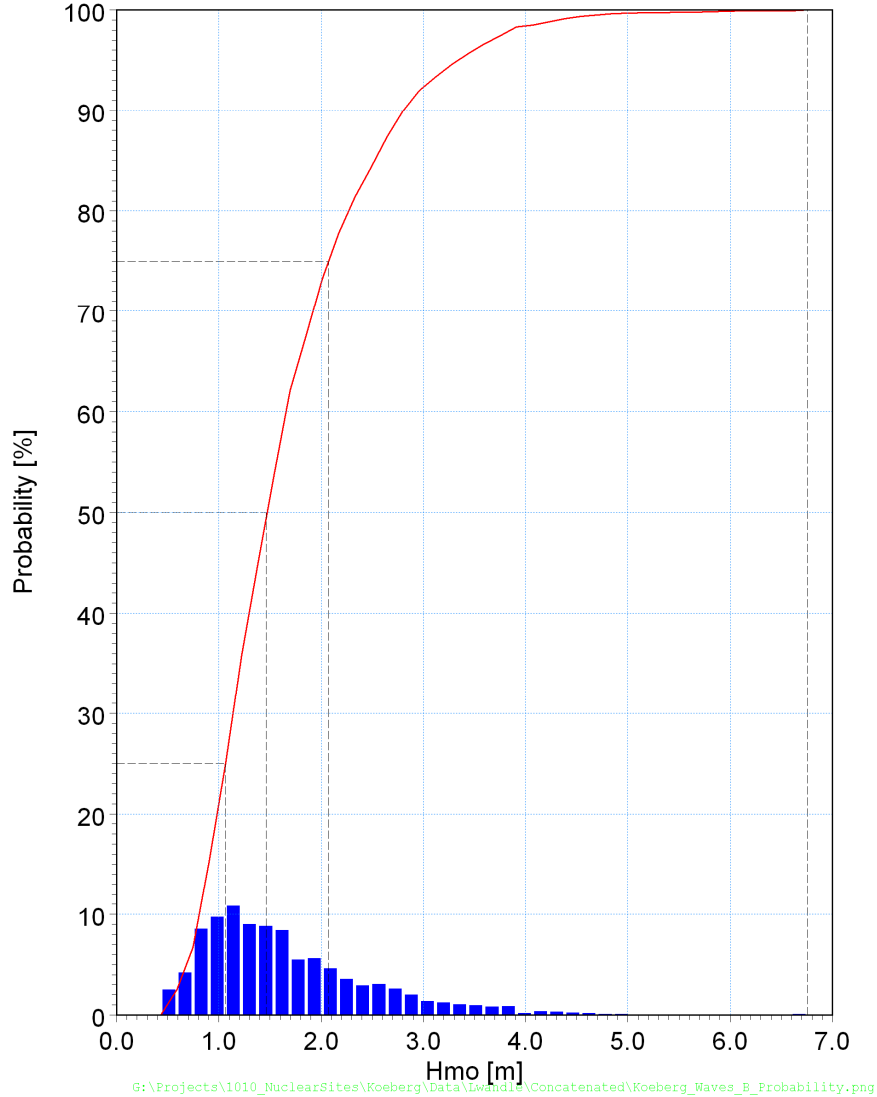
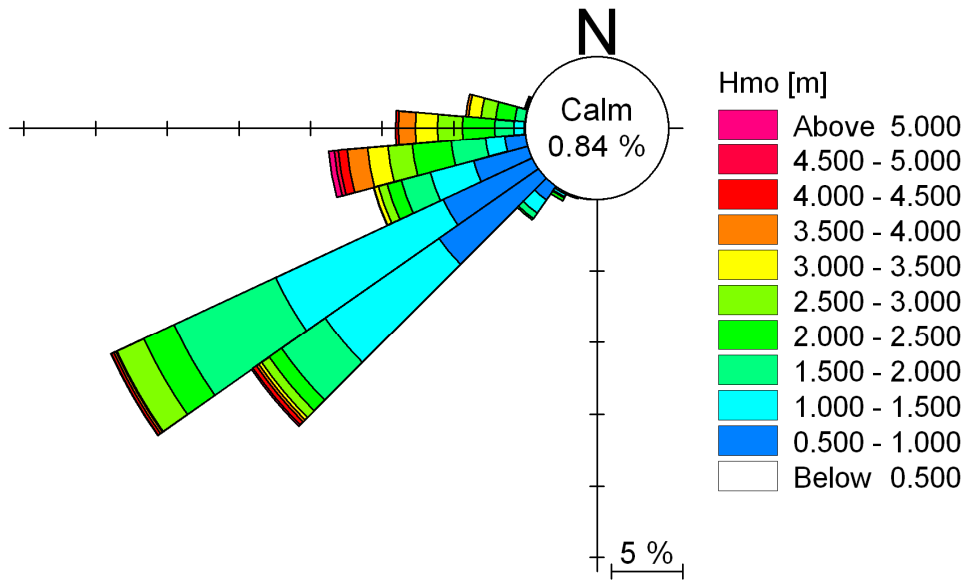
**Title:** Wave measurements at Duynfontein Site A (refer to Figure 1.2 for instrument position).  
 Wave rose and histogram of wave heights.

Wave Rose

Wave Height Histogram

000.0%: 0.44139  
 025.0%: 1.06334  
 050.0%: 1.46171  
 075.0%: 2.07210  
 100.0%: 6.75659

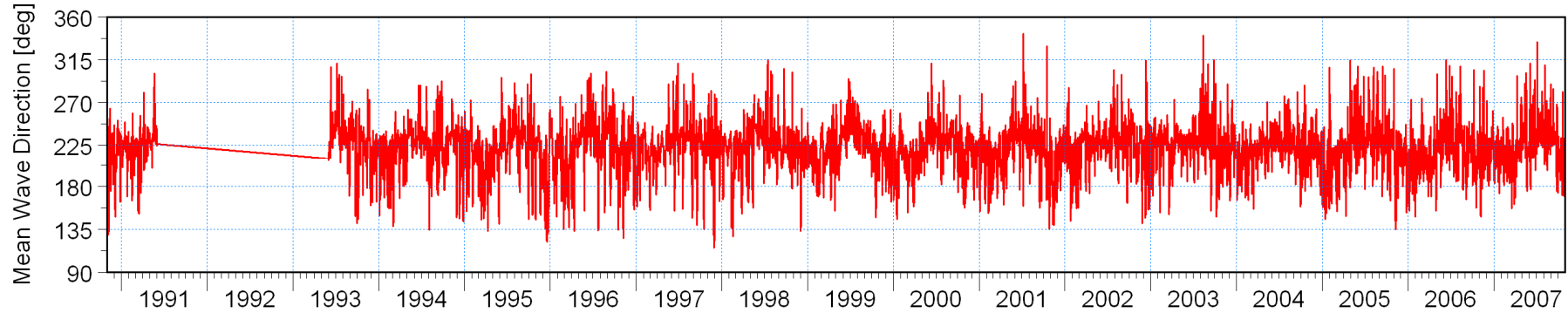
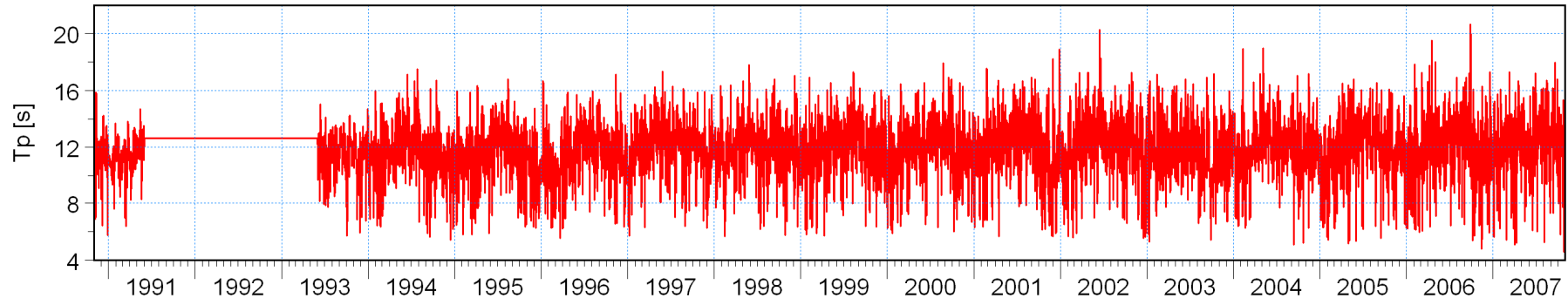
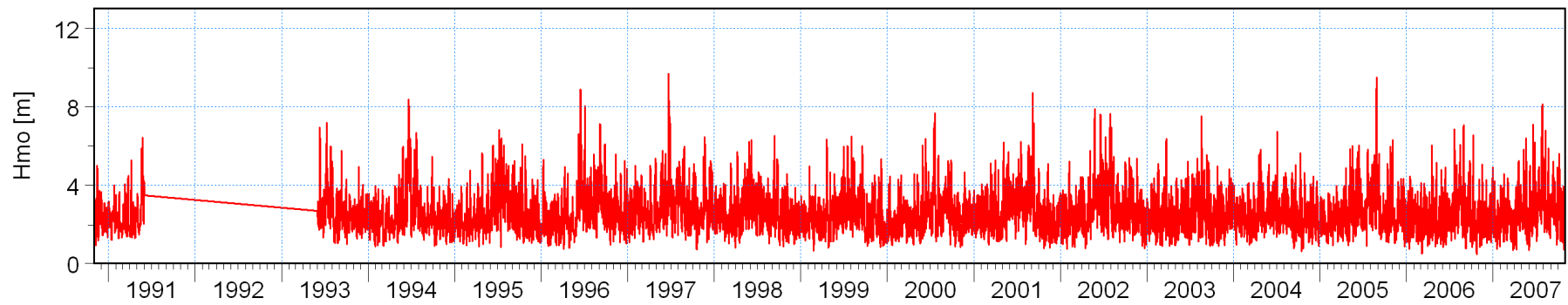
G:\Projects\1010\_NuclearSites\Koeberg\Data\Lwandle\Concatenated\Koeberg\_Waves\_B\_Rose.png



G:\Projects\1010\_NuclearSites\Koeberg\Data\Lwandle\Concatenated\Koeberg\_Waves\_B\_Probability.png



**Title:** Wave measurements at Duynefontein Site B (refer to Figure 1.2 for instrument position).  
 Wave rose and histogram of wave heights.

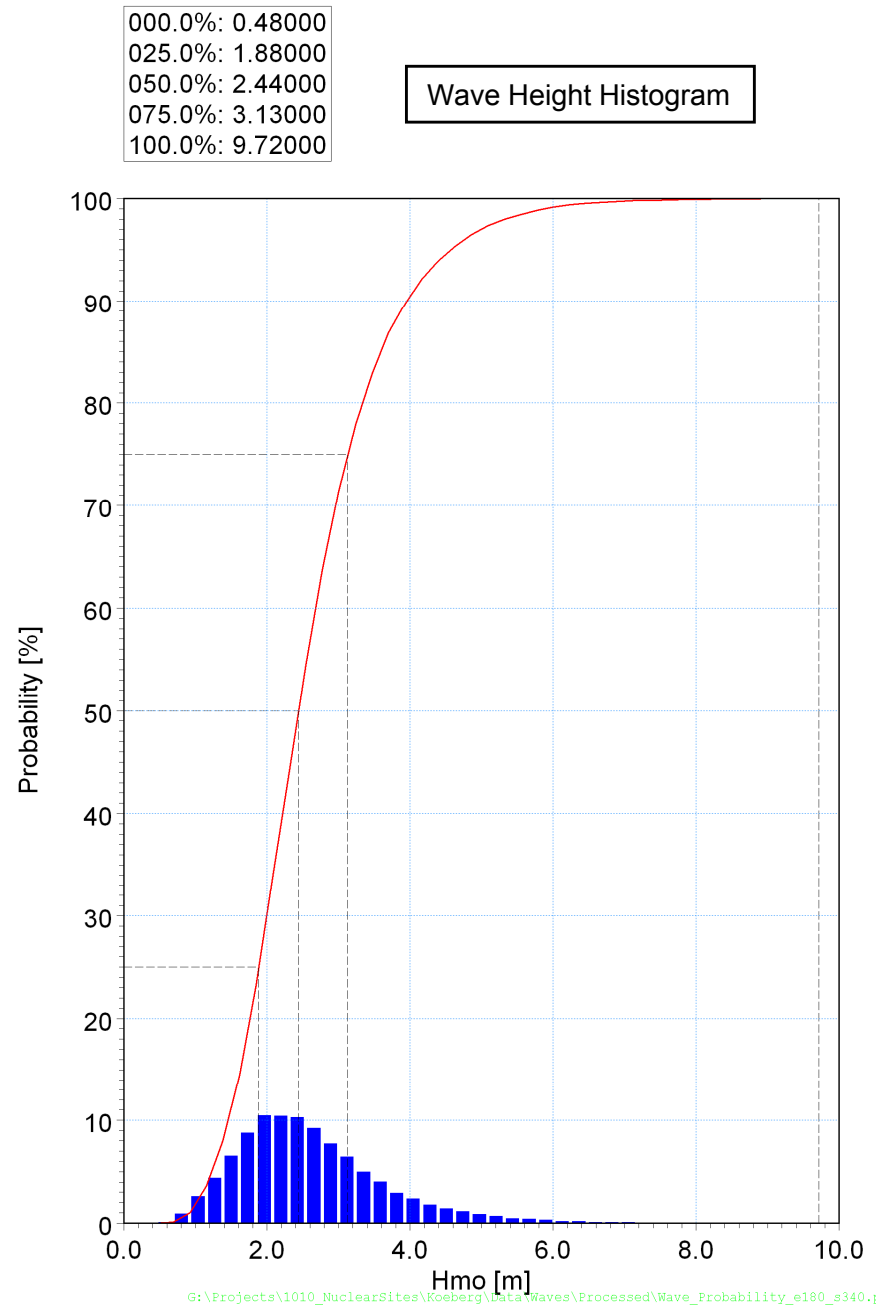
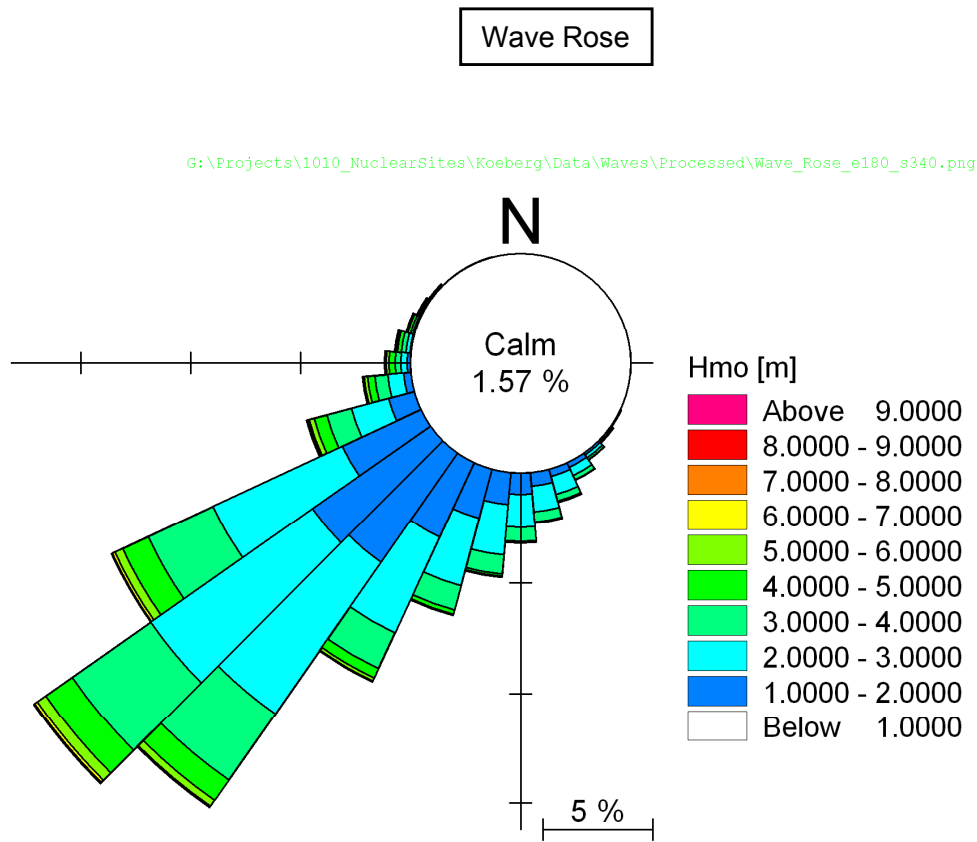


G:\Projects\1010\_NuclearSites\Koeberg\Data\Waves\Processed\Wave\_Parameters\_Oceanor\_e180\_s340\_Timeseries.png



**Title:** Time-series of offshore wave hindcast parameters.  
**Position is 40 km south-west of Cape Town in 200 m depth at position E 18.0°, S 34.0° (refer to Figure 6.6).**

**Figure No.**  
**6.4**

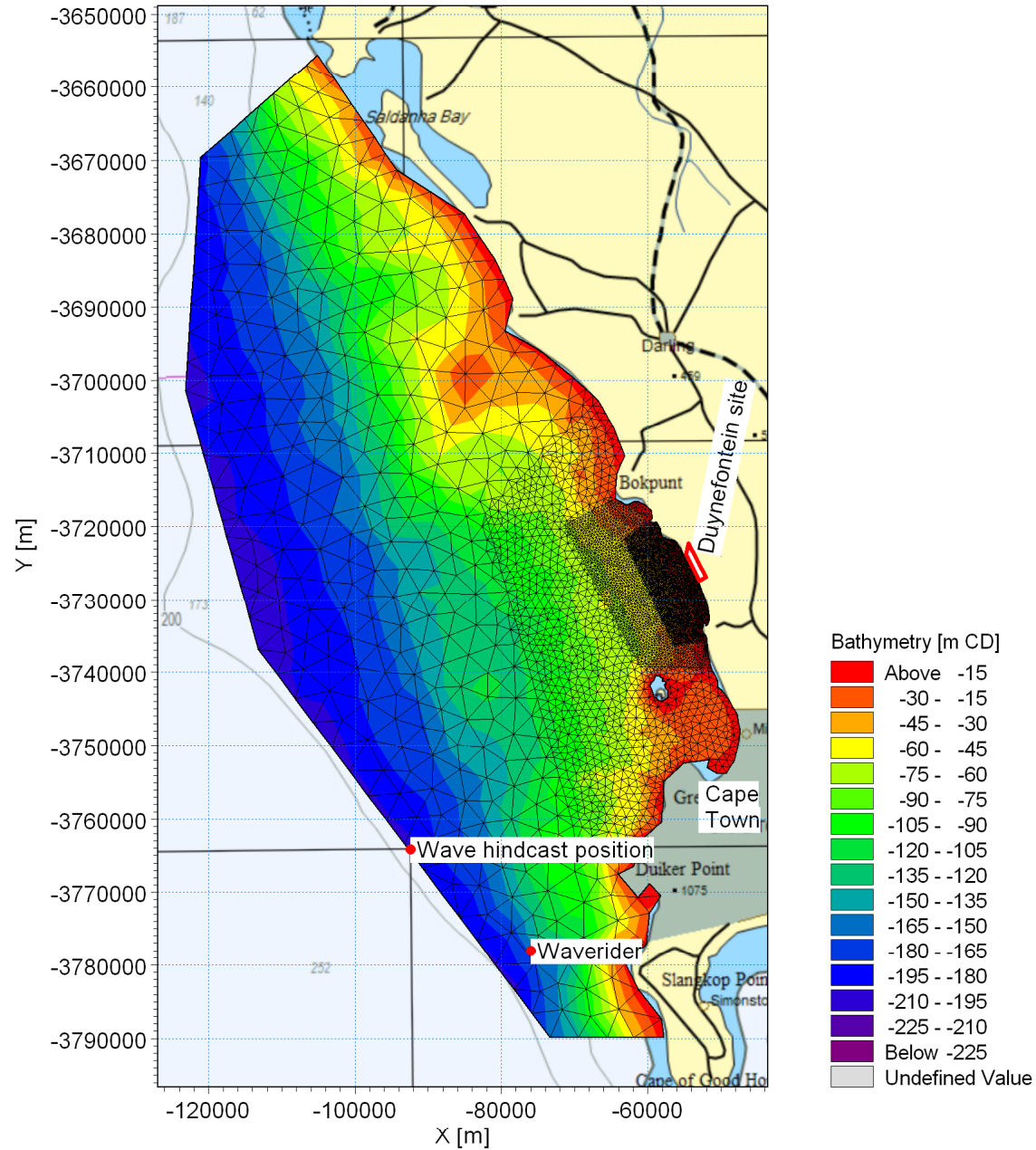


**Title:**

**Rose and histogram of offshore wave hindcast data.  
Position is 40 km south-west of Cape Town in 200 m depth at position E 18.0°, S 34.0° (refer to  
Figure 6.6).**

**Figure No.**

**6.5**

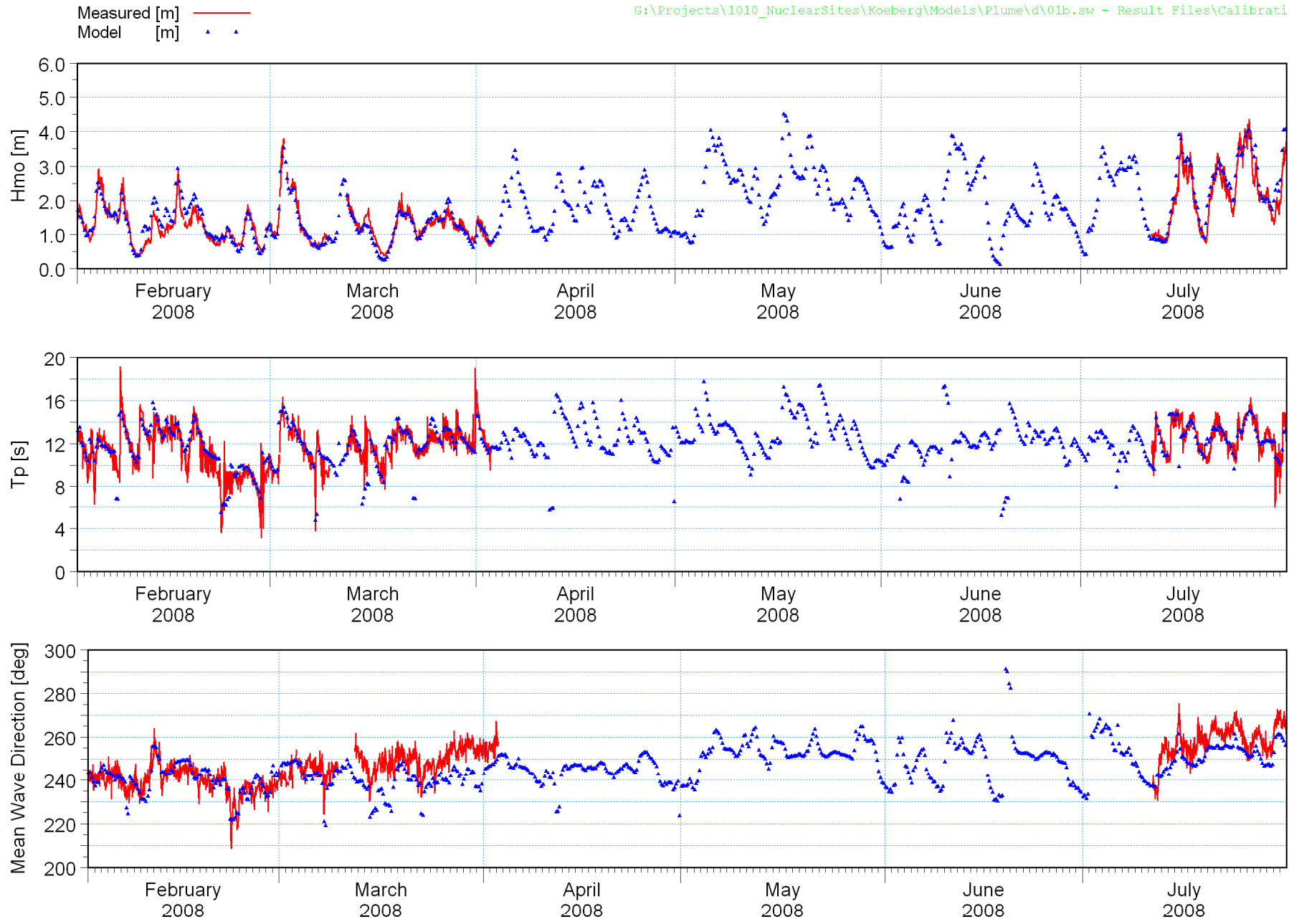


Title:

Numerical mesh used for wave refraction modelling.

Figure No.

6.6

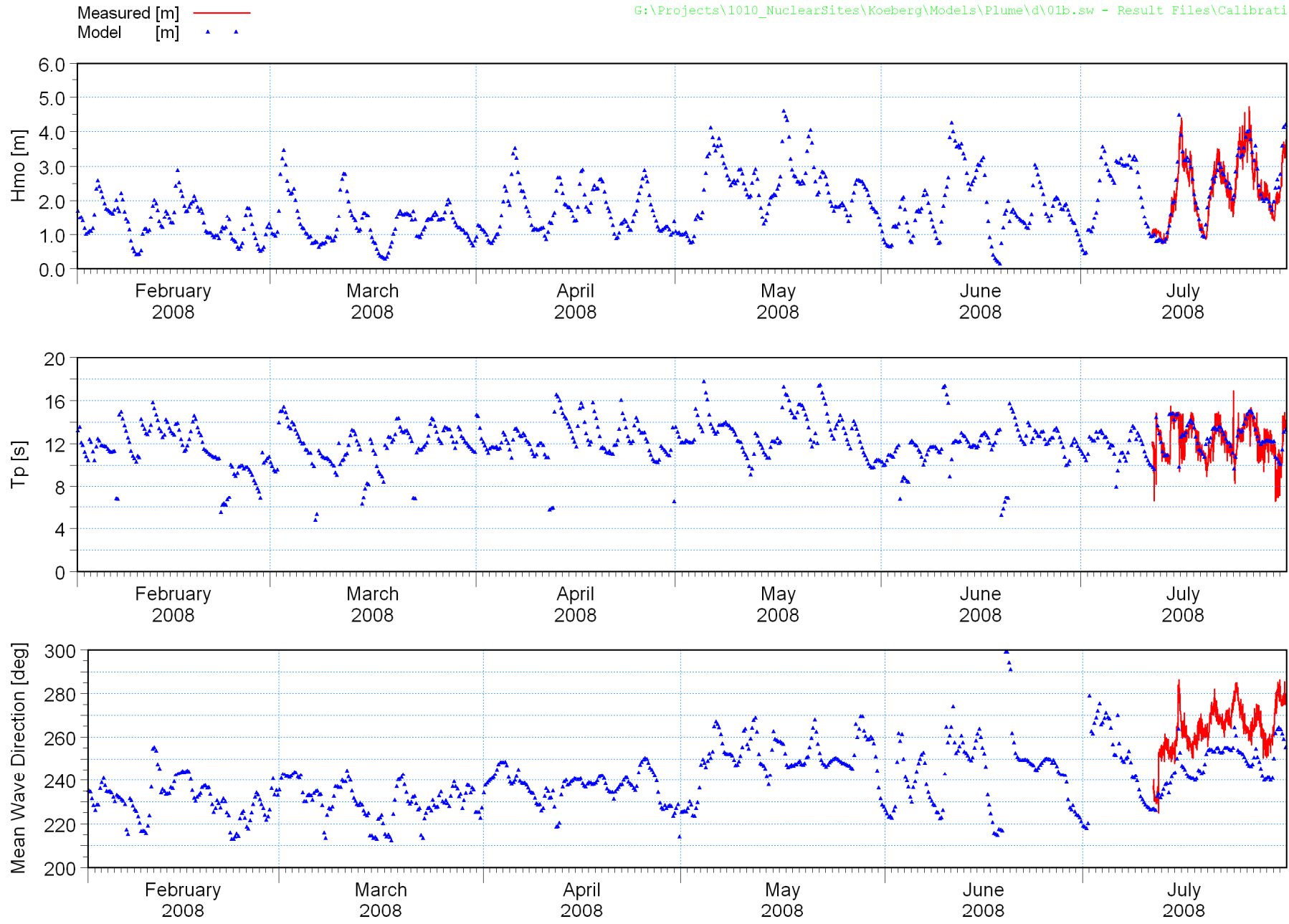


Title:

**Calibration of wave model.  
Measured and modelled time-series of wave parameters at Site A (refer to Figure 1.2 for location).**

Figure No.

**6.7**

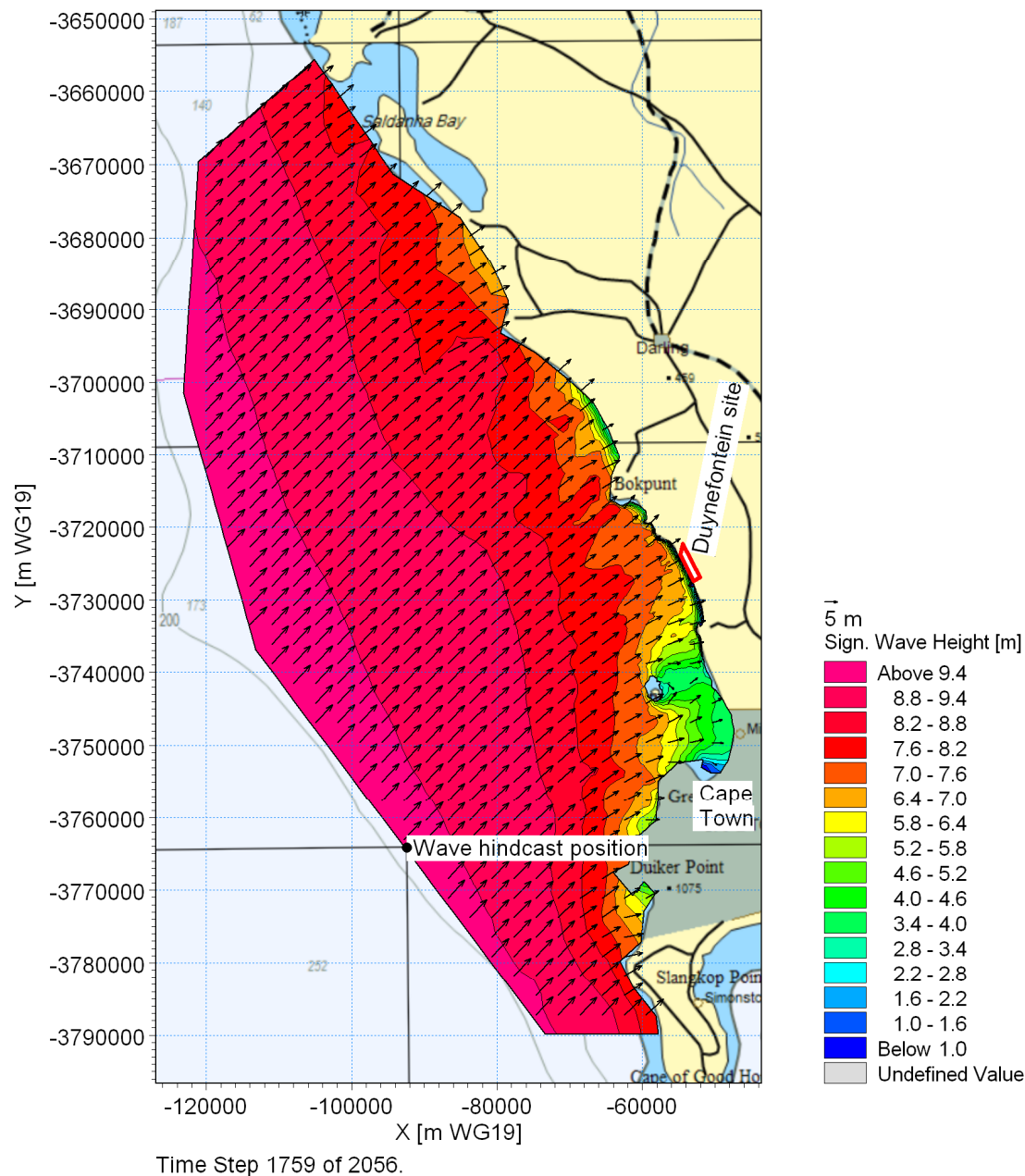


Title:

**Calibration of wave model.  
Measured and modelled time-series of wave parameters at Site B (refer to Figure 1.2 for location).**

Figure No.

**6.8**

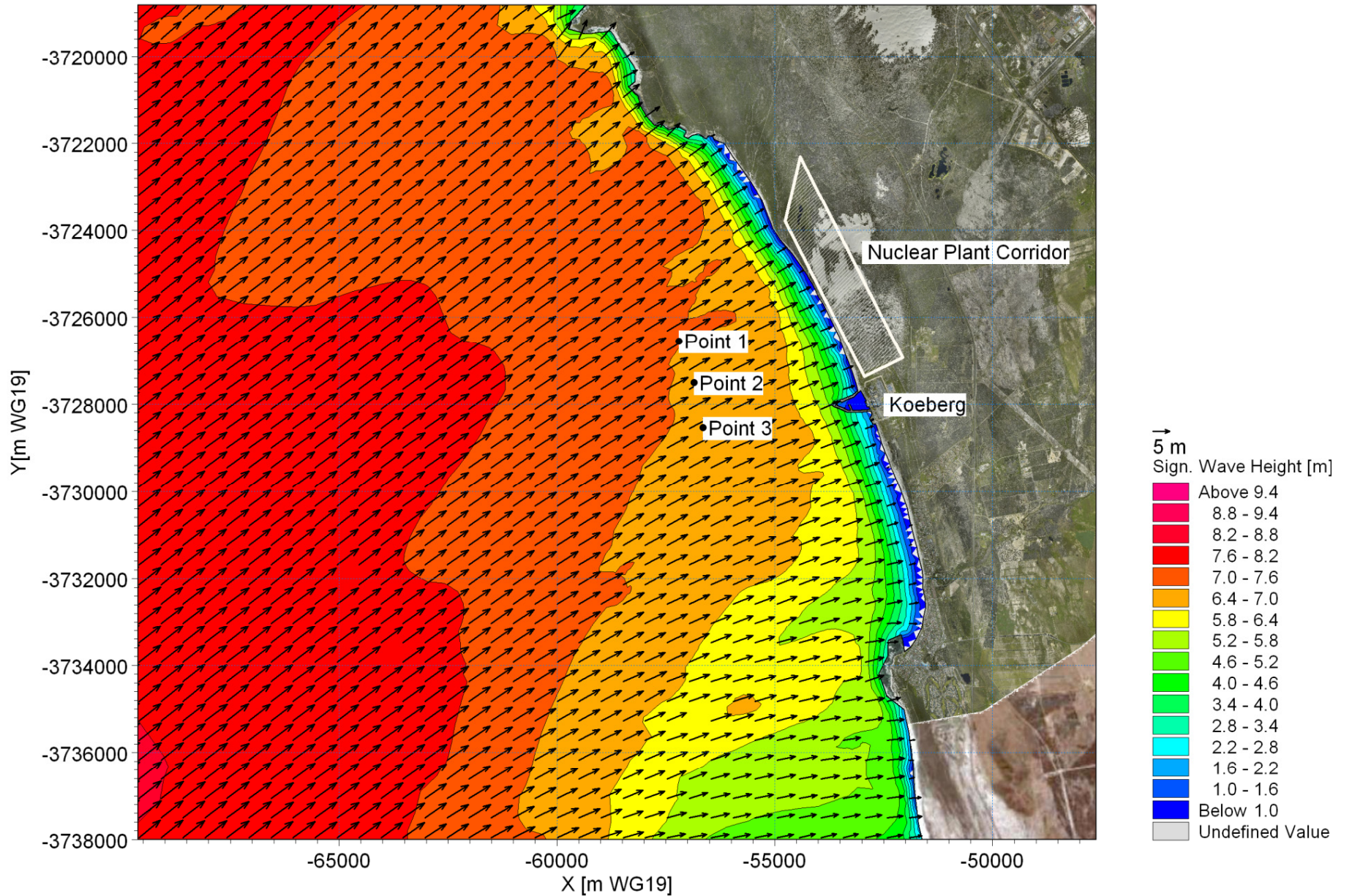


Title:

**Example of wave refraction from offshore to Duynfontein site.  
 Deepwater wave condition:  $H_{m0} = 9.5$  m,  $T_p = 16.5$  s, Mean direction =  $224^\circ$ .**

Figure No.

6.9



Title:

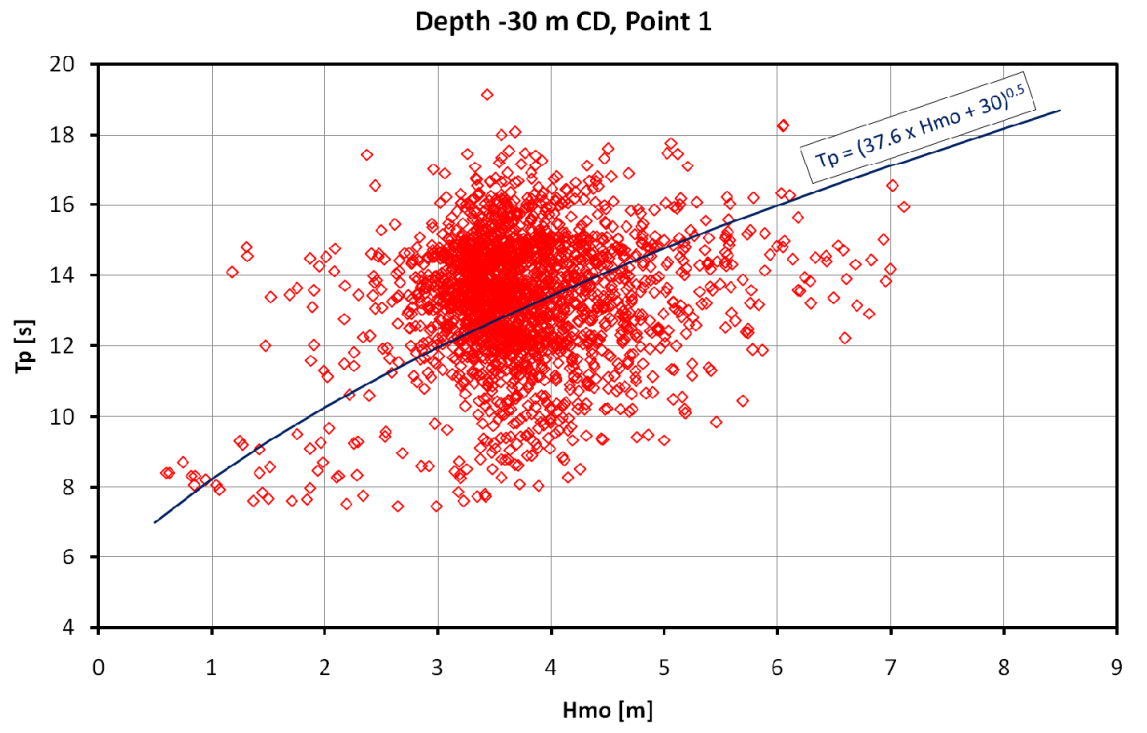
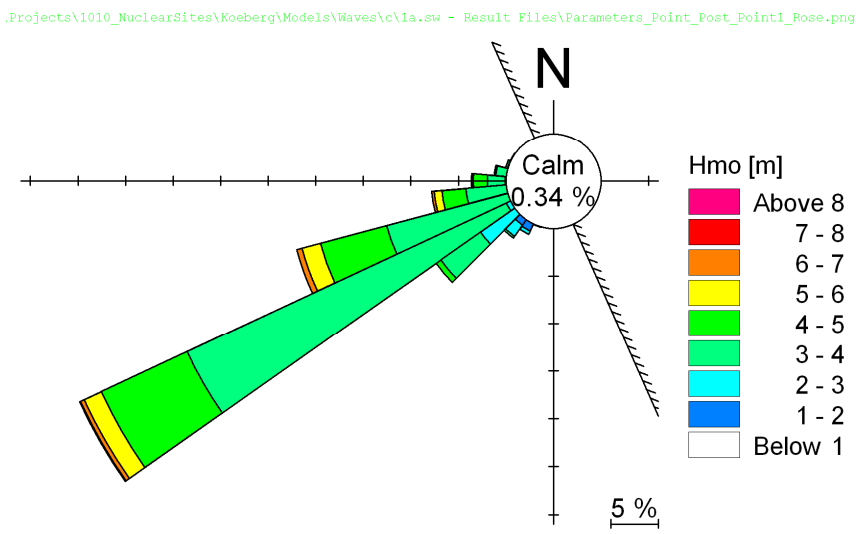
**Example of wave refraction from offshore to Dufnefontein site.  
 Deepwater wave condition:  $H_{m0} = 9.5$  m,  $T_p = 16.5$  s, Mean Dir = 224°.  
 Model output points along -30 m CD contour indicated.**

Figure No.

**6.10**

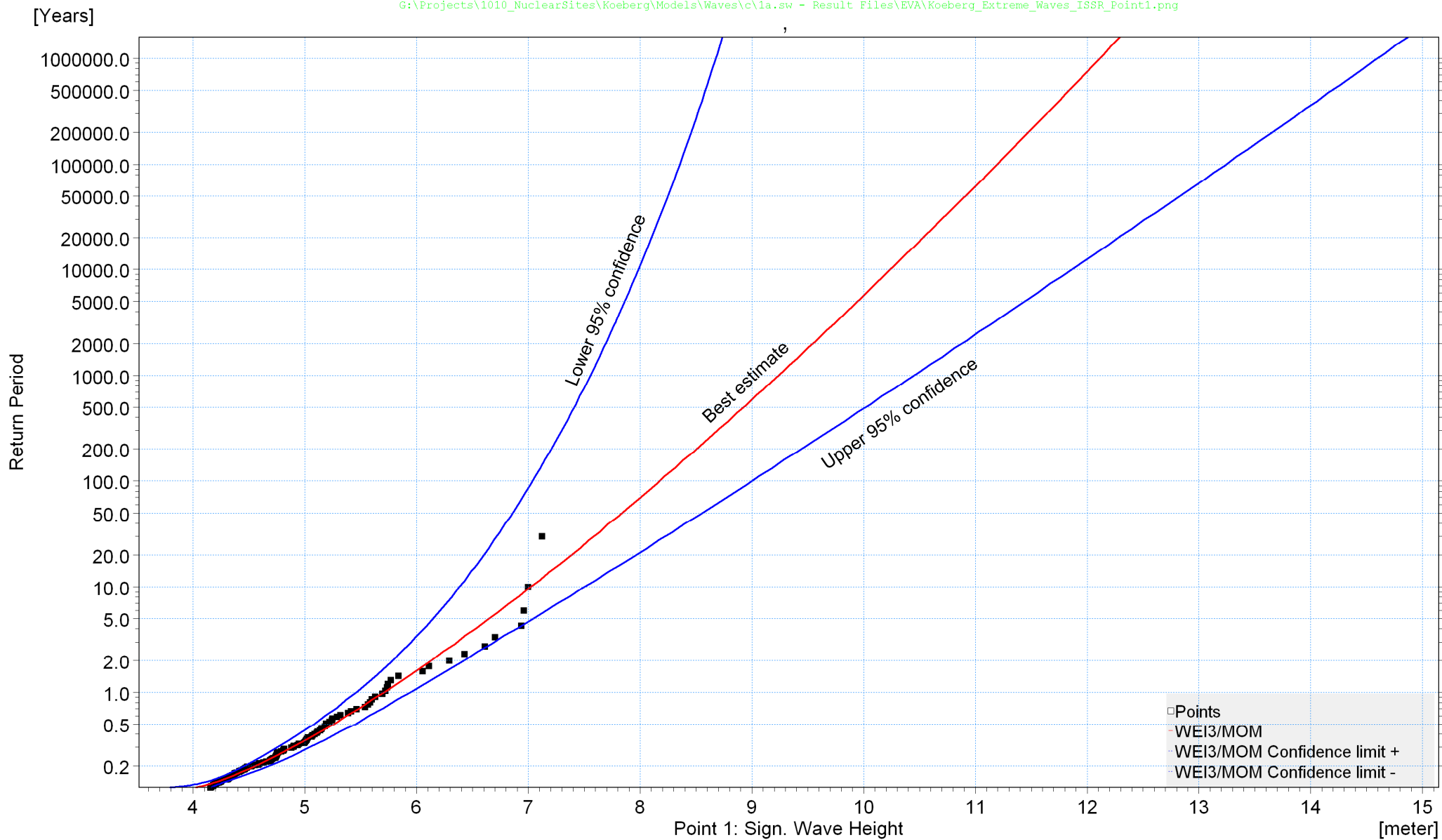
Wave Rose

Wave Height – Period Relationship



Title: **Characterisation of storm waves refracted to -30 m CD depth contour at Duynfontein site. Point 1. Includes only storms where the offshore  $H_{m0} > 4.0$  m.**

Figure No. **6.11**



Title:

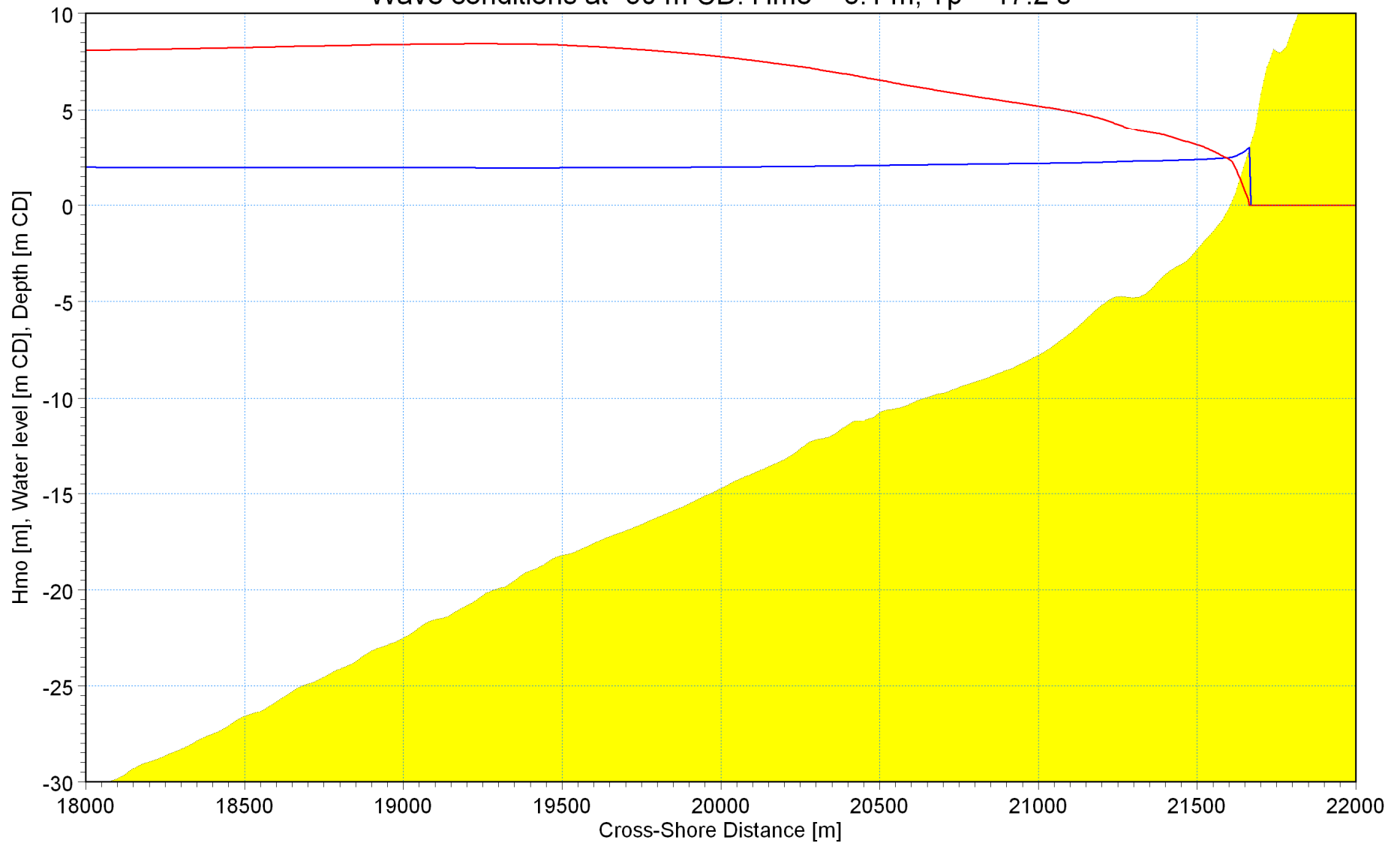
Extreme value analysis of waves at -30 m CD depth at Duynefontein (Point 1).

Figure No.

6.12

Depth [m]   
Water level [m]   
Hmo [m] 

Wave conditions at -30 m CD:  $H_{mo} = 8.1$  m,  $T_p = 17.2$  s



01/01/90 00:00:00:000



Title:

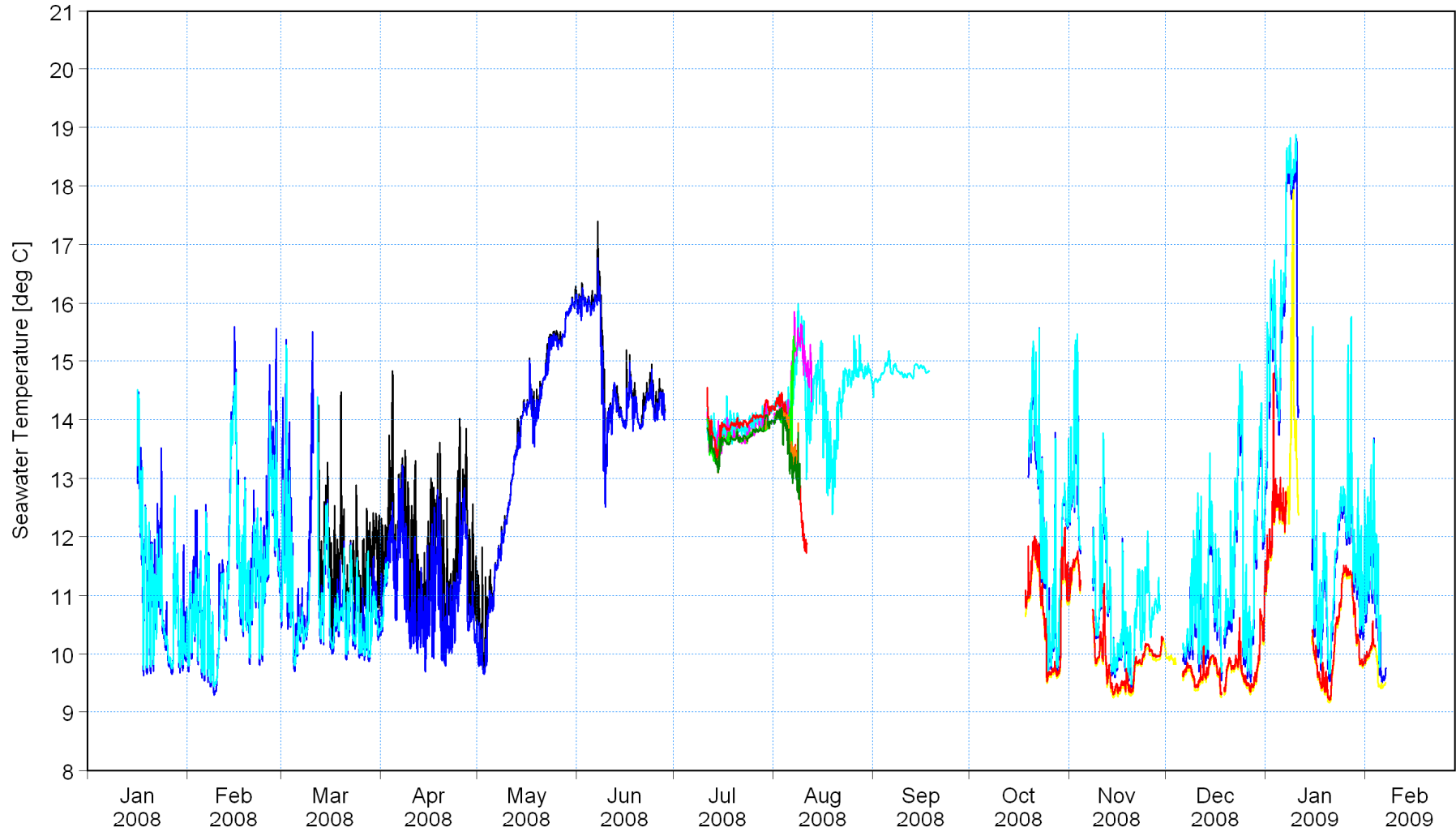
Example of cross-shore wave transformation modelling from -30 m CD depth to shoreline.

Figure No.

6.13

Site A, Water depth = 10 m, Instrument depth = 4 m [deg C] ———  
 Site A, Water depth = 10 m, Instrument depth = 10 m [deg C] ———  
 Site A, Water depth = 10 m, Instrument depth = 10 m [deg C] ———  
 Site B, Water depth = 30 m, Instrument depth = 9 m [deg C] ———  
 Site B, Water depth = 30 m, Instrument depth = 19 m [deg C] ———  
 Site B, Water depth = 30 m, Instrument depth = 28 m [deg C] ———  
 Site B, Water depth = 30 m, Instrument depth = 28 m [deg C] ———  
 Site B, Water depth = 30 m, Instrument depth = 29 m [deg C] ———  
 Site B, Water depth = 30 m, Instrument depth = 30 m [deg C] ———

G:\Projects\1010\_NuclearSites\Koeberg\Data\Lwandle\Concatenated\Koeberg\_Temperature\_All\_Timeseries.png



Title:

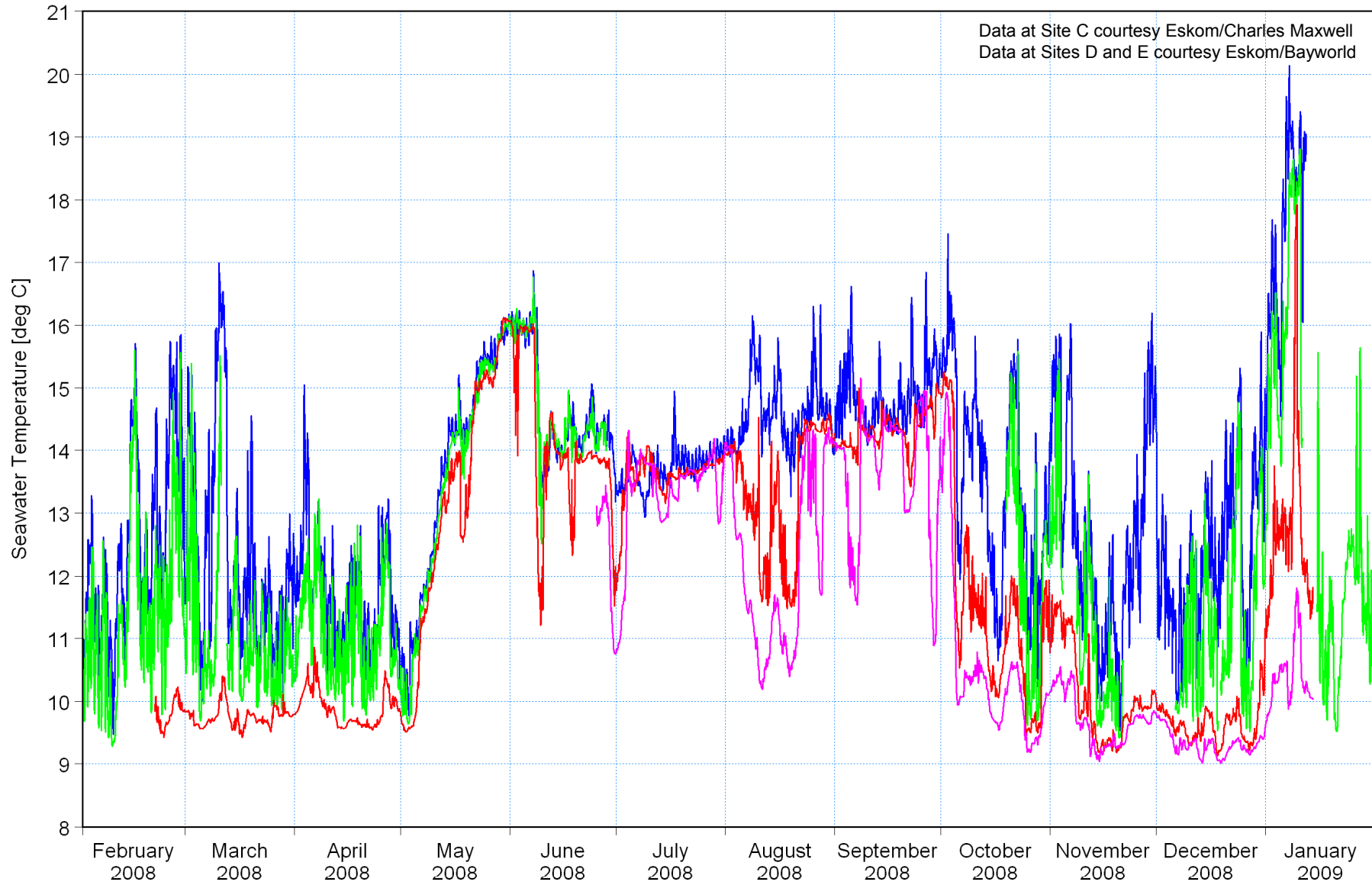
**Seawater temperatures measured at Duynefontein for SSR.  
 (Refer to Figure 1.2 for instrument positions).**

Figure No.

7.1

Site C, Water depth = 3 m, Instrument depth = 3 m [deg C] — blue  
Site A, Water depth = 10 m, Instrument depth = 10 m [deg C] — green  
Site D, Water depth = 27 m, Instrument depth = 27 m [deg C] — red  
Site E, Water depth = 50 m, Instrument depth = 50 m [deg C] — magenta

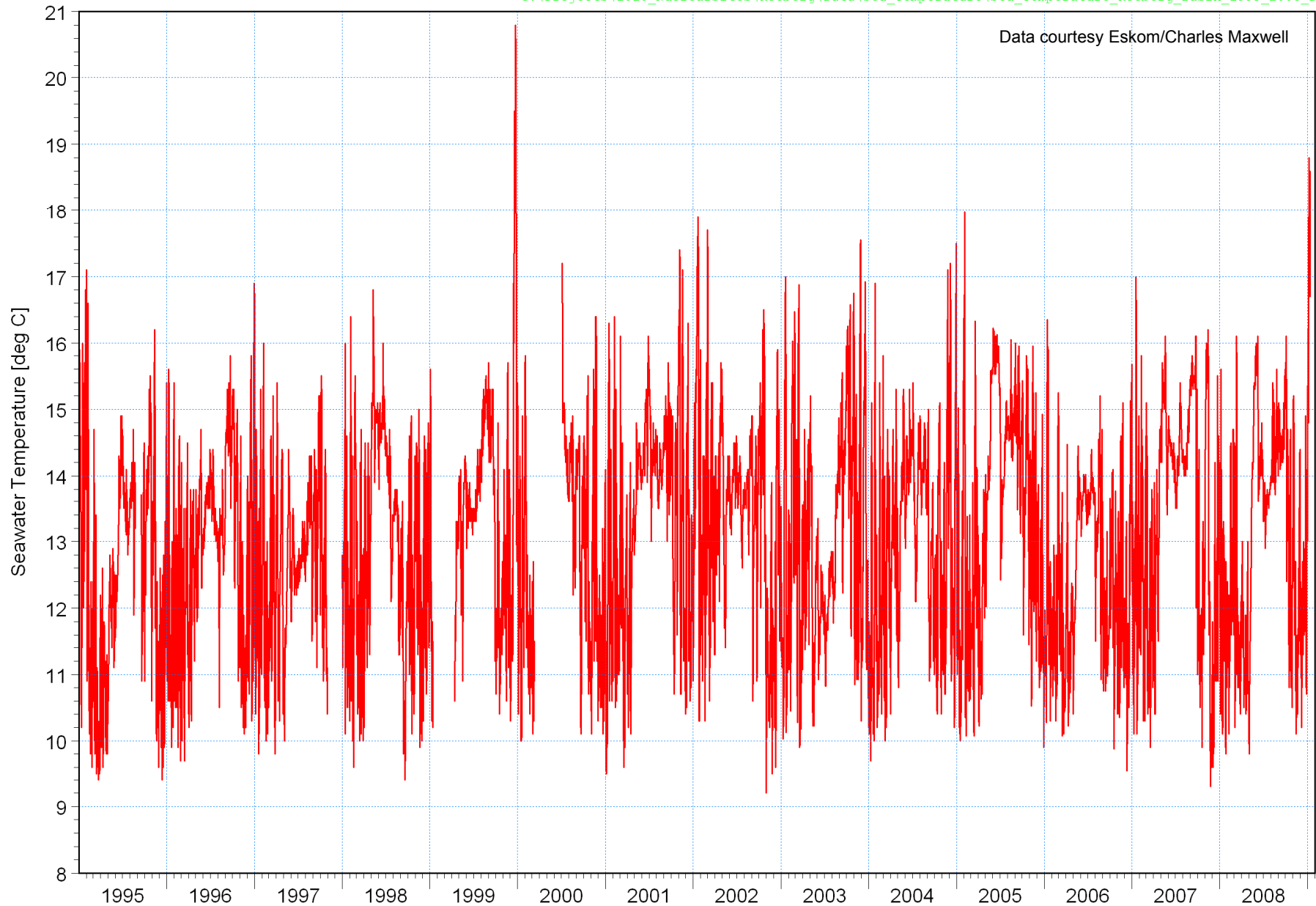
G:\Projects\1010\_NuclearSites\Koeberg\Data\Sea\_Temperature\Sea\_Temperature\_Koeberg\_Stratification\_2008.png



**Title:** Seawater temperatures measured at Duynefontein showing decrease in temperature with depth.  
(Refer to Figure 1.2 for instrument positions).

**Figure No.**  
7.2

Data courtesy Eskom/Charles Maxwell



**Title:**

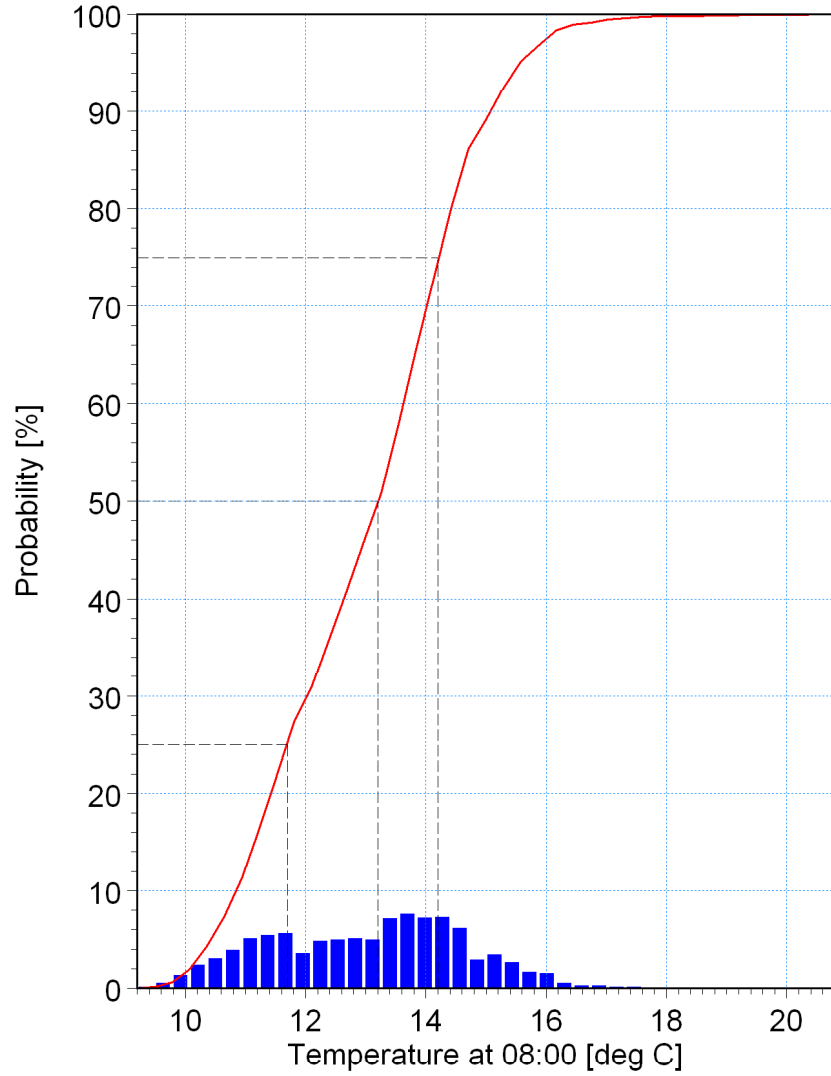
**Seawater temperatures measured at 08:00 inside cooling water intake basin at Koeberg.  
Site C, Water depth = 3 m, Instrument depth = 3 m. (Refer to Figure 1.2 for instrument position).**

**Figure No.**

**7.3**

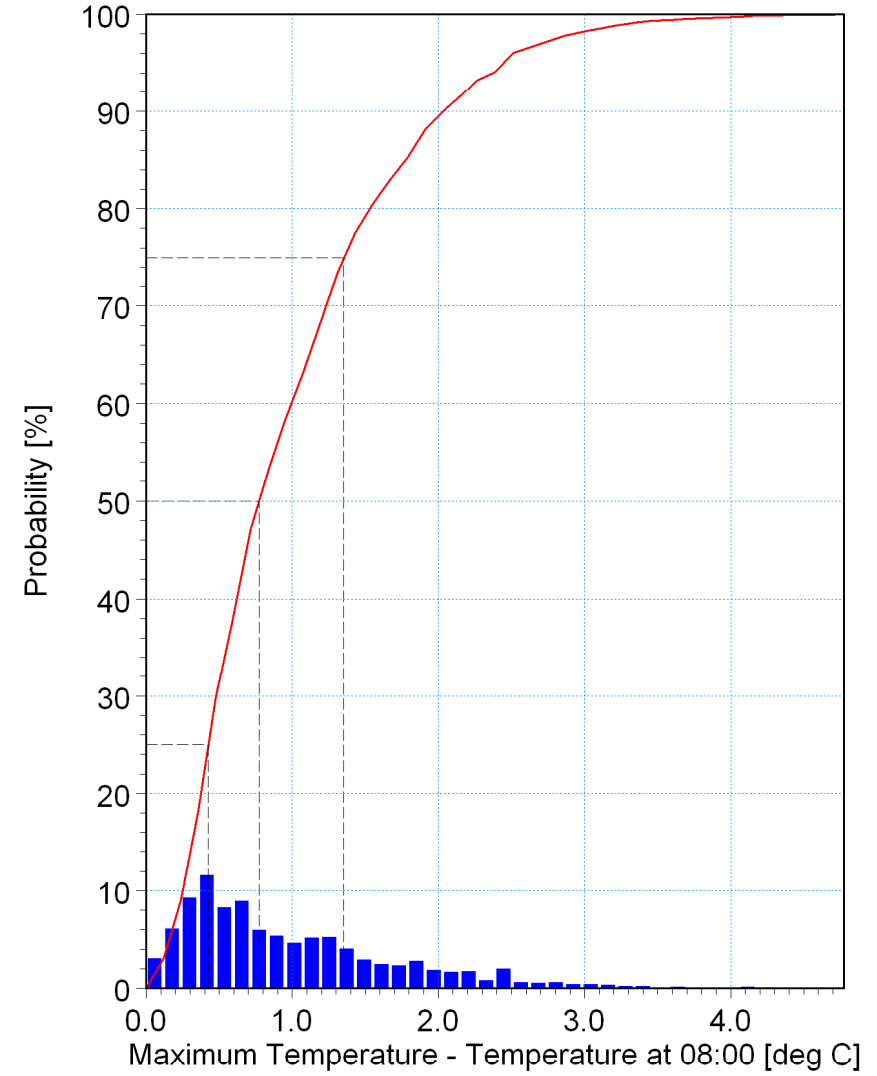
000.0%: 9.20000  
 025.0%: 11.70000  
 050.0%: 13.20000  
 075.0%: 14.20000  
 100.0%: 20.80000

Sea\_Temperature\_Koeberg\_Basin\_1995\_20  
 08\_Daily\_Probability.png



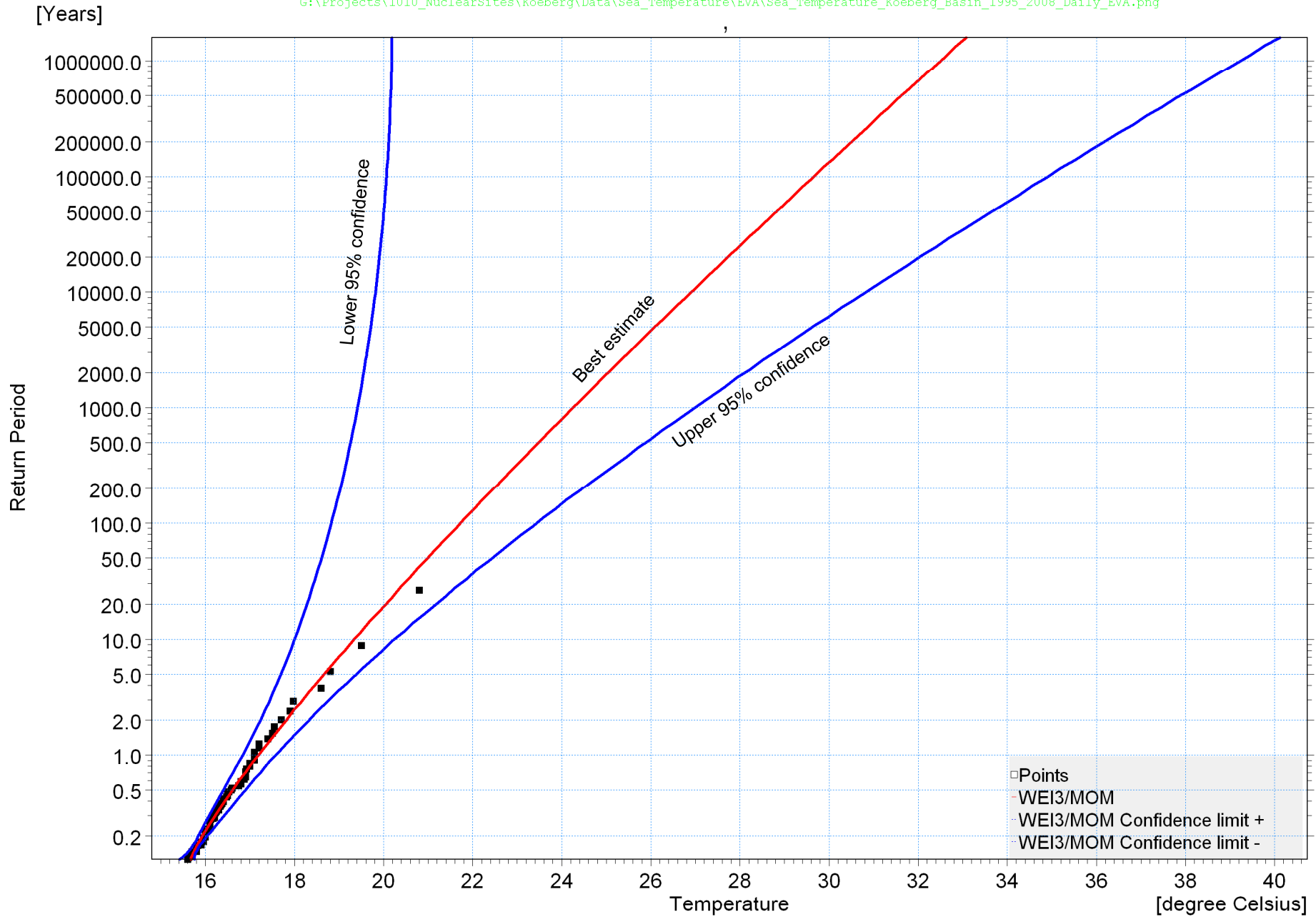
000.0%: 0.00000  
 025.0%: 0.42500  
 050.0%: 0.77500  
 075.0%: 1.35000  
 100.0%: 4.77500

Sea\_Temperature\_Koeberg\_Basin\_2003\_20  
 08\_Hourly\_Daily\_Max\_Probability.png

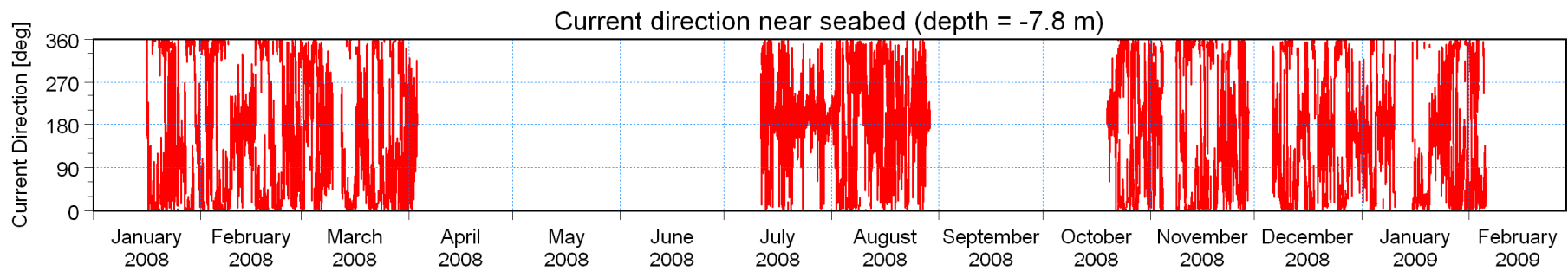
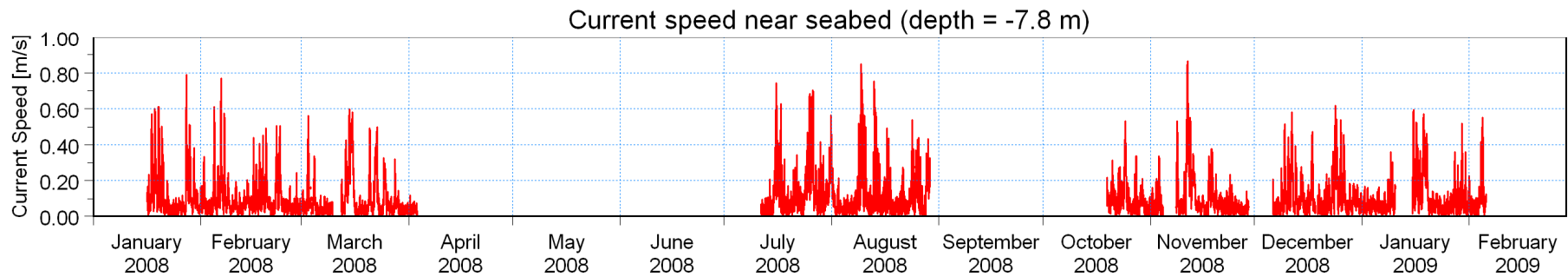
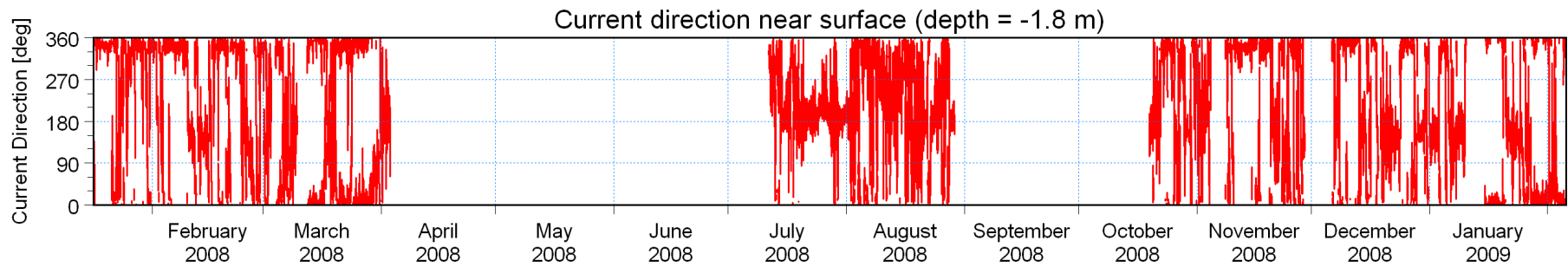
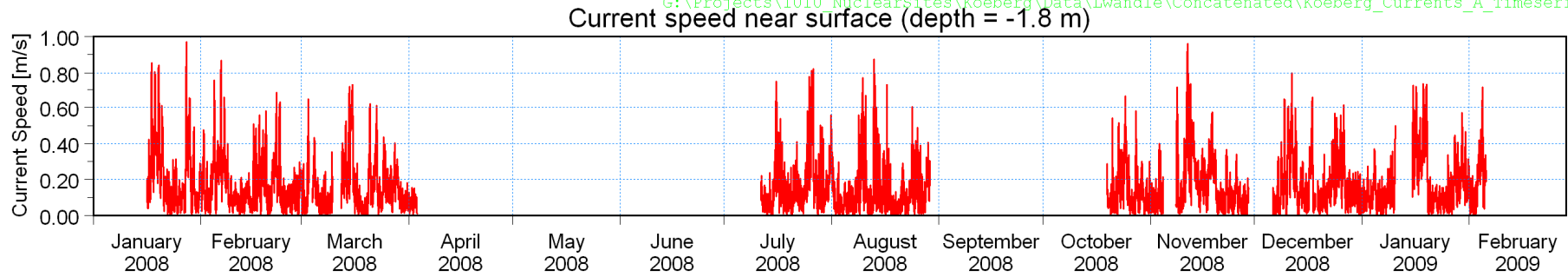


**Title: Histograms of measured seawater temperatures in the cooling water intake basin at Koeberg.**  
**Left: Temperature measured at 08:00.**  
**Right: Difference between the maximum daily temperature and the temperature at 08:00.**

**Figure No.**  
**7.4**



**Title:** Extreme Value Analysis of measured seawater temperatures at 08:00 in the cooling water intake basin at Koeberg.

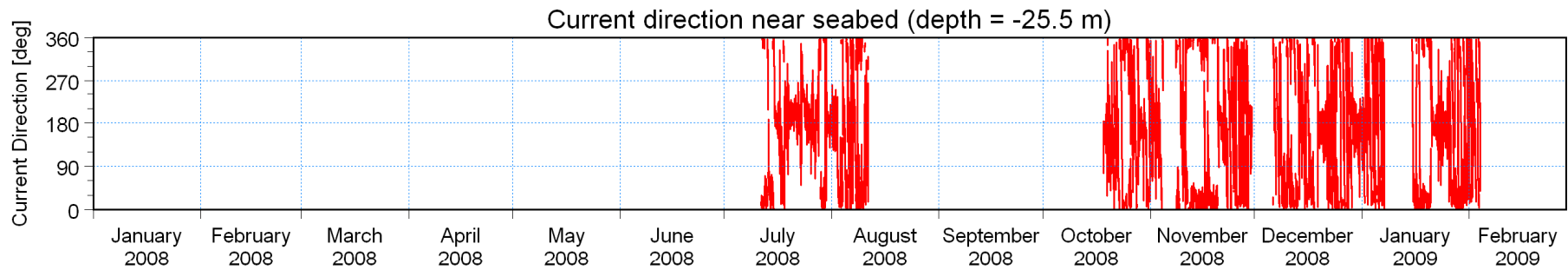
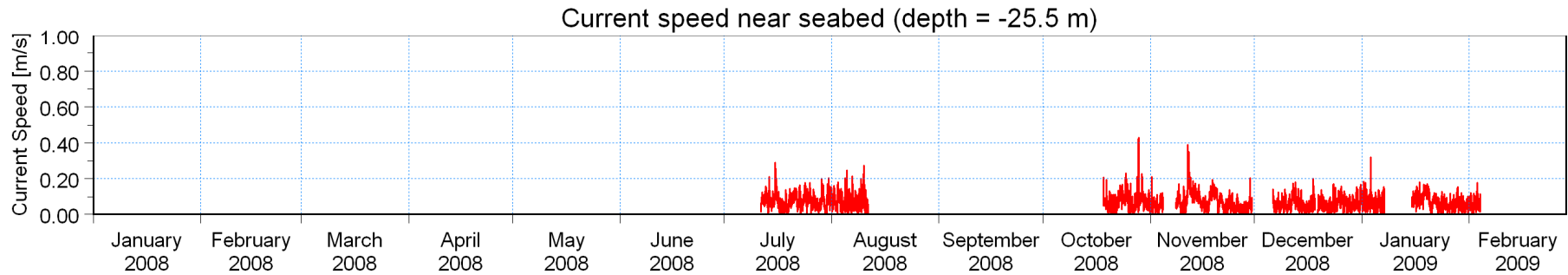
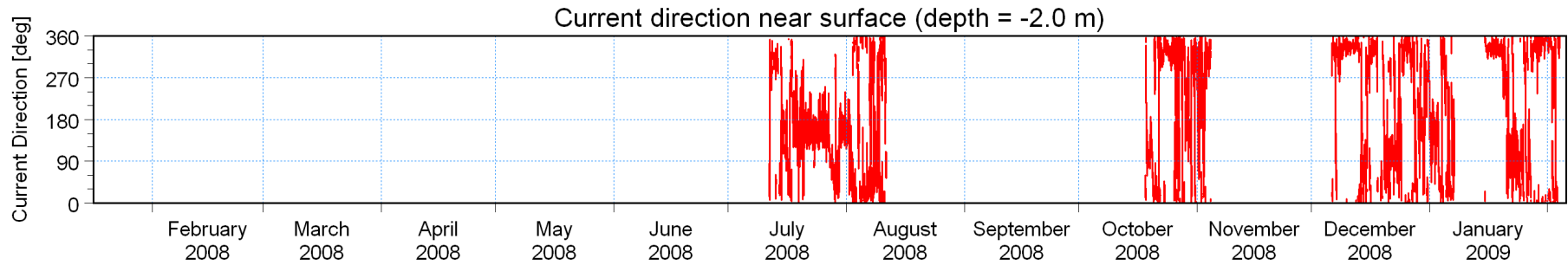
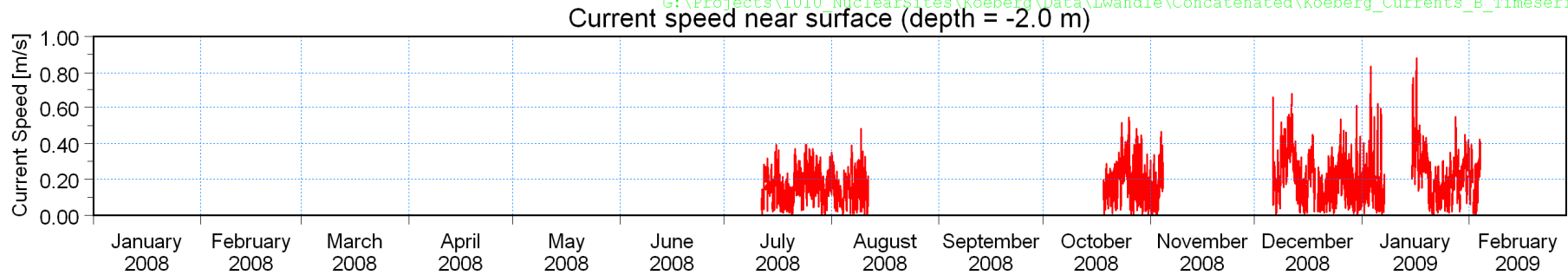


Title:

**Current measurements at Site A, water depth = 10 m (refer to Figure 1.2 for position).  
Time-series of surface and bottom currents.**

Figure No.

8.1

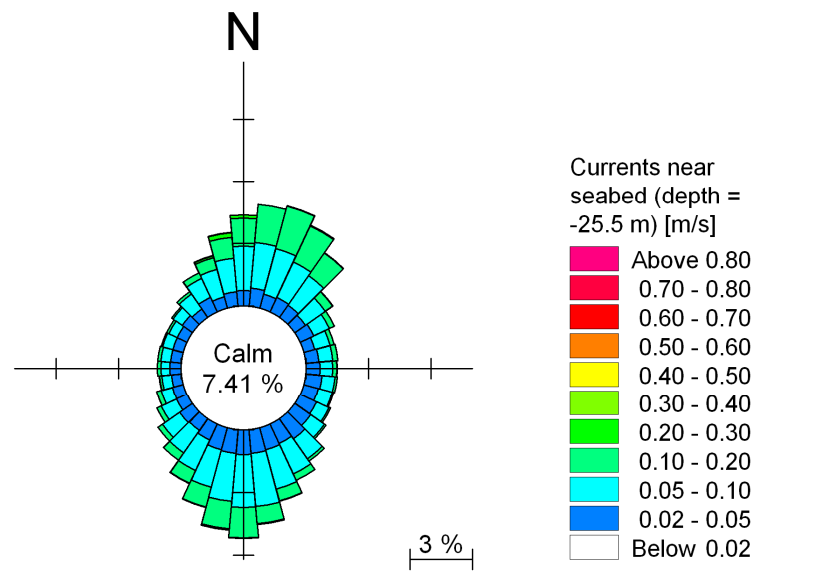
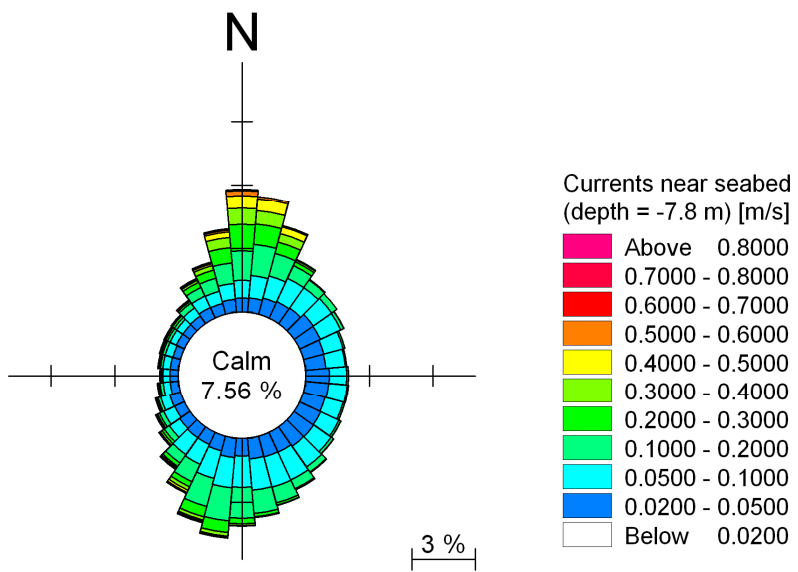
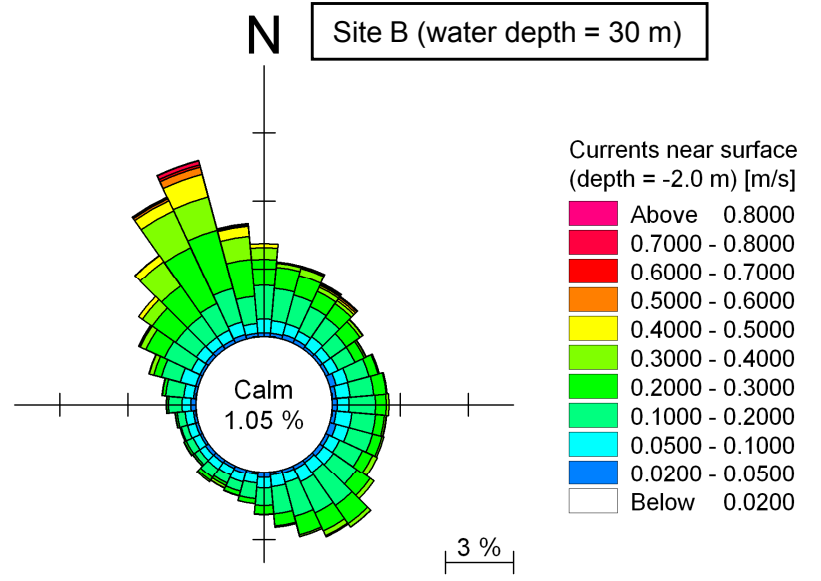
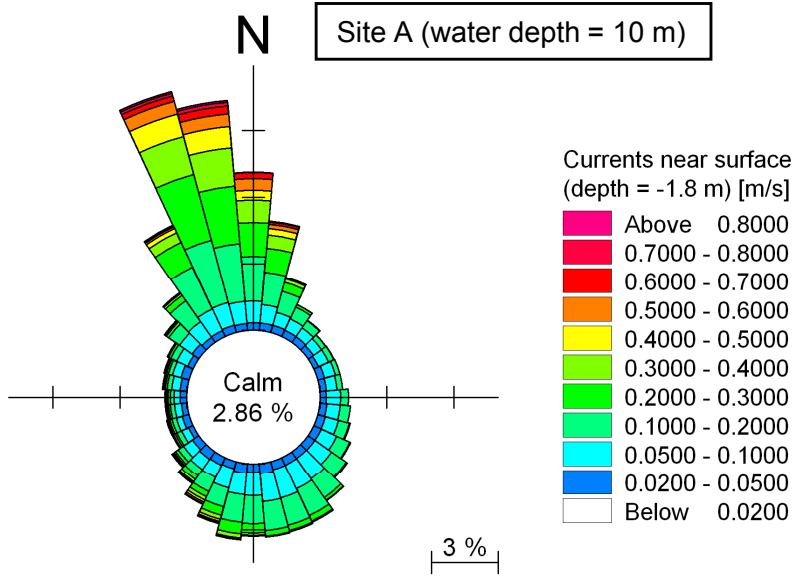


Title:

**Current measurements at Site B, water depth = 30 m (refer to Figure 1.2 for position).  
Time-series of surface and bottom currents.**

Figure No.

8.2



G:\Projects\1010\_NuclearSites\Koeberg\Data\Lwandle\Concatenated\Koeberg\_Currents\_A\_Roses.png

G:\Projects\1010\_NuclearSites\Koeberg\Data\Lwandle\Concatenated\Koeberg\_Currents\_B\_Roses.png

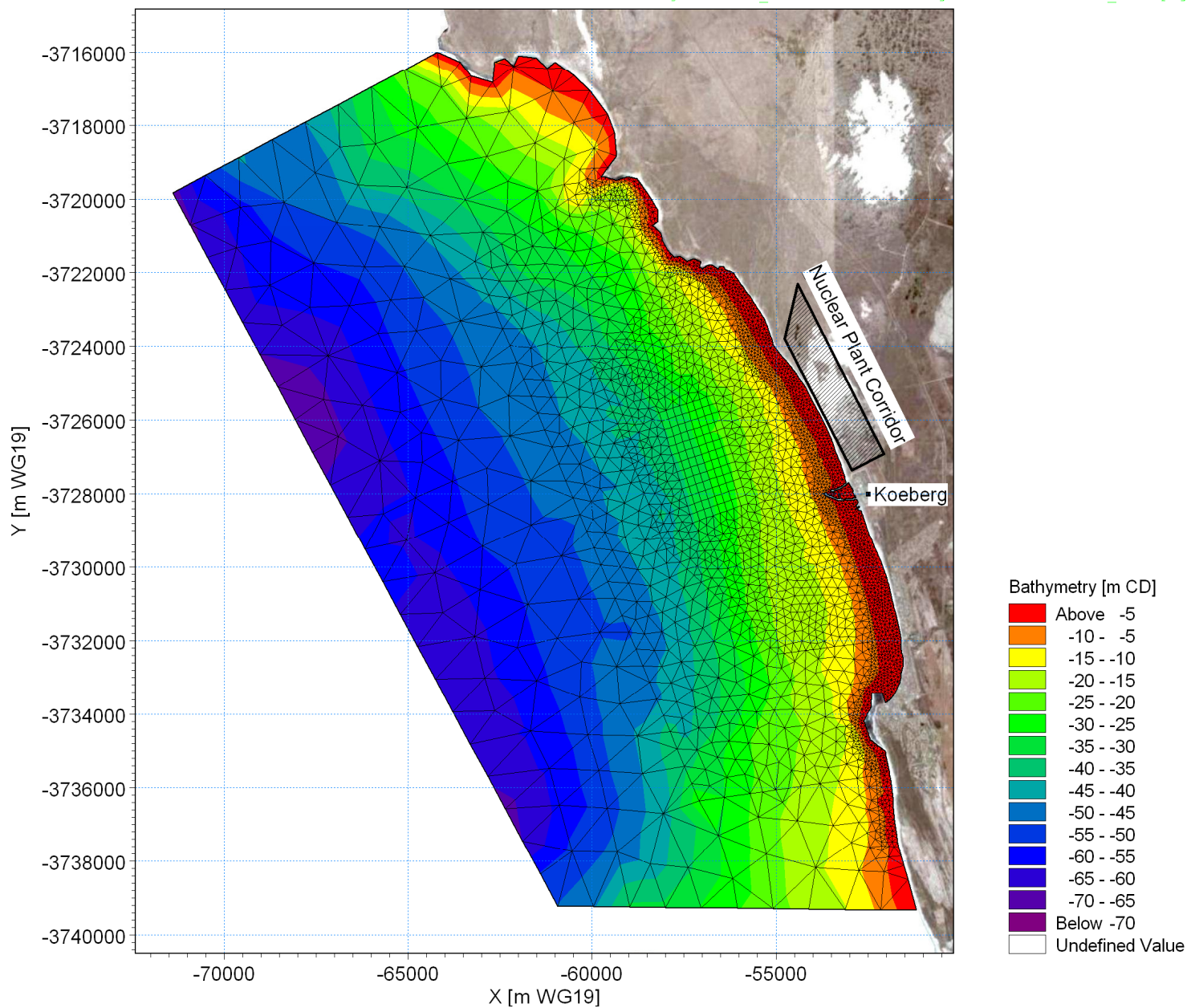


Title:

**Current measurements at Sites A and B (refer to Figure 1.2 for locations).  
Surface and seabed current rose plots.**

Figure No.

**8.3**



Title:

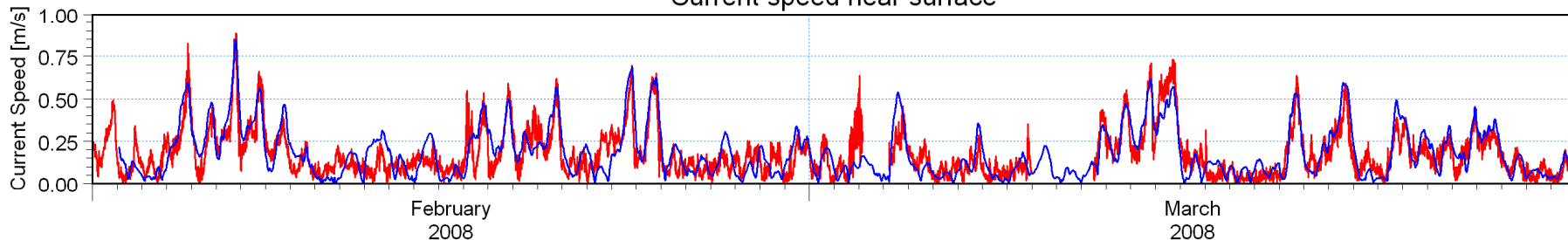
Numerical mesh and bathymetry used for hydrodynamic modelling.

Figure No.

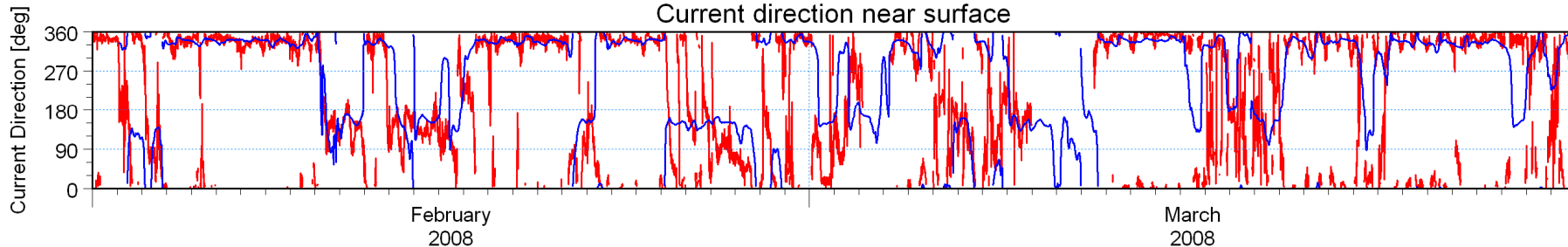
8.4

Measured [m/s] — (red line)  
Model [m/s] — (blue line)

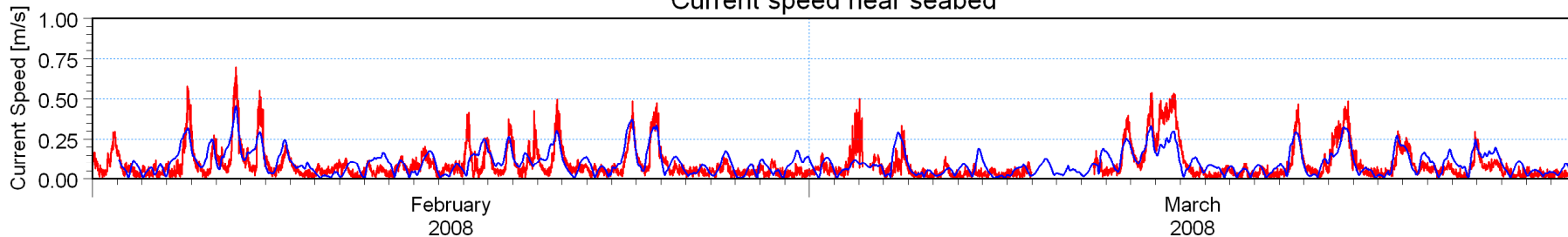
### Current speed near surface



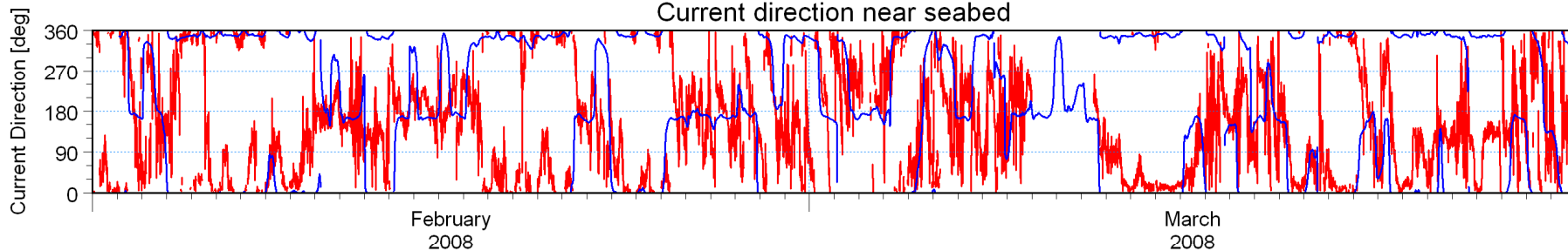
### Current direction near surface



### Current speed near seabed

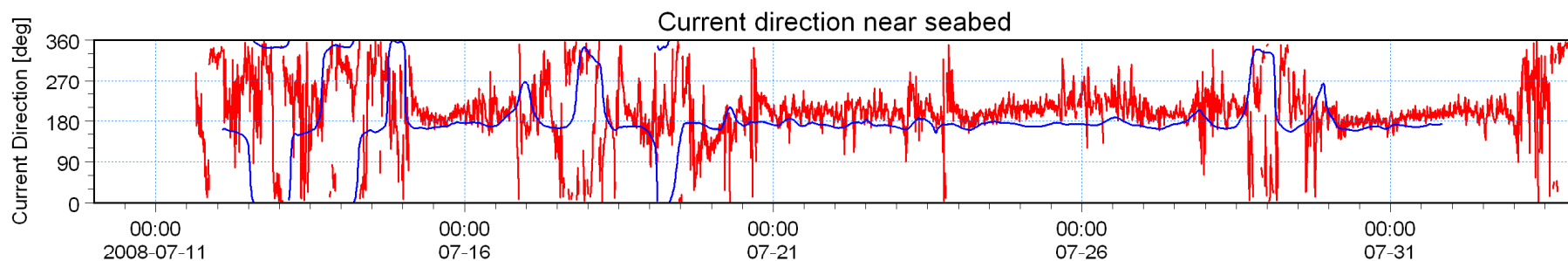
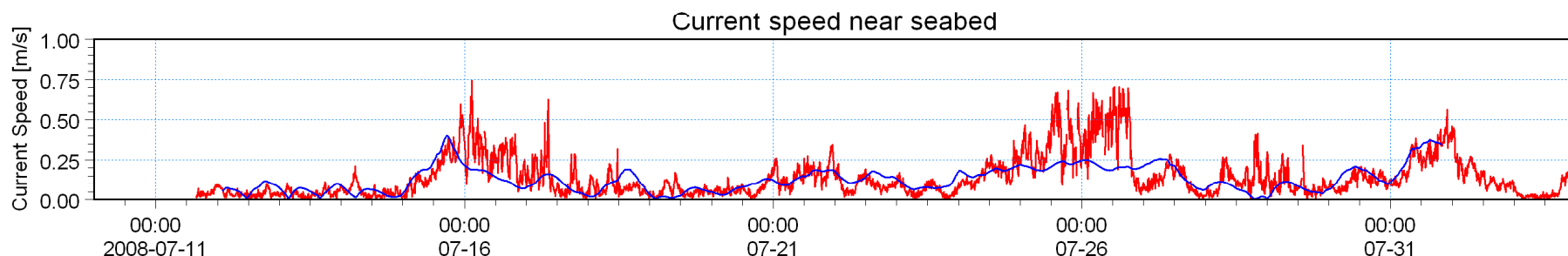
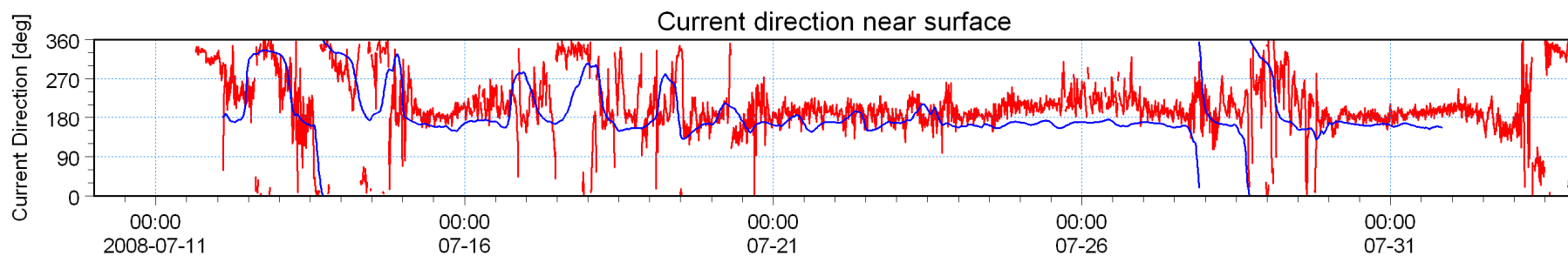
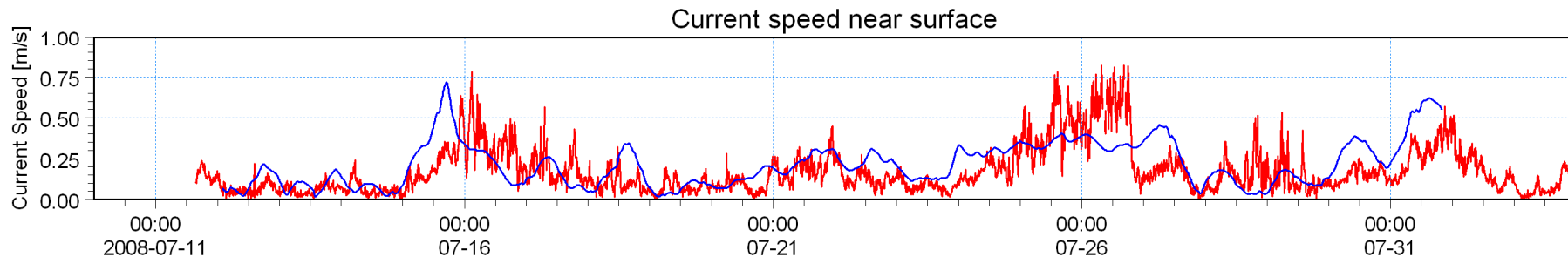


### Current direction near seabed



**Title: Calibration of hydrodynamic model: current speed and direction.  
Measured and modelled time-series of currents at Site A for period February to March 2008.  
(refer to Figure 1.2 for location).**

Measured [m/s] — (red line)  
Model [m/s] — (blue line)



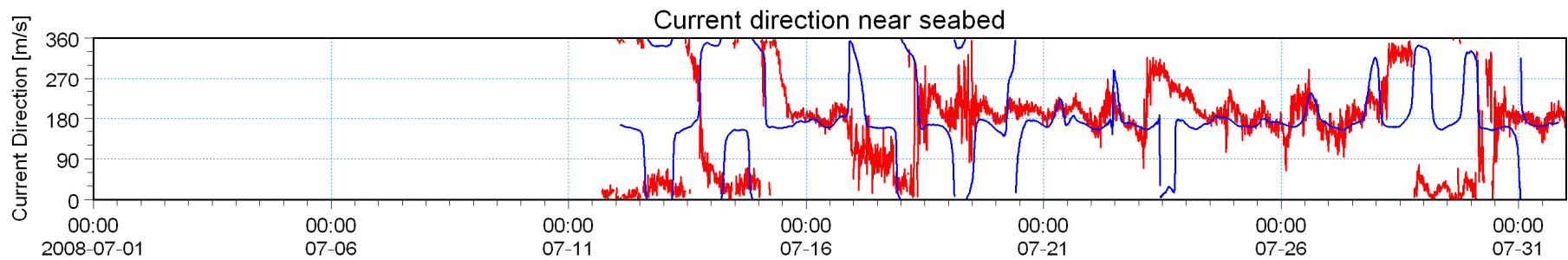
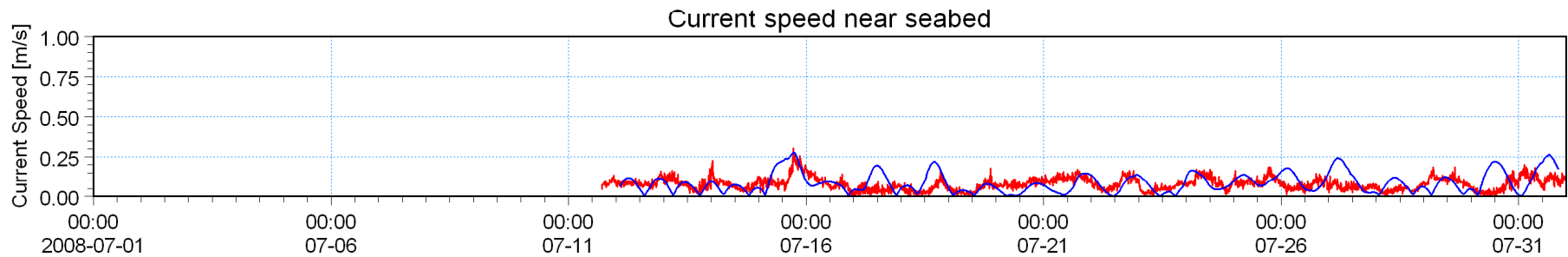
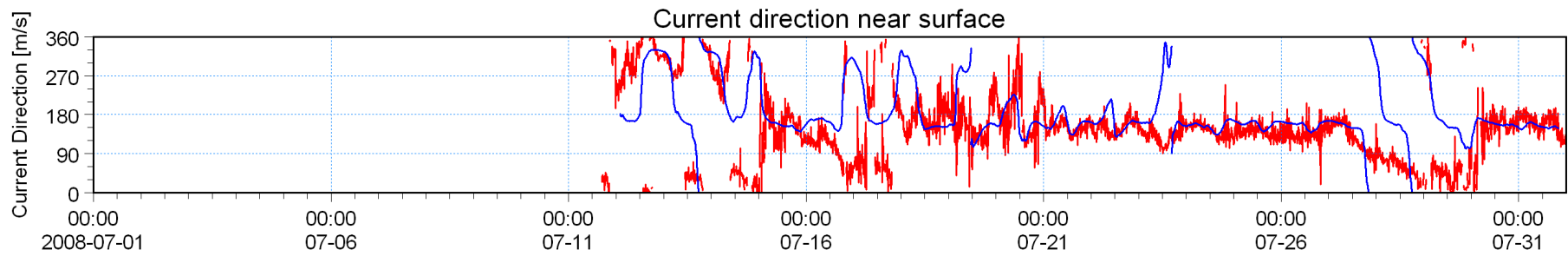
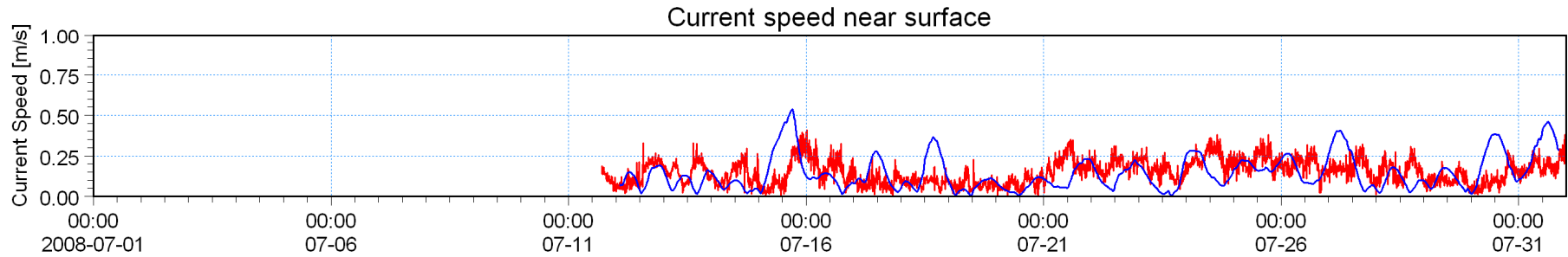
Title:

**Calibration of hydrodynamic model: current speed and direction.  
Measured and modelled time-series of currents at Site A for period July 2008.  
(refer to Figure 1.2 for location).**

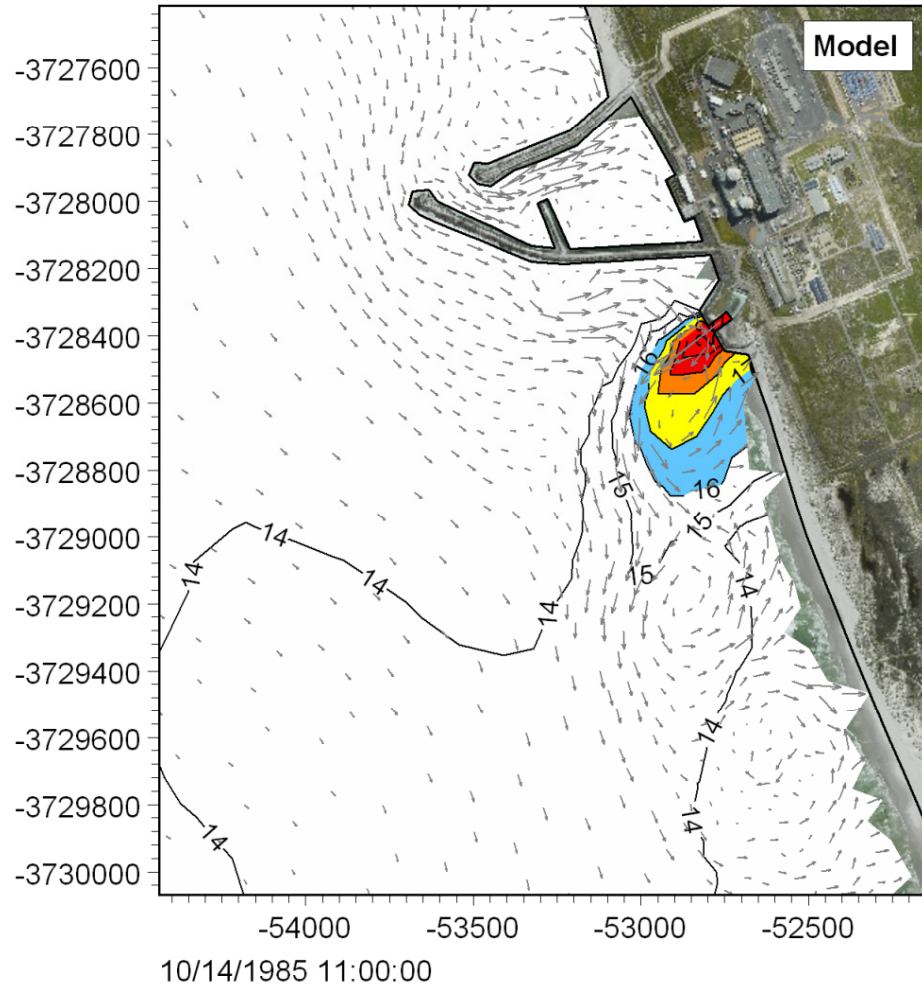
Figure No.

8.6

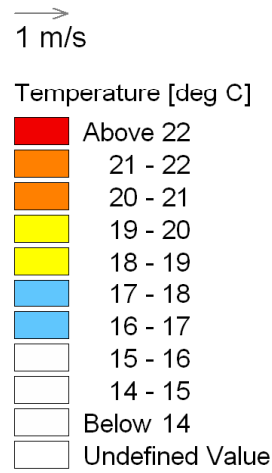
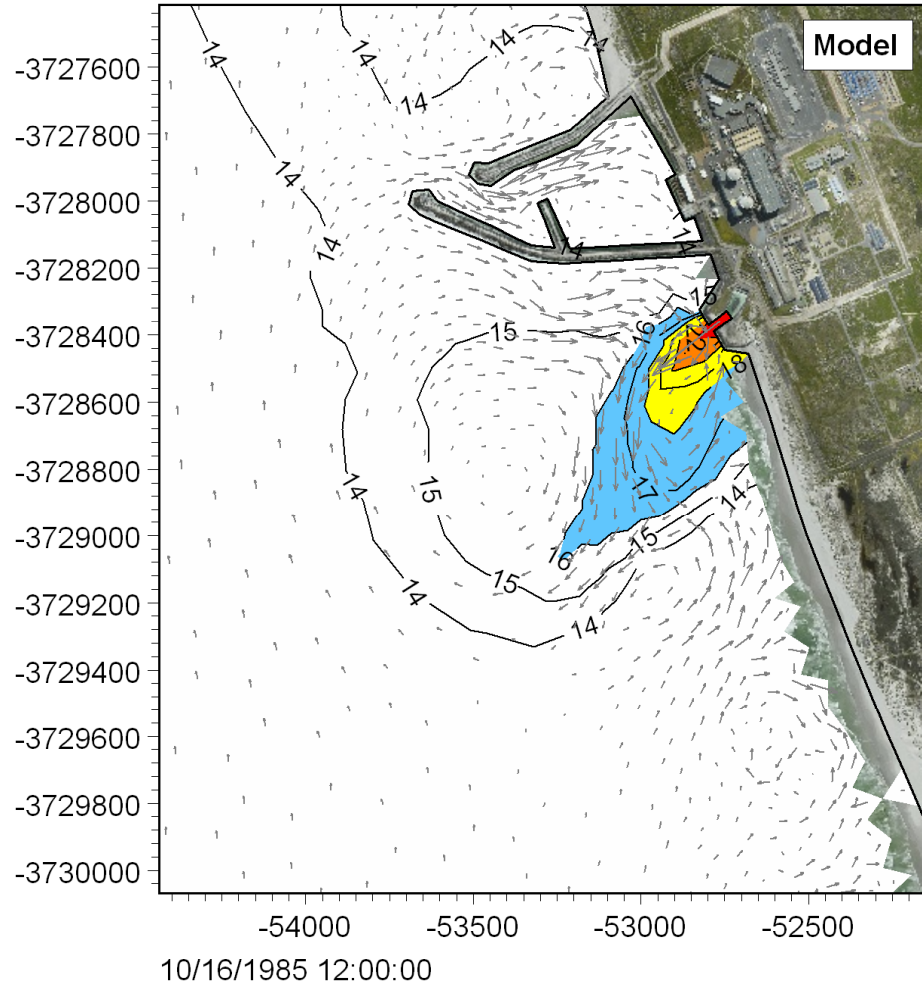
Measured [m/s] — (red line)  
Model [m/s] — (blue line)



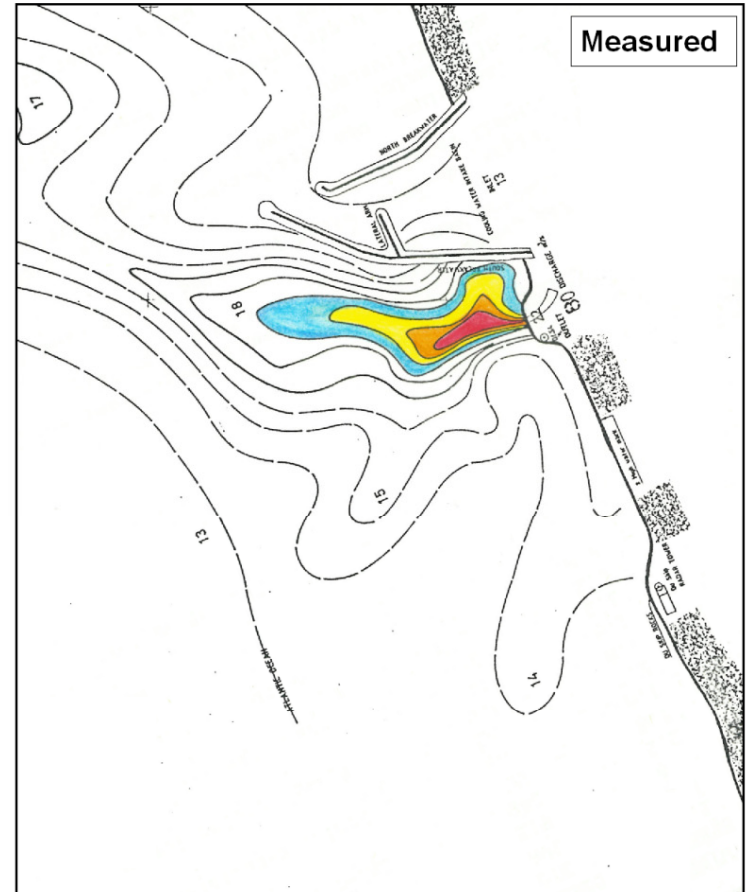
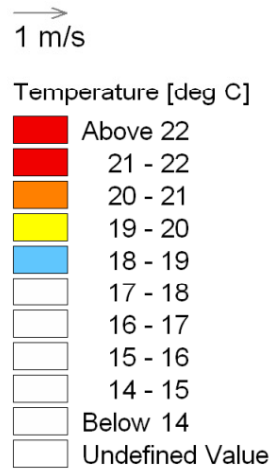
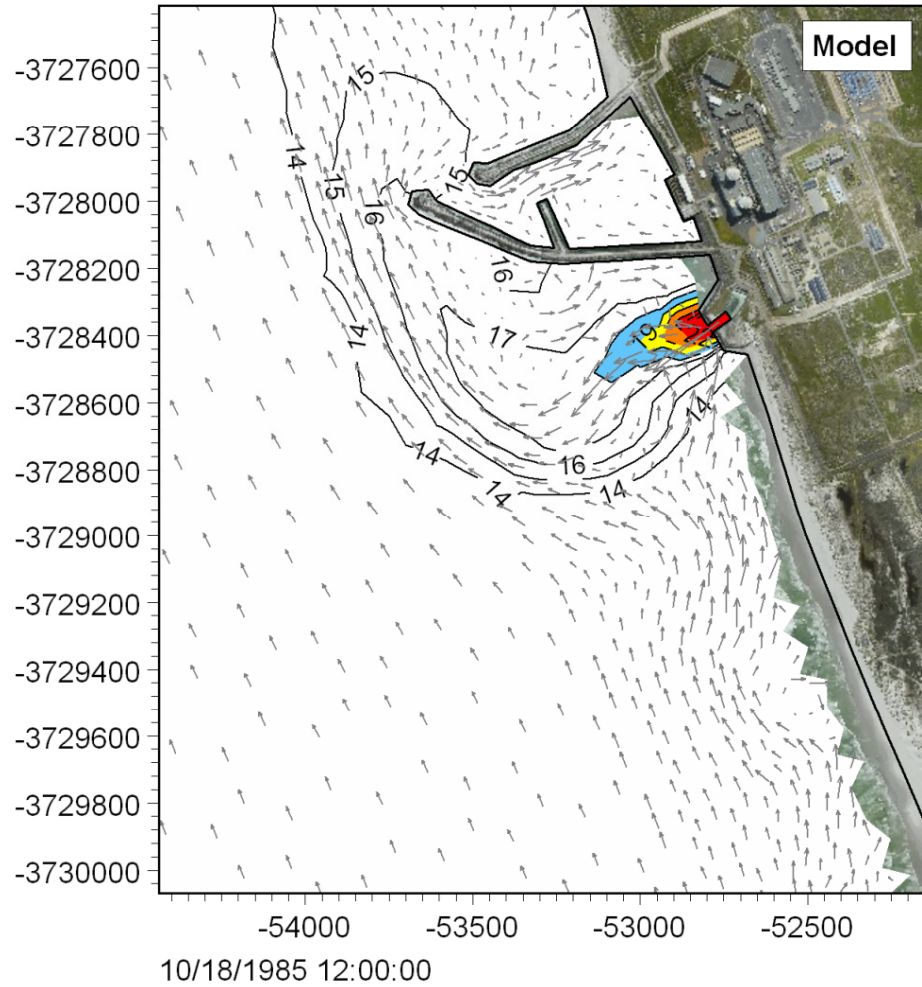
**Title:** Calibration of hydrodynamic model: current speed and direction.  
Measured and modelled time-series of currents at Site B for period July 2008.  
(refer to Figure 1.2 for location).



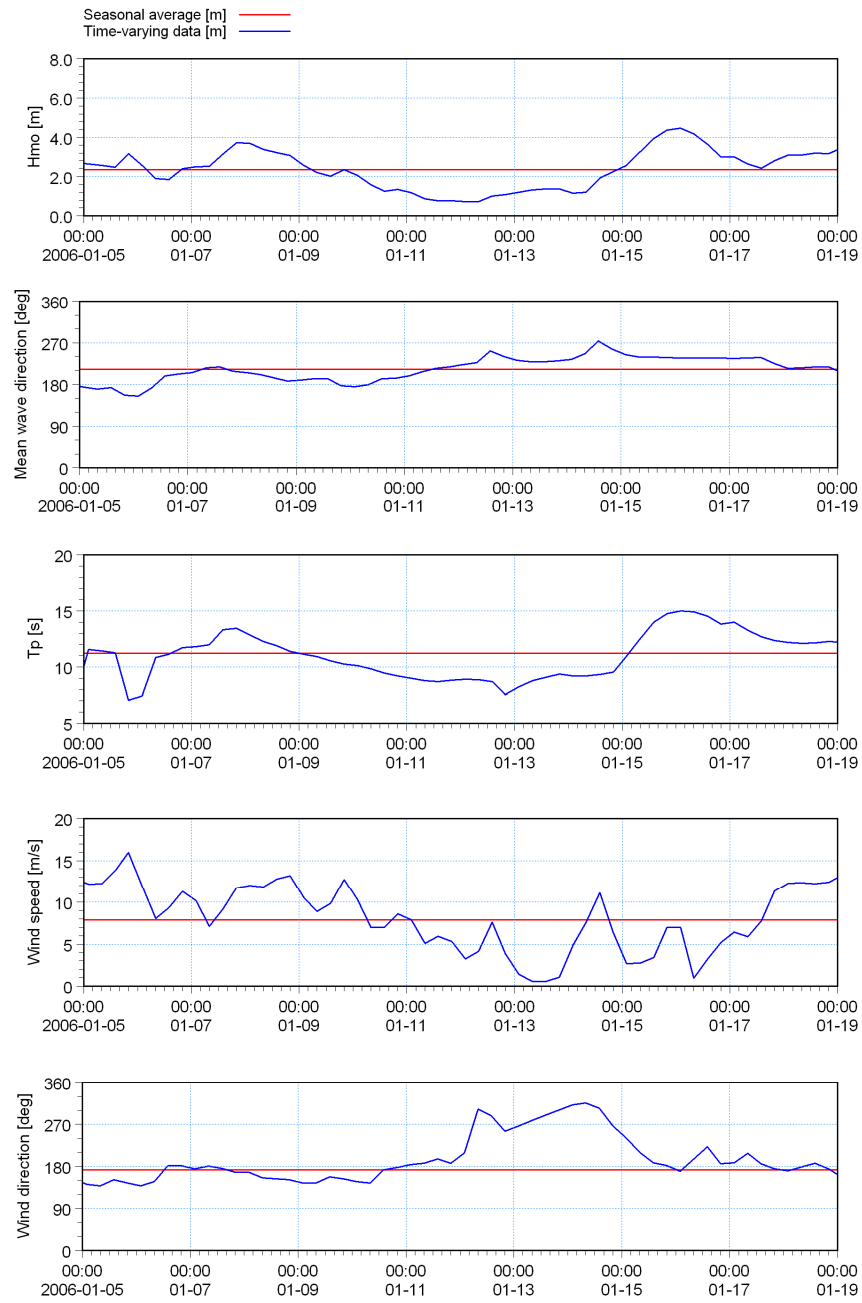
**Title:** Calibration of hydrodynamic model: thermal plume dispersion.  
 Modelled surface temperatures at 11:00 and measured surface temperatures between 11:20 and 11:50 on 14 October 1985. Vectors show modelled currents.



**Title:** Calibration of hydrodynamic model: thermal plume dispersion.  
**Modelled surface temperatures at 12:00 and measured surface temperatures between 11:30 and 12:15 on 16 October 1985. Vectors show modelled currents.**



**Title:** Calibration of hydrodynamic model: thermal plume dispersion.  
**Modelled surface temperatures at 12:00 and measured surface temperatures between 11:18 and 12:10 on 18 October 1985. Vectors show modelled currents.**



I:\WaveSim\Kobberg\_Average\_Conditions.dbo  
 I:\WaveSim\Kobberg\_Average\_Conditions.dbo  
 I:\WaveSim\Kobberg\_Average\_Conditions.dbo  
 I:\WaveSim\Kobberg\_Average\_Conditions.dbo  
 I:\WaveSim\Kobberg\_Average\_Conditions.dbo

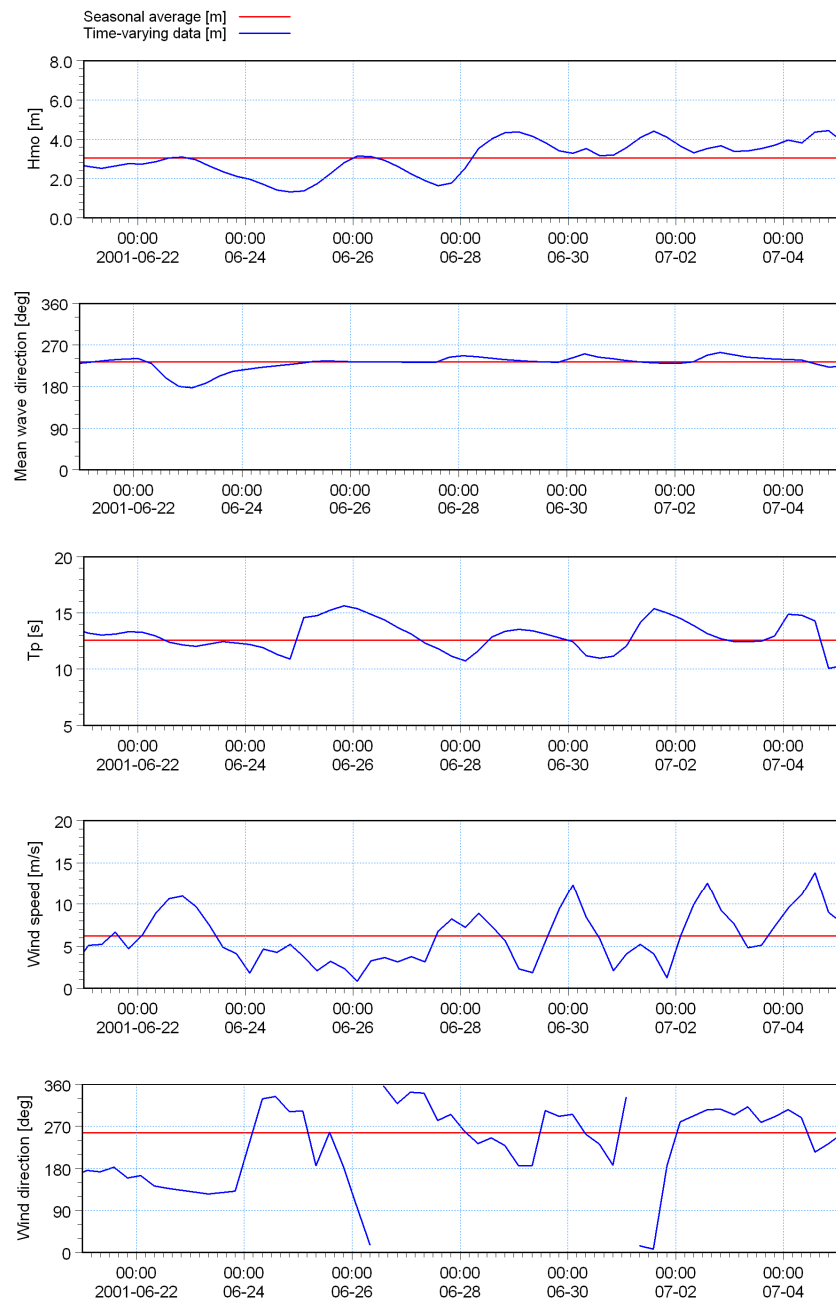


Title:

**Wave and wind time-series used in hydrodynamic and plume modelling.  
14 day summer simulation period.**

Figure No.

**8.11**



I:\Waves\Process\Kobberg\_Average\_Conditions.dbo  
 C:\ProgramData\Interpret\2001\_2003.dbo  
 I:\Waves\Process\Kobberg\_Average\_Conditions.dbo  
 C:\ProgramData\Interpret\2001\_2003.dbo  
 I:\Waves\Process\Kobberg\_Average\_Conditions.dbo  
 C:\ProgramData\Interpret\2001\_2003.dbo  
 I:\Waves\Process\Kobberg\_Average\_Conditions.dbo  
 C:\ProgramData\Interpret\2001\_2003.dbo

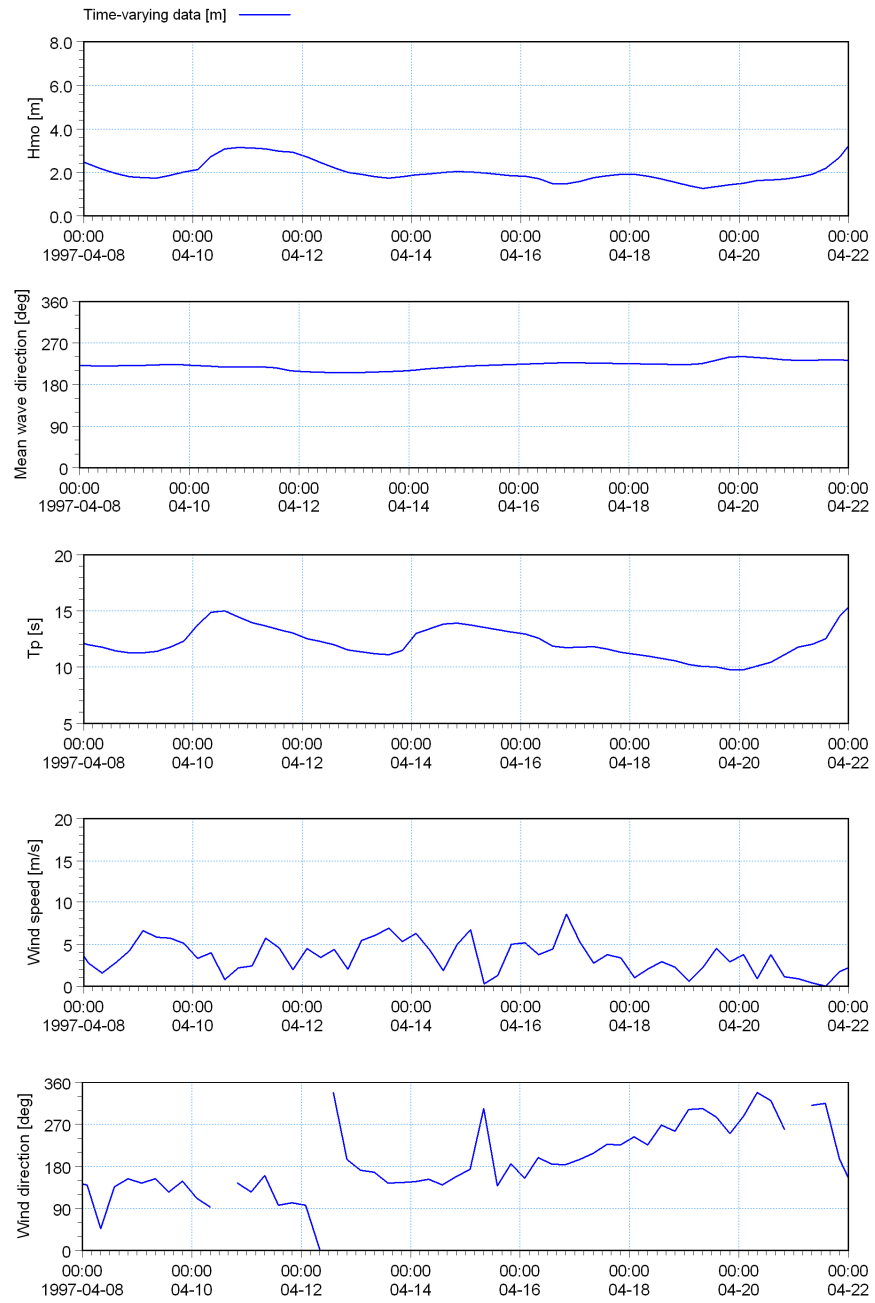


Title:

**Wave and wind time-series used in hydrodynamic and plume modelling.  
14 day winter simulation period.**

Figure No.

8.12



s\_Parameters\_Oceanor\_e180\_s340\_1997\_2006.dfo  
 \_Parameters\_Oceanor\_e180\_s340\_1997\_2006.dfo  
 e\_Parameters\_Oceanor\_e180\_s340\_1997\_2006.dfo  
 L\_Oceanor\_e180\_s340\_Interpolate2\_1997\_2006.dfo  
 sanor\_e180\_s340\_Interpolate2\_1997\_2006.dfo

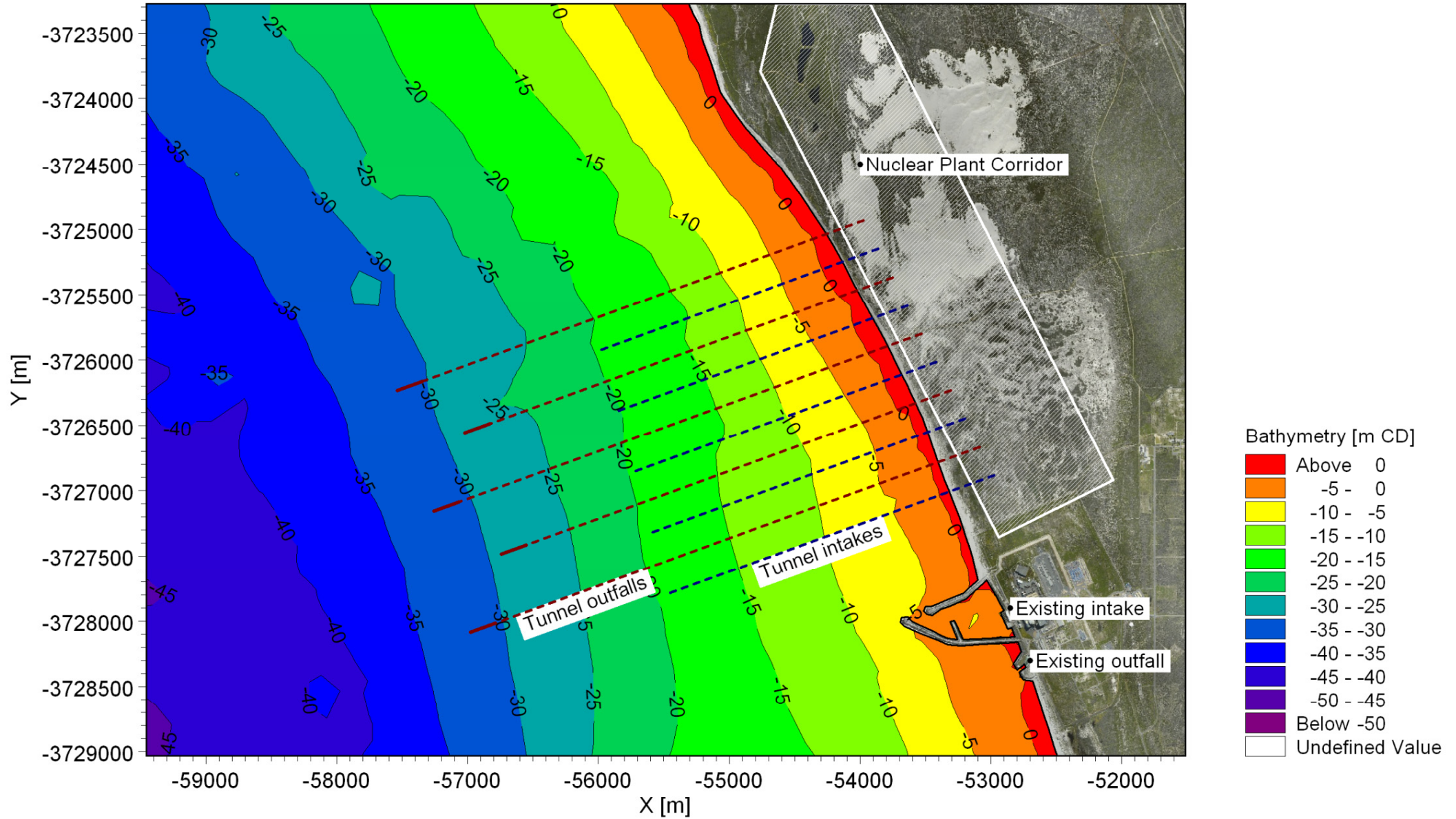


Title:

**Wave and wind time-series used in hydrodynamic and plume modelling.  
 14 day calm simulation period.**

Figure No.

8.13

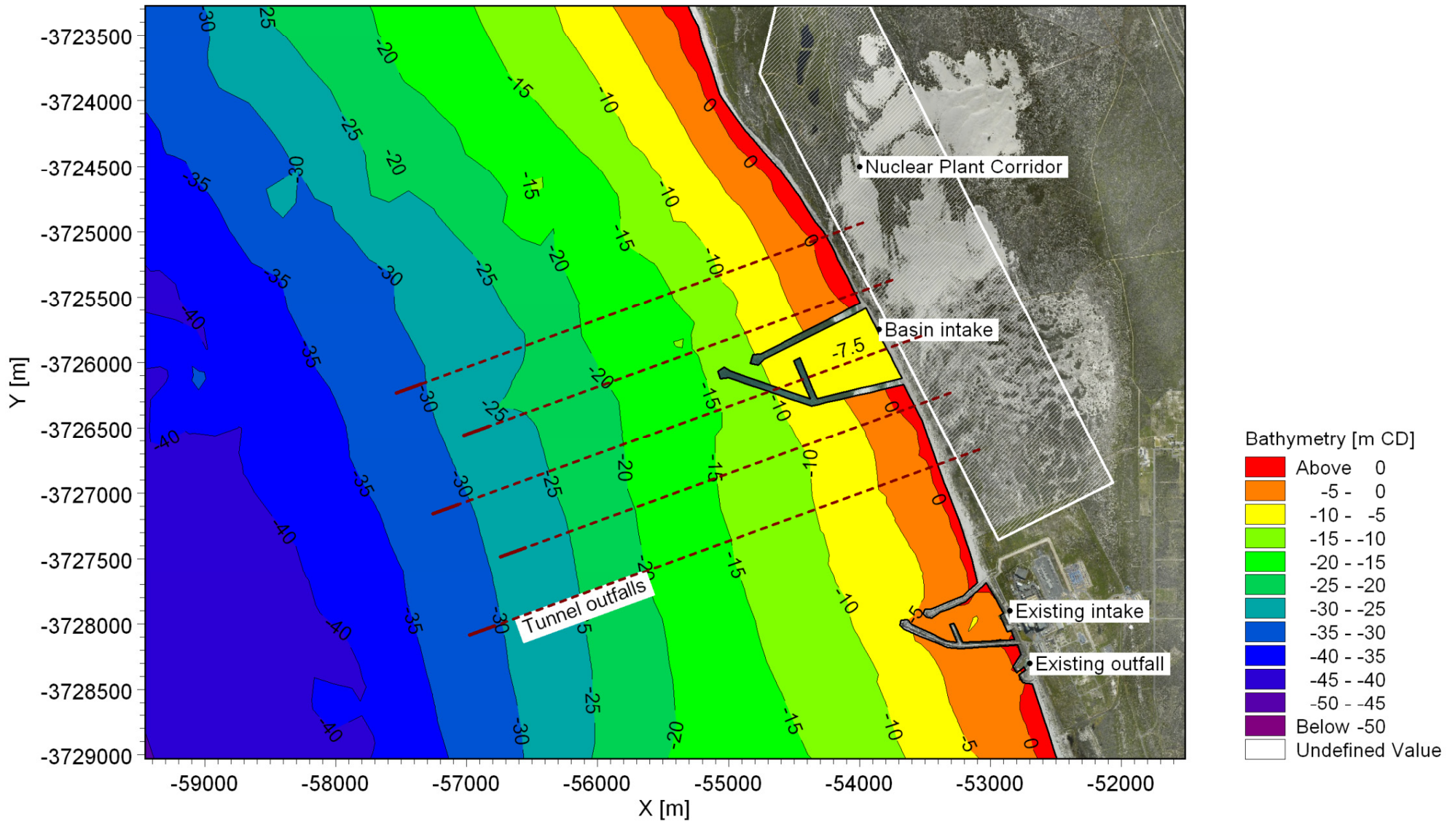


Title:

Layout 1: Offshore tunnel intake and offshore tunnel outfall.

Figure No.

9.1

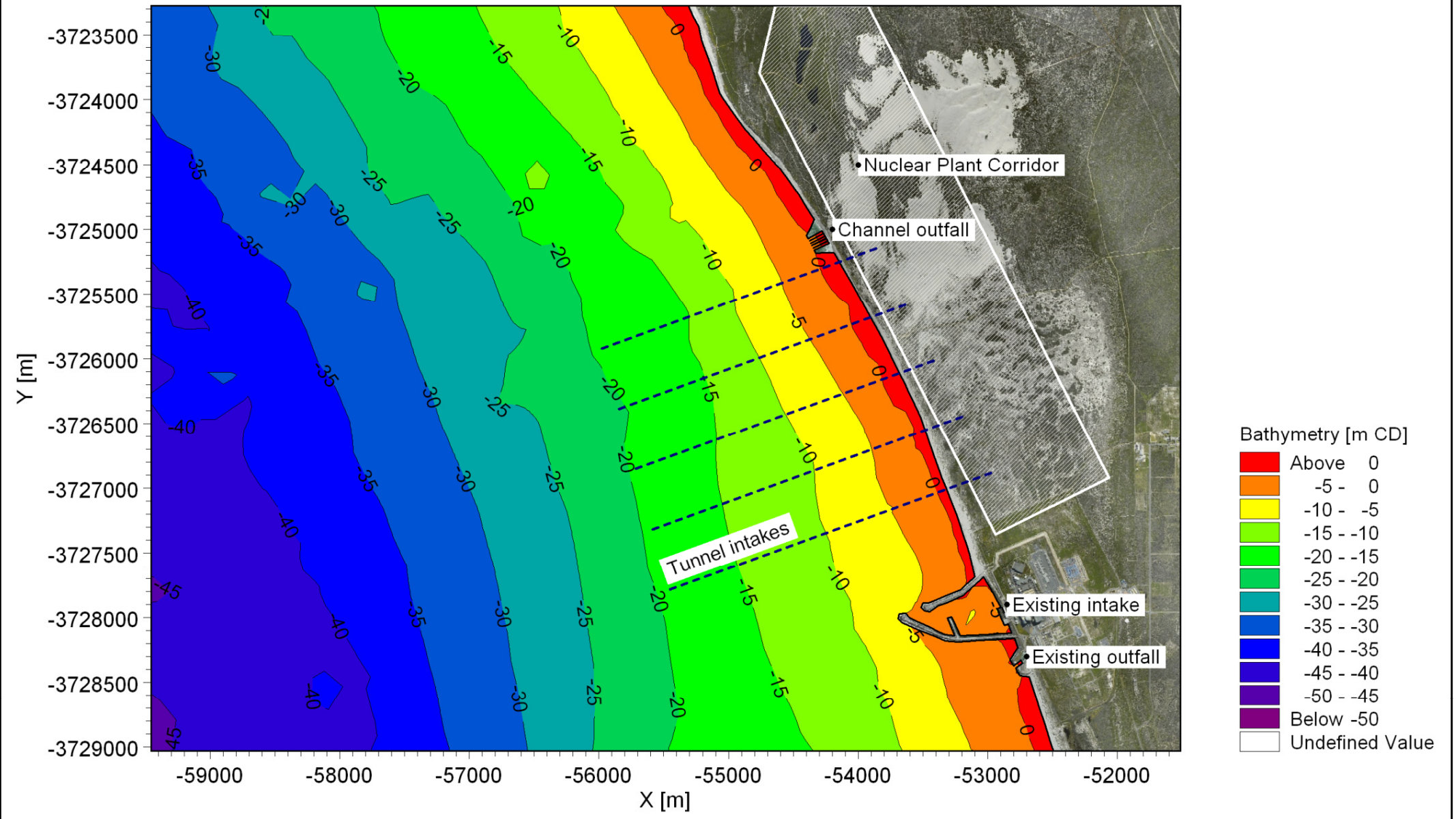


Title:

Layout 2: Basin intake and offshore tunnel outfall.

Figure No.

9.2

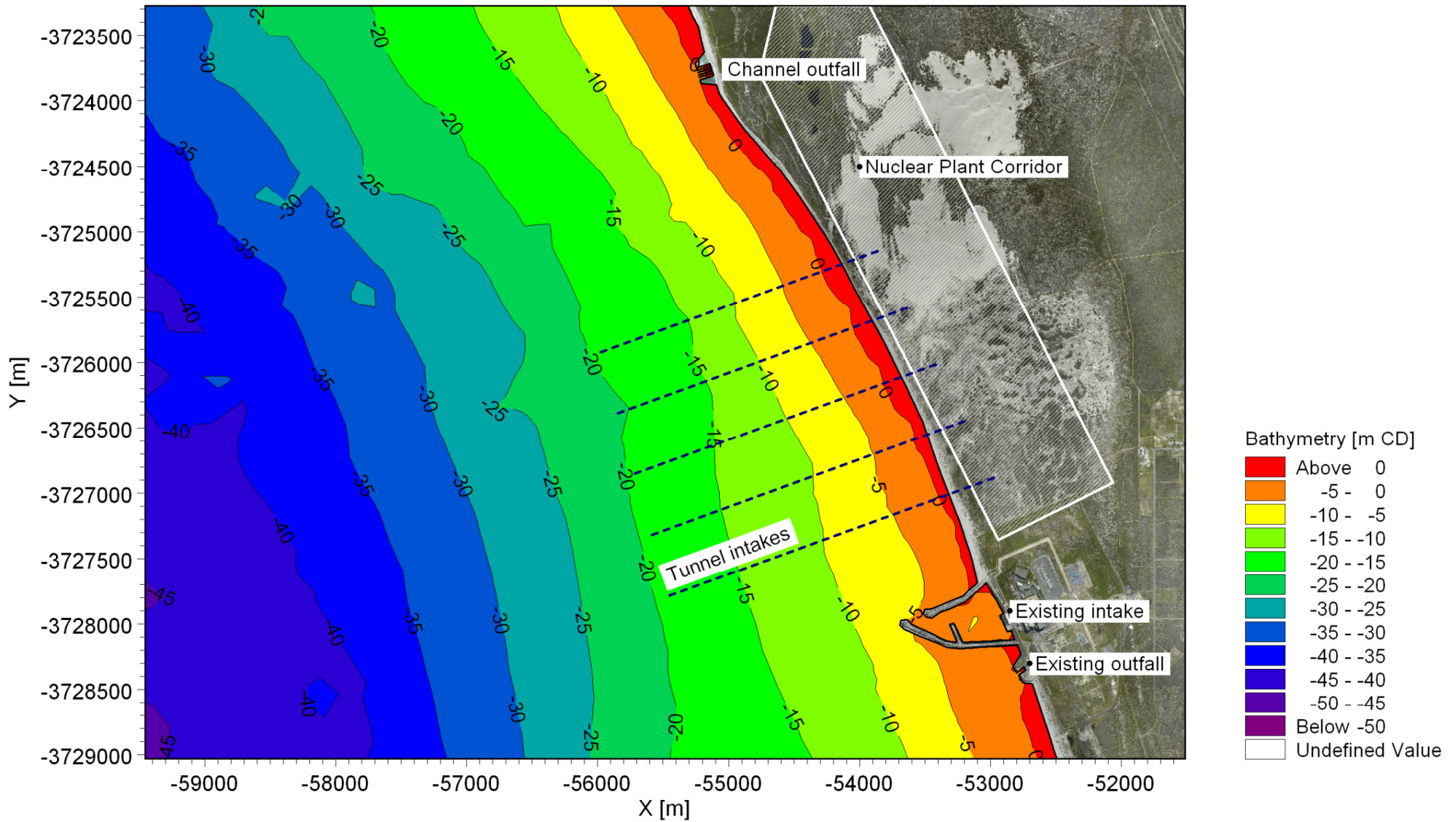


Title:

Layout 3: Offshore tunnel intake and nearshore channel outfall 3 km north.

Figure No.

9.3

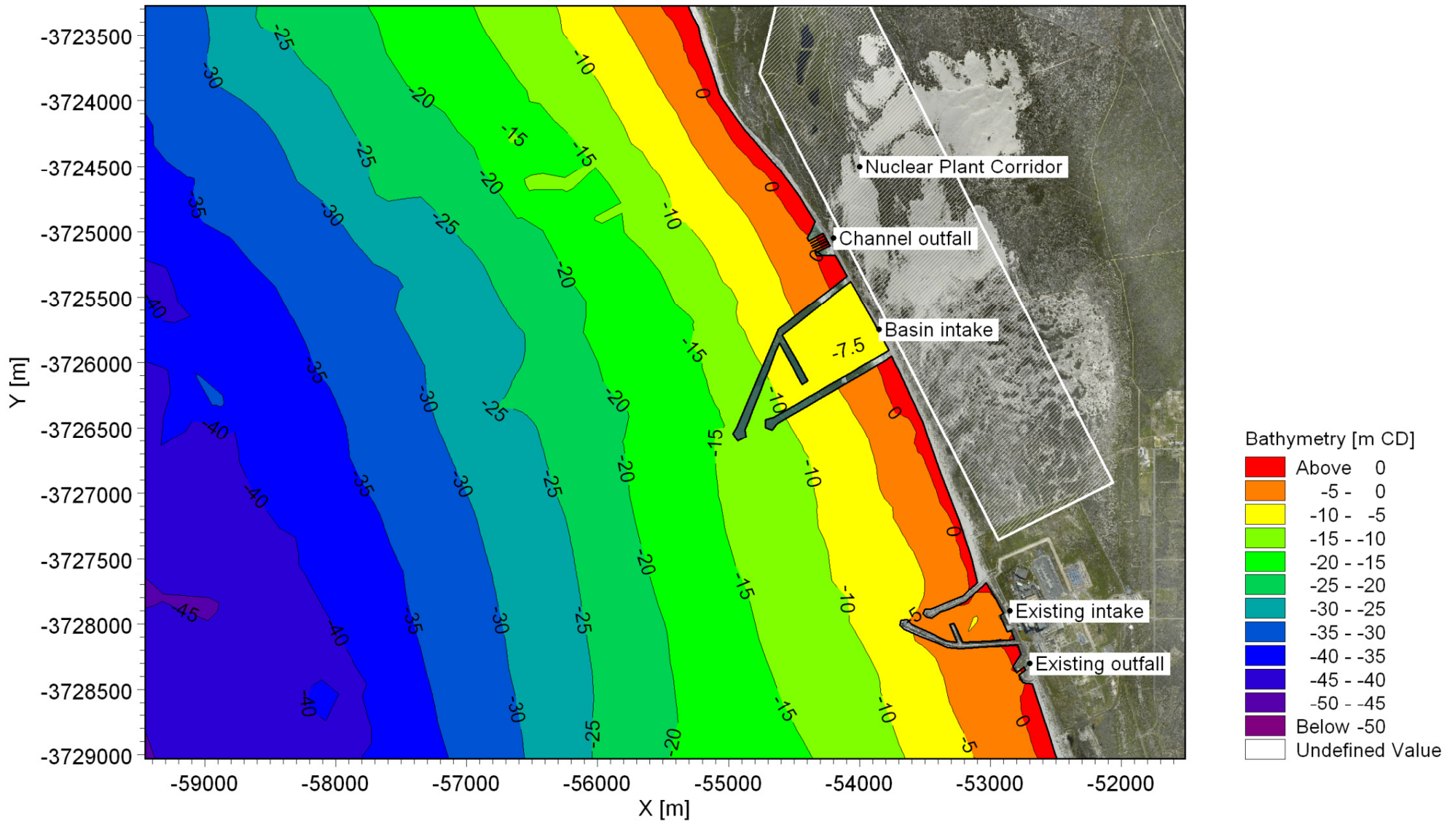


Title:

Layout 4: Offshore tunnel intake and nearshore channel outfall 4.5 km north.

Figure No.

9.4

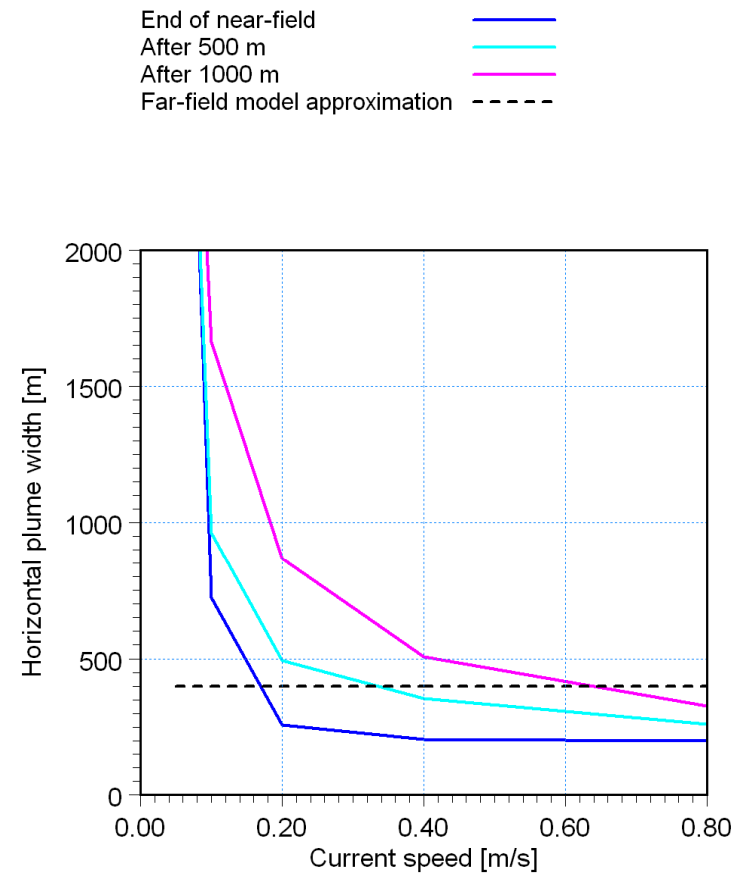
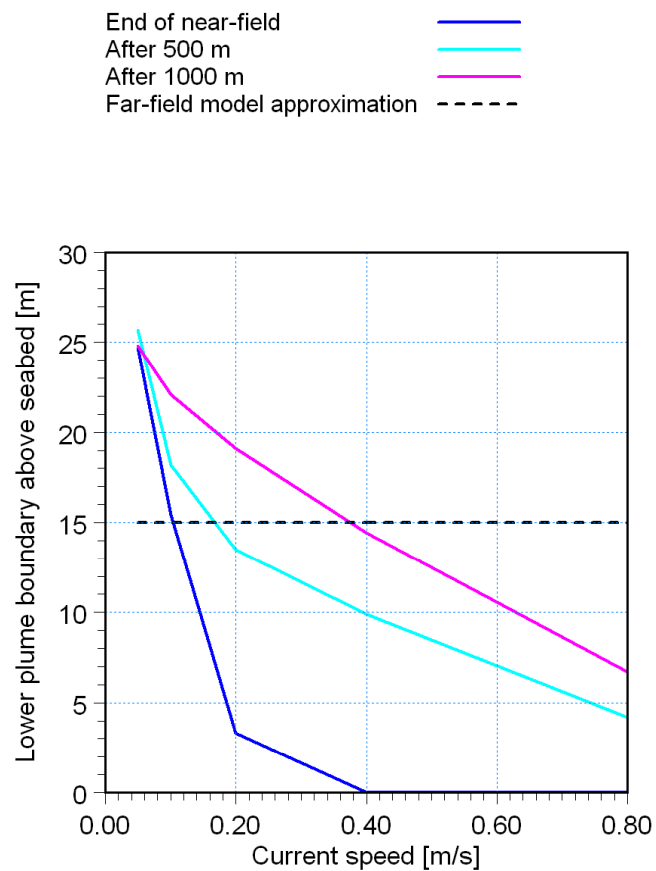
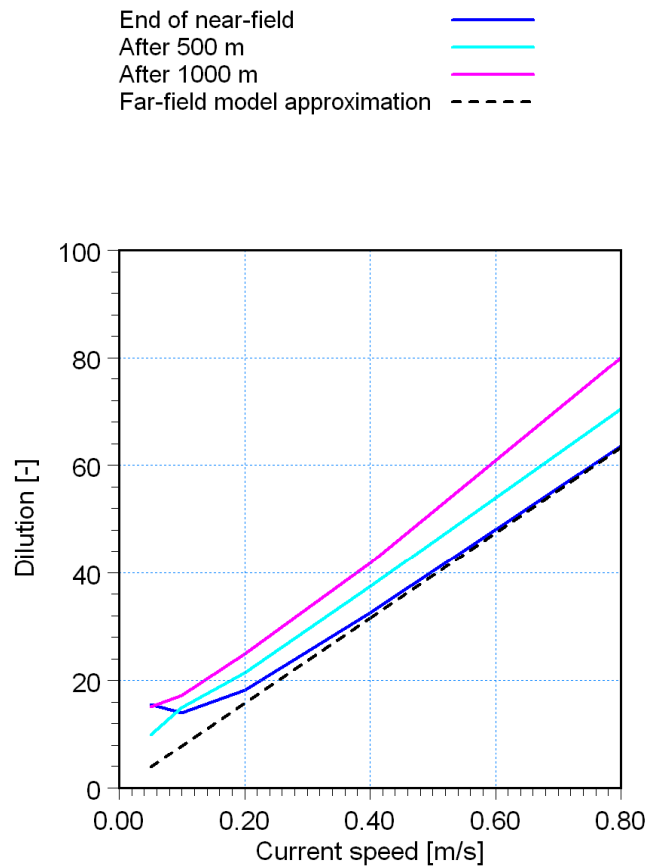


Title:

Layout 5: Basin intake and nearshore channel outfall.

Figure No.

9.5



G:\Projects\1010\_NuclearSites\General\Data\Discharges\Cormix.png

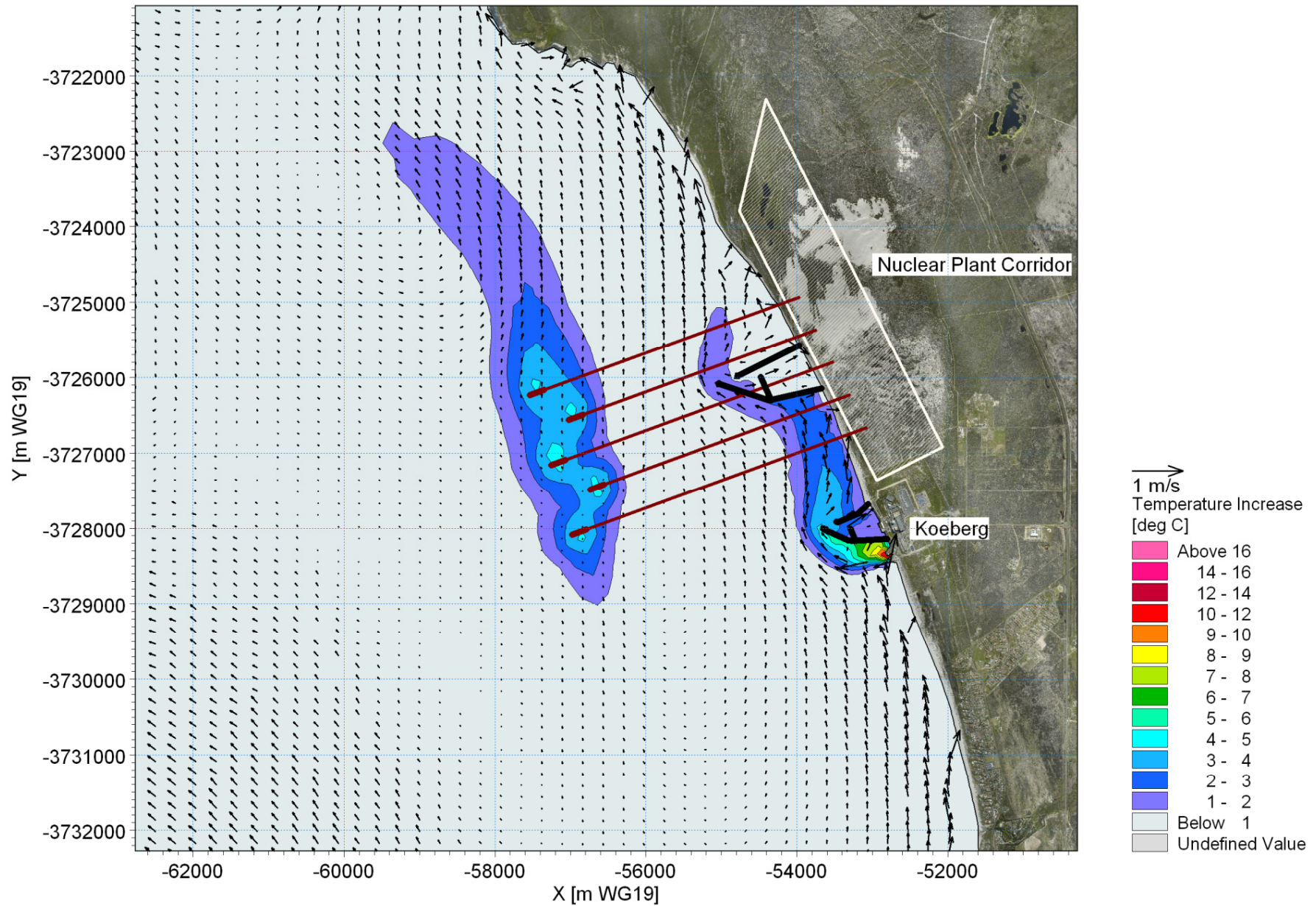


Title:

Near-field dilution modelling results (summer).

Figure No.

9.6



20:00:00 2020-01-03 Time Step 42 of 1008. Sigma Layer No. 5 of 5.

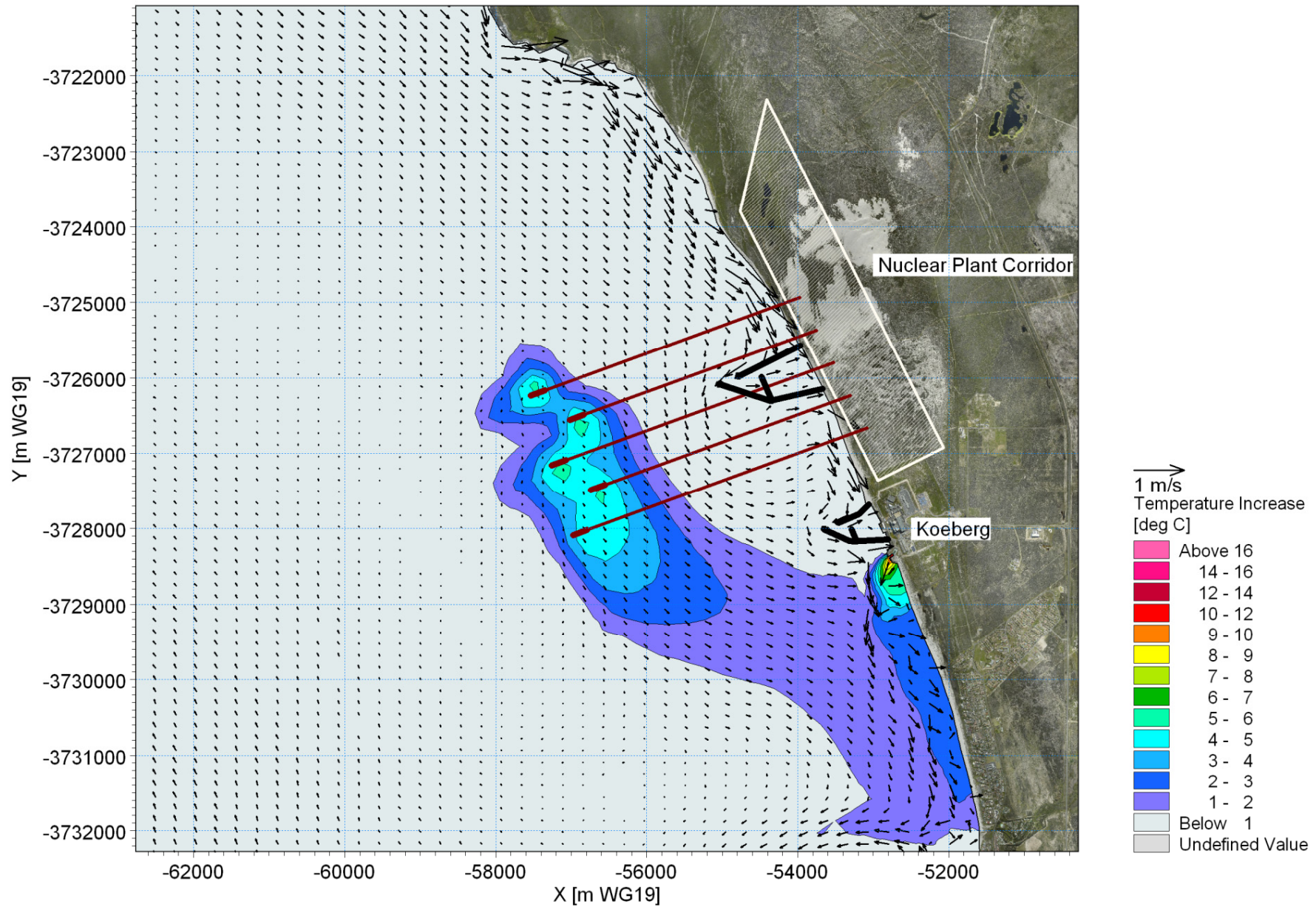


Title:

**Example of modelled currents and thermal plume near water surface at a time when the currents are northward.**

Figure No.

**9.7**



12:00:00 2020-01-28 Time Step 634 of 1008. Sigma Layer No. 5 of 5.



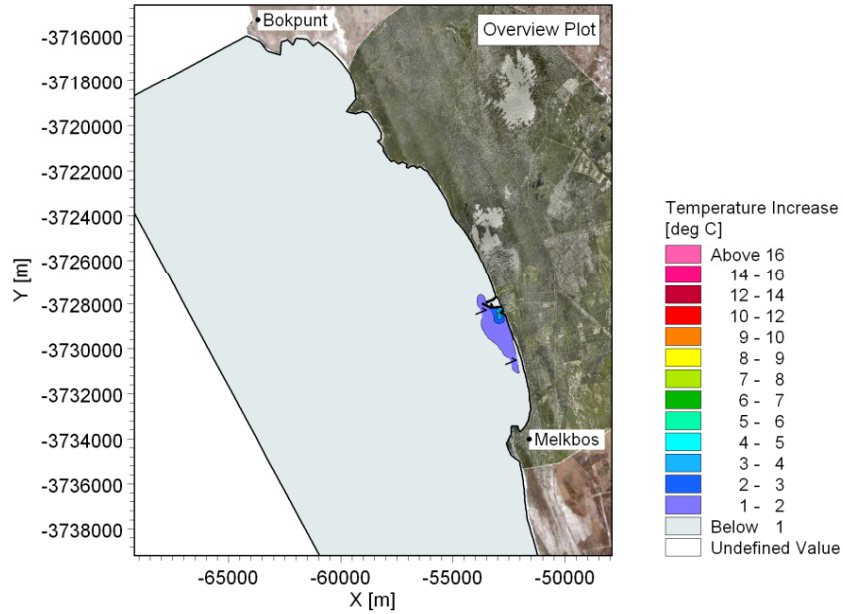
Title:

**Example of modelled currents and thermal plume near water surface at a time when the currents are southward.**

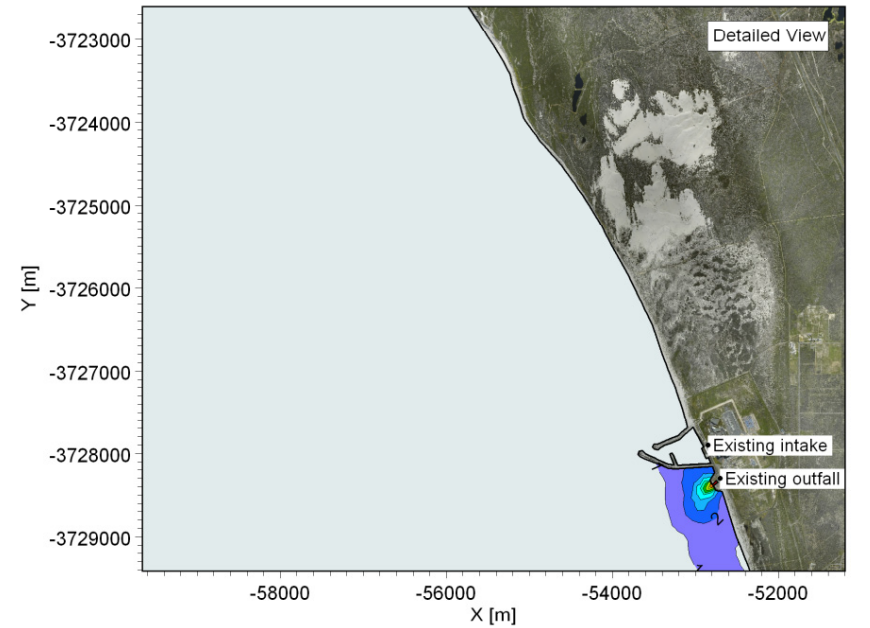
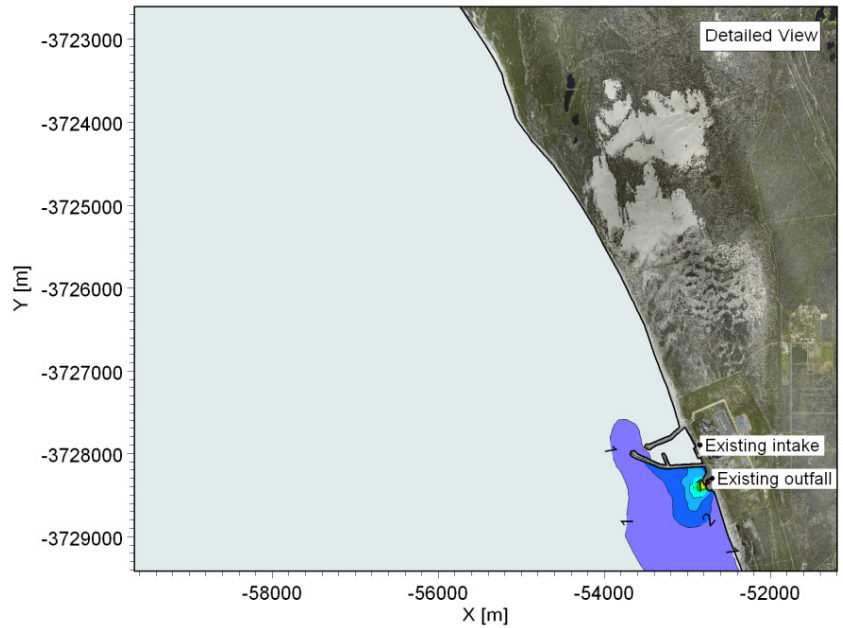
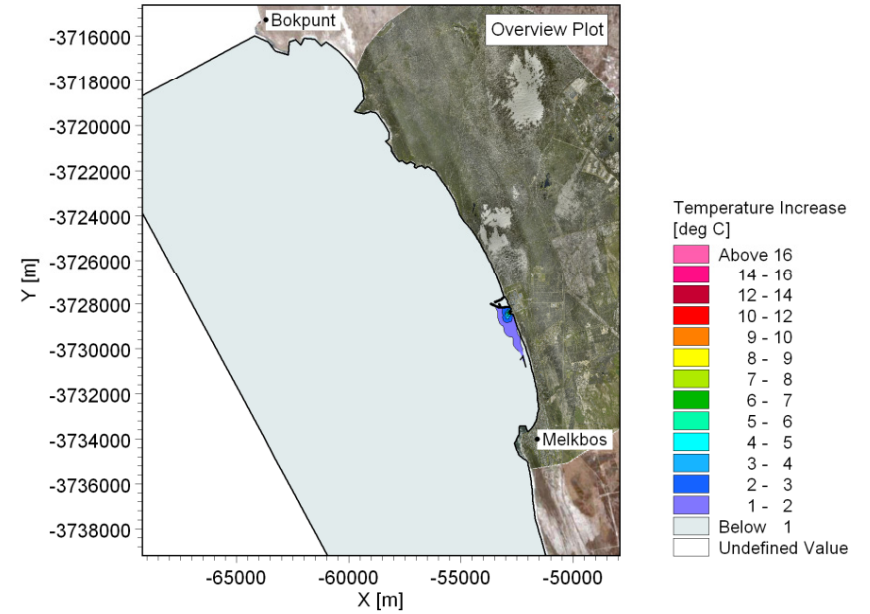
Figure No.

**9.8**

**Mean Increase in Temperature Near Water Surface**



**Mean Increase in Temperature Near Seabed**



G:\Projects\1010\_NuclearSites\Koeberg\Models\Plume\F\11a00a.m3fm - Result Files\Temp\_Mean\_Lay5.png

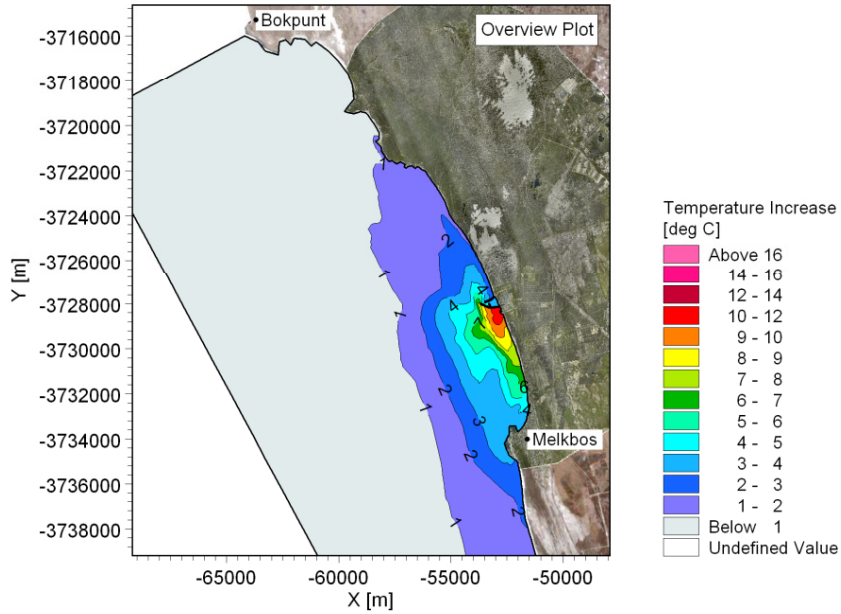
G:\Projects\1010\_NuclearSites\Koeberg\Models\Plume\F\11a00a.m3fm - Result Files\Temp\_Mean\_Lay1.png



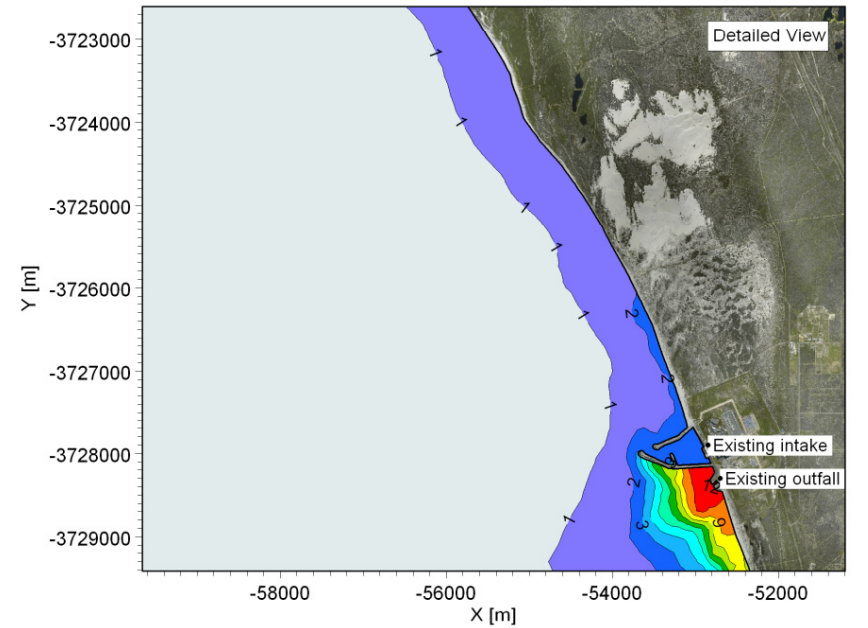
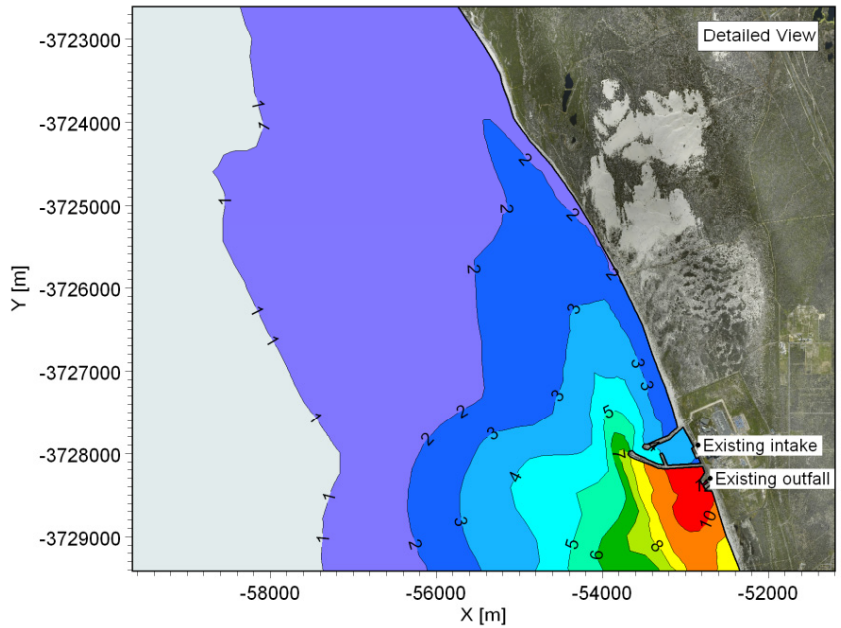
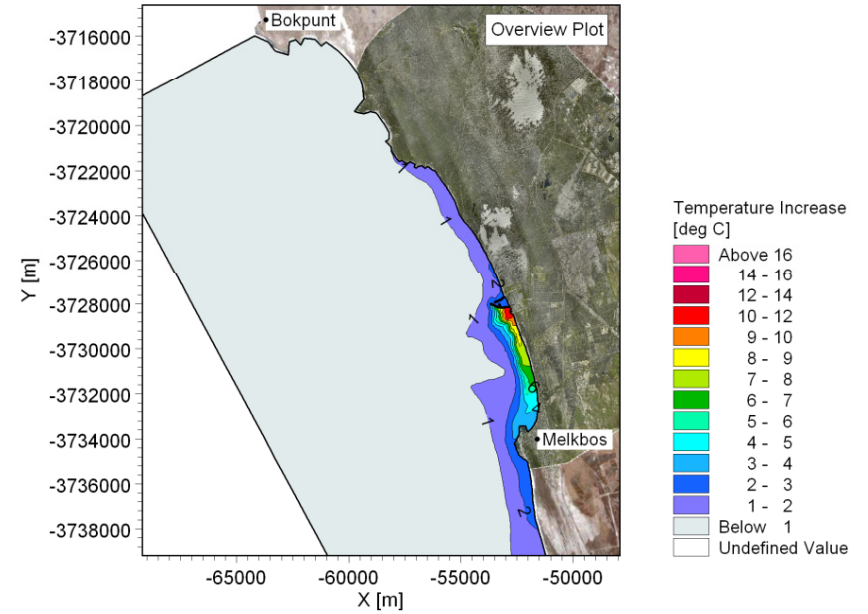
**Title:** Thermal plume modelling: Mean increase in temperature due to power station.  
**Layout 0: Existing Koeberg Layout.**  
**Power output: Koeberg = 1800 MWe.**

**Figure No.**  
**9.9**

**Maximum Increase in Temperature Near Water Surface**



**Maximum Increase in Temperature Near Seabed**



G:\Projects\1010\_NuclearSites\Koeberg\Models\Plume\F\11a00a.m3fm - Result Files\Temp\_Max\_Lay5.png

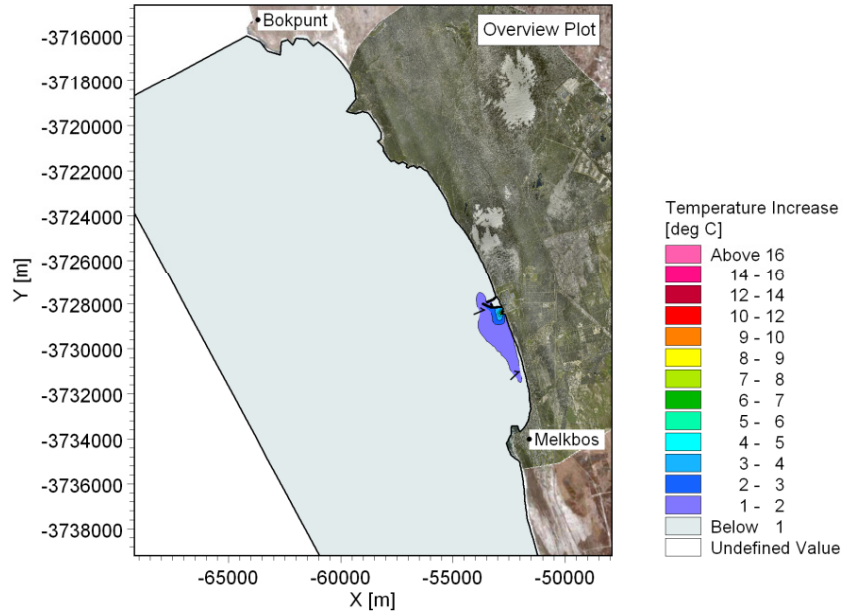
G:\Projects\1010\_NuclearSites\Koeberg\Models\Plume\F\11a00a.m3fm - Result Files\Temp\_Max\_Lay1.png



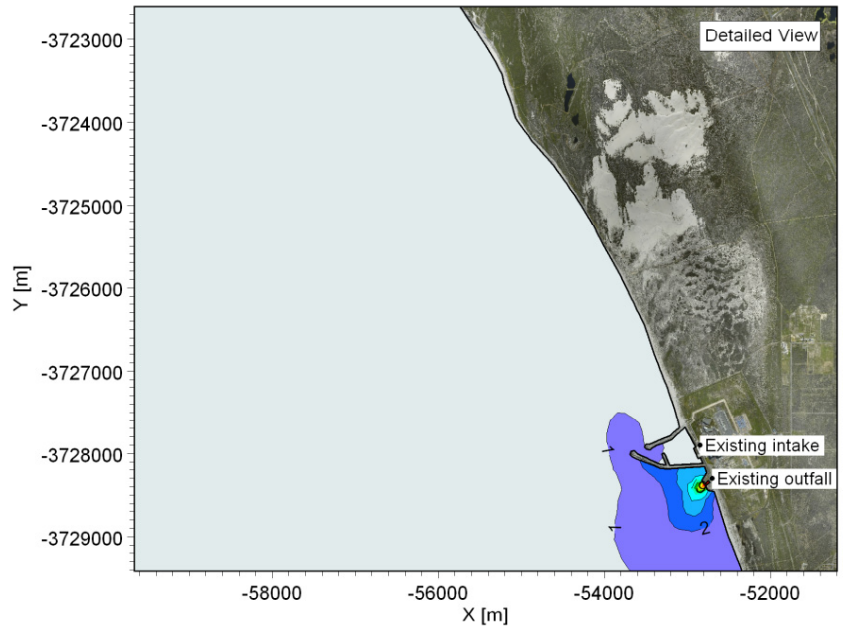
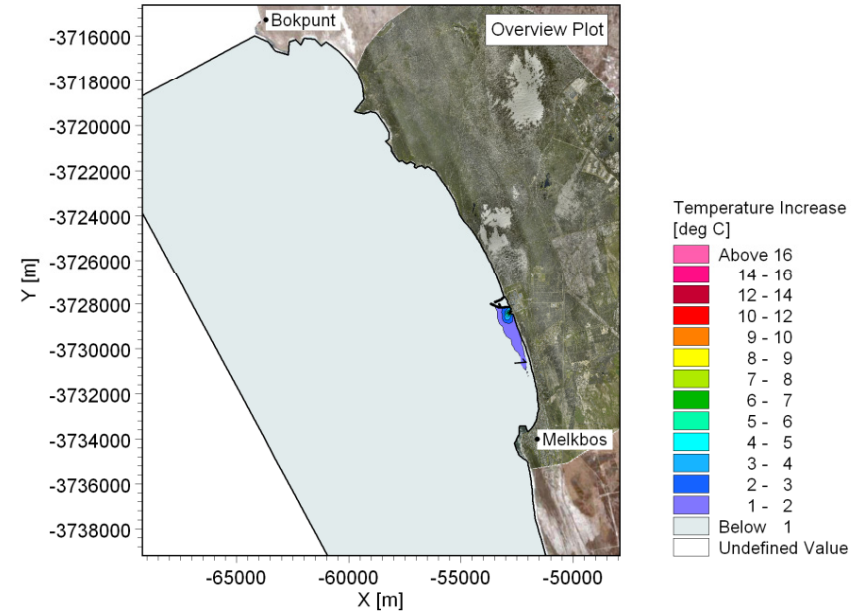
**Title: Thermal plume modelling: Maximum increase in temperature due to power station.  
Layout 0: Existing Koeberg Layout.  
Power output: Koeberg = 1800 MWe.**

**Figure No.  
9.10**

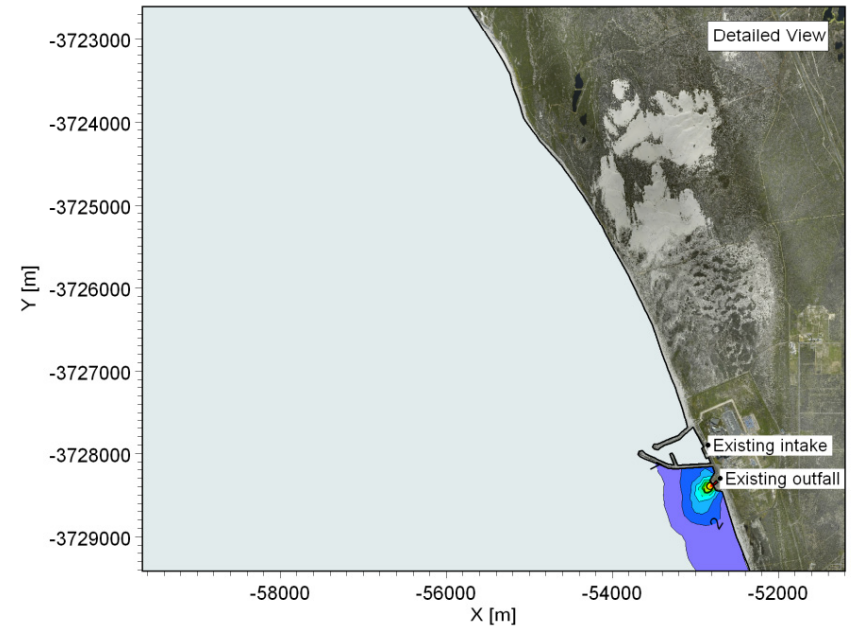
**Mean Increase in Temperature Near Water Surface**



**Mean Increase in Temperature Near Seabed**



G:\Projects\1010\_NuclearSites\Koeberg\Models\Plume\F\11a01a.m3fm - Result Files\Temp\_Mean\_Lay5.png



G:\Projects\1010\_NuclearSites\Koeberg\Models\Plume\F\11a01a.m3fm - Result Files\Temp\_Mean\_Lay1.png



Title:

**Thermal plume modelling: Mean increase in temperature due to power station.**

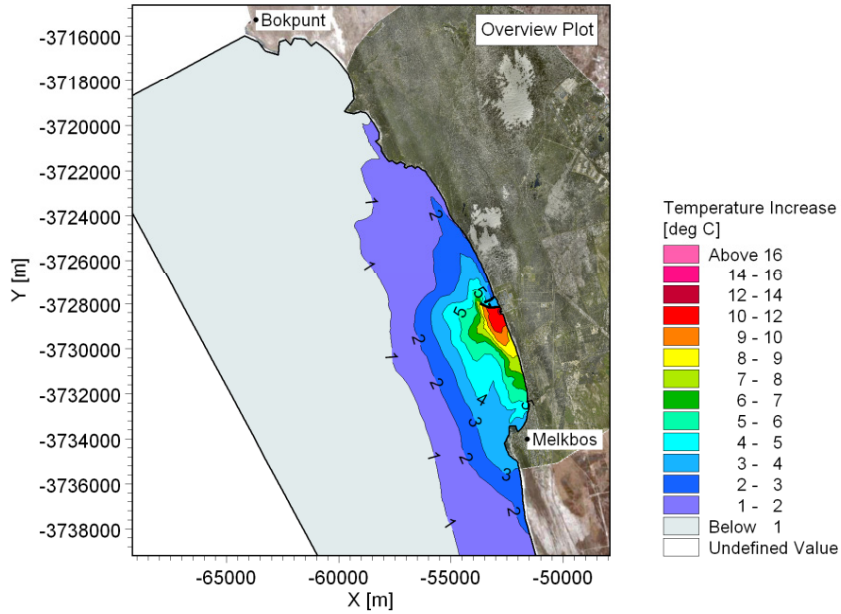
**Layout 0: Existing Koeberg Layout plus PBMR.**

**Power output: Koeberg = 1800 MWe, PBMR = 165 MWe.**

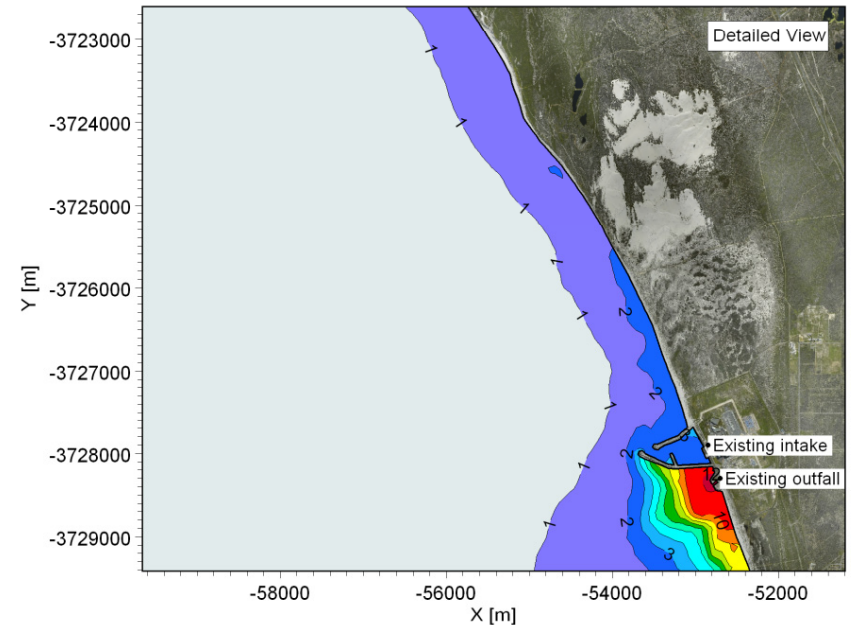
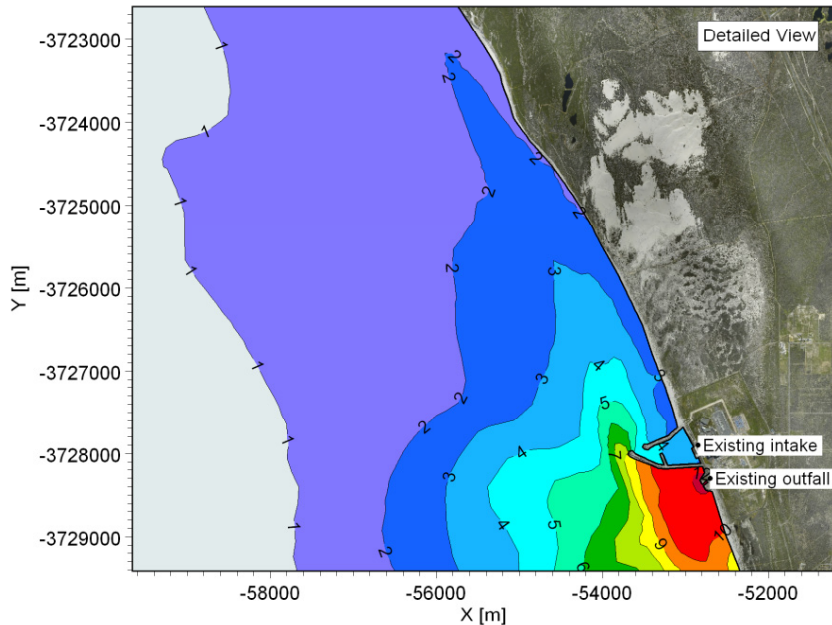
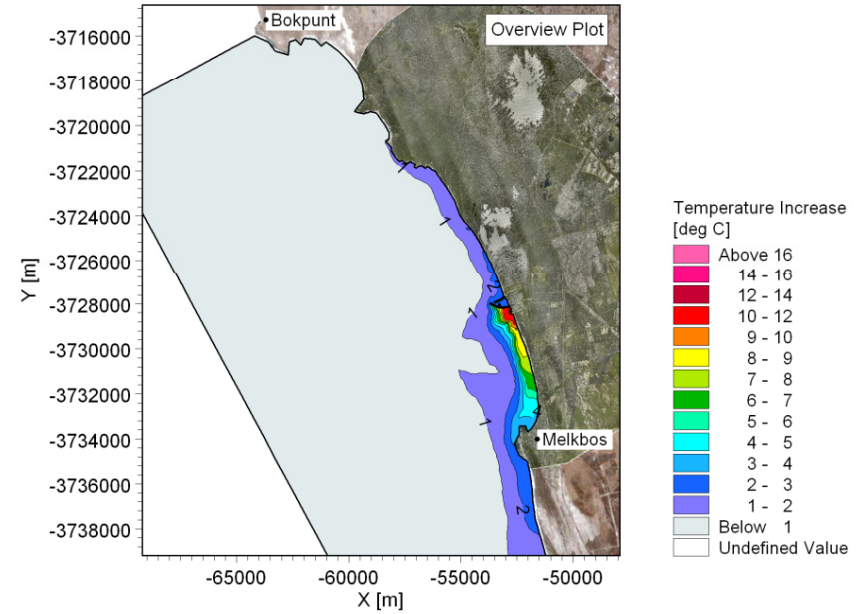
Figure No.

**9.11**

**Maximum Increase in Temperature Near Water Surface**



**Maximum Increase in Temperature Near Seabed**



G:\Projects\1010\_NuclearSites\Koeberg\Models\Plume\F\11a01a.m3fm - Result Files\Temp\_Max\_Lay5.png

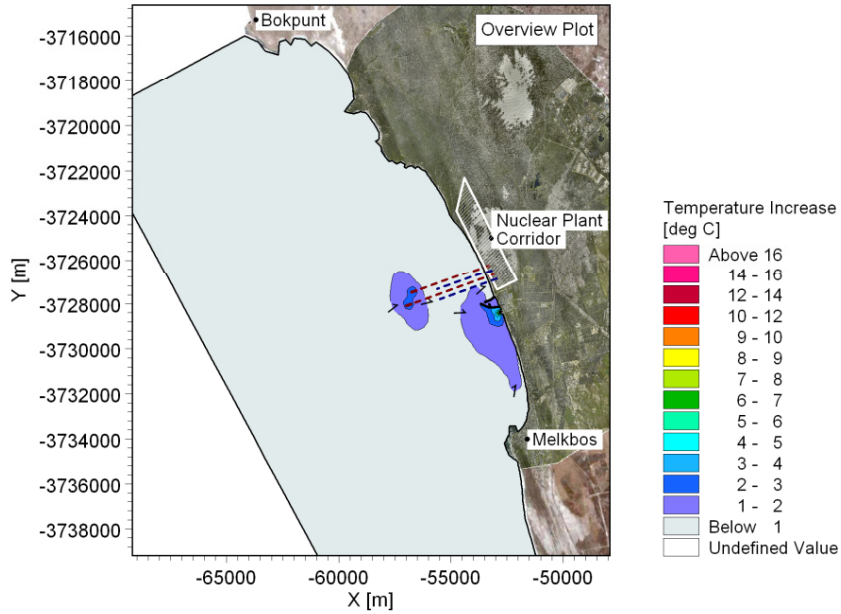
G:\Projects\1010\_NuclearSites\Koeberg\Models\Plume\F\11a01a.m3fm - Result Files\Temp\_Max\_Lay1.png



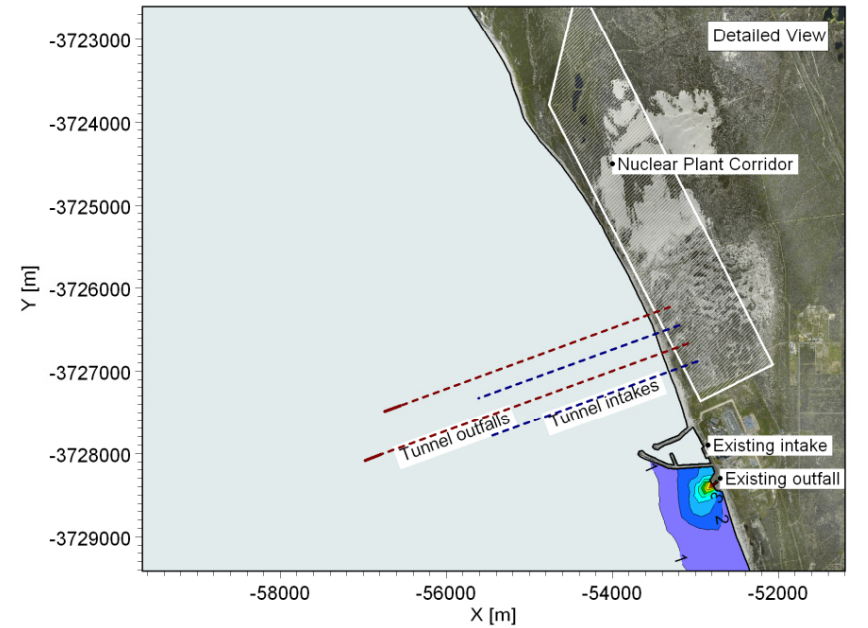
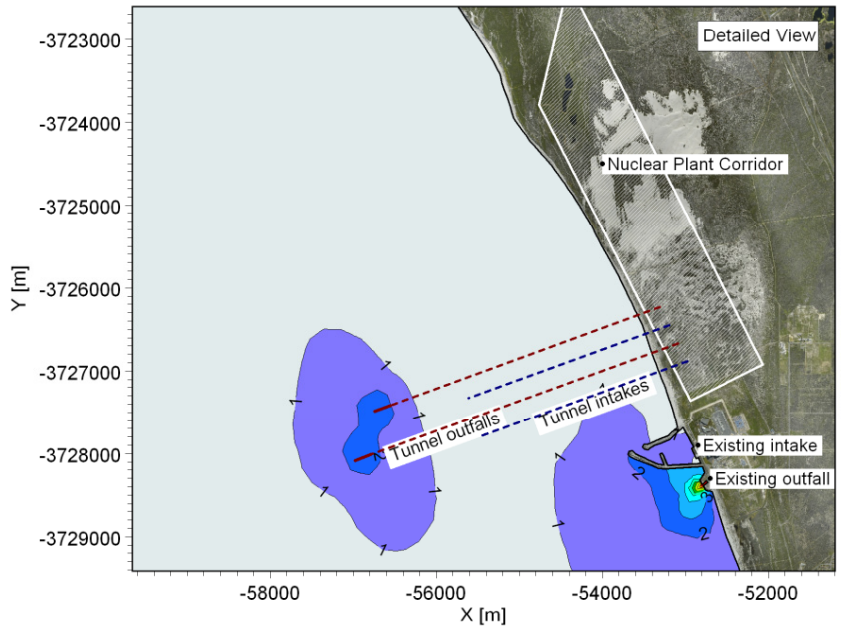
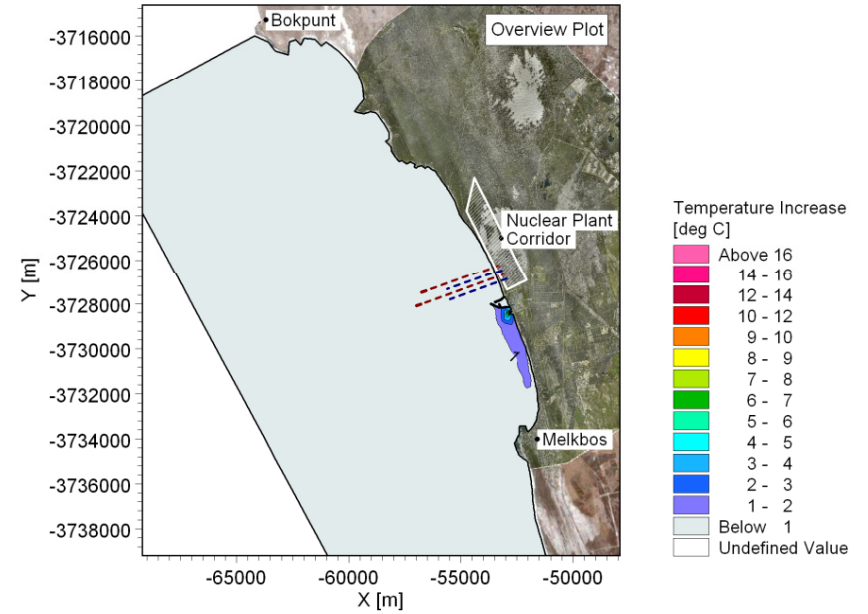
**Title: Thermal plume modelling: Maximum increase in temperature due to power station.  
Layout 0: Existing Koeberg Layout plus PBMR.  
Power output: Koeberg = 1800 MWe, PBMR = 165 MWe.**

**Figure No.  
9.12**

**Mean Increase in Temperature Near Water Surface**



**Mean Increase in Temperature Near Seabed**



G:\Projects\1010\_NuclearSites\Koeberg\Models\Piume\F\11a13a.m3fm - Result Files\Temp\_Mean\_Lay5.png

G:\Projects\1010\_NuclearSites\Koeberg\Models\Piume\F\11a13a.m3fm - Result Files\Temp\_Mean\_Lay1.png



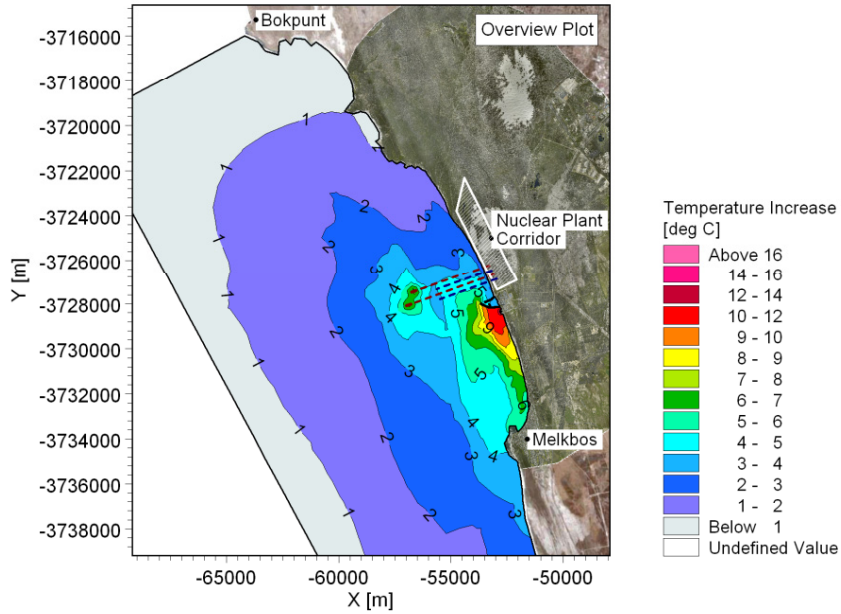
**Title:**

**Thermal plume modelling: Mean increase in temperature due to power station.  
Layout 1: Offshore tunnel intake and offshore tunnel outfall.  
Power output: Koeberg = 1800 MWe, PBMR = 165 MWe, Nuclear-1 = 4000 MWe.**

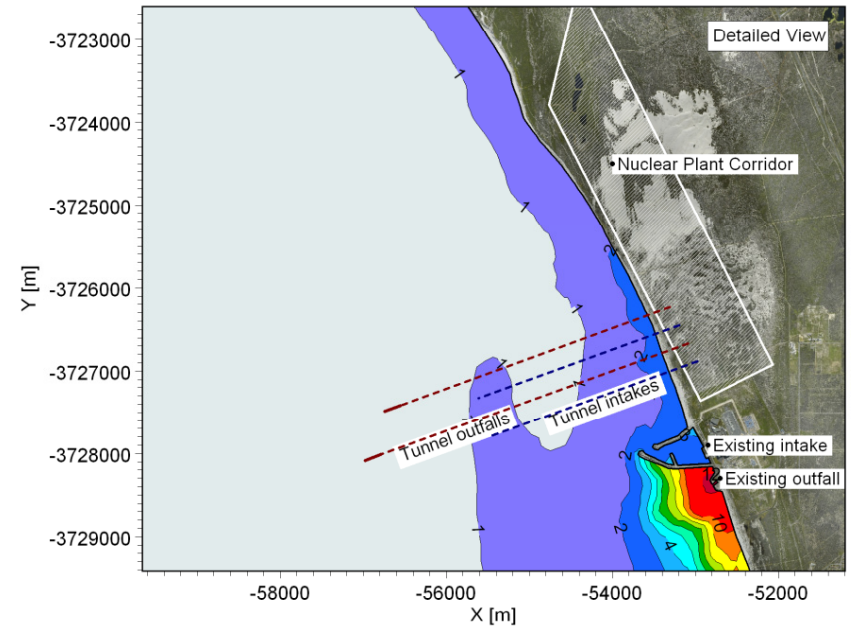
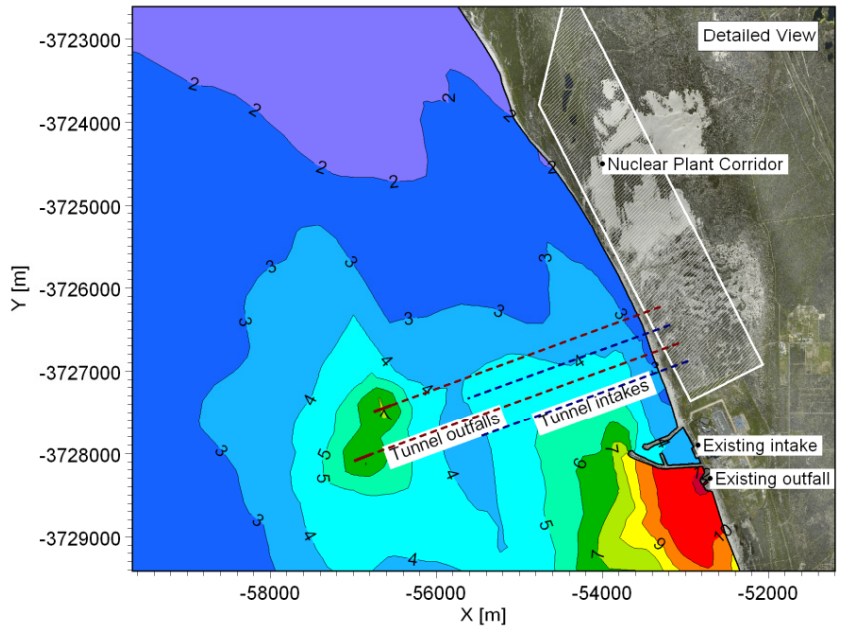
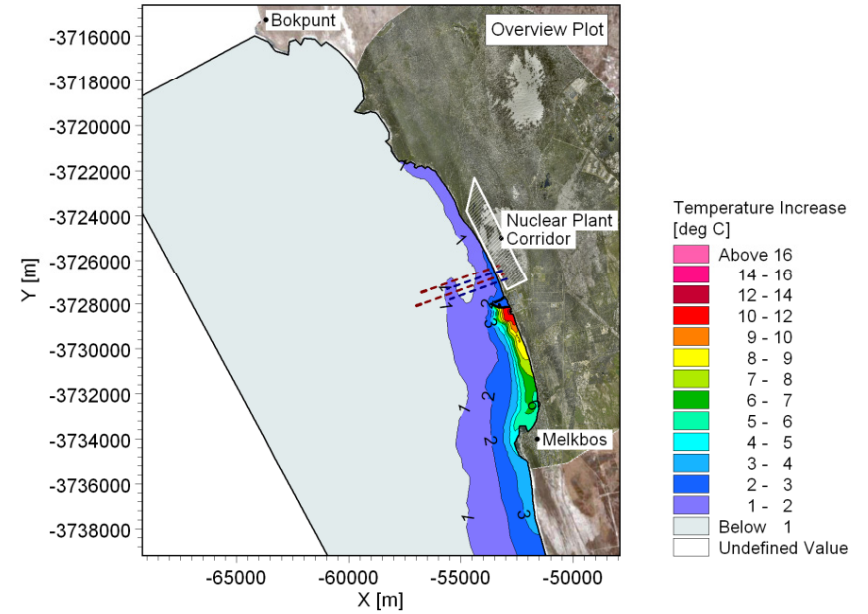
**Figure No.**

**9.13**

**Maximum Increase in Temperature Near Water Surface**



**Maximum Increase in Temperature Near Seabed**



G:\Projects\1010\_NuclearSites\Koeberg\Models\Plume\F\11a13a.m3fm - Result Files\Temp\_Max\_Lay5.png

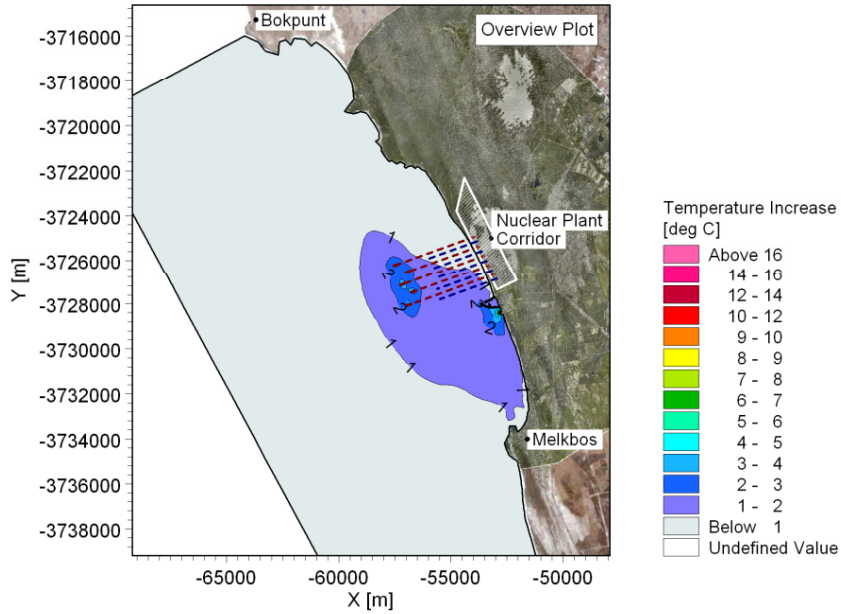
G:\Projects\1010\_NuclearSites\Koeberg\Models\Plume\F\11a13a.m3fm - Result Files\Temp\_Max\_Lay1.png



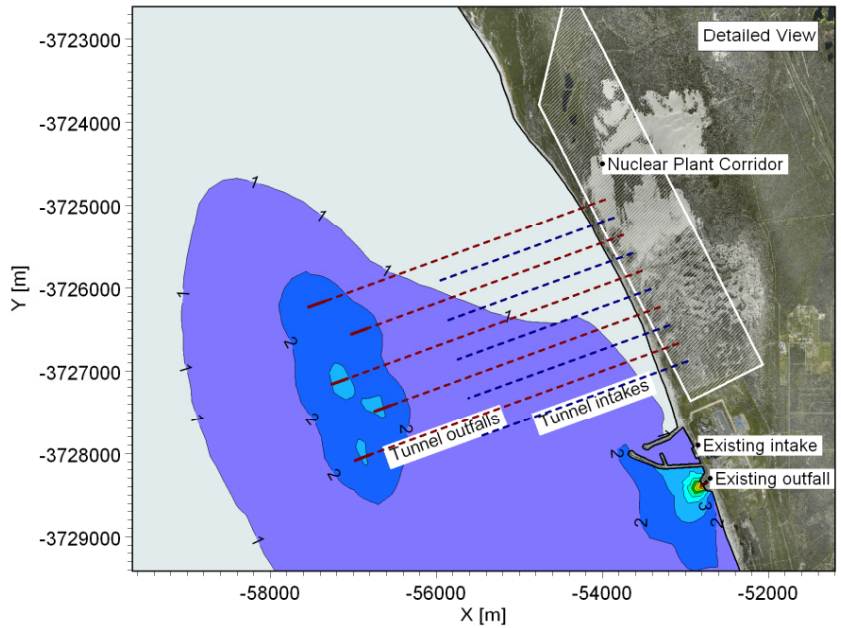
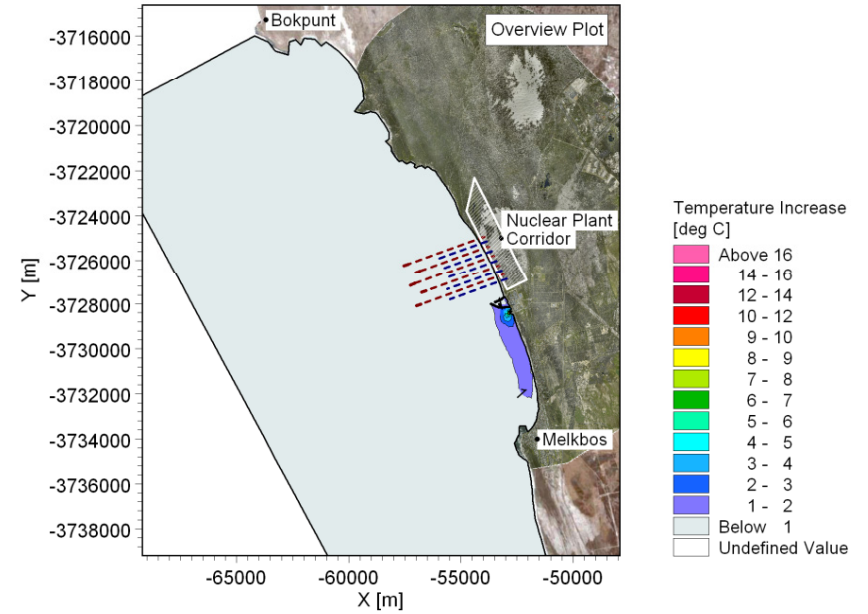
**Title: Thermal plume modelling: Maximum increase in temperature due to power station.  
Layout 1: Offshore tunnel intake and offshore tunnel outfall.  
Power output: Koeberg = 1800 MWe, PBMR = 165 MWe, Nuclear-1 = 4000 MWe.**

**Figure No.  
9.14**

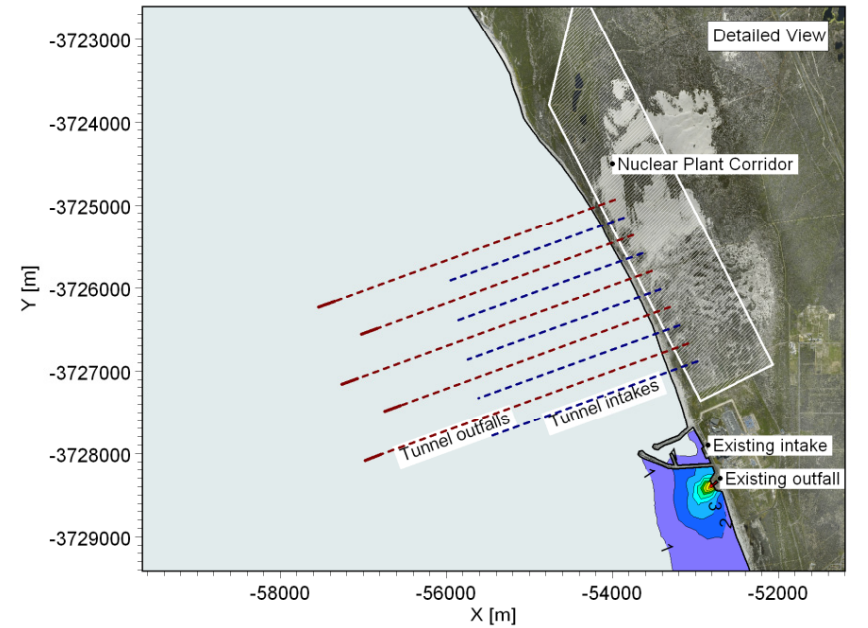
**Mean Increase in Temperature Near Water Surface**



**Mean Increase in Temperature Near Coastal**



G:\Projects\1010\_NuclearSites\Koeberg\Models\Plume\F\11a12a.m3fm - Result Files\Temp\_Mean\_Lay5.png



G:\Projects\1010\_NuclearSites\Koeberg\Models\Plume\F\11a12a.m3fm - Result Files\Temp\_Mean\_Lay1.png



**Title:**

**Thermal plume modelling: Mean increase in temperature due to power station.**

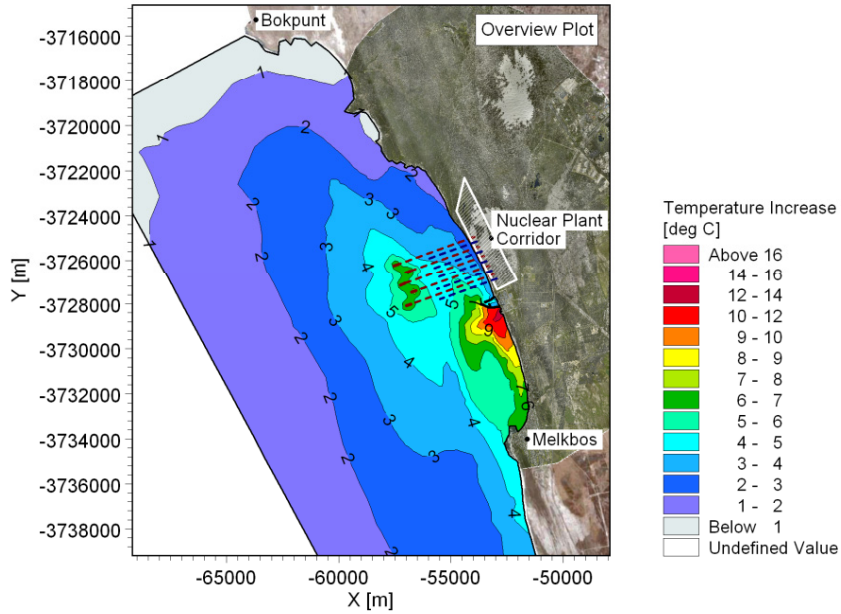
**Layout 1: Offshore tunnel intake and offshore tunnel outfall.**

**Power output: Koeberg = 1800 MWe, PBMR = 165 MWe, Nuclear-1 + expansion = 8250 MWe.**

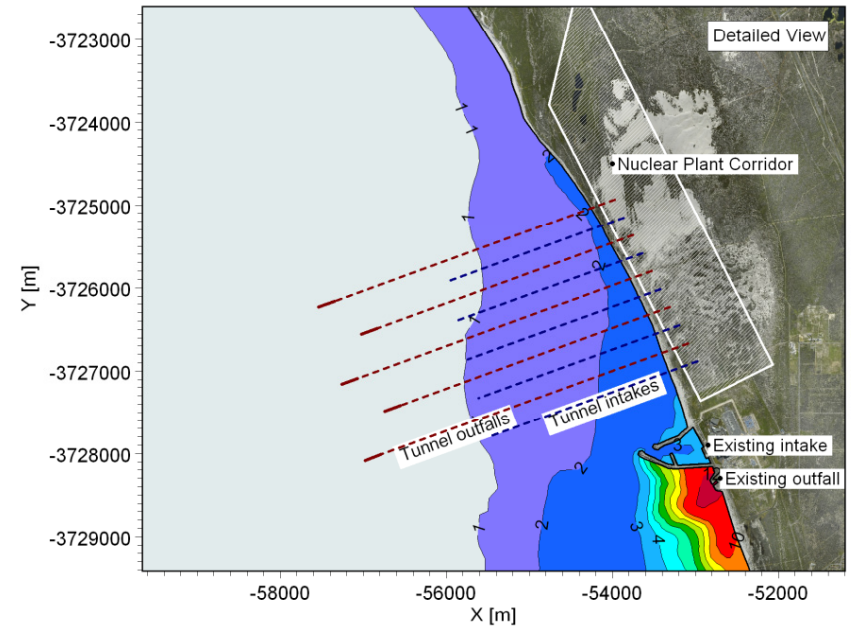
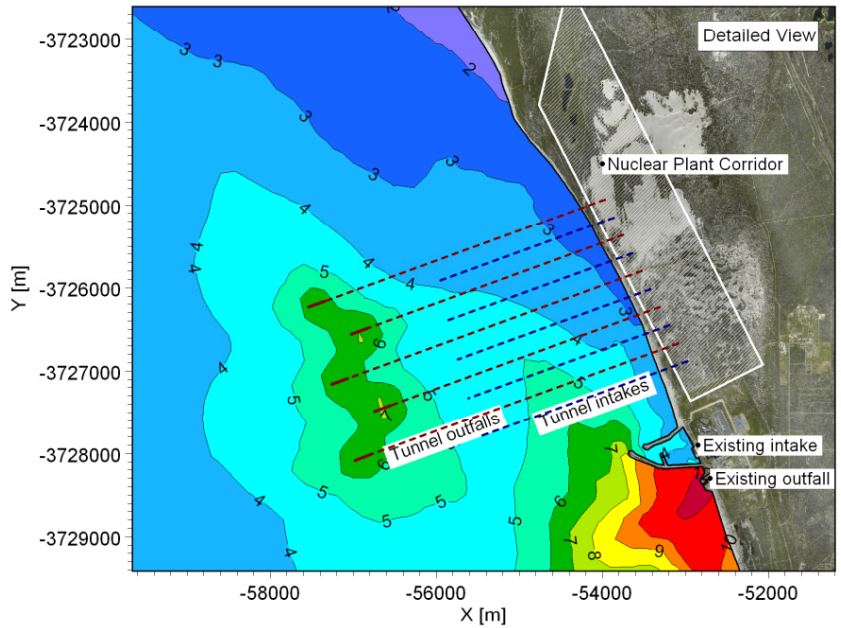
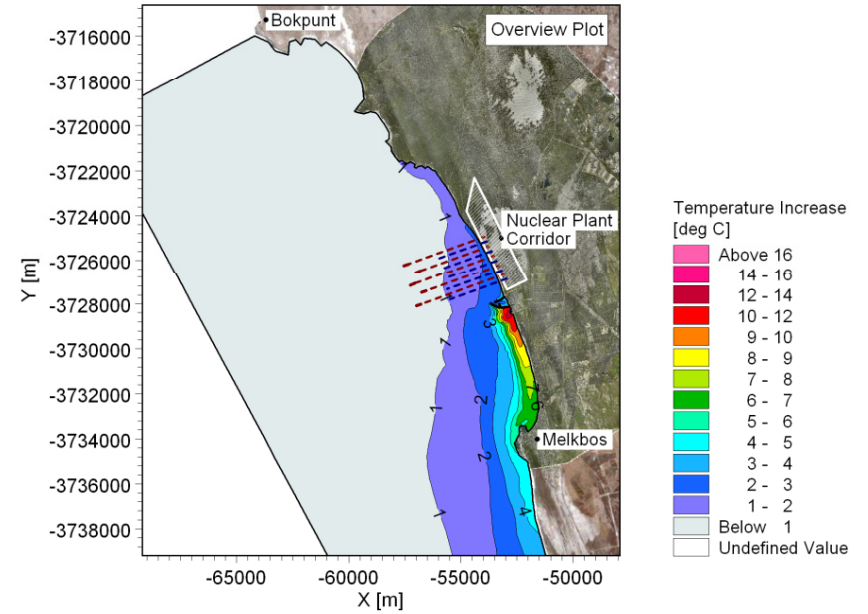
**Figure No.**

**9.15**

**Maximum Increase in Temperature Near Water Surface**



**Maximum Increase in Temperature Near Seabed**



G:\Projects\1010\_NuclearSites\Koeberg\Wdels\FIume\F\11a12a.m3fm - Result Files\Temp\_Max\_Lay5.png

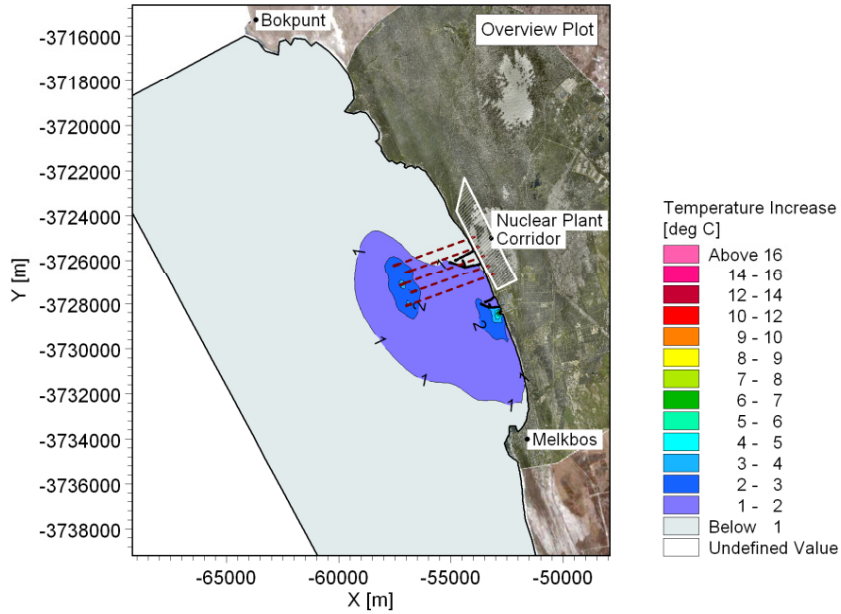
G:\Projects\1010\_NuclearSites\Koeberg\Wdels\FIume\F\11a12a.m3fm - Result Files\Temp\_Max\_Lay1.png



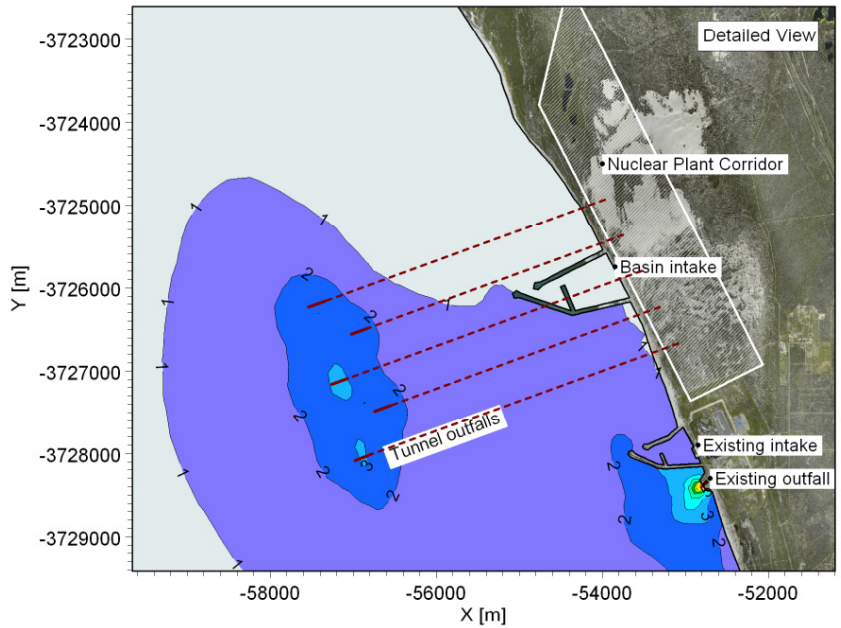
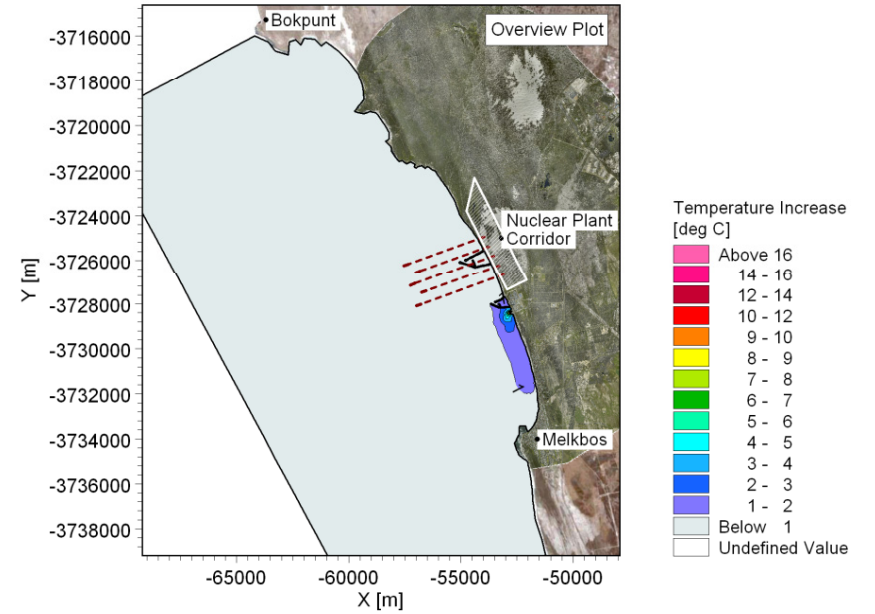
**Title: Thermal plume modelling: Maximum increase in temperature due to power station.  
Layout 1: Offshore tunnel intake and offshore tunnel outfall.  
Power output: Koeberg = 1800 MWe, PBMR = 165 MWe, Nuclear-1 + expansion = 8250 MWe.**

**Figure No.  
9.16**

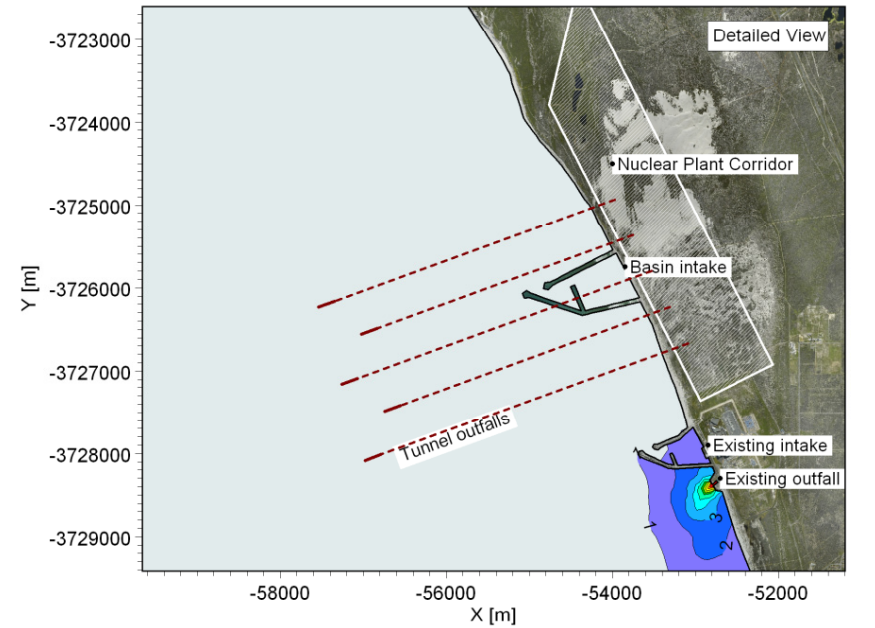
**Mean Increase in Temperature Near Water Surface**



**Mean Increase in Temperature Near Seabed**



G:\Projects\1010\_NuclearSites\Koeberg\Models\Plume\F\12a22a.m3fm - Result Files\Temp\_Mean\_Lay5.png



G:\Projects\1010\_NuclearSites\Koeberg\Models\Plume\F\12a22a.m3fm - Result Files\Temp\_Mean\_Lay1.png



**Title:**

**Thermal plume modelling: Mean increase in temperature due to power station.**

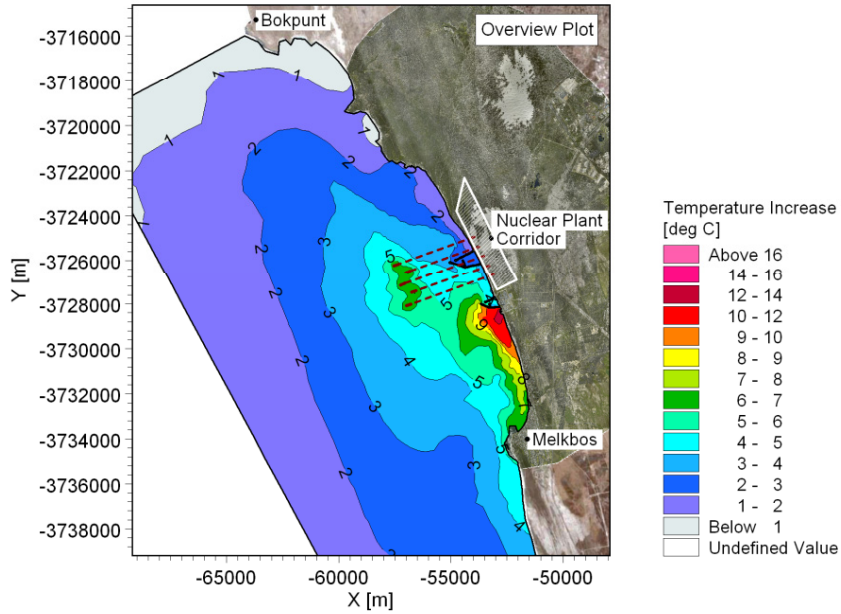
**Layout 2: Basin intake and offshore tunnel outfall.**

**Power output: Koeberg = 1800 MWe, PBMR = 165 MWe, Nuclear-1 + expansion = 8250 MWe.**

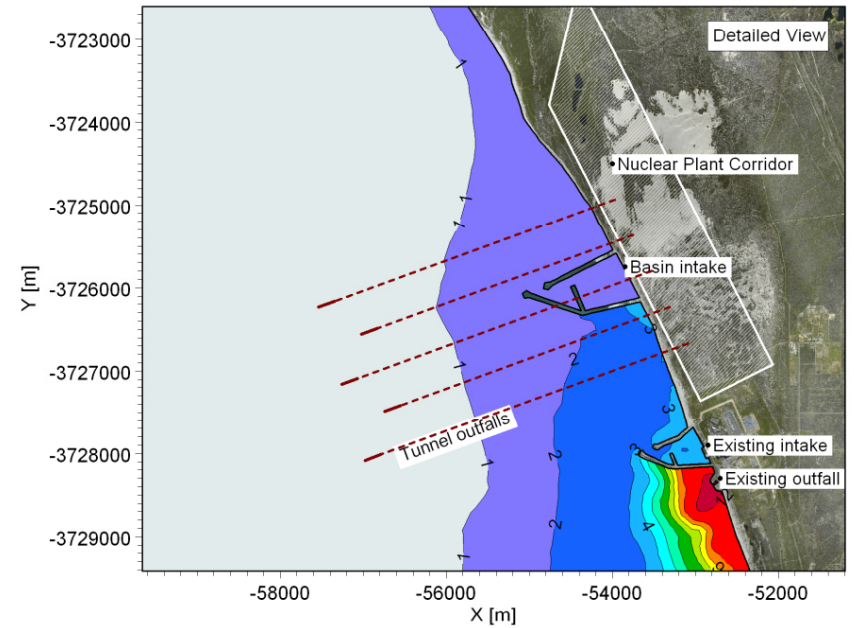
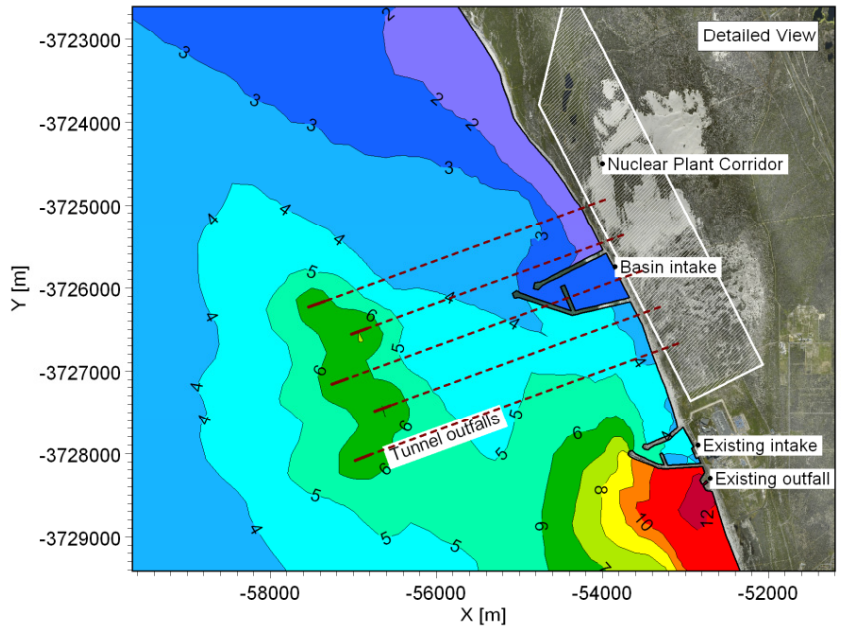
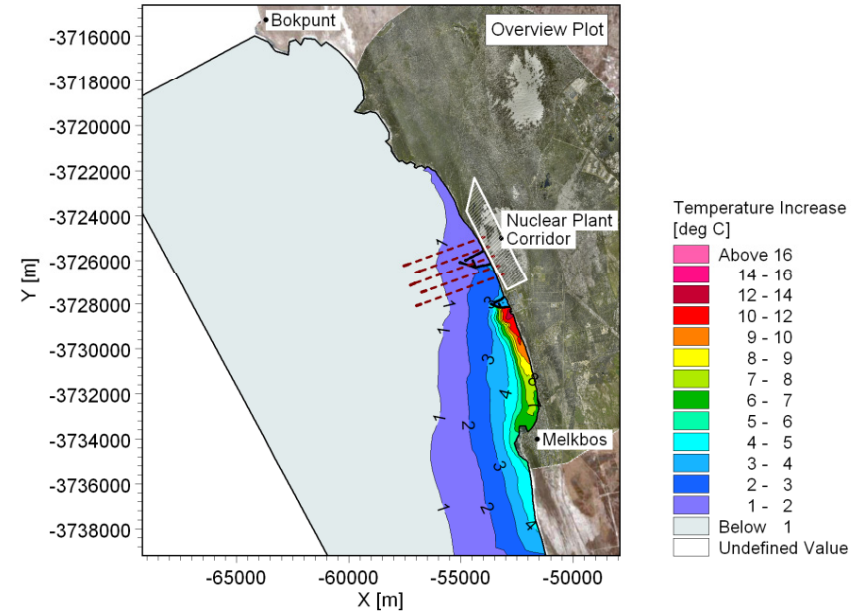
**Figure No.**

**9.17**

### Maximum Increase in Temperature Near Water Surface



### Maximum Increase in Temperature Near Seabed



G:\Projects\1010\_NuclearSites\Koeberg\Wodels\FIume\F\12a22a.m3fm - Result Files\Temp\_Max\_Lay5.png

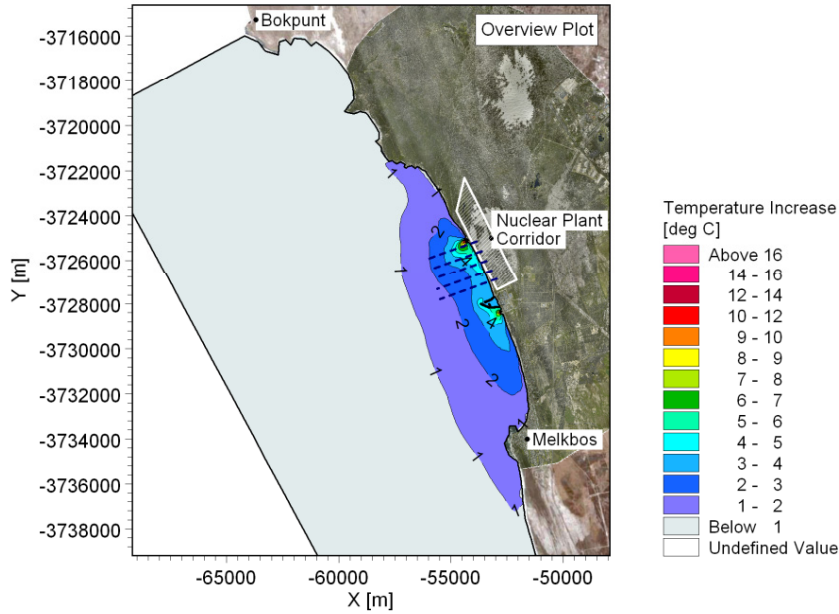
G:\Projects\1010\_NuclearSites\Koeberg\Wodels\FIume\F\12a22a.m3fm - Result Files\Temp\_Max\_Lay1.png



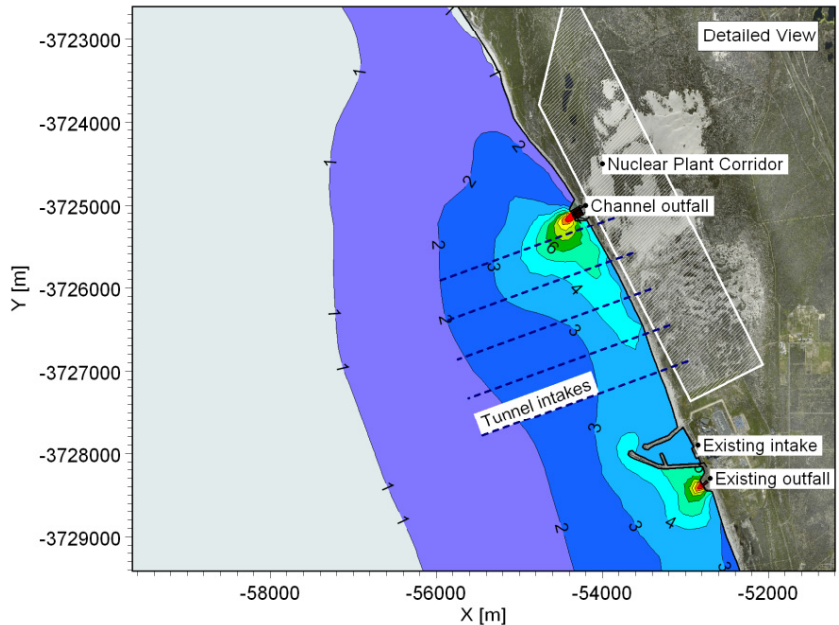
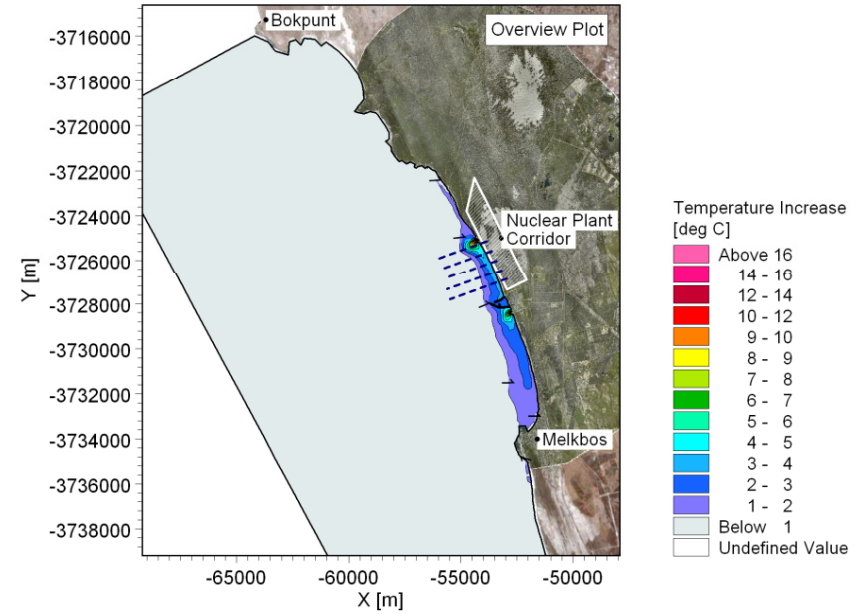
**Title:** Thermal plume modelling: Maximum increase in temperature due to power station.  
**Layout 2: Basin intake and offshore tunnel outfall.**  
**Power output: Koeberg = 1800 MWe, PBMR = 165 MWe, Nuclear-1 + expansion = 8250 MWe.**

**Figure No.**  
**9.18**

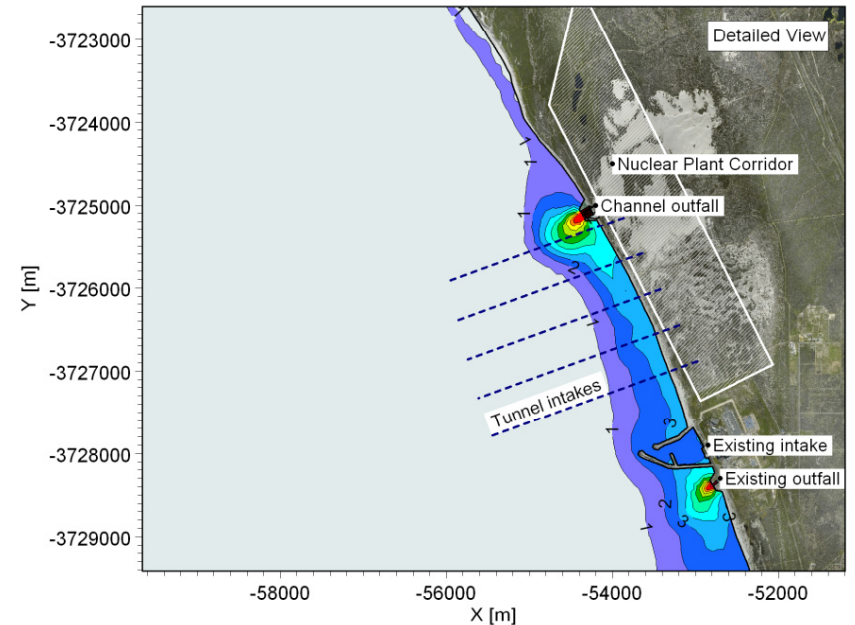
**Mean Increase in Temperature Near Water Surface**



**Mean Increase in Temperature Near Seabed**



G:\Projects\1010\_NuclearSites\Koeberg\Models\Plume\F\13a32a.m3fm - Result Files\Temp\_Mean\_Lay5.png



G:\Projects\1010\_NuclearSites\Koeberg\Models\Plume\F\13a32a.m3fm - Result Files\Temp\_Mean\_Lay1.png



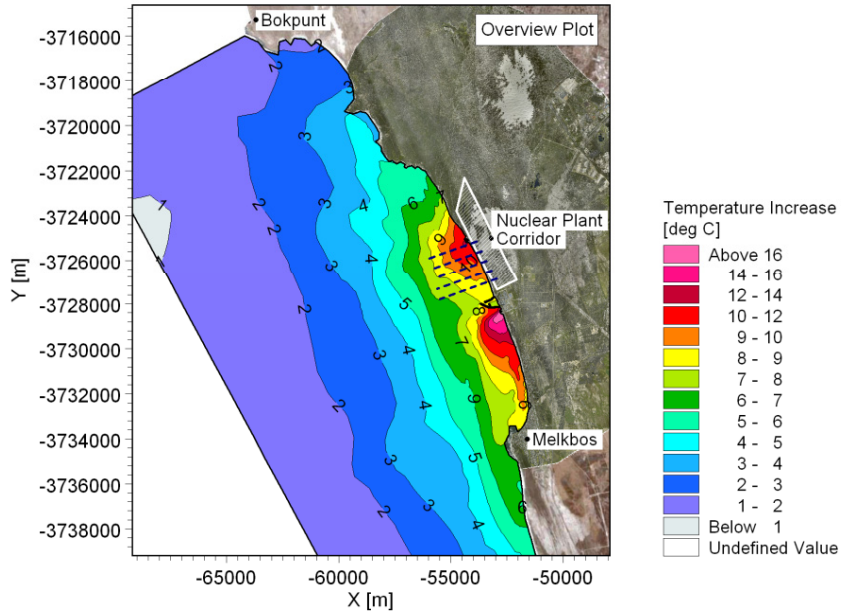
Title:

**Thermal plume modelling: Mean increase in temperature due to power station.  
Layout 3: Offshore tunnel intake and nearshore channel outfall 3 km north.  
Power output: Koeberg = 1800 MWe, PBMR = 165 MWe, Nuclear-1 + expansion = 8250 MWe.**

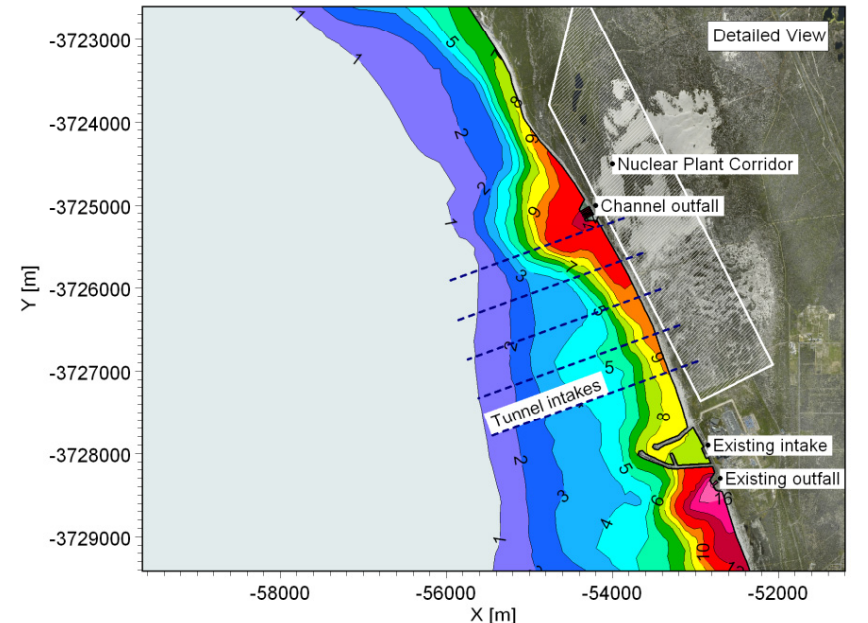
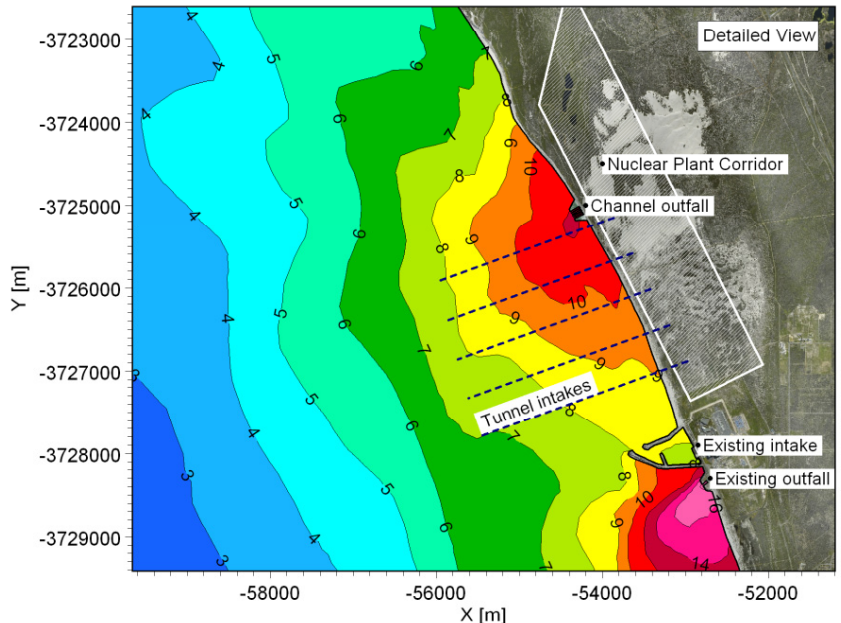
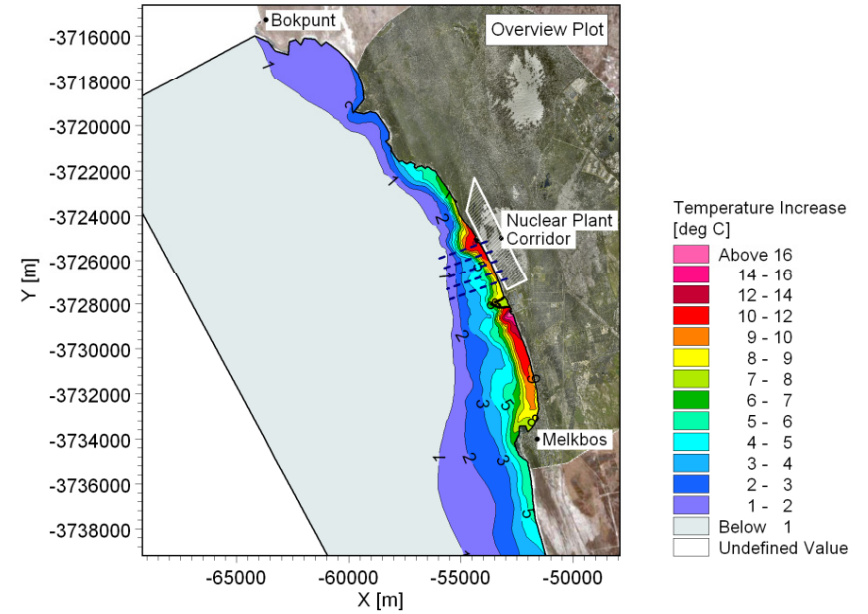
Figure No.

**9.19**

**Maximum Increase in Temperature Near Water Surface**



**Maximum Increase in Temperature Near Seabed**



G:\Projects\1010\_NuclearSites\Koeberg\Wdels\FIume\F\13a32a.m3fm - Result Files\Temp\_Max\_Lay5.png

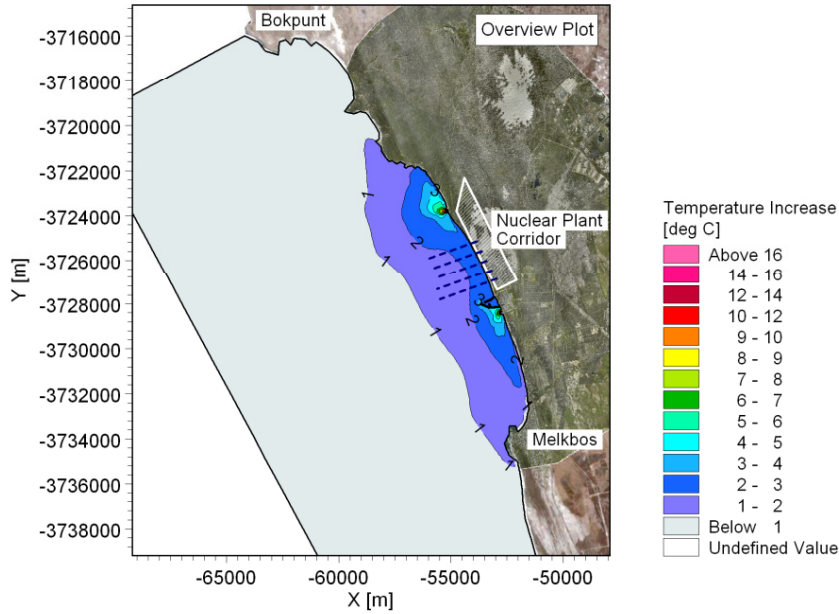
G:\Projects\1010\_NuclearSites\Koeberg\Wdels\FIume\F\13a32a.m3fm - Result Files\Temp\_Max\_Lay1.png



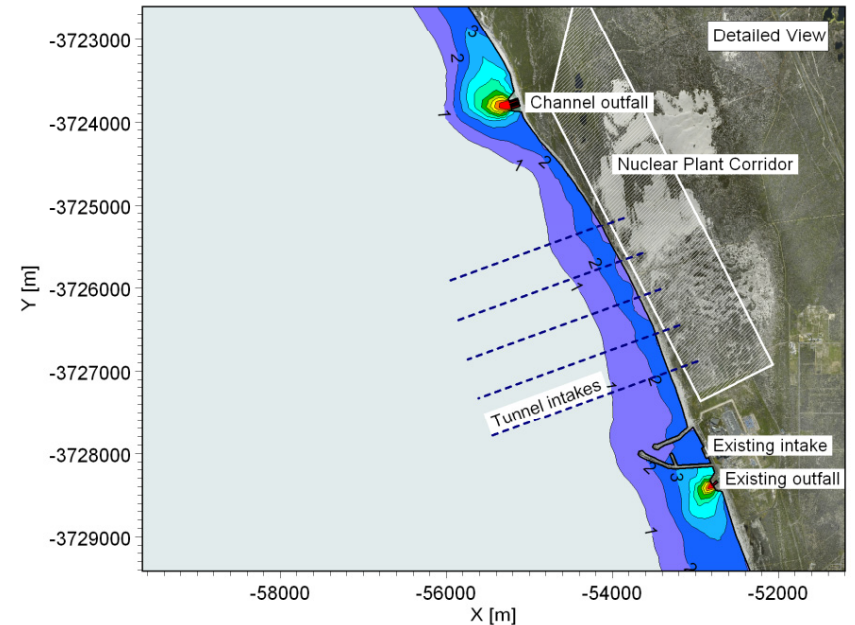
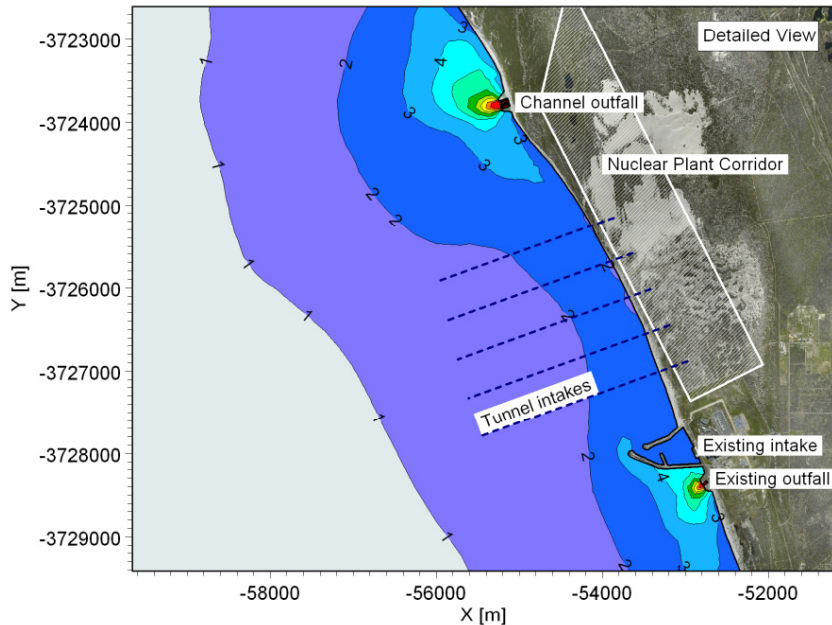
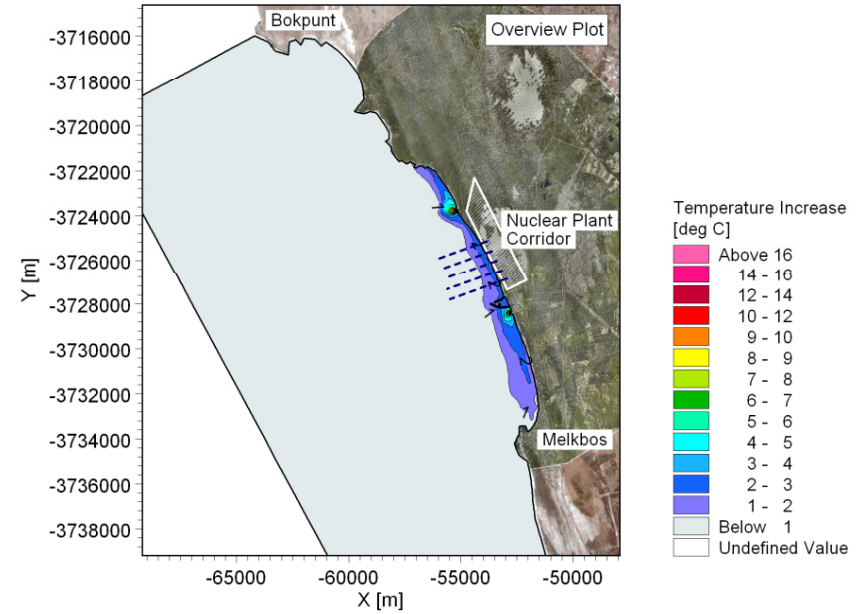
**Title: Thermal plume modelling: Maximum increase in temperature due to power station.  
Layout 3: Offshore tunnel intake and nearshore channel outfall 3 km north.  
Power output: Koeberg = 1800 MWe, PBMR = 165 MWe, Nuclear-1 + expansion = 8250 MWe.**

**Figure No.  
9.20**

**Mean Increase in Temperature Near Water Surface**



**Mean Increase in Temperature Near Seabed**



G:\Projects\1010\_NuclearSites\Koeberg\Models\Plume\F\14a42a.m3fm - Result Files\Temp\_Mean\_Lay5.png

G:\Projects\1010\_NuclearSites\Koeberg\Models\Plume\F\14a42a.m3fm - Result Files\Temp\_Mean\_Lay1.png



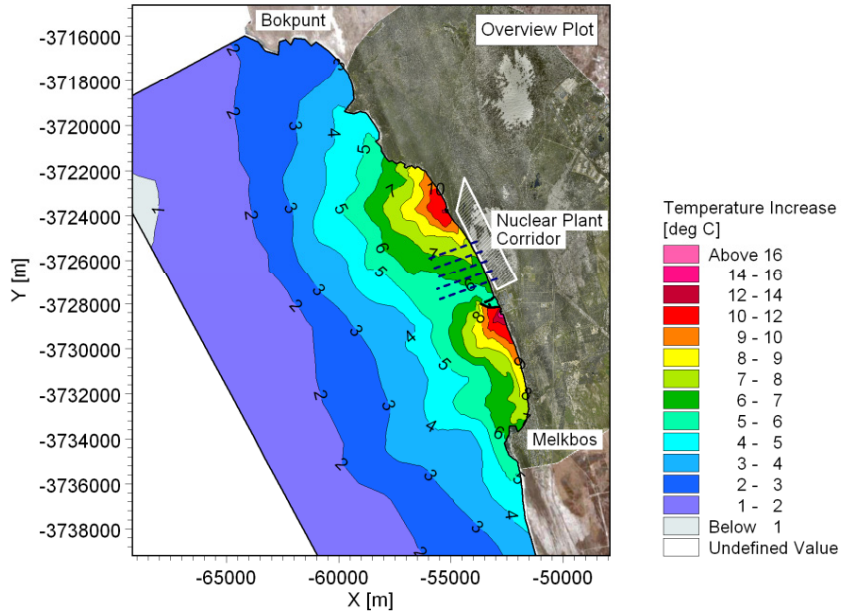
**Title:**

**Thermal plume modelling: Mean increase in temperature due to power station.  
Layout 4: Offshore tunnel intake and nearshore channel outfall 4.5 km north.  
Power output: Koeberg = 1800 MWe, PBMR = 165 MWe, Nuclear-1 + expansion = 8250 MWe.**

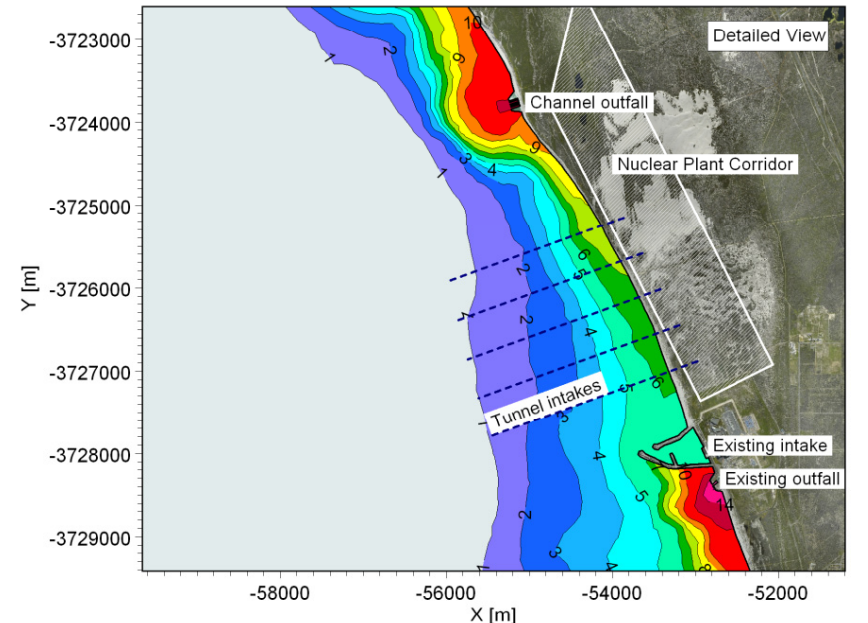
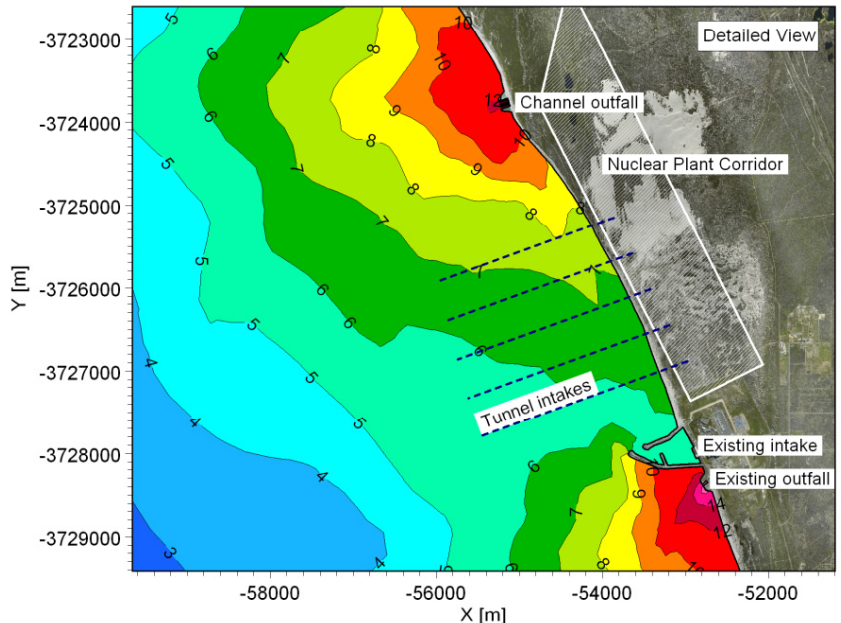
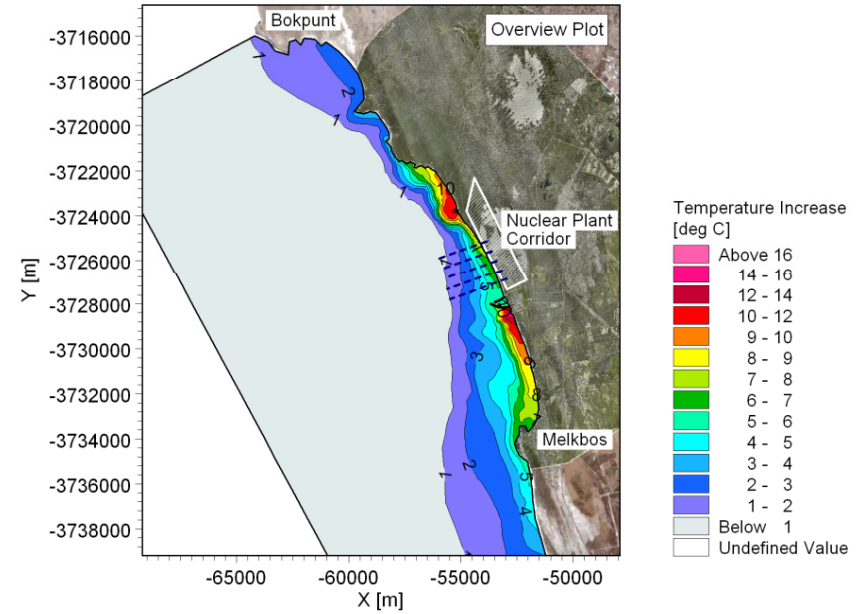
**Figure No.**

**9.21**

**Maximum Increase in Temperature Near Water Surface**



**Maximum Increase in Temperature Near Seabed**



G:\Projects\1010\_NuclearSites\Koeberg\Wodels\FIume\F\1442a.m3fm - Result Files\Temp\_Max\_Lay5.png

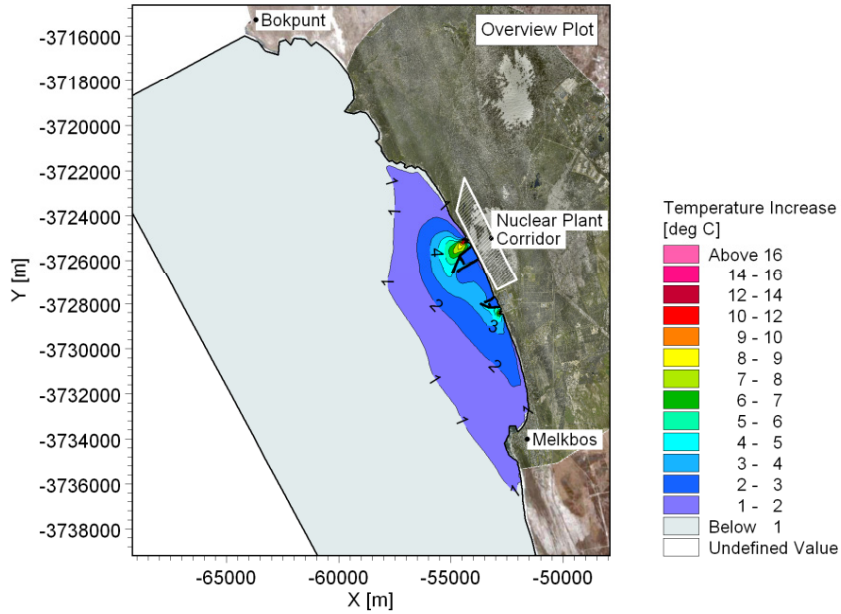
G:\Projects\1010\_NuclearSites\Koeberg\Wodels\FIume\F\1442a.m3fm - Result Files\Temp\_Max\_Lay1.png



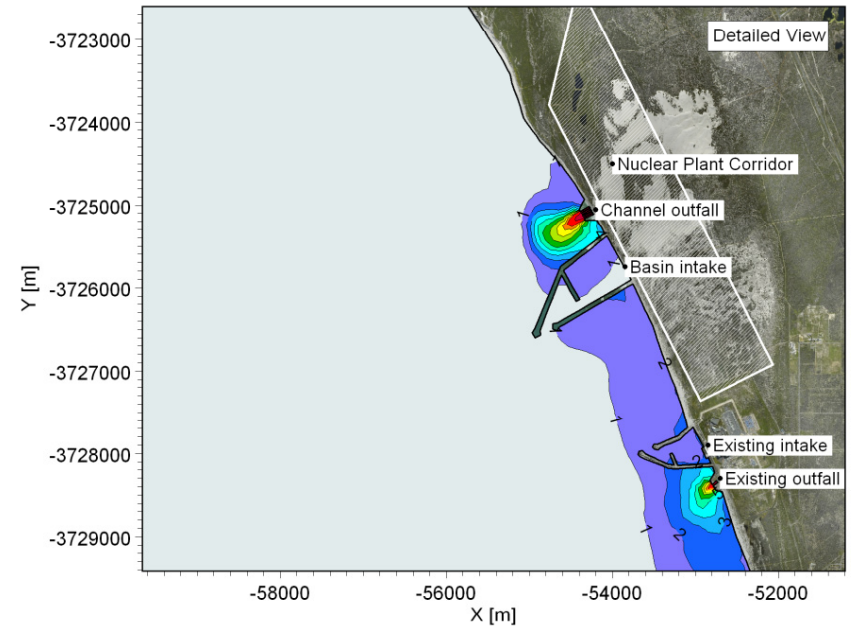
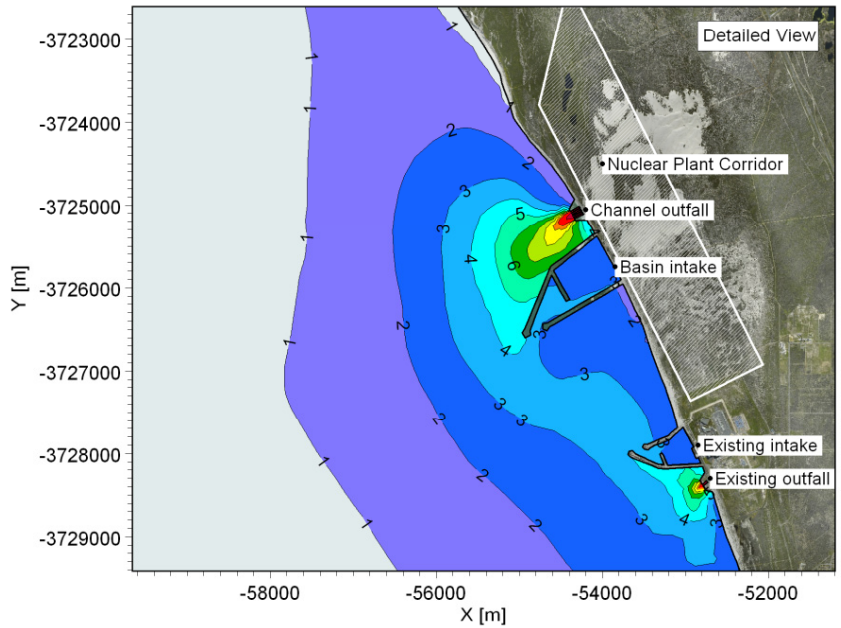
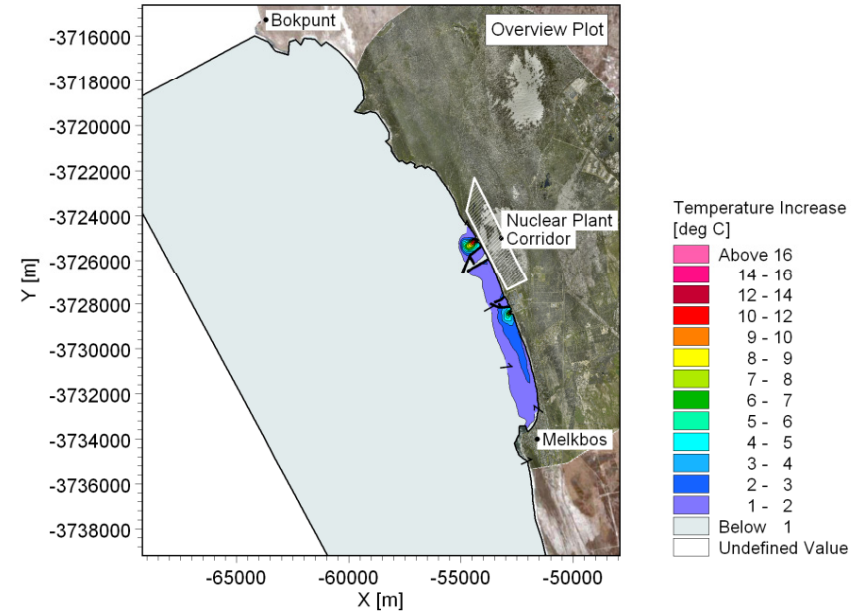
**Title: Thermal plume modelling: Maximum increase in temperature due to power station.  
Layout 4: Offshore tunnel intake and nearshore channel outfall 4.5 km north.  
Power output: Koeberg = 1800 MWe, PBMR = 165 MWe, Nuclear-1 + expansion = 8250 MWe.**

**Figure No.  
9.22**

**Mean Increase in Temperature Near Water Surface**



**Mean Increase in Temperature Near Seabed**



G:\Projects\1010\_NuclearSites\Koeberg\Models\Plume\F\15a52a.m3fm - Result Files\Temp\_Mean\_Lay5.png

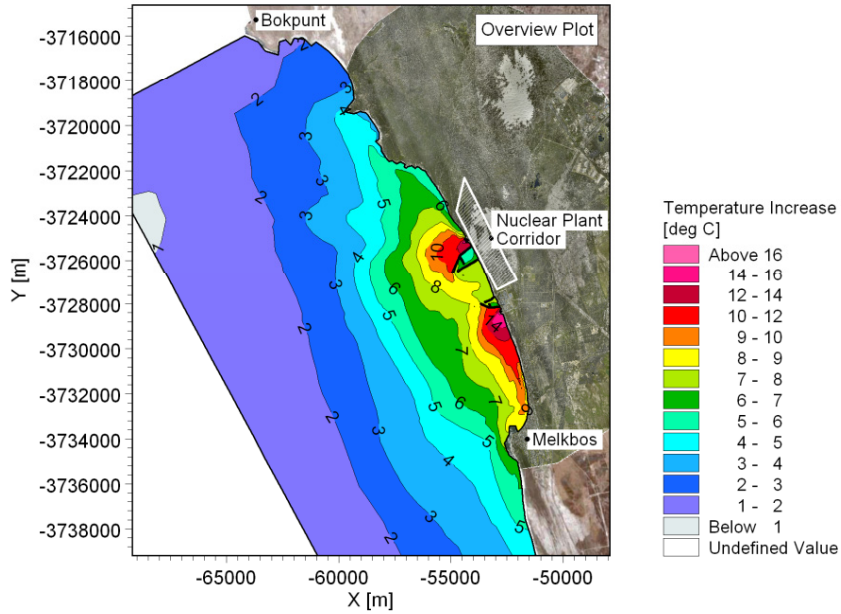
G:\Projects\1010\_NuclearSites\Koeberg\Models\Plume\F\15a52a.m3fm - Result Files\Temp\_Mean\_Lay1.png



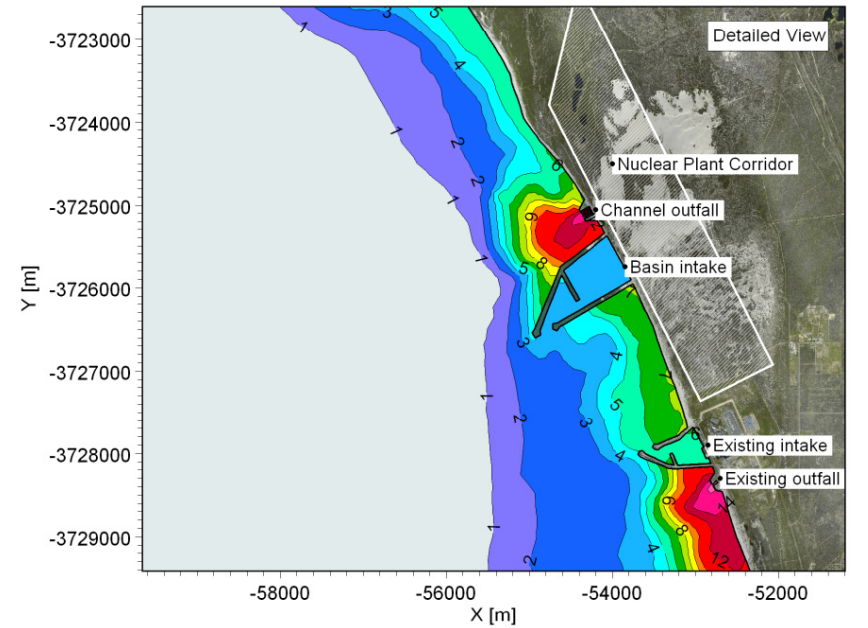
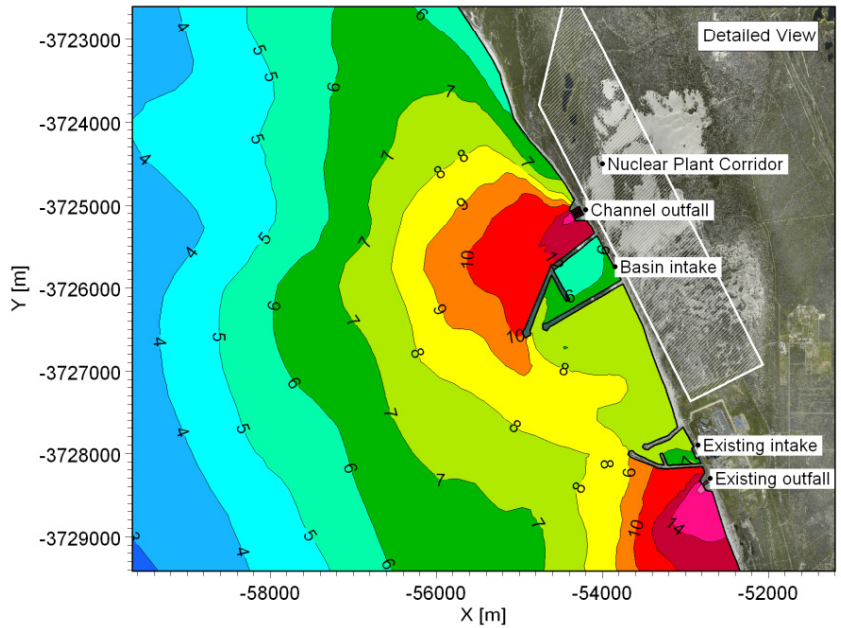
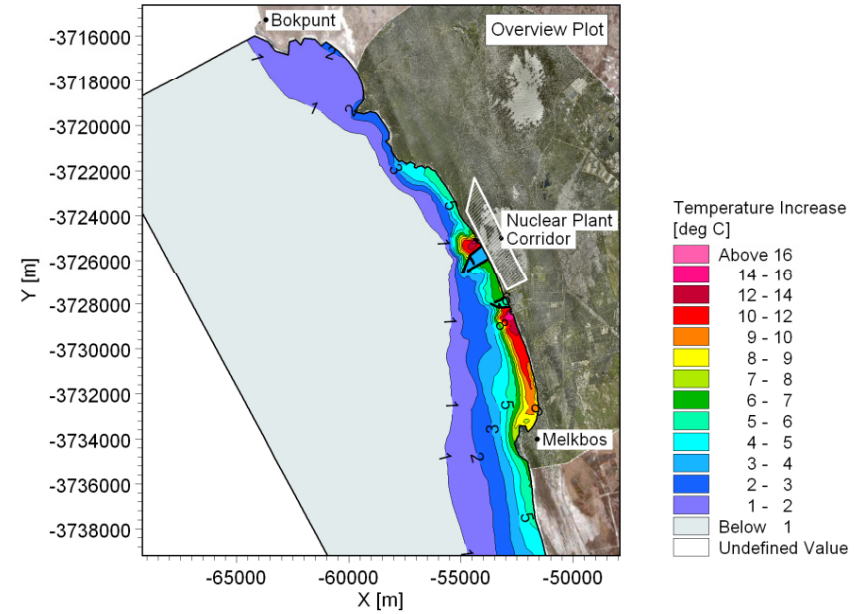
**Title: Thermal plume modelling: Mean increase in temperature due to power station.  
Layout 5: Basin intake and nearshore channel outfall.  
Power output: Koeberg = 1800 MWe, PBMR = 165 MWe, Nuclear-1 + expansion = 8250 MWe.**

**Figure No.  
9.23**

**Maximum Increase in Temperature Near Water Surface**



**Maximum Increase in Temperature Near Seabed**



G:\Projects\1010\_NuclearSites\Koeberg\Wodels\Flume\F\15a52a.m3fm - Result Files\Temp\_Max\_Lay5.png

G:\Projects\1010\_NuclearSites\Koeberg\Wodels\Flume\F\15a52a.m3fm - Result Files\Temp\_Max\_Lay1.png

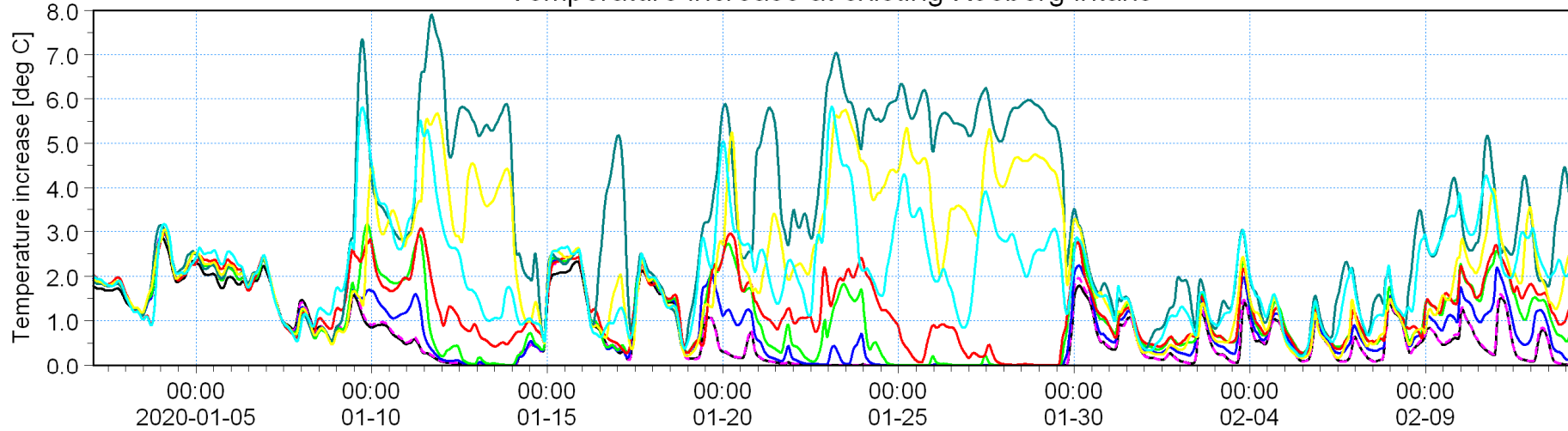


**Title: Thermal plume modelling: Maximum increase in temperature due to power station.  
Layout 5: Basin intake and nearshore channel outfall.  
Power output: Koeberg = 1800 MWe, PBMR = 165 MWe, Nuclear-1 + expansion = 8250 MWe.**

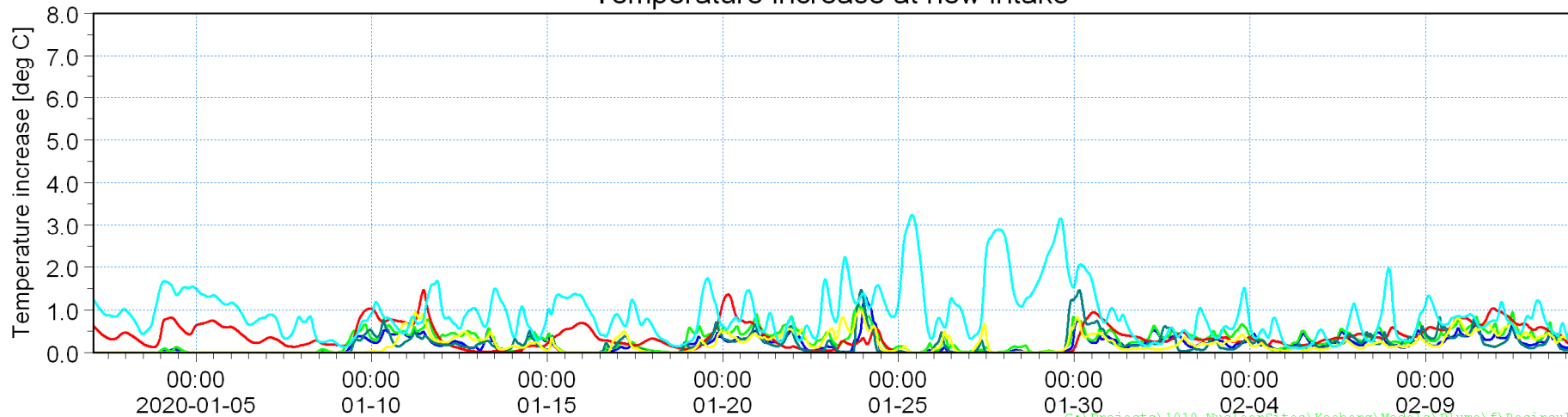
**Figure No.  
9.24**

Layout 0: Koeberg (1800 MWe) [deg C] —  
 Layout 0: Koeberg (1800 MWe) + PBMR (165 MWe) [deg C] - - -  
 Layout 1: Koeberg (1800 MWe) + PBMR (165 MWe) + Nuclear-1 (4000 MWe) [deg C] —  
 Layout 1: Koeberg (1800 MWe) + PBMR (165 MWe) + Nuclear-1 + expansion (8250 MWe) [deg C] —  
 Layout 2: Koeberg (1800 MWe) + PBMR (165 MWe) + Nuclear-1 + expansion (8250 MWe) [deg C] —  
 Layout 3: Koeberg (1800 MWe) + PBMR (165 MWe) + Nuclear-1 + expansion (8250 MWe) [deg C] —  
 Layout 4: Koeberg (1800 MWe) + PBMR (165 MWe) + Nuclear-1 + expansion (8250 MWe) [deg C] —  
 Layout 5: Koeberg (1800 MWe) + PBMR (165 MWe) + Nuclear-1 + expansion (8250 MWe) [deg C] —

Temperature increase at existing Koeberg intake



Temperature increase at new intake



G:\Projects\1010\_NuclearSites\Koeberg\Models\Plume\F\Recirculation.png

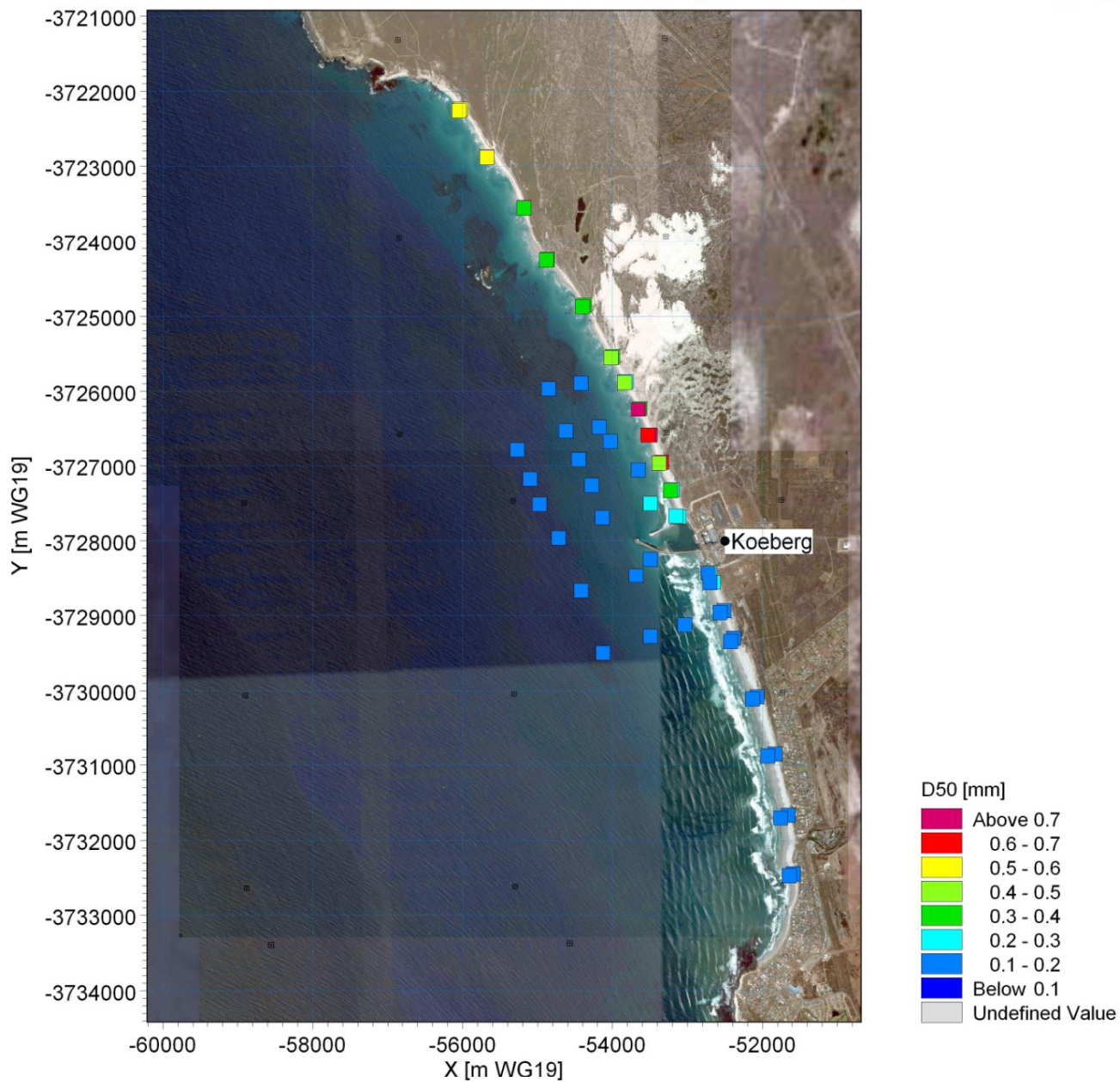


Title:

**Thermal plume modelling: time-series of recirculation results showing the increase in temperature at the intakes for the various layouts and power outputs modelled.**

Figure No.

**9.25**

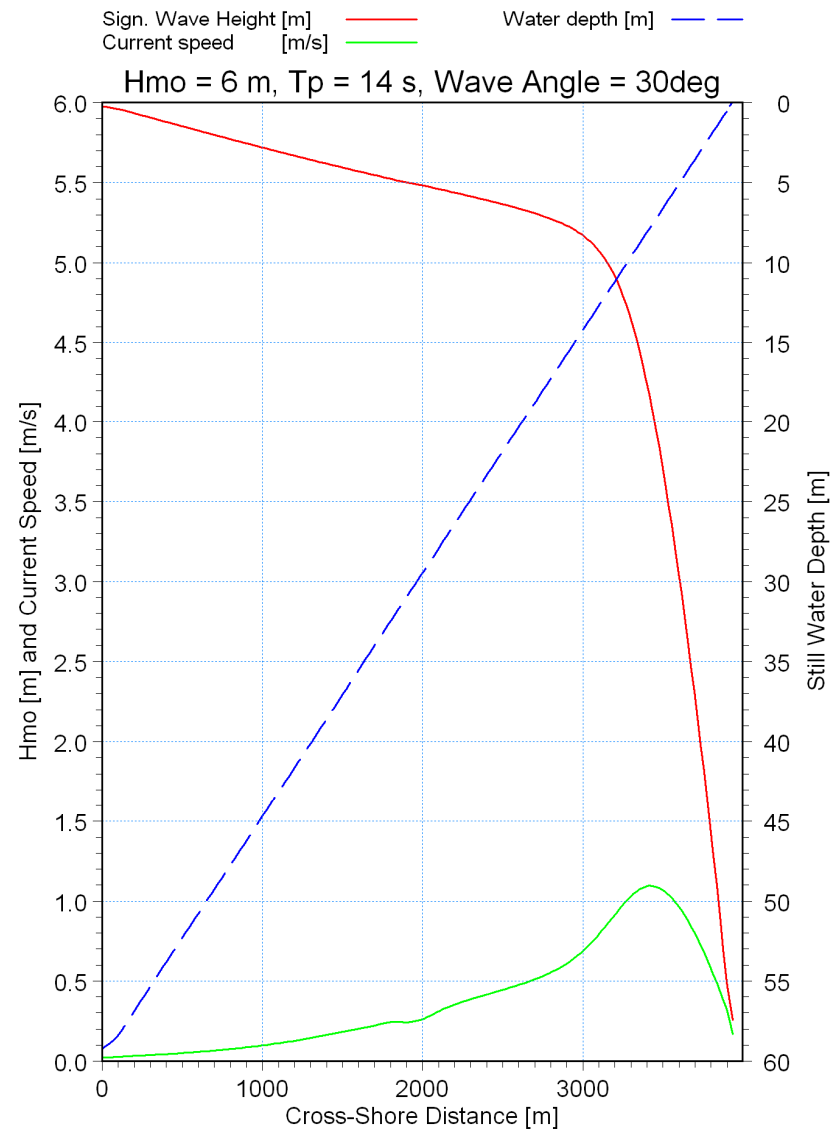
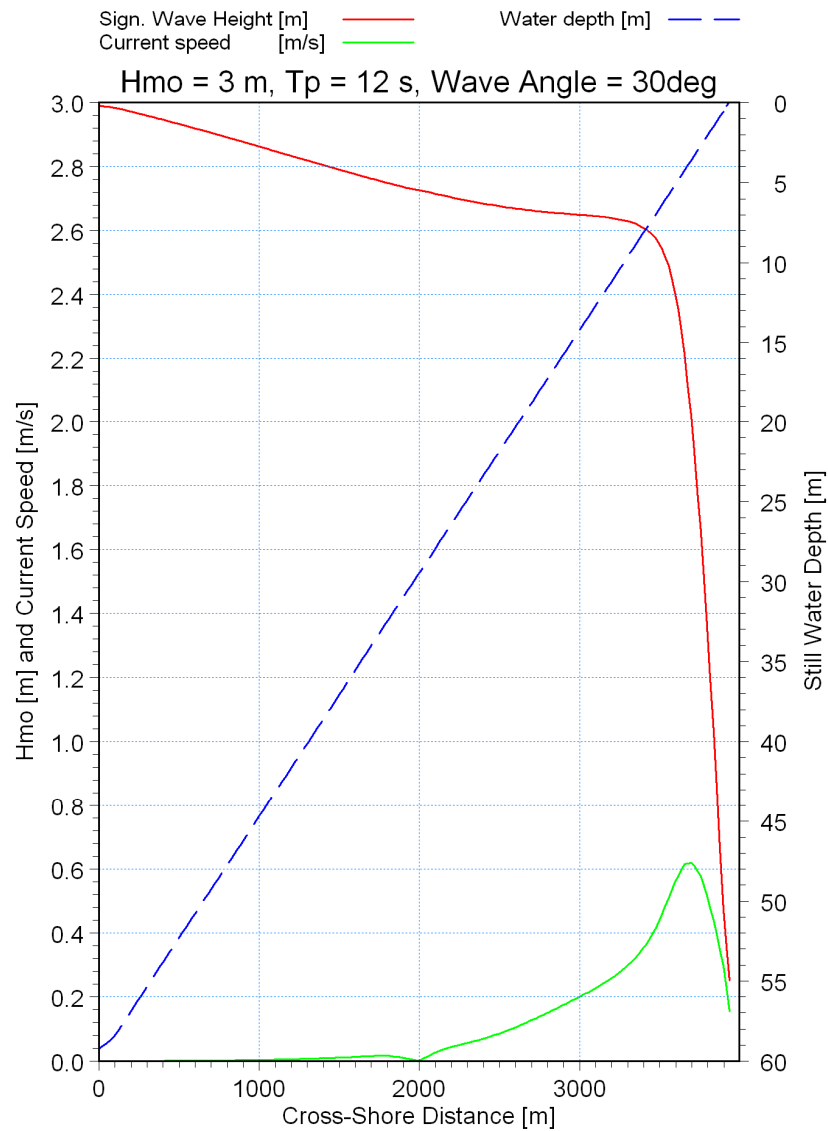


Title:

Sediment transport modelling.  
Measured  $D_{50}$  grain size.

Figure No.

10.1

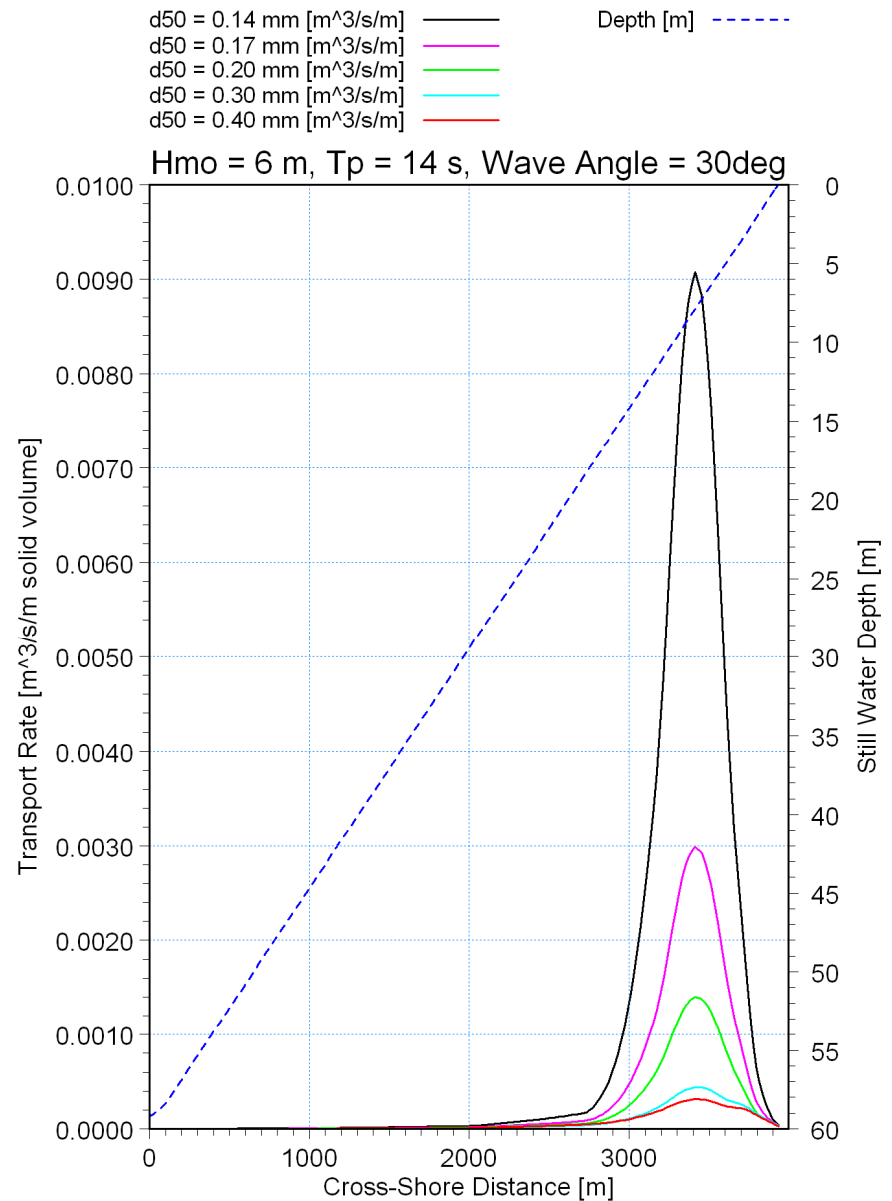
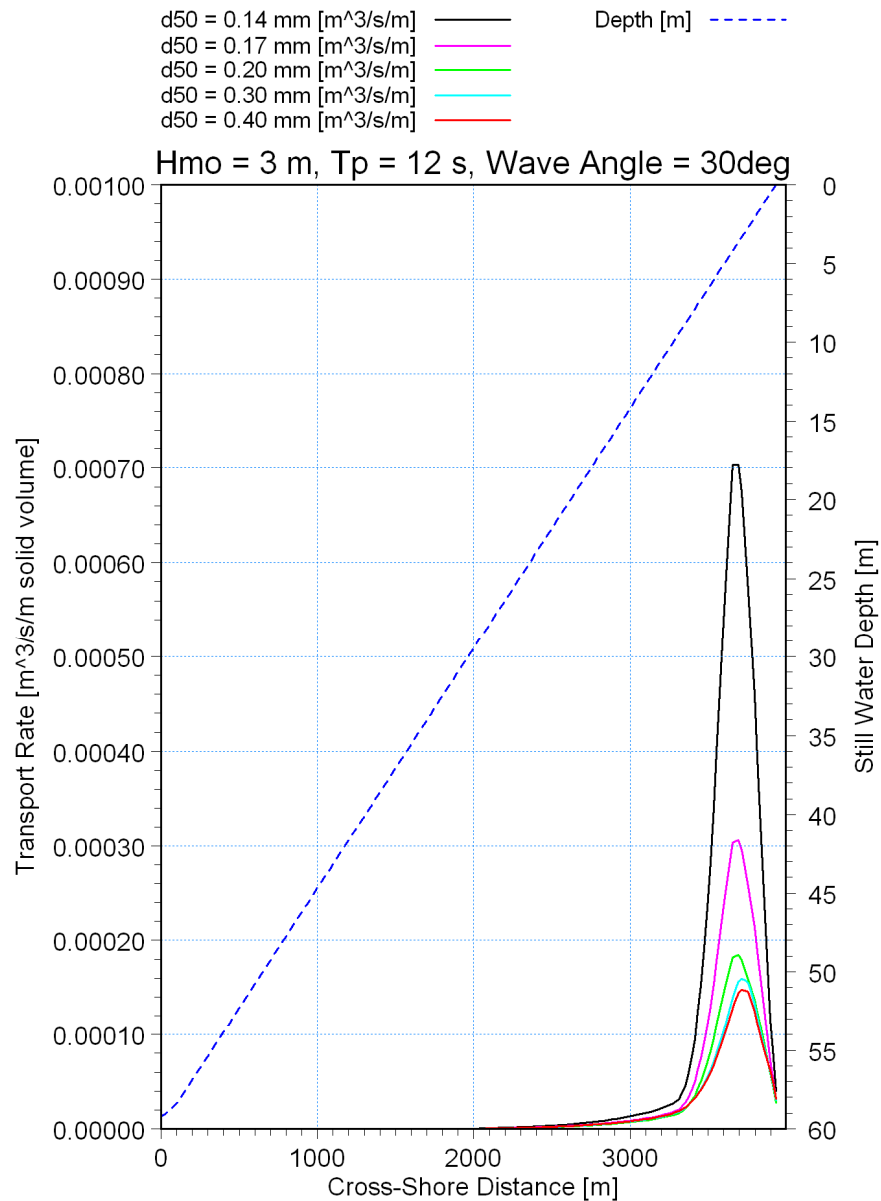


Title:

**Sediment transport modelling.**  
**Testing of wave and current modules in a simplified model comprising a uniform 1:67 beach slope with a wave approaching 30° from normal.**

Figure No.

**10.2**

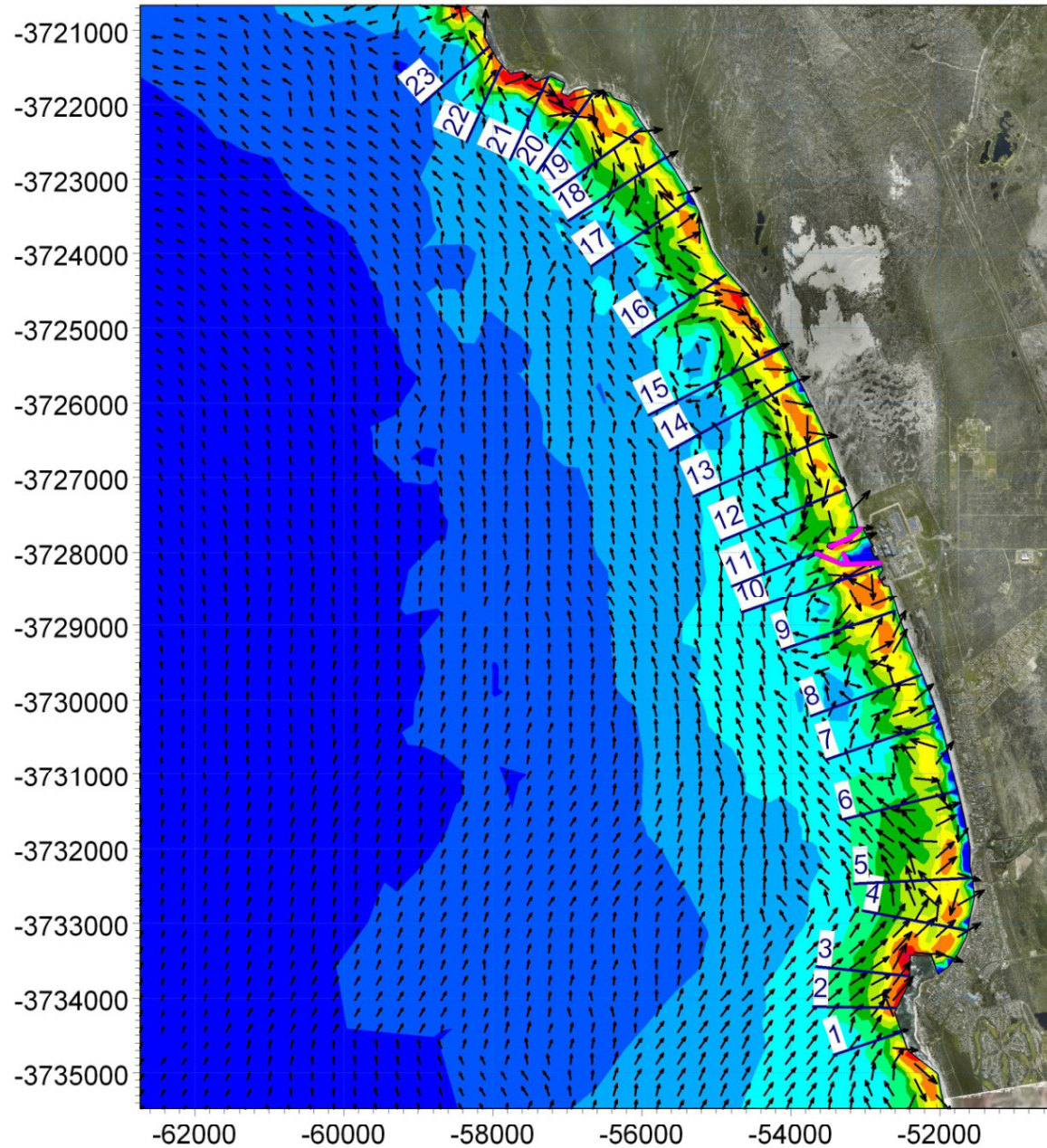


Title:

**Sediment transport modelling.**  
**Testing of the coupled wave, current and sediment transport model for a simplified case with a uniform 1:67 beach slope and a wave approaching 30° from normal.**

Figure No.

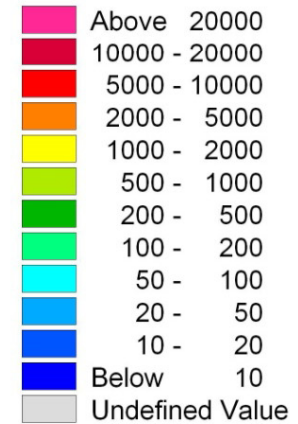
10.3



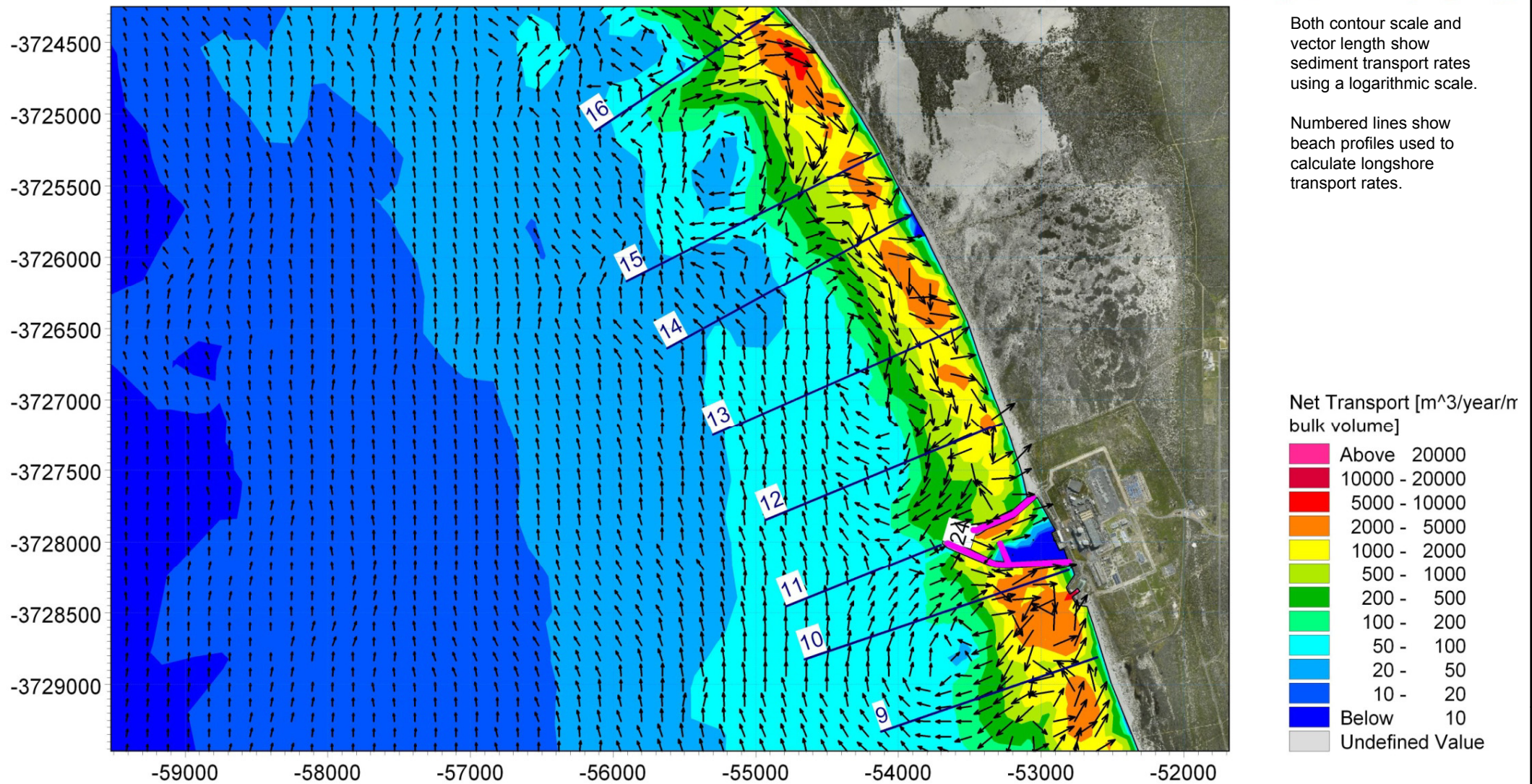
Both contour scale and vector length show sediment transport rates using a logarithmic scale.

Numbered lines show beach profiles used to calculate longshore transport rates.

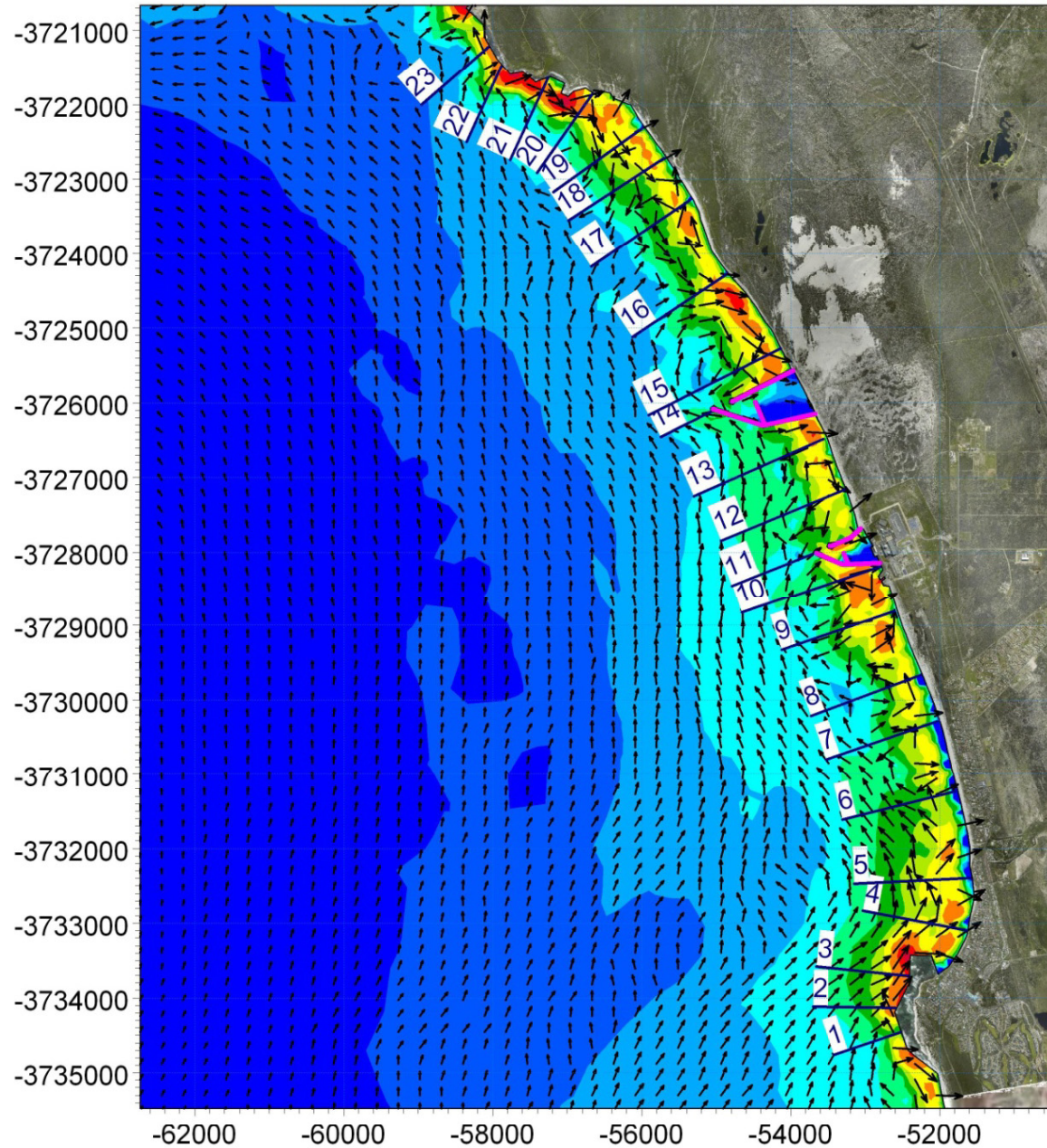
Net Transport [ $m^3/year/n$  bulk volume]



Title: **Sediment transport modelling: Potential net sediment transport for  $D_{50} = 0.2$  mm.**  
**Layout 0: Existing Koeberg Layout.**  
**Overview plot.**



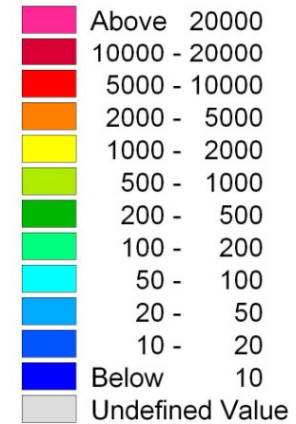
Title: **Sediment transport modelling: Potential net sediment transport for  $D_{50} = 0.2$  mm.  
Layout 0: Existing Koeberg Layout.  
Detailed view.**



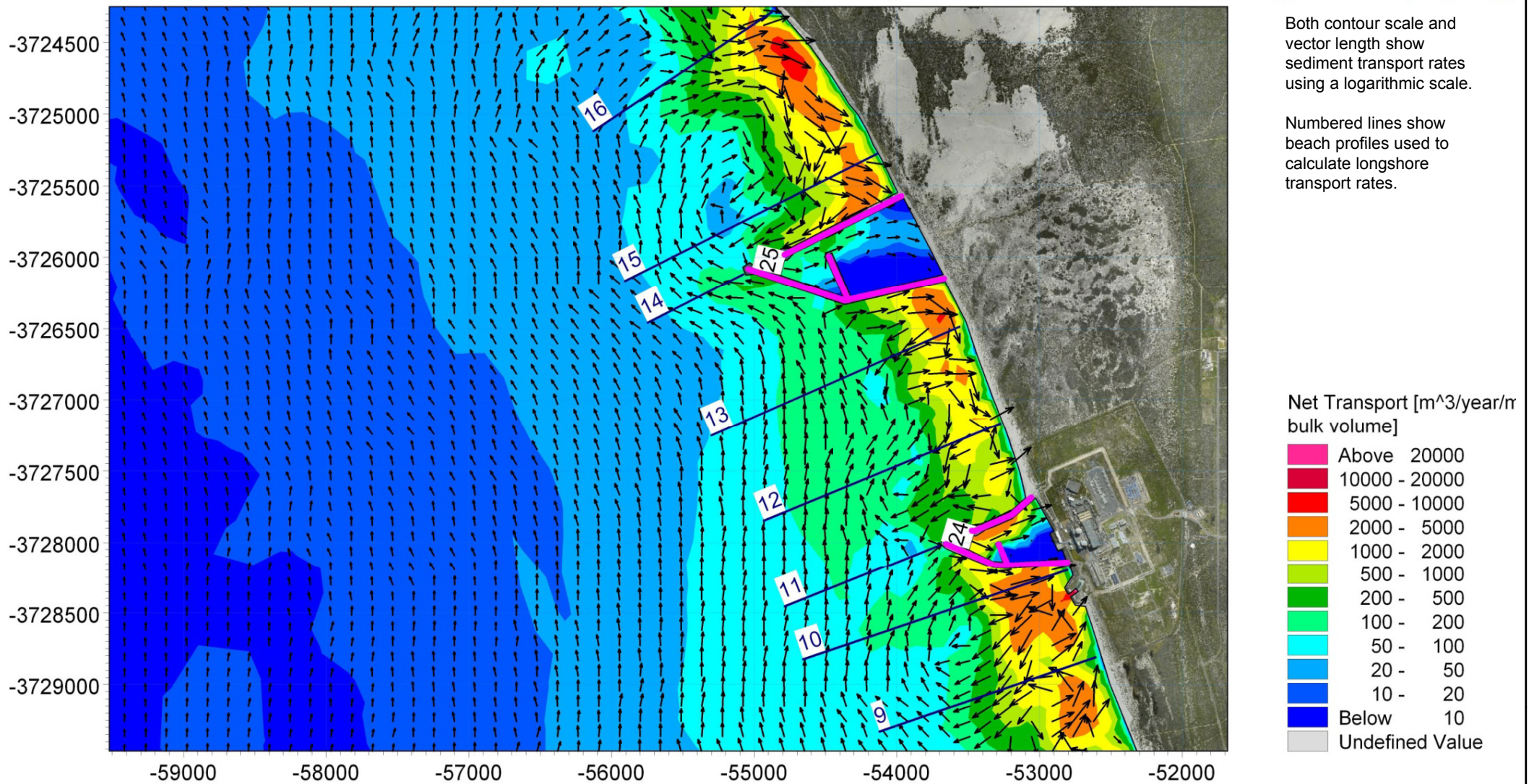
Both contour scale and vector length show sediment transport rates using a logarithmic scale.

Numbered lines show beach profiles used to calculate longshore transport rates.

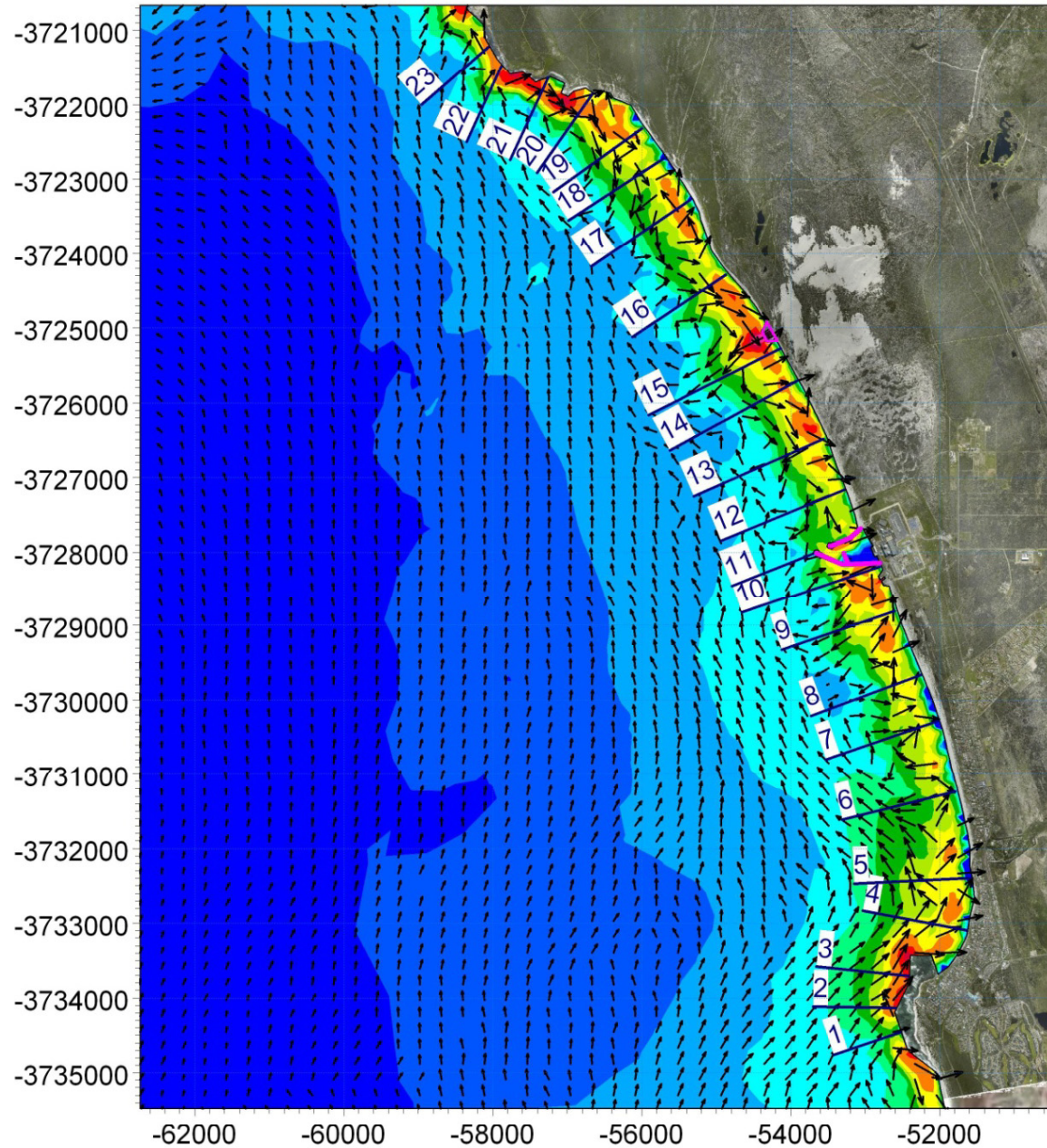
Net Transport [ $m^3/year/n$  bulk volume]



Title: **Sediment transport modelling: Potential net sediment transport for  $D_{50} = 0.2$  mm.**  
**Layout 2: Basin intake and offshore tunnel outfall.**  
**Overview plot.**



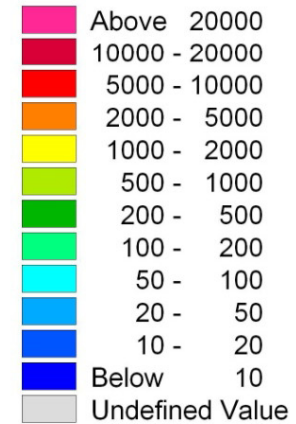
Title: **Sediment transport modelling: Potential net sediment transport for  $D_{50} = 0.2$  mm.**  
**Layout 2: Basin intake and offshore tunnel outfall.**  
**Detailed view.**



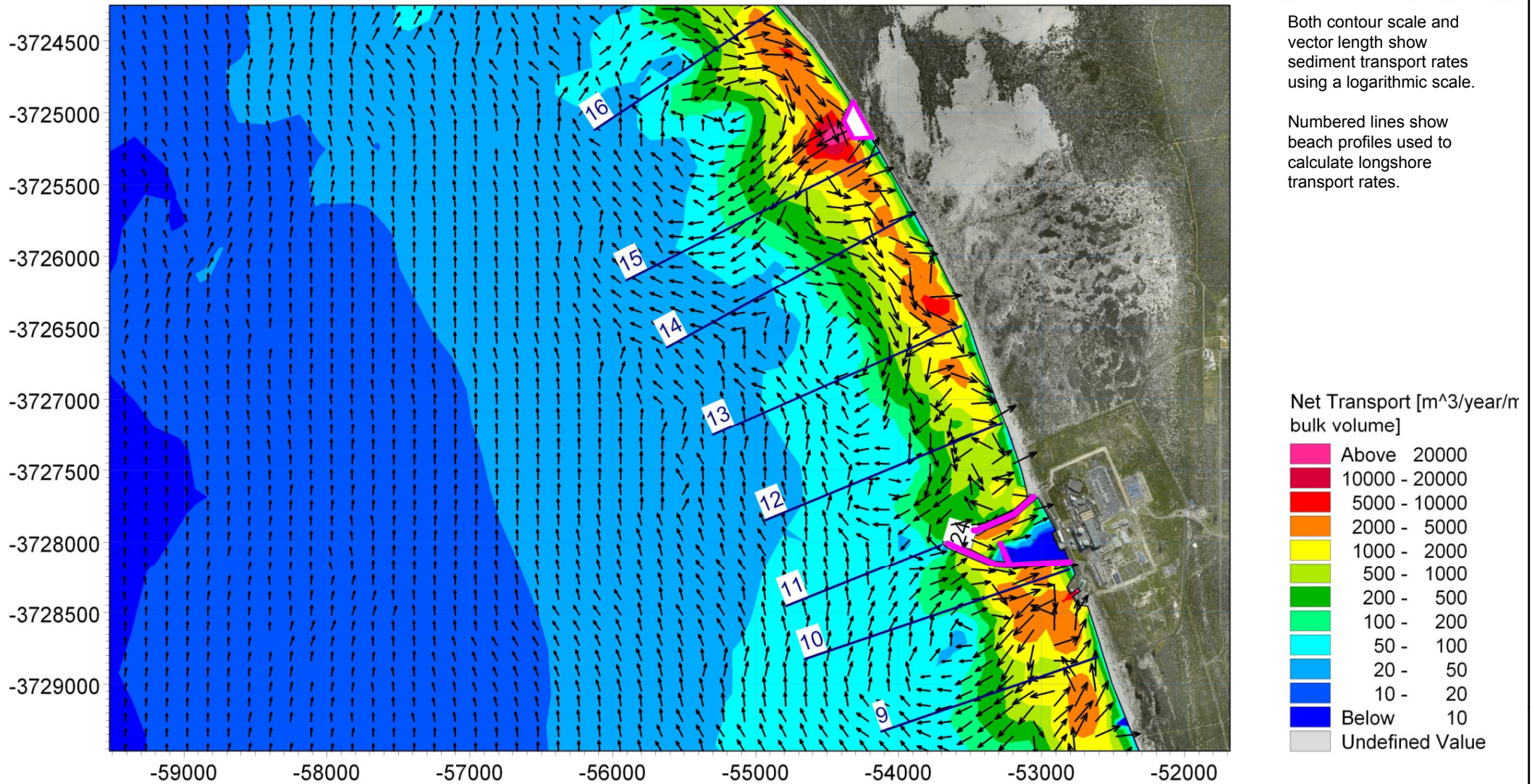
Both contour scale and vector length show sediment transport rates using a logarithmic scale.

Numbered lines show beach profiles used to calculate longshore transport rates.

Net Transport [ $m^3/year/n$  bulk volume]

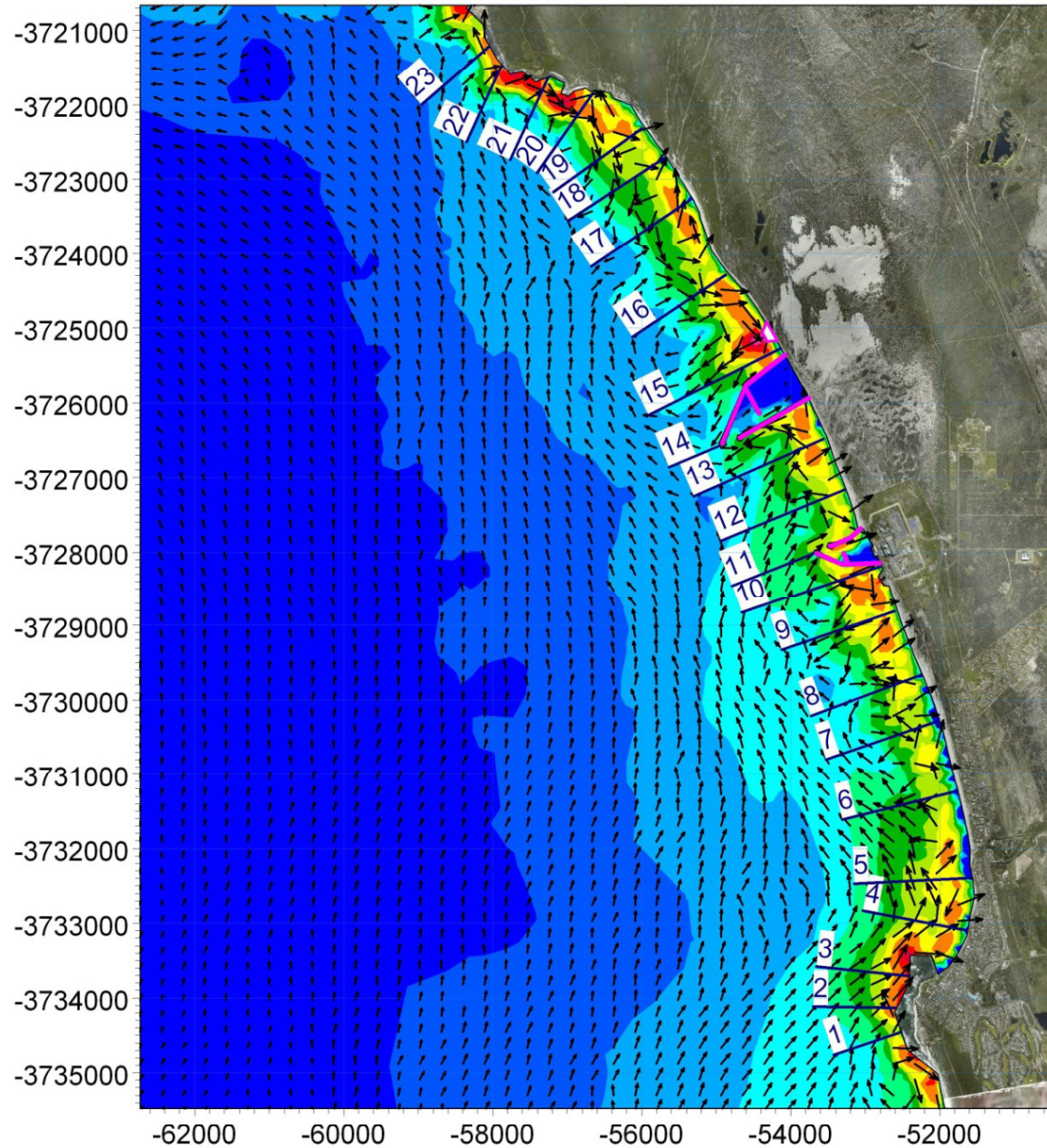


Title: **Sediment transport modelling: Potential net sediment transport for  $D_{50} = 0.2$  mm.**  
**Layout 3: Offshore tunnel intake and nearshore channel outfall.**  
**Overview plot.**



Title: **Sediment transport modelling: Potential net sediment transport for  $D_{50} = 0.2$  mm.  
Layout 3: Offshore tunnel intake and nearshore channel outfall.  
Detailed view.**

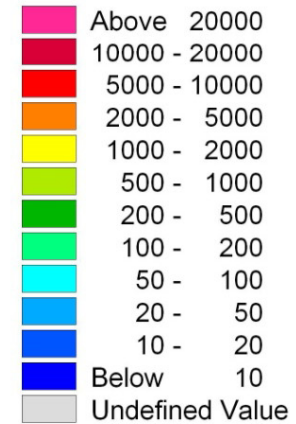
Figure No.  
**10.9**



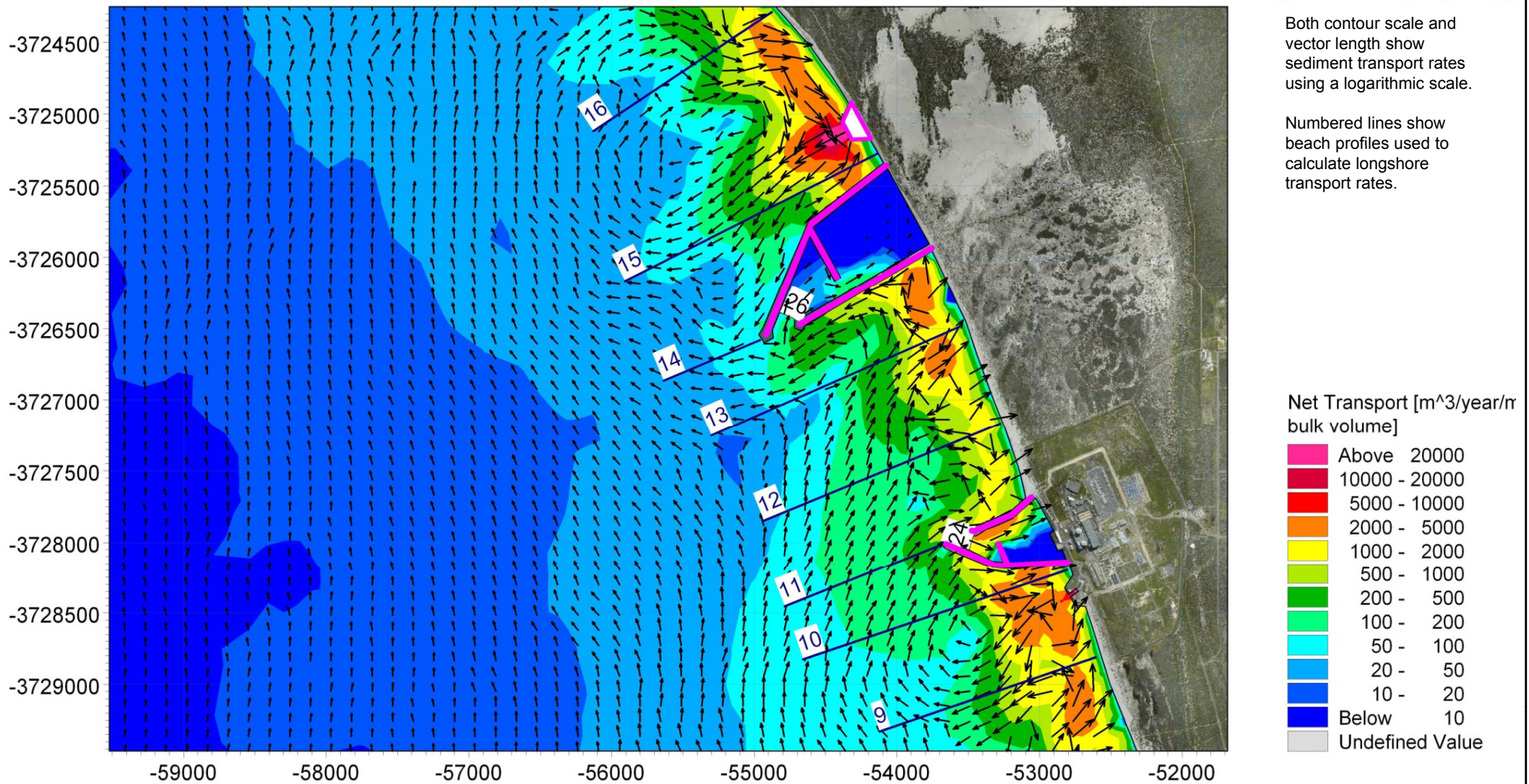
Both contour scale and vector length show sediment transport rates using a logarithmic scale.

Numbered lines show beach profiles used to calculate longshore transport rates.

Net Transport [ $m^3/year/n$  bulk volume]

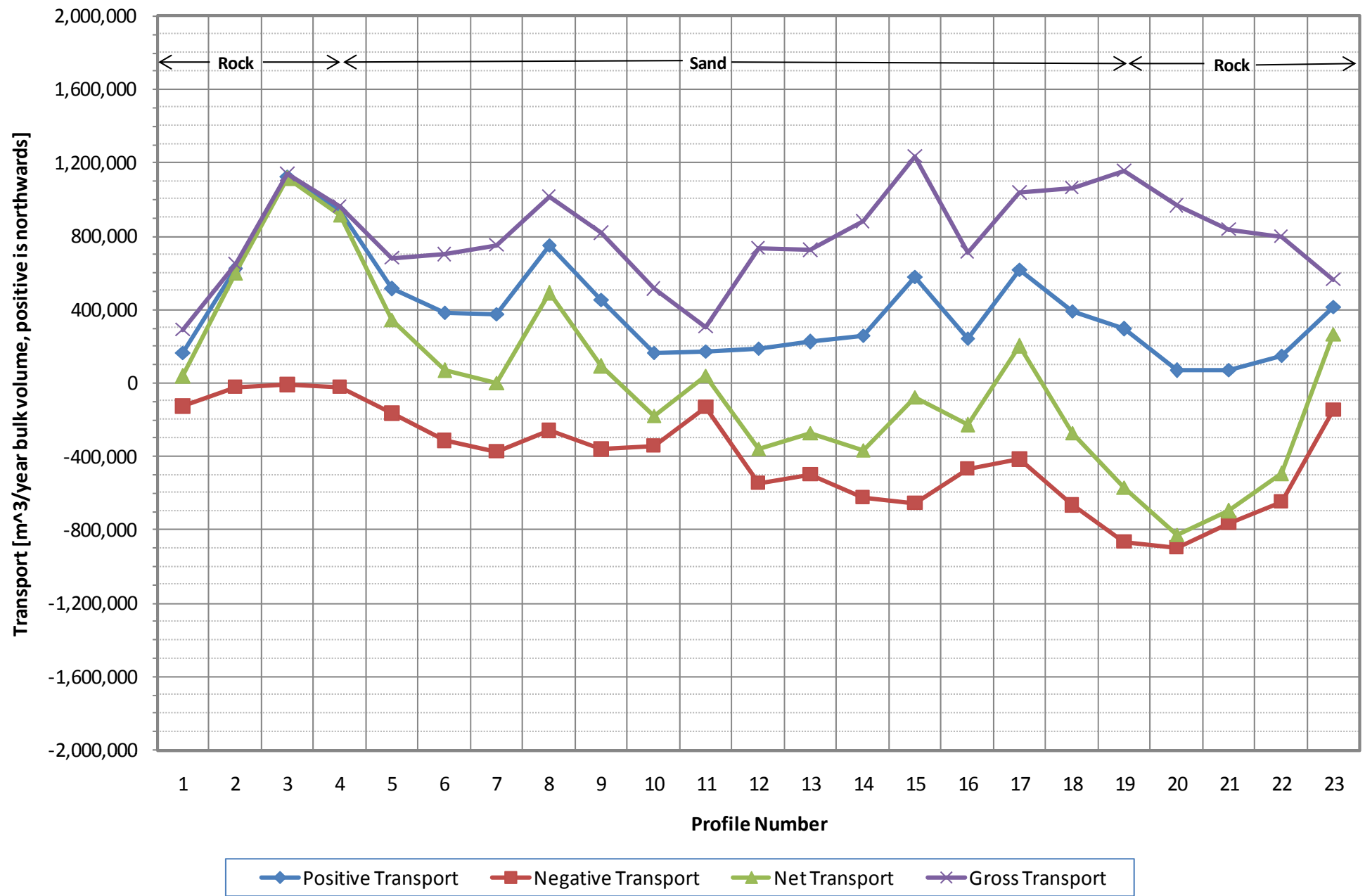


**Title:** Sediment transport modelling: Potential net sediment transport for  $D_{50} = 0.2$  mm.  
 Layout 5: Basin intake and nearshore channel outfall.  
 Overview plot.



Title: **Sediment transport modelling: Potential net sediment transport for  $D_{50} = 0.2$  mm.  
Layout 5: Basin intake and nearshore channel outfall.  
Detailed view.**

Figure No.  
**10.11**

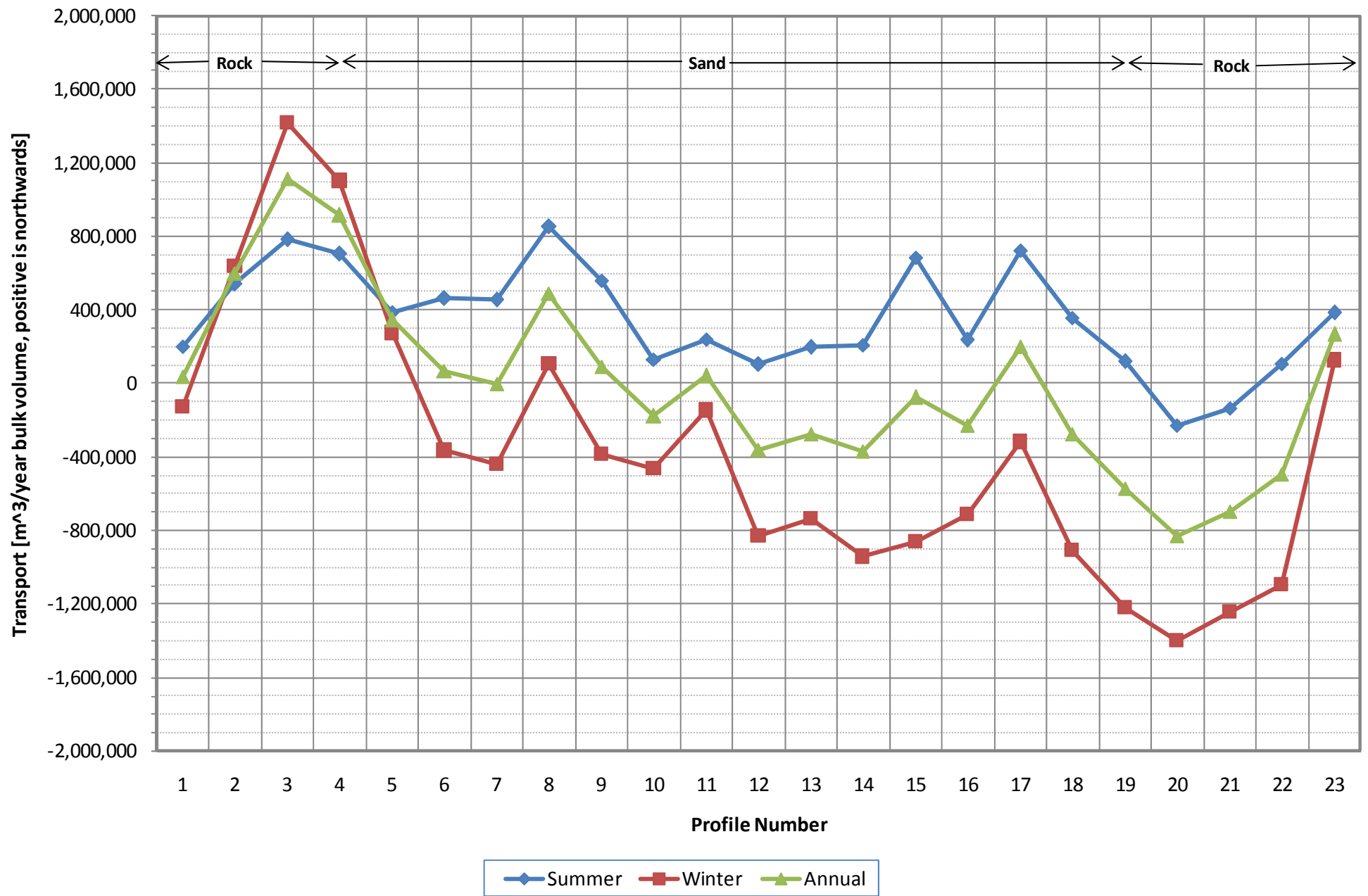


Title:

**Sediment transport modelling.**  
**Alongshore transport rates. Layout 0.  $D_{50} = 0.2$  mm.**  
**Refer to Figure 10.4 for profile locations.**

Figure No.

**10.12**

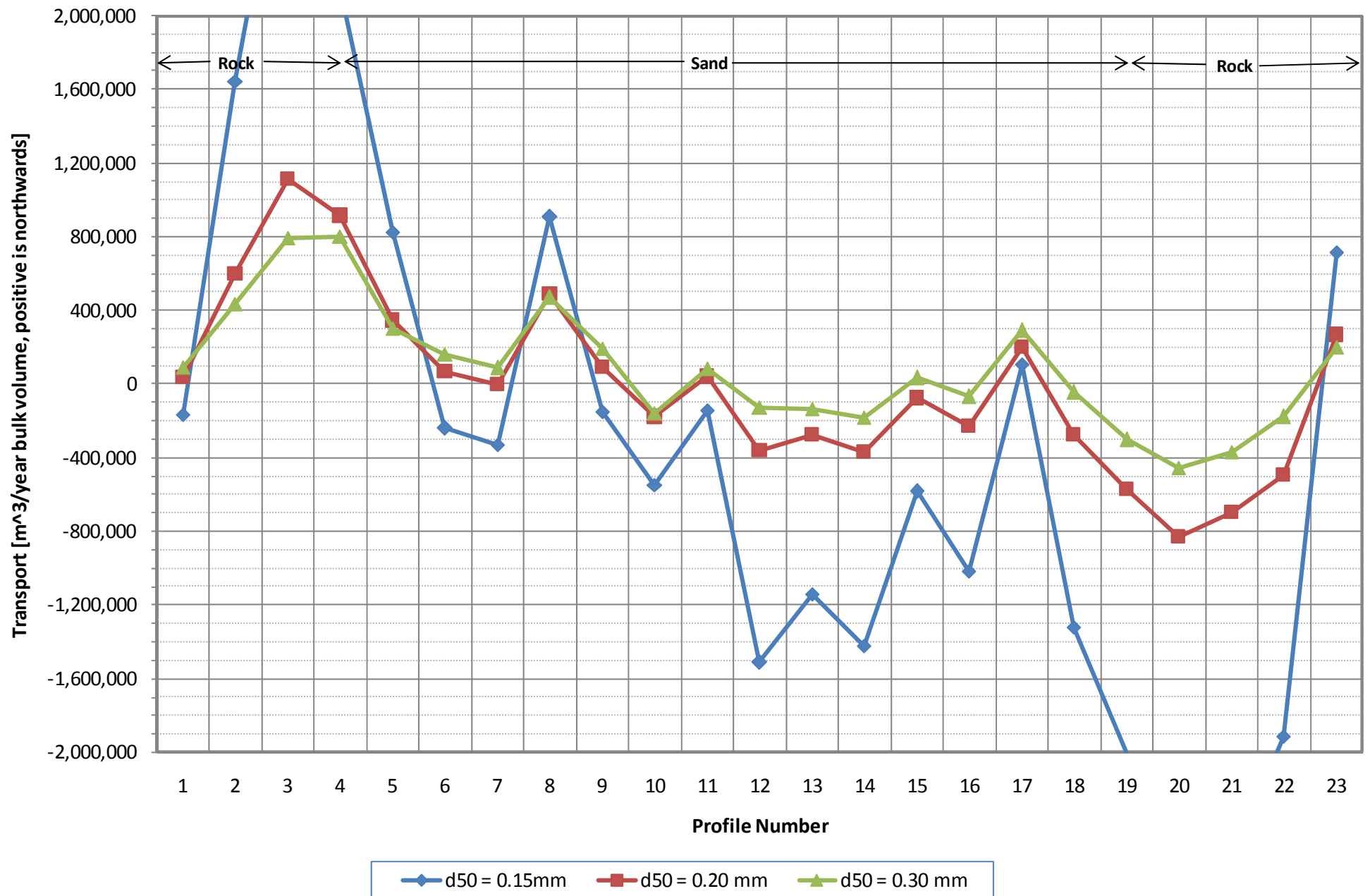


Title:

**Sediment transport modelling.**  
**Influence of season on net alongshore transport rates. Layout 0.  $D_{50} = 0.2$  mm.**  
**Refer to Figure 10.4 for profile locations.**

Figure No.

**10.13**

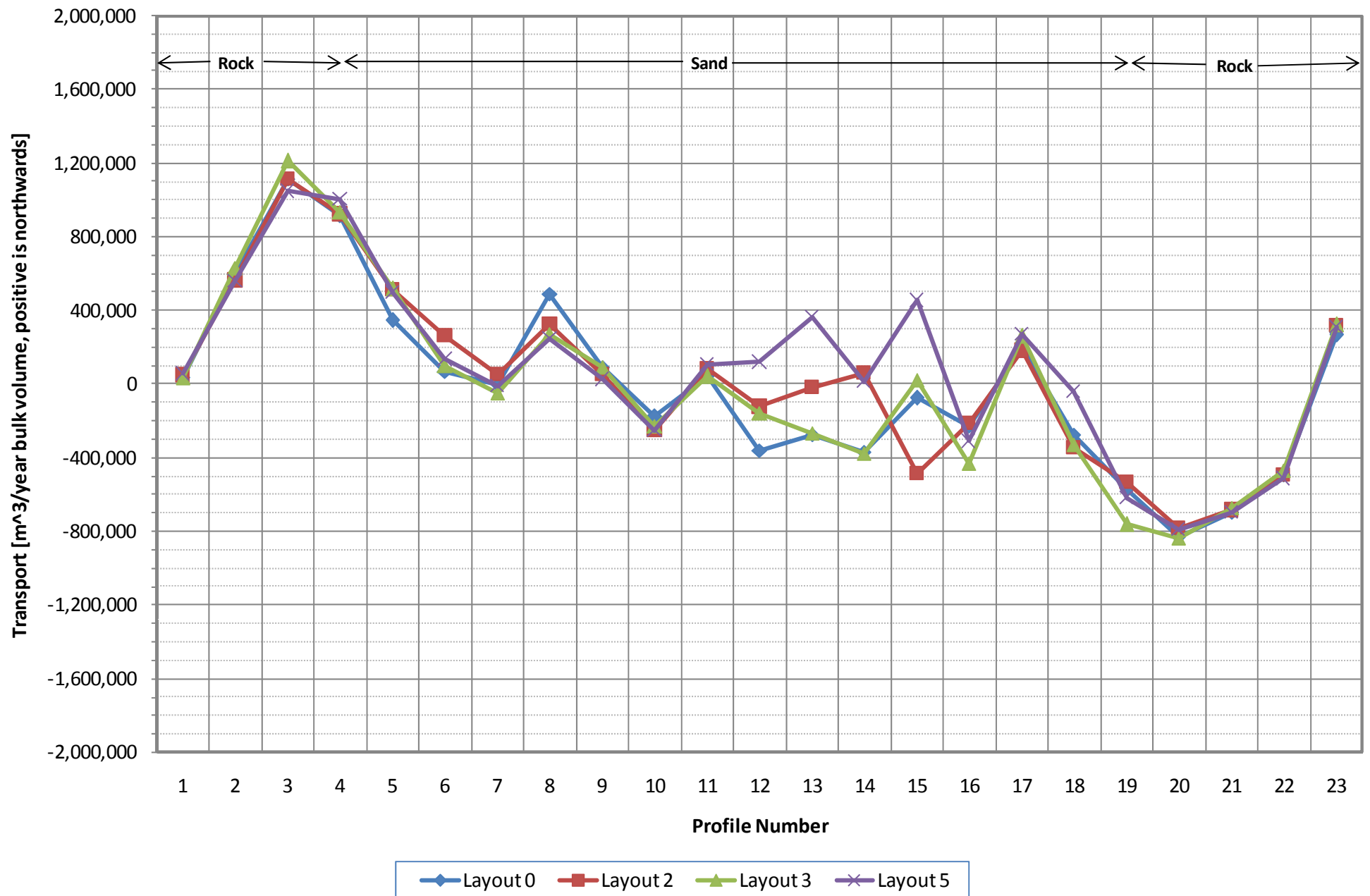


Title:

**Sediment transport modelling.**  
**Influence of grain size on net alongshore transport rates. Layout 0.  $D_{50} = 0.2$  mm.**  
**Refer to Figure 10.4 for profile locations.**

Figure No.

**10.14**

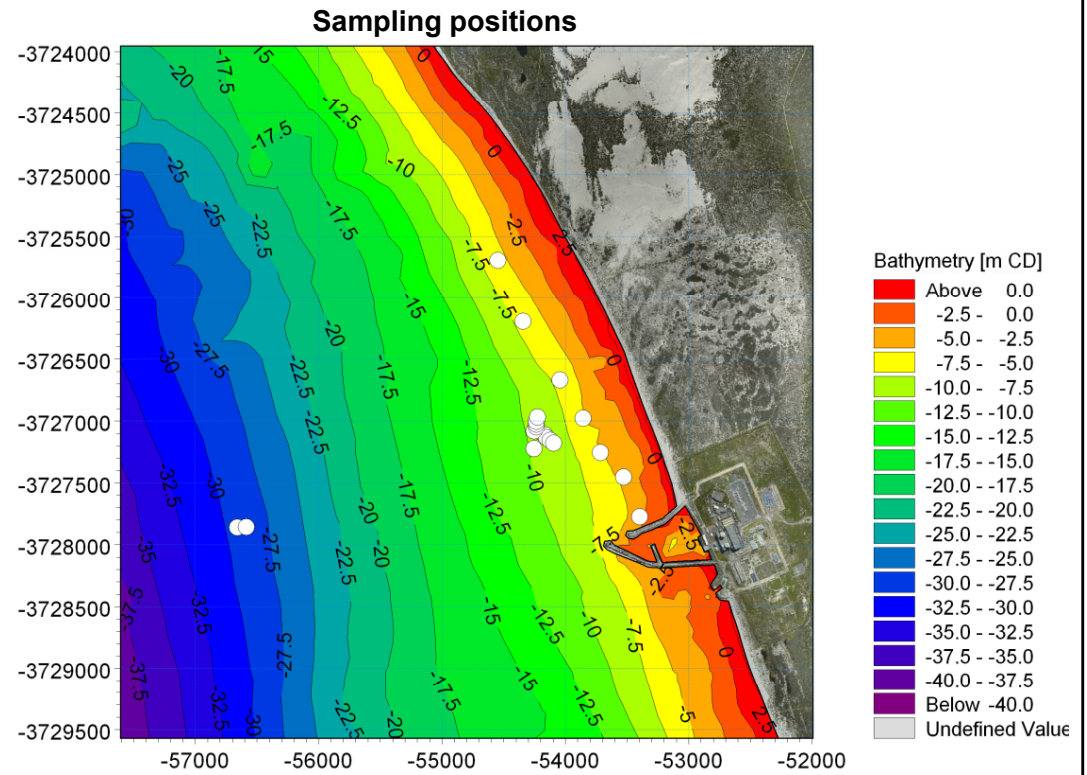
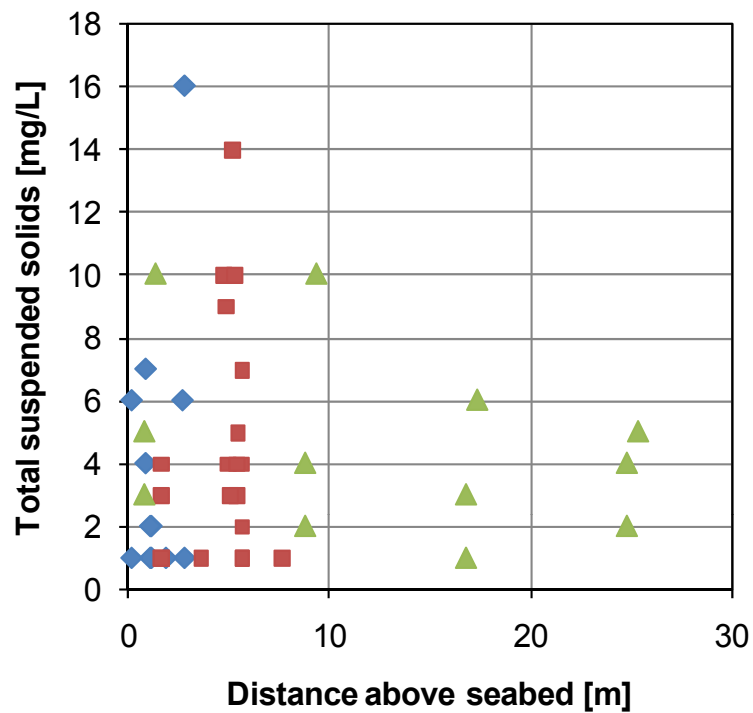


Title:

**Sediment transport modelling.**  
**Influence of layout on net alongshore transport rates.  $D_{50} = 0.2$  mm.**  
**Refer to Figure 10.4 for profile locations.**

Figure No.

**10.15**



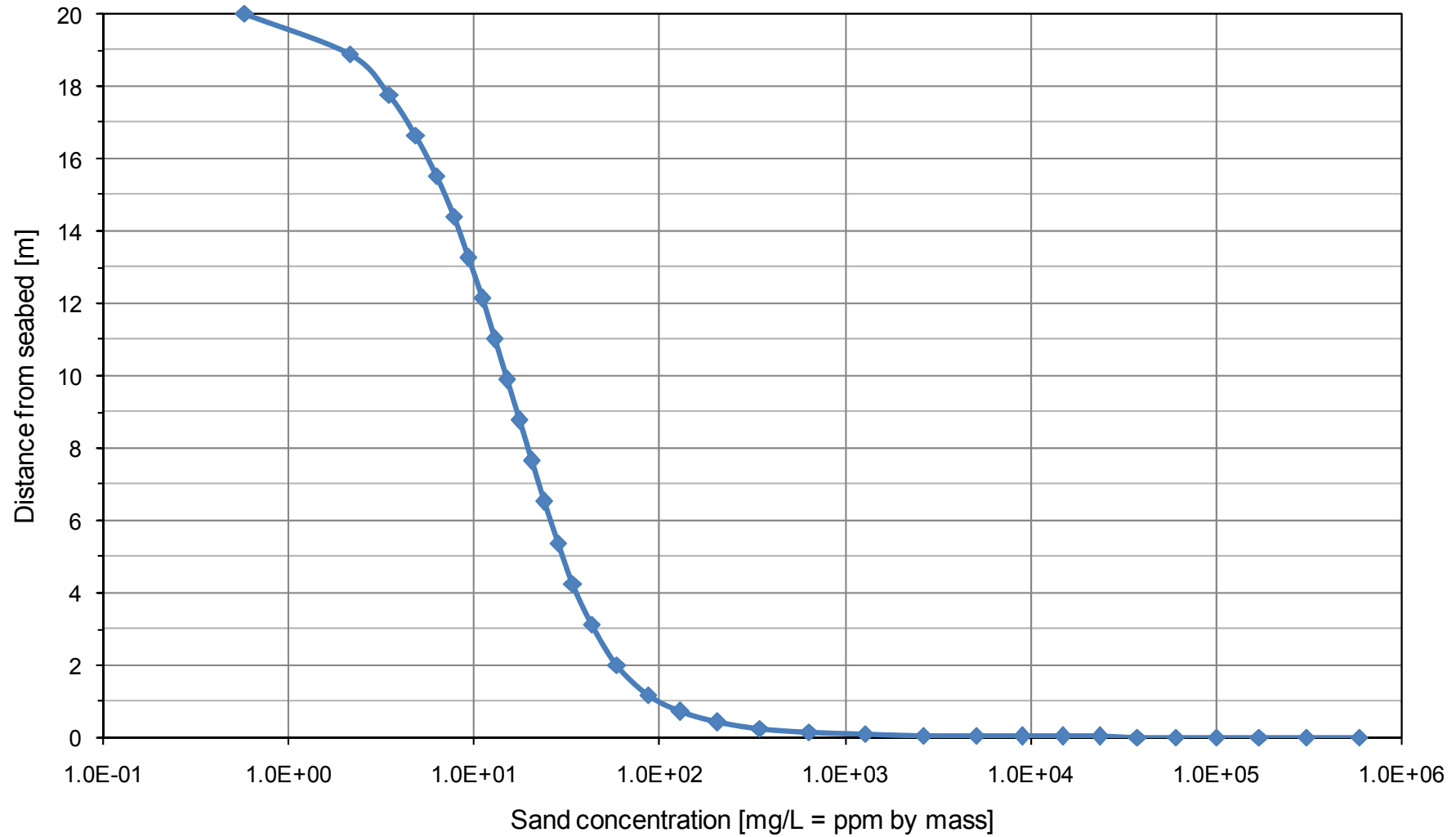
Title:

Measured total suspended solids and sampling positions.

Figure No.

10.16

Model input parameters: depth = 20 m,  $H_{m0} = 6.7$  m, wave direction =  $263^\circ$ ,  $T_p = 14$  s, current speed = 0.4 m/s, current direction =  $163^\circ$ ,  $D_{50} = 0.12$  mm, sediment grading = 1.5



Title:

Example of modelled vertical profile of suspended sand concentration.

Figure No.

10.17